Cooperative Properties of Lipid Bilayers: Collective Director Fluctuations and the Effects of Hydrophobic Mismatch in Protein/Lipid Membrane Systems

Thesis by
Paula Ivonne Watnick

In Partial Fulfillment
of the Requirements for
the Degree of Doctor of Philosophy

California Institute of Technology
Pasadena, California

1989
(submitted August 1, 1988)

Pasadena

This morning
Our jagged peaks
Crisp, a clear brilliant
Purple-Grey.
A beautiful day.

So many days
The air is
Purple-grey,
And the mountains
Vaguely present
In the distance.

Acknowledgements

Caltech has provided me with five of the happiest years of my life. I have many collegues and friends to thank for these years. First of all, I would like to thank Dr. Lila Gierasch for introducing me to scientific research in the context of a supportive, enthusiastic environment. I owe my interest in research to her. I would also like to thank my undergraduate research advisor, Dr. Robert Austin, for being himself and for proving that one need not compromise one's individuality to survive in the scientific arena.

My scientific maturation has been forwarded by many mentors. First of all, I would like to thank my research advisor, Sunney Chan, for teaching me to work independently and confidently and for consistently attracting talented and helpful individuals to his research group. Dr. Phoebe Dea has been a special collaborator and friend during the past five years. In addition to providing crucial assistance in many experiments, her advice and encouragement have been an integral part of my achievements at Caltech. Dr. Akbar Nayeem must be credited with the utmost patience in explaining the theoretical aspects of NMR relaxation to me. This work would not have been possible without the expert assistance of Drs. James Yesinowski and Hellmut Eckert of the NSF Regional NMR Facility. I would also like to thank them both for their friendship and James, in particular, for single-handedly making Brahms a common household word. I would like to thank Dr. Dan Weitekamp for sharing his insights into the theory of NMR and also for providing an excellent role model for young, aspiring scientists.

The students which I encountered when I first joined the Chan group were a particularly individualistic yet harmonious bunch. I am especially grateful to Dave Blair, Jeff Gelles, and Hsin Wang for their friendship, patience, and support

while I was getting started in the lab. Those were some of my most trying times at Caltech. Dave and Jeff will both be wonderful academic research advisors some day.

As any graduate student in chemistry will attest, the current Chan group includes an equally interesting cast of characters. I thank them all. I have had many belly laughs with Denise. Mark has taught me that I can come to know and like one whose moral philosophy of life is diametrically opposed to my own. I would like to thank Joel for his friendship and for the many interesting discussions we shared on those rare days when we had both managed to get up on the right side of the bed. Elise is not only a good friend but also one of those people who unifies a research group by her unflagging support of and interest in the work of the other members. Finally, I would like to thank Kathy for being a loyal and true friend who has fought, cried, and laughed with me during the past five years. Without her expert guidance, I would never have known which route to take or where to park in Pasadena.

Many friends outside the Chan group have brightened my stay. I would like to thank Miriam Zietlow for many Monday lunches. I will always remember warmly Christmas dinners with Miriam, Tom, and her parents. Tinar Kramer has also been a good friend throughout my stay at Caltech. We have commiserated and laughed over Chinese, Thai, Indonesian, and Mexican meals. I wish her all the best in the coming years.

The Caltech chamber music program has added a second dimension to my life here. I am particularly grateful to Delores and Bill Bing for their friendship and their dedication to and support of this program. I have shared many years of quartet playing and friendship with Karl Irikura and Julian Pranata. During the

past year, it has been a pleasure to rehearse and perform Mozart and Mendelssohn trios with Leslie Sonder and Tad White. They are both sensitive and talented musicians. Music has kept my heart from atrophying in the scientific environment.

Finally, I would like to thank my parents and my sister whose love throughout my life has equipped me with the confidence to act upon my own values and beliefs in spite of pressures from without.

Abstract

Cooperative director fluctuations in lipid bilayers have been postulated for many years. ^{2}H-NMR T_1^{-1}, $T_{1\rho}^{-1}$, and T_2^{-1} measurements have been used identify these motions and to determine the origin of increased slow bilayer motion upon addition of unlike lipids or proteins to a pure lipid bilayer.

The contribution of cooperative director fluctuations to NMR relaxation in lipid bilayers has been expressed mathematically using the approach of Doane et al.[1] and Pace and Chan.[2] The T_2^{-1}'s of pure dimyristoyllecithin (DML) bilayers deuterated at the 2, 9 and 10, and all positions on both lipid hydrocarbon chains have been measured. Several characteristics of these measurements indicate the presence of cooperative director fluctuations. First of all, T_2^{-1} exhibits a linear dependence on S_{CD}^2. Secondly, T_2^{-1} varies across the ^{2}H-NMR powder pattern as $\sin^2(2\beta)$, where β is the angle between the average bilayer director and the external magnetic field. Furthermore, these fluctuations are restricted near the lecithin head group suggesting that the head group does not participate in these motions but, rather, anchors the hydrocarbon chains in the bilayer.

T_2^{-1} has been measured for selectively deuterated liquid crystalline DML bilayers to which a host of other lipids and proteins have been added. The T_2^{-1} of the DML bilayer is found to increase drastically when chlorophyll *a* (chl *a*) and Gramicidin A′ (GA′) are added to the bilayer. Both these molecules interfere with the lecithin head group spacing in the bilayer. Molecules such as myristic acid, distearoyllecithin (DSL), phytol, and cholesterol, whose hydrocarbon regions are quite different from DML but which have small,neutral polar head groups, leave cooperative fluctuations in the DML bilayer unchanged.

The effect of chl *a* on cooperative fluctuations in the DML bilayer has been

examined in detail using ^{2}H-NMR T_1^{-1}, $T_{1\rho}^{-1}$, and T_2^{-1} measurements. Cooperative fluctuations have been modelled using the continuum theory of the nematic state of liquid crystals. Chl *a* is found to decrease both the correlation length and the elastic constants in the DML bilayer.

A mismatch between the hydrophobic length of a lipid bilayer and that of an added protein has also been found to change the cooperative properties of the lecithin bilayer. Hydrophobic mismatch has been studied in a series GA′/lecithin bilayers. The dependence of ^{2}H-NMR order parameters and relaxation rates on GA′ concentration has been measured in selectively deuterated DML, dipalmitoyllecithin (DPL), and DSL systems. Order parameters, cooperative lengths, and elastic constants of the DML bilayer are most disrupted by GA′, while the DSL bilayer is the least perturbed by GA′. Thus, it is concluded that the hydrophobic length of GA′ best matches that of the DSL bilayer. Preliminary Raman spectroscopy and Differential Scanning Calorimetry experiments of GA′/lecithin systems support this conclusion. Accommodation of hydrophobic mismatch is used to rationalize the absence of H_{II} phase formation in GA′/DML systems and the observation of H_{II} phase in GA′/DPL and GA′/DSL systems.

1. J. W. Doane and D. L. Johnson, *Chem. Phys. Lett.*, **6**, 291-295 (1970).
2. R. J. Pace and S. I. Chan, *J. Chem. Phys.*, **76**, 4217-4227 (1982).

TABLE OF CONTENTS

List of Figures and Tables

Chapter IV

Chapter V

Chapter VI

Chapter VII

Chapter I

Introduction

The most elementary conception of the cell membrane is that of a barrier allowing definition of the aqueous interior and exterior of the cell. This barrier is primarily composed of lipids which form bilayer structures in an aqueous environment. In addition, the lipid bilayer serves as a solvent system in which enzymatic, transport and gating functions of membrane-bound proteins may be carried out. The physical properties of the bilayer matrix will determine the efficiency of these functions. In turn, the proteins may alter the physical properties of the bilayer. The proper lipid and protein composition, therefore, is essential to the membrane's role as a solvent. This work is part of the on-going effort to understand how membrane lipids and proteins influence each other.

Lipids are composed of a hydrophilic headgroup region attached to a hydrophobic hydrocarbon region. Dimyristoyllecithin (DML), a diacyllecithin with two 14 carbon chains, is depicted in Figure 1. In aqueous environments, lipids arrange into configurations which expose the head groups to water, while shielding the hydrocarbon region from water. The packing of the hydrocarbon chains in the hydrophobic region also determines the preferred structure of a lipid system. Three commonly found arrangements are the bilayer, cubic, and hexagonal (H_{II}) phases. These are illustrated in Figure 2. Trends in the size, charge, extent of hydration of the head group, and length of the hydrocarbon chains correlate well with the phase in which a lipid system is found.[1–3]

The bilayer phase is the most prevalent in biological systems. Diacyl lipids with charged or amphiphilic head groups are generally found in bilayers. In this configuration, two lipid monolayers are arranged in a long sheet with hydrophobic tails pointing towards the center and head groups facing the aqueous environment. The vector perpendicular to the plane defined by the lipid head groups is the

Figure 1: The structure DML, a lecithin with two fourteen carbon chains.[31]

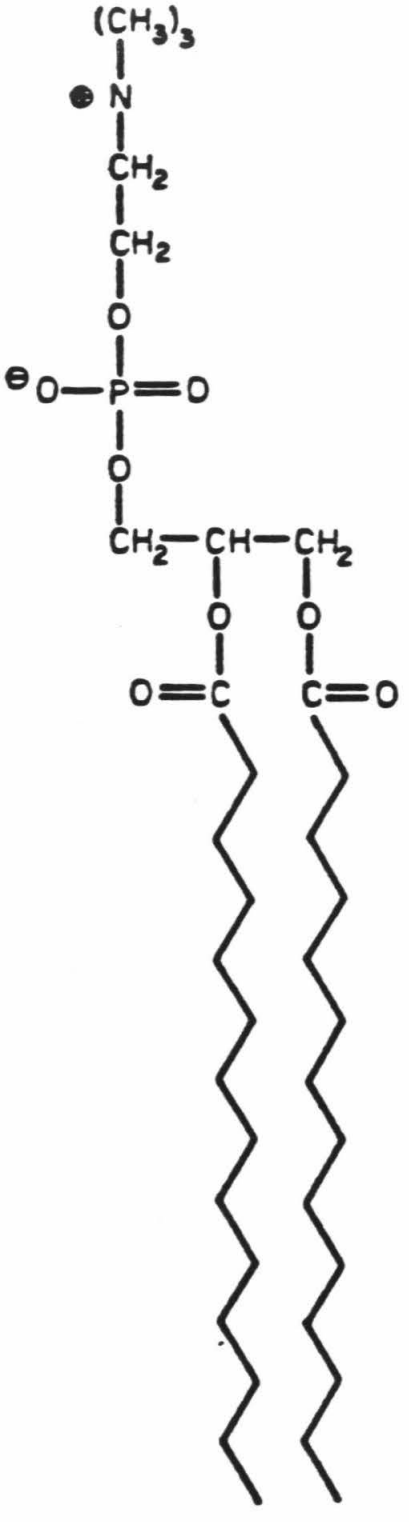

Figure 2: The three dimensional arrangement of the (a) bilayer, (b) cubic, and (c) H_{II} lipid phases.[32]

(a)

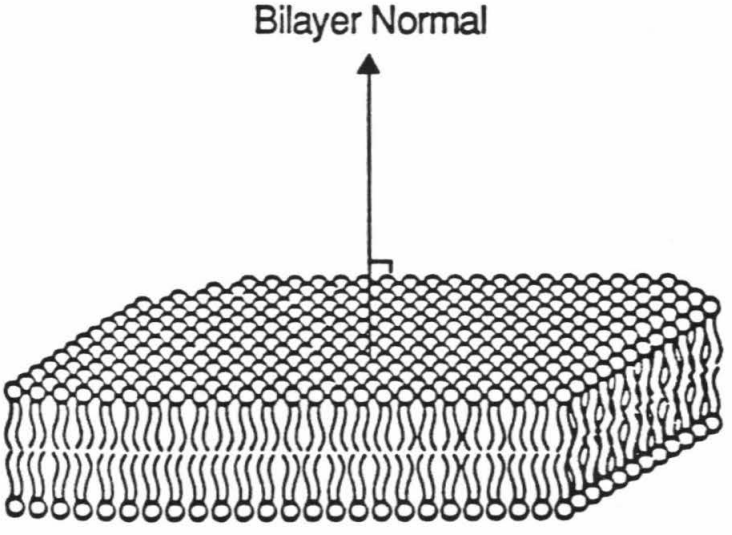

(b)

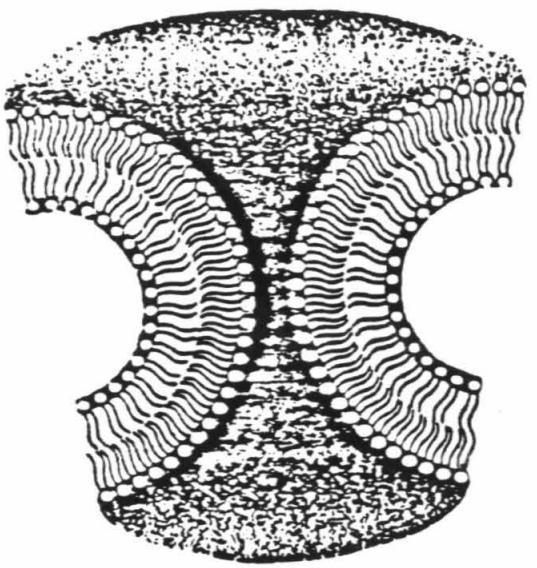

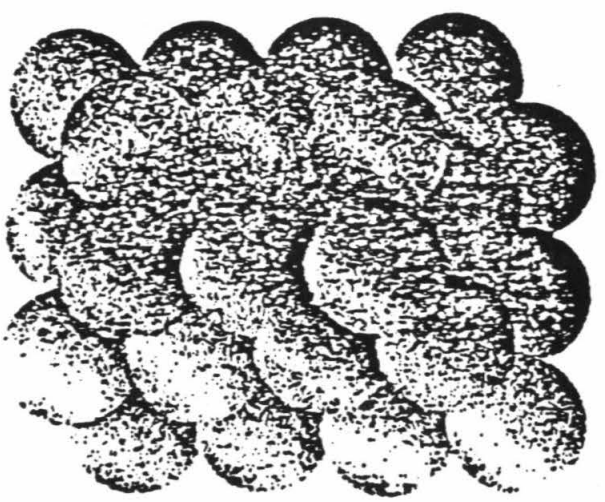

(c)

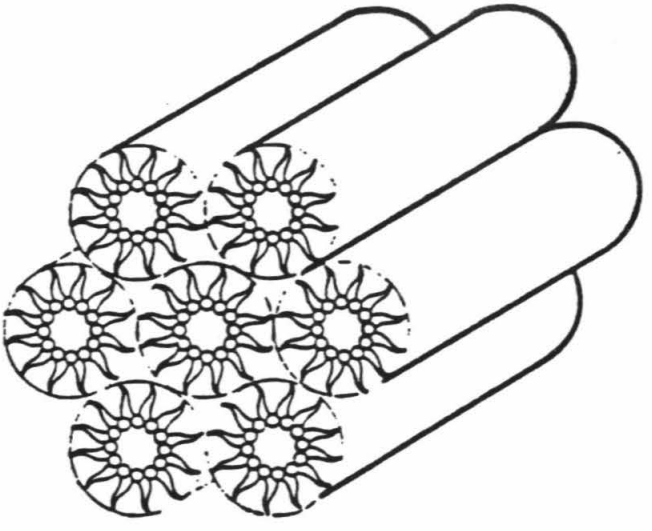

bilayer normal. The characteristics of the bilayer phase vary with temperature. At low temperatures, the bilayer is in the $L_{\beta'}$ or gel state. In this state, the lipid acyl chains are fully extended in an all-trans configuration. In addition, the chains are tilted by 30° with respect to the bilayer normal. At high temperatures, the L_{α} or liquid crystalline state is observed. In the liquid-crystalline state, the chains are much more fluid and, on average, are oriented parallel to the bilayer normal. In pure lipid bilayers, $P_{\beta'}$, a state occurring at intermediate temperatures, is observed. In this state, the chains are rigid as in the $L_{\beta'}$ state. They are not, however, tilted with respect to the bilayer normal. As proteins or other lipids are added to a lipid bilayer, the transition from the $P_{\beta'}$ state into the $L_{\beta'}$ state is often lost. For a given polar head group, the temperature (T_c) at which the bilayer crosses from the gel into the liquid-crystalline state is determined by the head group charge, the head group size, the degree of unsaturation of the hydrocarbon chains, and the length of the hydrocarbon chains. In saturated diacyllecithins, for example, T_c increases by approximately twenty degrees for every addition of two carbons to the hydrocarbon chains.

The cubic phase is believed to be a transition state in the passage of a lipid system from bilayer to hexagonal phase.[4] The inner region of this phase is an aqueous sphere rather than a cylinder. As in hexagonal phase, the hydrophobic chains line the exterior. It is theorized that cubic phase forms within two monolayers when two bilayers approach each other.

If the hydrophobic cross-section of a diacyl lipid with a small, uncharged polar head group is much larger than the hydrophilic cross-section, this lipid is best accommodated by hexagonal phase. In this phase, the polar head groups are pointed towards an inner cylinder of water, while the hydrocarbon chains point

outwards towards the chains of other cylinders. Because this phase presents a hydrophobic phase to the exterior medium, it self-associates in excess water to form large aggregates. In addition, high temperatures and low water contents promote hexagonal phase in pure lipid systems. The structural implications of the bilayer and H_{II} phases will be further discussed in chapter 5.

An important step in the characterization of a lipid or lipid/protein system is the construction of a phase diagram. The temperatures and enthalpies characterizing phase boundary traversals may be accurately determined by Differential Scanning Calorimetry (DSC) measurements.[5–7] Phospholipids in the bilayer gel, bilayer liquid crystalline, cubic, and H_{II} phases have characteristic ^{31}P Nuclear Magnetic Resonance (NMR) spectra.[8–10] At a given temperature, therefore, NMR allows identification of the state and phase of a phospholipid system. Furthermore, by measuring the temperature dependence of the ^{31}P-NMR spectrum, the types of phase boundaries crossed in the phase diagram may be determined. The ^{31}P-NMR spectra for lipid systems in the bilayer, cubic, and H_{II} phases are shown in Figure 3.

The motional and structural properties of a lipid phase vary with the types of lipids and membrane-bound proteins involved in the phase. Although a phase diagram indicates the three dimensional arrangement of the lipid system at a given temperature, it does not detail the properties of each phase for a particular lipid system. The exact dimensions of a given lipid phase may be determined by X-ray diffraction. For the bilayer phase, this technique yields the repeat distances between bilayers.[11,12] For H_{II} phase, X-ray diffraction provides the spacing between aqueous cylinder. The motions of the lipids in a given phase may be observed by multiple pulse NMR,[13,14] fluorescence anisotropy and quenching,[15–17] and other

Figure 3: The ^{31}P-NMR spectra of the (a) bilayer, (b) cubic, and (c) H_{II} lipid phases.[10]

(a)

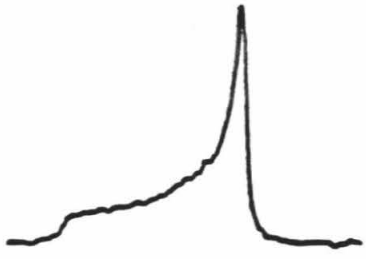

(b)

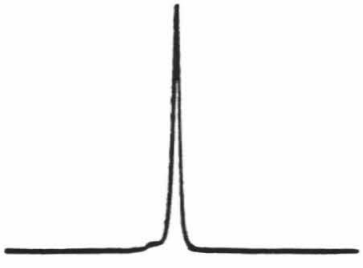

(c)

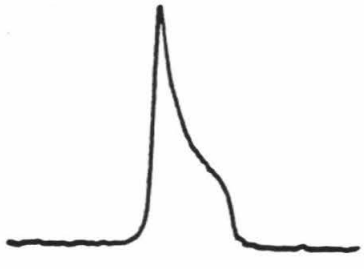

techniques.

In this work, the changes in the structural and motional properties of a homogeneous lipid system upon addition of another type of lipid or protein will be studied. Only if the phases of the homogeneous lipid system are well characterized, is it possible to determine the effects of adding other lipids or proteins. The additions may cause a gross change of phase, a change in the structural characteristics of a phase, or simply change the mobility of lipids in a given phase.

Nuclear Magnetic Resonance (NMR) relaxation experiments are especially well-suited to the study of motional parameters in lipid bilayer systems.[18–20] From these experiments, it has been deduced that the motions of lipids in the liquid crystalline phase are characterized by one of two time scales.[21,22] One motional time scale is much faster than 10^{-10} seconds, while the other is slower than 10^{-6} seconds. The faster time scale is associated with motions involving a single lipid molecule such as bond rotation and bond reorientation. The slower time scale is associated with motions perpendicular to the bilayer normal. These motions involve reorientation of the lipid chains with respect to the bilayer normal. If these molecules do not move coherently, such reorientation will result in collisions with neighboring lipid molecules. Close association of the lipid chains, therefore, forces them to move cooperatively in the direction perpendicular to the bilayer normal. Because of the large distances over which these cooperative motions extend, they are much slower than non-cooperative motions.

Upon addition of a protein to a deuterated lipid bilayer, the ^{2}H-NMR signal is significantly broadened.[23–25] Three explanations have been suggested for this result. It has been proposed that the broadness of the NMR signal is due to a superposition of several NMR spectra arising from lipids in different types of

protein environments.[26] Another hypothesis involves the formation of protein/lipid complexes which severely limit the motion of individual lipid molecules.[27] Finally, it has been suggested that the the broadness of the NMR signal is a result of a change in the cooperative motions of the lipid bilayer.[28] The protein, therefore, somehow perturbs the cooperativity between bilayer lipids. The latter hypothesis is the subject of this work.

After a brief introduction to NMR relaxation of the ^{2}H nucleus, relaxation rates of a variety of mixed lipid and protein/lipid systems will be surveyed. When compared with the relaxation rates of the pure lipid bilayer, these mixed systems may be separated into two groups. In group one, the frequency profile of cooperative motion is similar to that of the pure bilayer. In group two, the frequency profile is very different from that of the pure bilayer. Cooperative motions in the pure lipid bilayer are similar to cooperative motions in nematic liquid crystals. Consequently, changes in these motions upon addition of another lipid or protein will be described using the continuum theory of the nematic state.[28–30]

To determine how certain lipids and proteins affect cooperative motions in lipid bilayers, two systems will be studied in detail. These are chlorophyll *a* (chl *a*) in DML and Gramicidin A′ (GA′) in lecithin bilayers of various chain lengths. Chl *a* has a large porphyrin head group. In the chl *a*/DML system, accommodation of the porphyrin head group is correlated with changes in cooperative motions of the lipid bilayer.

In the GA/lecithin systems, the effect of mismatched protein and lipid bilayer hydrophobic lengths on cooperative motion is examined. In addition, a model is proposed for the induction of H_{II} phase by the addition of GA′ to the longer chain length lipid bilayers.

The changes in cooperative motions upon addition of a protein are important in the characterization of lipid/protein interactions in the lipid bilayer. The activity of a protein in a lipid bilayer may depend on the coupling of cooperative lipid motions to the internal motions in the protein. In this case, the frequency profile of cooperative motions and protein fluctuations must be matched. In this work, the frequency profile of cooperative lipid motions is measured. A determination of the time scale of protein fluctuations will be the subject of future investigations.

References

1. J. N. Israelachvili, D. J. Mitchell, and B. W. Ninham, *Biochim. Biophys. Acta*, **470**, 185-201 (1977).
2. G. L. Kirk, S. M. Gruner, and D. L. Stein, *Biochemistry*, **23**, 1093-1102 (1984).
3. S. M. Gruner, *Proc. Natl. Acad. Sci. USA*, **82**, 3665-3669 (1985).
4. D. P. Siegel, *Biophys. J.*, **49**, 1155-1170 (1986).
5. D. Chapman and J. Urbina, *J. Biol. Chem.*, **249**, 2512-2521 (1974).
6. S. Mabrey and J. Sturtevant, *Proc. Natl. Acad. Sci. USA*, **73**, 3862-3866 (1976).
7. I. Hatta, K. Suzuki, and S. Imaizumi, *J. Phys. Soc. Japan*, **52**, 2790-2797 (1983).
8. P. R. Cullis and B. De Kruijff, *Biochim. Biophys. Acta*, **507**, 207-218 (1978).
9. A. M. Thayer and S. J. Kohler, *Biochemistry*, **20**, 6831-6834 (1981).
10. S. M. Gruner, P. R. Cullis, M. J. Hope, and C. P. S. Tilcock, *Ann. Rev. Biophys. Biophys. Chem.*, **14**, 211-238 (1985).
11. B. A. Lewis and D. M. Engelman, *J. Mol. Biol.*, **166**, 211-217 (1983).
12. B. F. Cornell and F. Separovic, *Biochim. Biophys. Acta*, **733**, 189-198 (1983).
13. P. Meier, E. Ohmes, G. Kothe, A. Blume, J. Weldner, and H. Eibl, *J. Phys. Chem.*, **87**, 4904-4912 (1983).
14. B. De Kruijff, G. A. Morris, and P. R. Cullis, *Biochim. Biophys. Acta*, **598**, 206-211 (1980).
15. F. Jaehnig, *Proc. Natl. Acad. Sci. USA*, **76**, 6361-6353 (1979).
16 H. Vogel and F. Jaehnig, *Proc. Natl. Acad. Sci. USA* , **82**, 2029-2033 (1985).
17. E. London and G. W. Feigenson, *Biochemistry*, **20**, 1932-1938 (1981).
18. B. A. Cornell and J. M. Pope, *Chem. Phys. Lip.*, **27**, 151-164 (1980).
19. Y. C. W. van Der Leeuw and G. Stulen, *J. Magn. Res.*, **42**, 434-445 (1981).
20. M. F. Brown, *J. Chem. Phys.*, **77**, 1576-1599 (1982).
21. G. W. Feigenson and S. I. Chan, *J. Am. Chem. Soc.* , **96**, 1312-1319 (1973).

22. N. O. Petersen, and S. I. Chan, *Biochemistry*, **16**, 2657-2667 (1977).

23. D. Rice and E. Oldfield, *Biochemistry*, **18**, 3272-3279 (1979).

24. S. Y. Kang, H. S. Gutowsky, J. C. Hsung, R. Jacobs, T. E. King, D. Rice, and E. Oldfield, *Biochemistry*, **18**, 3257-3267 (1979).

25. A. J. Deese, E. A. Dratz, F. W. Dahlquist, and M. R. Paddy, *Biochemistry*, **20**, 6420-6427 (1981).

26. A. Bienvenue, M. Bloom, J. H. Davis, and P. F. Devaux, *J. Biol. Chem.*, **257**, 3032-3038 (1982).

27. B. A. Cornell, R. G. Hiller, J. Raison, F. Separovic, R. Smith, J. C. Vary, and G. Morris, *Biochem. Biophys. Res. Comm.*, **732**, 473-478 (1983).

28. J. W. Doane and D. L. Johnson, *Chem. Phys. Lett.*, **6**, 291-295 (1970).

29. P. G. de Gennes, **The Physics of Liquid Crystals** (Oxford University Press, New York, 1974).

30. S. Chandrasekhar, **Liquid Crystals** (Cambridge University Press, New York, 1977).

31. P. I. Watnick, P. Dea, A. Nayeem, and S. I. Chan, *J. Chem. Phys.*, **86**, 5789-5800 (1987).

32. A. J. Verkleij, *Biochim. Biophys. Acta*, **779**, 43-63 (1984).

Chapter II

Chemical Shift Anisotropy, the Quadrupolar Hamiltonian, and Deuterium Relaxation Rates in Lipid Bilayers

Introduction

In order to extract motional information from NMR experiments carried out on lipid bilayers, one must have a model for the types of motions undergone by the bilayer. The effect of these motions on the nuclear spin Hamiltonian must also be understood. The following chapters include studies of both ^{31}P and ^{2}H nuclei in lipid systems. For ^{2}H and ^{31}P nuclei, quadrupolar and chemical shift interactions, respectively, dominate the spin Hamiltonian. In this chapter, therefore, expressions for the quadrupolar and chemical shift Hamiltonians in the presence of anisotropic motional averaging are derived.

Although quadrupolar and chemical shift interactions have distinct origins, the treatment of these two interactions for systems undergoing anisotropic motion in the presence of a strong magnetic field is quite similar. The form of quadrupolar Hamiltonian in the instance of anisotropic motion in lipid bilayers, therefore, will be derived in detail. The chemical shift interaction will subsequently be presented by analogy.

The Quadrupolar Hamiltonian and Deuterium Relaxation Rates

I. *The Static Quadrupolar Hamiltonian in Zero Field*

In nuclei with $I \geq 1$, an asymmetric distribution of charge within the nucleus leads to a nuclear electric quadrupole moment. The electrostatic interaction of the quadrupole moment with the electronic field gradient at the nucleus is represented by a quadrupolar term in the nuclear spin Hamiltonian. The electric nuclear

quadrupole interaction may be represented by a three dimensional tensor $\hat{Q}$. The Hamiltonian is:[1]

$$H^Q = \hat{\mathrm{I}} \cdot \hat{Q} \cdot \hat{\mathrm{I}} \tag{1}$$

This expression may be expanded to give:[2]

$$H^Q = \frac{eQ}{4I(2I-1)}[V_0(3\hat{I}_c^2 - \hat{I}^2) + V_{\pm}\hat{I}_{\mp}\hat{I}_c + \hat{I}_c\hat{I}_{\mp}) + V_{\pm 2}\hat{I}_{\mp}^2] \tag{2}$$

where Q represents the scalar quadrupole moment of the nucleus ($2.875\times10^{27}\mathrm{cm}^2$ for $^2\mathrm{H}$), e is the elementary charge, I is the nuclear spin ($I = 1$ for $^2\mathrm{H}$), $I_{\pm}$ are raising and lowering operators, and the V_m are:

$$V_0 = V_{cc} \tag{3a}$$

$$V_{\pm 1} = V_{ac} \pm iV_{bc} \tag{3b}$$

$$V_{\pm 2} = \frac{1}{2}(V_{aa} - V_{bb} \pm 2iV_{ab}) \tag{3c}$$

The V_{ij} are second derivatives of the electrostatic potential at the quadrupolar nucleus. In the interest of simplicity, components of the quadrupolar Hamiltonian may be factored and expressed in terms of their second order irreducible spherical tensor components. In this case, the Hamiltonian takes the form:[3]

$$H^Q = \frac{eQ}{4}\sum_{l=0}^{2}\sum_{m=-2}^{2} V_{l,m}A_{l,-m}^Q \tag{4}$$

The spatial spherical tensor components are:

$$V_{2,0} = V_{cc} \tag{5a}$$

$$V_{2,\pm 1} = \pm\sqrt{\frac{2}{3}}(V_{ac} \pm iV_{bc}) \tag{5b}$$

$$V_{2,\pm 2} = \sqrt{\frac{1}{6}}(V_{aa} - V_{bb} \pm 2iV_{ab}) \tag{5c}$$

and the spin spherical tensor components are:

$$A^{Q}_{2,0} = 3\hat{I}_c^2 - I(I+1) \tag{6a}$$

$$A^{Q}_{2,\pm 1} = \sqrt{\frac{3}{2}}(\hat{I}_c\hat{I}_\pm + \hat{I}_\pm\hat{I}_c) \tag{6b}$$

$$A^{Q}_{2,\pm 2} = \sqrt{\frac{3}{2}}(\hat{I}_\pm)^2 \tag{6c}$$

Only the components which are non-zero in both space and spin are given above. Note that the quadrupolar tensor is traceless.

The proper choice of coordinate axis greatly simplifies expression of the quadrupolar Hamiltonian.[4] The principal coordinate system is defined to be one in which the electric field gradient tensor is diagonal. This coordinate system is also known as the quadrupolar frame. In the absence of a magnetic field, the nuclear spins are quantized in the principal coordinate system as well. Because off-diagonal elements are zero, $V_{2,\pm 1}$=0. If one makes the following substitutions,[5]

$$eq = V_{cc} \tag{7a}$$

$$\eta = \frac{V_{aa} - V_{bb}}{V_{cc}} \tag{7b}$$

the components of the electric field gradient become:

$$V_{2,0} = eq \tag{8a}$$

$$V_{2,\pm 1} = 0 \tag{8b}$$

$$V_{2,\pm 2} = \sqrt{\frac{1}{6}}\eta eq \tag{8c}$$

For a deuteron involved in a C-D bond, η is only 0.05. The field gradient, therefore, is approximated as being axially symmetric, and $\eta \approx 0$. For aliphatic systems, the axis of approximate axial symmetry coincides with the C-D bond vector. Thus, the orientations of the C-D bond vector and the principal axis system are equivalent. Because only $A^Q_{2,0}$ is non-zero, the Hamiltonian is further simplified to:

$$H^Q = \frac{e^2qQ}{4}(3\hat{I}_z^2 - I(I+1)) \tag{9}$$

II. *The Static Quadrupolar Hamiltonian in a Strong Magnetic Field*

In the presence of a strong external magnetic field, the degeneracy of the nuclear spin states is broken. The spins become quantized along the magnetic field direction, and the spin tensor is described as being diagonal in the laboratory frame. This effect is known as the Zeeman interaction. The quadrupolar interaction may be treated as a small perturbation of spin quantization along the magnetic field direction. In this case, the total Hamiltonian may be expressed as:[5]

$$H = H^z + H^Q \tag{10}$$

where:

$$H^Q = H_0^Q + H_1^Q + H_2^Q \tag{11},$$

H^z arises from the Zeeman interaction, and the H_p^Q represent the corrections to the Hamiltonian based on perturbation theory. The various H_p^Q correspond to respective terms in the quadrupolar Hamiltonian containing $I_\pm^p$ where p=0,1,2. The

form of the H^Q is complicated in the presence of a strong external magnetic field. As a result of this field, the spin tensor becomes diagonal in the laboratory frame, while the electric field gradient remains diagonal in the principal axis system. It is desirable to express H^Q as the product of diagonal spin and spatial tensors. This is made possible by the use of Wigner rotation matrices.[6] A spin tensor expressed in the laboratory frame may, thus, be rotated into the quadrupolar frame. The elements of the rotation matrix are denoted as $D^{(2)}_{pm}(\alpha,\beta,\gamma)$, where α, β, and γ are the Euler angles which rotate the axes of the laboratory frame into those of the quadrupolar frame. The axes about which these rotations are performed are shown in Figure 1. The elements of a rotation matrix may be separated into a product of terms involving only one Euler angle using the following formula:[6]

$$D^2_{pm}(\alpha\beta\gamma) = \exp(-ip\alpha)d^2_{pm}(\beta)\exp(-im\gamma) \tag{12}$$

The reduced matrix elements d^2_{pm} are given in Table I. The new tensor components for the quadrupolar spin interaction are calculated using:[4]

$$A^Q_{2,0} = \sum_{p=-2}^{2} A_{2,p}D^2_{p0}(\alpha\beta\gamma) \tag{13}$$

where the $A_{2,p}$ are the tensor components of the quadrupolar interaction in the laboratory frame. In order to obtain the correct form for the quadrupolar Hamiltonian in a strong magnetic field, Eqn. 13 must be substituted into Eqn. 4. This substitution yields:

$$H^Q_p = \frac{eQ}{4}V_{2,0}A_{2,p}D^2_{p0}(\alpha\beta\gamma) \tag{14}$$

A simplification of H^Q is often possible when motion exists in the system under study.

Figure 1: The Euler angles (a) α, (b) β, and (c) γ, which are used to rotate one coordinate system into another.[13]

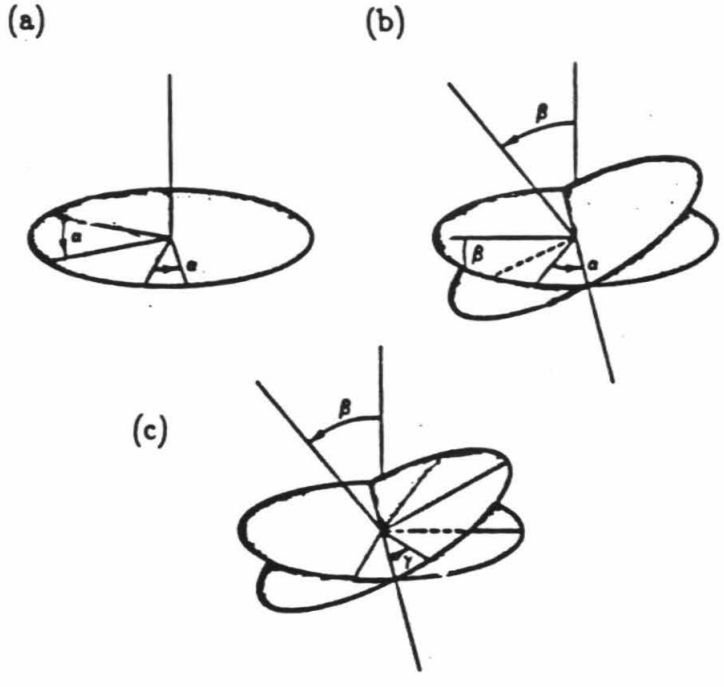
(a)
α
e
(b)
β
β
α
(c)
β
γ

Table I: The reduced Wigner rotation matrix elements of order two.

Table I[1]

$$d^2_{22} = d^2_{-22} = \cos^4(\frac{\beta}{2})$$

$$d^2_{21} = -d^2_{12} = -d^2_{-2-1}$$

$$= d^2_{-1-2} = -\frac{1}{2}\sin\beta(1+\cos\beta)$$

$$d^2_{20} = d^2_{02} = d^2_{-20} = d^2_{0-2} = \sqrt{\frac{3}{8}}\sin^2\beta$$

$$d^2_{2-1} = d^2_{1-2} = d^2_{-21} = d^2_{-12} = \frac{1}{2}\sin\beta(\cos\beta - 1)$$

$$d^2_{2-2} = d^2_{-22} = \sin^4\frac{\beta}{2}$$

$$d^2_{11} = d^2_{-1-1} = \frac{1}{2}(2\cos\beta - 1)(\cos\beta + 1)$$

$$d^2_{1-1} = d^2_{-11} = \frac{1}{2}(2\cos\beta + 1)(1 - \cos\beta)$$

$$d^2_{10} = d^2_{0-1} = d^2_{01} = d^2_{-10} = -\sqrt{\frac{3}{2}}\sin\beta\cos\beta$$

$$d^2_{00} = \frac{1}{2}(3\cos^2\beta - 1)$$

III. *The Quadrupolar Hamiltonian in the Presence of Anisotropic Motion*

Anisotropic motion is characterized by rapid averaging about one or several axes with much slower averaging occurring about other axes. The motion experienced by a deuteron on a lipid hydrocarbon chain in a multilamellar system is believed to be anisotropic.[7] Motion occurs most rapidly about three axes. Rotation of the C-D bond vector about the hydrocarbon chain axis occurs very rapidly about the lipid hydrocarbon C-C chain segment. Locally, lipid molecules in a bilayer are oriented in the same direction with respect to the magnetic field. This orientation is represented by a unit vector known as the director. On the NMR time scale, lipid chains oscillate less rapidly about the average director orientation. Because of close contact between lipid chains, these oscillations can be cooperative. The collective position of the lipid chains at any instant is referred to as the instantaneous director orientation. Finally, hydrocarbon chain isomerizations occur about the instantaneous director orientation.[8] Motion about all other directions in space is slow on all time scales relevant to this work.

The average quadrupolar Hamiltonian is most simply expressed if motional averaging about the hydrocarbon chain and director is considered in the transformation of the spin tensor into the principal axis frame. The rotation must be divided into four sub-rotations. These are 1) a rotation from the laboratory coordinate system into an axis system with the z direction along the average director, 2) a rotation from the coordinate system of the average director into that of the instantaneous director, 3) a rotation from the instantaneous director axis system into the axis system of the hydrocarbon chain segment, and, finally, 4) a rotation from the chain segment orientation into the principal coordinate system. The corresponding Euler angles for these rotations will be represented by:

$$\Omega \equiv (\alpha, \beta, \gamma) \tag{15a}$$

$$\delta\Omega \equiv (\delta\alpha, \delta\beta, \delta\gamma)$$

$$\Omega' \equiv (\alpha', \beta', \gamma') \tag{15b}$$

$$\Omega'' \equiv (\alpha'', \beta'', \gamma'') \tag{15c}$$

These rotations are diagrammed in Figure 2. The δ notation in $\delta\Omega$ is used to signify that the director fluctuations are very small perturbations of the average director orientation.[9] The rotation of the spin tensor is denoted as follows:

$$A^{Q}_{2,0} = \sum_{k=-2}^{2} \sum_{q=-2}^{2} \sum_{n=-2}^{2} A_{2,p} D^{2}_{pq}(\Omega) D^{2}_{qk}(\delta\Omega) D^{2}_{kn}(\Omega') D^{2}_{n0}(\Omega'') \tag{16}$$

and the quadrupolar Hamiltonian becomes:

$$H^{Q}_{p} = \frac{e^2 qQ}{4} \sum_{k=-2}^{2} \sum_{q=-2}^{2} \sum_{n=-2}^{2} A_{2,p} D^{2}_{pq}(\Omega) D^{2}_{qk}(\delta\Omega) D^{2}_{kn}(\Omega') D^{2}_{n0}(\Omega'') \tag{17}$$

By assuming the type of motional averaging found in the hydrocarbon region of lipid bilayers, Eqn. (15) may be further simplified.

As suggested above, fluctuations in Ω, $\delta\Omega$, Ω', and Ω'' occur on very different time scales. The orientation of the average director with respect to the magnetic field direction, which is represented by Ω, remains constant on the NMR time scale. Fluctuations of the instantaneous director orientation about the average director, which involve changes in $\delta\Omega$, are slow but observable on the NMR time scale. The frequency of the latter motions is thought to be in the range $10^{-5} - 10^{-8}$ sec^{-1}.[7] Trans-gauche isomerizations about C-C bonds along the lipid hydrocarbon chain, which will result in fluctuations about the instantaneous director orientation, are

Figure 2: The intermediate Euler angles used to rotate the nuclear spin tensor from the laboratory frame into the quadrupolar frame: (a) the rotation from the laboratory frame into the frame of the average director, (b) the rotation from the coordinate system of the average director into the coordinate system of the instantaneous director, (c) the rotation from the coordinate system of the instantaneous director into the chain segment coordinate system, and (d) the rotation from the chain segment coordinate system into the quadrupolar or C-D bond frame.(Picture modified from reference 14.)

(a)

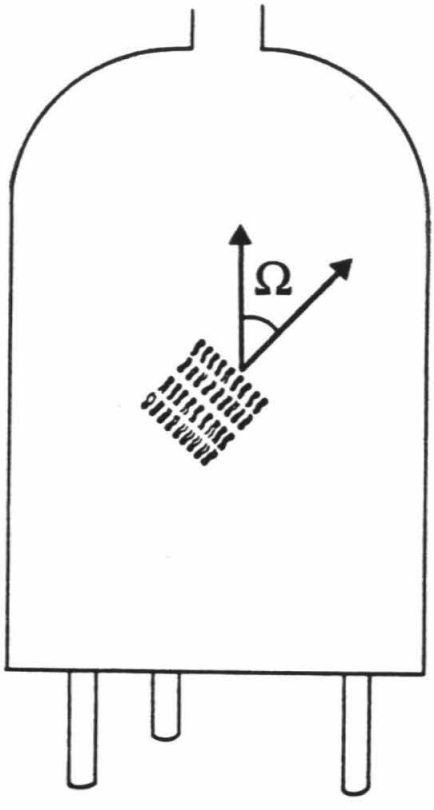

(b)

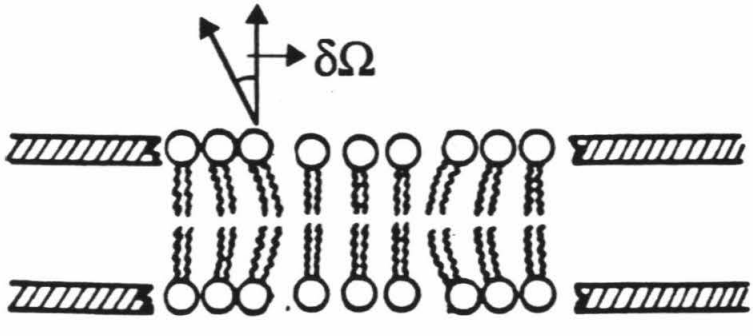

(c)

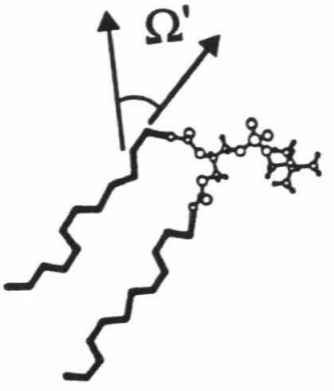

(d)

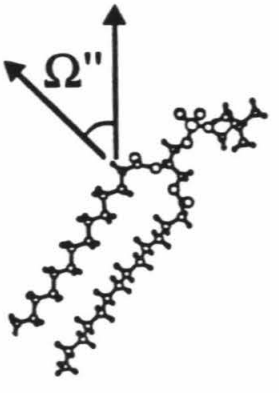

probably quite slow for segments in the central portion of the hydrocarbon chain.[8] This region extends from position 3 to approximately position 10 of the lipid chain. In this region, hydrocarbon chains of nearby lipid molecules are closely packed, and isomerizations of the lipid chain segments are likely to be restricted by the conformations of neighboring lipid chains. Finally, rotations of the C-D bond about the hydrocarbon chain segment, which affect Ω'', occur very quickly on the NMR time scale. They are estimated to be in the range of $10^{-10} - 10^{-11}$ sec^{-1}.[7] Because the time scales of these four motions are very different, they are assumed to be uncorrelated. Consequently, in $< H_p^Q >$, their ensemble averages may be taken separately.

In addition, the time dependence of the director orientation is contained in $\delta\Omega$. The average director orientation, therefore, is time-independent. As a result of these approximations, the average Hamiltonian becomes:

$$< H_p^Q >= \frac{e^2qQ}{4} \sum_{k=-2}^{2} \sum_{q=-2}^{2} \sum_{n=-2}^{2} A_{2,p} D_{pq}^2(\Omega) < D_{qk}^2(\delta\Omega) > < D_{kn}^2(\Omega') >< D_{n0}^2(\Omega'') > \quad (18)$$

The distribution of instantaneous directors about the average director orientation is taken to be cylindrically symmetric. Furthermore, the fluctuations of γ are taken to be independent of fluctuations in α and β. Using the relationship,

$$\int_\gamma \exp(ik\gamma) d\gamma = \delta_{k,0},$$

it is concluded that $D_{pq}^2(\Omega)$ will be non-zero only for $q = 0$.

On average, chain segments are also distributed about the instantaneous director with cylindrical symmetry, and fluctuations about $\delta\gamma$ are not correlated

with fluctuations in $\delta\beta$ and $\delta\gamma$. Again, only rotation matrix elements, $D^2_{qk}(\delta\Omega)$, with k=0 will be non-zero.

Finally, using similar approximations for the motions of the C-D bond vector about the chain segment orientation, it is concluded that only rotation elements with n=0 will be non-zero. These approximations lead to the simplest form of the Hamiltonian:

$$< H_p^Q >= \frac{e^2qQ}{4} A_{2,p} D^2_{p0}(\Omega) < D^2_{00}(\delta\Omega) >< D^2_{00}(\Omega') >< D^2_{00}(\Omega'') > \qquad (19)$$

Recall that the instantaneous director deviates only slightly from the average director orientation. In this case, the following approximations are made:

$$\cos(\delta\beta) \approx 1 \qquad (20a)$$

$$\sin(\delta\beta) \approx \delta\beta \qquad (20b)$$

This leads to the following relationship:

$$D^2_{00}(\delta\Omega) = \frac{1}{2}(3\cos^2(\delta\beta) - 1) = 1 \qquad (21)$$

By substituting Eqn. (21) into Eqn. (18), the final expression for the time averaged quadrupolar Hamiltonian becomes:

$$< H_p^Q >= \frac{e^2qQ}{4} A_{2,p} D^2_{p0}(\Omega) < D^2_{00}(\Omega') >< D^2_{00}(\Omega'') > \qquad (22)$$

IV. *Simulation of Deuterium Spectra in the Presence of Anisotropic Motion*

For the purposes of spectral simulation, a first order correction to the Hamiltonian is sufficient. In this case, $I_{\pm}$ terms may be neglected, and only terms with p=0 need be considered. This leads to:

$$< H_0^Q >= \frac{e^2qQ}{4} A_{2,0} D^2_{00}(\Omega) < D^2_{00}(\Omega') >< D^2_{00}(\Omega'') > \tag{23}$$

This may be rewritten as:

$$< H_0^Q >= \frac{e^2qQ}{4} S_{CD}[\frac{1}{2}(3cos^2\beta - 1)][3I_z^2 - 2]] \tag{24}$$

where:

$$S_{CD} = S_{\beta'} S_{\beta''} \tag{25a}$$

$$S_{\beta'} =< \frac{1}{2}(3cos^2\beta' - 1) > \tag{25b}$$

$$S_{\beta''} =< \frac{1}{2}(3cos^2\beta'' - 1) > \tag{25c}$$

S_{CD}, $S_{\beta'}$, and $S_{\beta''}$ are known as order parameters.

The resonant frequencies for the transitions m=0 $\rightarrow \pm 1$, which are observed in the NMR spectrum are given by:

$$\nu = \nu_0 \pm \frac{3}{4\hbar} e^2qQ S_{CD}[\frac{1}{2}(3cos^2\beta - 1)] \tag{26}$$

where ν_0 is the energy splitting due to the Zeeman interaction. The above expression illustrates the dependence of the resonant frequency on the orientation of the average director with respect to the magnetic field. Two transitions should be observed for each orientation. These transitions correspond to changes in nuclear spin with Δm=$\pm$1.

In randomly oriented multilayers, the number of equivalent orientations of the average director with respect to the magnetic field for a given angle β is proportional to $\sin(\beta)$. In the NMR spectrum, therefore, the intensity of a transition corresponding to an orientation of β with respect to the magnetic field is scaled by $\sin\beta$. A ^{2}H-NMR spectrum simulated using the above relationship for intensity is shown in Figure 3. An ensemble of randomly oriented lipid bilayers has been assumed in this simulation. Note that $\sin\beta$ is maximum at $\beta = 90°$. The singularities in the spectrum shown in Figure 3, therefore, arise from regions of bilayer whose director is oriented perpendicular to the magnetic field.

V. *The Order Parameter in Lipid Bilayers*

S_{CD} may be calculated from the frequency separation of the spectral singularities ($\Delta\nu_Q$) through the relationship:

$$S_{CD} = \frac{4}{3}\frac{\Delta\nu_Q \hbar}{e^2 qQ} \tag{27}$$

where:

$$\frac{e^2 qQ}{\hbar} = 170 \;\; KHz$$

is the static quadrupolar coupling constant.[2]

S_{CD} may change when a different lipid or protein is added to a pure lipid bilayer. This effect is frequently attributed to a change in the extent of motional averaging about the director axis. Eqn. (25) highlights the dependence of the order parameter not only on motional averaging, but also on the average values of β' and β''. Simulations of ^{2}H-NMR spectra for lipid bilayers show S_{CD} to be very sensitive to the average orientation of the C-D bond, but relatively insensitive

Figure 3: A simulated ^{2}H-NMR powder pattern with axial symmetry.

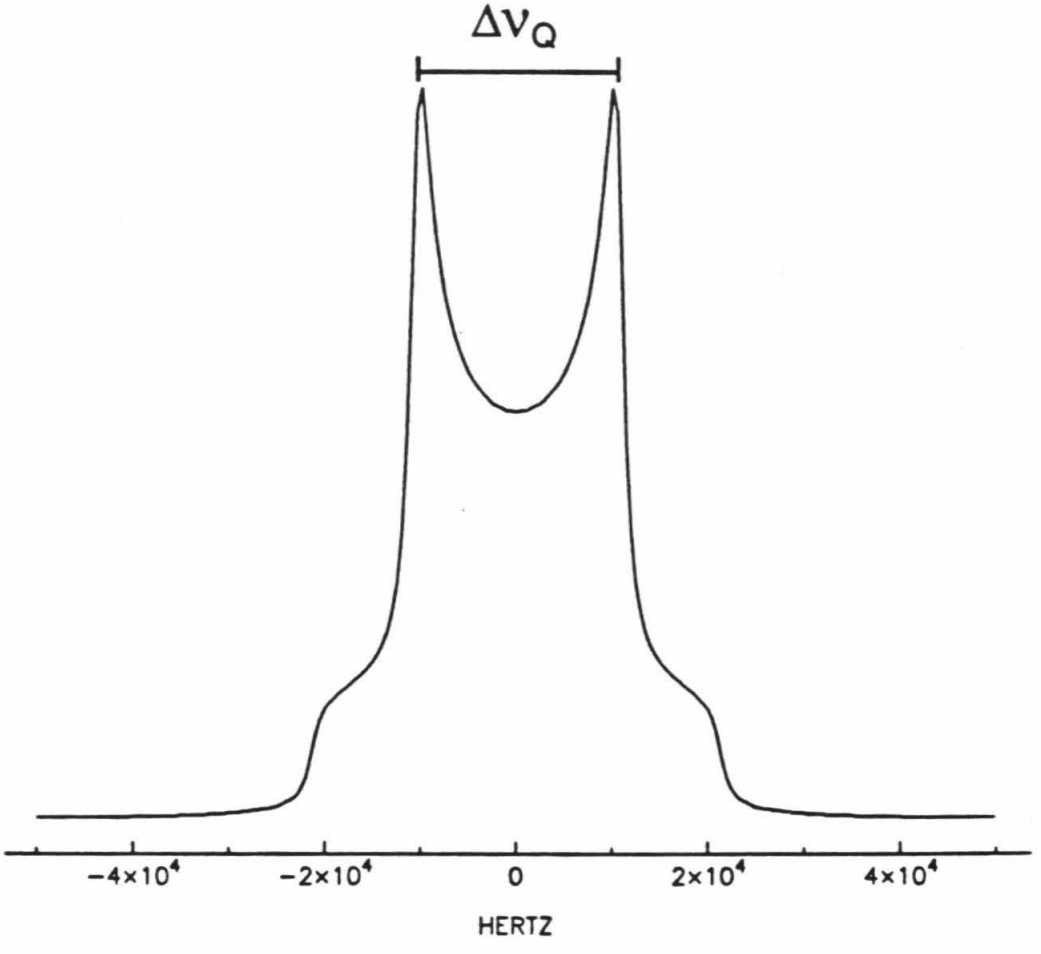
$\Delta\nu_Q$
-4×10^4
-2×10^4
0
2×10^4
4×10^4
HERTZ

to motional averaging. Thus, any changes in order parameter that are observed upon addition of another lipid or protein to a lipid bilayer are probably due to changes in chain orientation. This hypothesis may be tested by measuring ^{2}H-NMR relaxation rates in addition to the order parameter. The rate of motion in a system may be extracted from relaxation rate measurements. Such experiments, therefore, allow one to determine the relative contributions of orientation and motional averaging to S_{CD}.

There are two ways in which addition of an unlike lipid or protein to a pure lipid bilayer might affect the orientation of the C-D bond on a hydrocarbon chain. First of all, bilayer-forming lipid molecules, such as DML, are cylindrically-shaped. The addition of a cylindrically shaped lipid or protein to a DML bilayer will not perturb the orientation of the lipid chains significantly. Many lipids and most proteins, however, are not cylindrically shaped. When these are added to a DML bilayer, the DML molecules must accommodate the irregular shape. For example, a bulky amino acid side chain of the added protein may protrude into the lipid hydrocarbon region. To accommodate this side chain, the closest chain segments of the DML hydrocarbon chains must shift out of their usual alignment with respect to the instantaneous director orientation. This type of perturbation would only be expected to alter the S_{CD} of deuterons at chain positions in the vicinity of the shape irregularity of the added lipid or protein.

Secondly, both lipid bilayers and membrane-bound proteins are characterized by hydrophobic and hydrophilic regions. The lipid hydrocarbon chains constitute the hydrophobic portion of the bilayer. The surface of the portion of the membrane-bound protein that is meant to be immersed in the lipid hydrocarbon chains is also hydrophobic. When a protein is reconstituted with a bilayer-forming

lipid, a mismatch in the thicknesses of their hydrophobic regions may occur. The lipid may compensate for this mismatch in the following ways.[9,10] If the protein's hydrophobic region is thicker than that of the bilayer, the lipid chains may straighten. This corresponds to an increase in the population of trans conformers along the lipid chain. If the protein hydrophobic region is thinner than that of the bilayer, the lipid chains may tilt or the population of gauche conformers along the chain may increase. Adjustments that compensate for hydrophobic mismatch affect all positions along the hydrocarbon chain equally.

An added lipid or protein may perturb a lipid bilayer through shape irregularity and/or hydrophobic mismatch. The former alters S_{CD} in a particular region of the lipid chain, while the latter alters S_{CD} at each position along the chain. By measuring the change in S_{CD} at several positions on the lipid chain, perturbations of the lipid bilayer through hydrophobic mismatch and shape irregularity may be distinguished.

In conclusion, S_{CD} reflects the motion and orientational order of the C-D bond with respect to the director. In conjunction with relaxation rate measurements, S_{CD} may be used to determine the type of perturbation caused by addition of a different lipid or protein to a lipid bilayer. Upon addition of other lipids or proteins, it is hypothesized that changes in the S_{CD} of a deuteron in the hydrocarbon region of a lipid bilayer are due mainly to changes in average orientation with respect to the director. Both hydrophobic mismatch and shape irregularity are suggested as possible causes of changes in the average orientation of the C-D bond.

VI. *The Deuterium Relaxation Expressions*

Spin interactions such as chemical shift anisotropy, dipole-dipole interactions, and quadrupole interactions may all contribute to NMR relaxation rates. For

relaxation of the ^{2}H nucleus, which has spin I=1, the quadrupolar interaction is dominant. Thus, one need only consider quadrupolar interactions in the ^{2}H relaxation rate expressions. This work is concerned primarily with the spin-lattice (T_1^{-1}), rotating frame ($T_{1\rho}^{-1}$), and spin-spin (T_2^{-1}) relaxation rates. The well-known relaxation expressions for these rates are given below:[4]

$$\frac{1}{T_1} = \frac{3}{16}(\frac{e^2qQ}{\hbar})^2[J_1(\omega_D) + 4J_2(2\omega_D)] \tag{28a}$$

$$\frac{1}{T_{1\rho}} = \frac{3}{32}(\frac{e^2qQ}{\hbar})^2[3J_0(2\omega'_D) + 5J_1(\omega_D) + 2J_2(2\omega_D)] \tag{28b}$$

$$\frac{1}{T_2} = \frac{3}{32}(\frac{e^2qQ}{\hbar})^2[3J_0(0) + 5J_1(\omega_D) + 2J_2(2\omega_D)] \tag{28c}$$

where the spectral densities, $J_p(\omega)$ are given by:[12]

$$J_p(\omega) = \int_{-\infty}^{\infty} G_p(\tau)e^{-i\omega\tau}d\tau \tag{29}$$

and $G_p(\tau)$ is a correlation function which measures the decay of correlation between the state of a particle at time t=0 and t=τ. ω_D represents the Larmor frequency of the ^{2}H nucleus. In the $T_{1\rho}$ experiment, $2\omega'_D$ depends on the strength of the field used to lock the ^{2}H spins in the transverse plane.

Mathematically the correlation function at a time τ is expressed as:

$$G_p(\tau) = < H_p(0)H_p(\tau)^* > \tag{30a}$$

H_p is the Hamiltonian being modulated by motion. The subscript p corresponds to the order of the Hamiltonian. For example, p=0 will involve I and I_z terms in the Hamiltonian, while p=1 and p=2 will involve $I_\pm$ and $(I_\pm)^2$ terms, respectively. For

quadrupolar and chemical shift interactions in bilayers, the value of H_p depends only on the orientation of the lipid hydrocarbon C-D bond with respect to the external magnetic field. If one assumes that the orientational fluctuations are Markovian and described by a single correlation time, a single exponential decay of correlation is observed. Accordingly:

$$G_p(\tau) = < H_p(0)H_p(0)\exp(\frac{-\tau}{\tau_c}) > \qquad (30b)$$

where τ_c is the correlation time for the decay.

In Eqn. (28), it is shown that T_1^{-1} involves spectral densities at the resonant frequency of ^2H and twice the resonant frequency. For experiments conducted in an external magnetic field of strength 11.7 Tesla, the resonant frequency is 76 MHz. $T_{1\rho}^{-1}$ and T_2^{-1} involve spectral densities at $2\omega'_D$ and zero frequency, respectively. In the experiments to be described in the following chapters, $2\omega'_D$ is approximately equal to 56 KHz. $T_{1\rho}^{-1}$ and T_2^{-1}, therefore, are sensitive to much slower motions than T_1^{-1}.

Figure 4 shows a plot of the spectral density as a function of frequency.[12] The profile of the spectral density function is flat for $\omega \ll \tau_c^{-1}$. If $\tau_c^{-1} \gg 152$ MHz, $J_0(0)=J_1(76\text{ MHz})=J_2(152\text{ MHz})$. In this instance, the magnitudes of T_1^{-1}, $T_{1\rho}^{-1}$, and T_2^{-1} will be equal, and the motion is considered to be in the extreme narrowing regime. When $\tau_c^{-1} \ll 76$ MHz, $T_2^{-1} \gg T_1^{-1}$, and the motion is in the slow motional regime.

VII. *The Correlation Function for Lipid Bilayers*

In order to evaluate correlation functions, the form of the quadrupolar Hamiltonian, which is used for calculating spectra (Eqn. 23) is not sufficiently exact.

Figure 4: The dependence of the spectral density on frequency for a single motional correlation time, τ_c.[12]

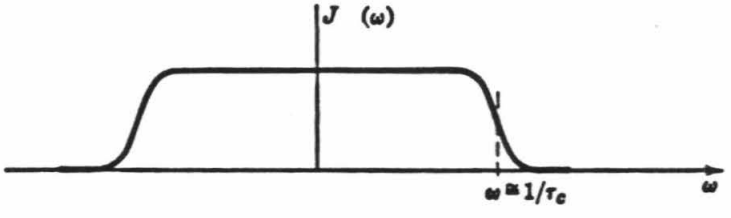
J (ω)
ω ≅ 1/τc
ω

This expression implies that H_1^Q and H_2^Q are zero and, hence, that $J_1(\omega_D) = J_2(2\omega_D) = 0$. Consequently, T_1 must be infinite. This is clearly not the case. Instead, the more exact Hamiltonian in Eqn. (17) is used to yield the following correlation function.

$$G_p(\tau) = (\frac{3}{4}e^2qQ)^2 \sum_{q=-2}^{2}\sum_{q'=-2}^{2}\sum_{k=-2}^{2}\sum_{k'=-2}^{2}\sum_{n=-2}^{2}\sum_{n'=-2}^{2} A_{2,p}^2$$
$$\times < D_{pq}^2(\Omega)_{t=0} D_{qk}^2(\delta\Omega)_{t=0} D_{kn}^2(\Omega')_{t=0} D_{n0}^2(\Omega'')_{t=0}$$
$$\times D_{p'q'}^2(\Omega)_{t=\tau}^* D_{q'k'}^2(\delta\Omega)_{t=\tau}^* D_{k'n'}^2(\Omega')_{t=\tau}^* D_{n'0}^2(\Omega'')_{t=\tau}^* > \qquad (31)$$

VIII. *The Correlation Function in the Presence of Anisotropic Motion*

Several approximations may be made based on motions of the four axis systems. This treatment is a modification of that used by Doane to treat the motions of liquid crystals.[9] More recently, the same treatment has been applied to lipid bilayers by Pace et al.[8] First of all, because of the very different time scales on which fluctuations of Ω, $\delta\Omega$, Ω', and Ω'' occur, these motions may be considered uncorrelated. The correlation functions involving each collection of Euler angles, therefore, may be treated separately.

Secondly, the orientation of the average director with respect to the magnetic field direction is taken to be constant on the experimental time scale. Thus, the correlation function involving $D_{pq}^2(\Omega)$ is merely equal to the square of the rotation matrix element. This leads to the following form of the total correlation function:

$$G_p(\tau) = (\frac{3}{4}e^2qQ)^2 \sum_{q=-2}^{2}\sum_{k=-2}^{2}\sum_{k'=-2}^{2}\sum_{n=-2}^{2}\sum_{n'=-2}^{2} A_{2,p}^2 [D_{pq}^2(\Omega)]^2$$
$$\times < D_{qk}^2(\delta\Omega)_{t=0} D_{q'k'}^2(\delta\Omega)_{t=\tau}^* >< D_{kn}^2(\Omega')_{t=0} D_{k'n'}^2(\Omega')_{t=\tau}^* >$$

$$\times < D^2_{n0}(\Omega'')_{t=0} D^2_{n'0}(\Omega'')^*_{t=\tau} > \qquad (32)$$

Furthermore, the correlation functions involving $\delta\gamma$ and γ' may be removed from those containing $D^2_{qk}(\delta\gamma)$ and $D^2_{kn}(\gamma')$, respectively. Fluctuations of $\delta\gamma$ should be much faster than those of $\delta\alpha$ and $\delta\beta$. Changes in $\delta\alpha$ require motion of the average director, which is time independent. Motions of $\delta\beta$ involve cooperative fluctuations of the instantaneous director, which are also slow. These differences in rates of motion allow the correlation function involving $\delta\gamma$ to be considered separately from that involving $\delta\alpha$ and $\delta\beta$. Similarly, motions of γ', which involve rotation of the C-D bond about the chain axis, are much faster than any other motions in the lipid bilayer, and the correlation function involving γ' may be separated from that involving α' and β'.

The motions of $\delta\gamma$ and γ' may be approximated as one dimensional circular diffusion. In this case the following relationship may be applied to correlation functions containing $\delta\gamma$ and γ':

$$< \exp(-ir\gamma(0)) \exp(-is\gamma(t)) >= \delta_{rs} \exp(\frac{-t}{\tau_m}) \qquad (33)$$

where τ_m is the correlation time for the motion. In the following treatment, τ_c and τ_b will represent the correlation times for $\delta\gamma$ and γ' diffusion, respectively.

In order to apply Eqn. (33) to $G_p(\tau)$, it is most convenient to separate $G_p(\tau)$ into terms that contain $\delta\gamma$ and γ' and terms that do not. This yields four terms with the following conditions: (1) $(k, k' \neq 0), (n, n' \neq 0)$; (2)$(k, k' \neq 0), (n, n' = 0)$; (3)$(k, k' = 0), (n, n' \neq 0)$; and (4) $(k, k' = 0), (n, n' = 0)$. For simplicity, the following substitution is made:

$$F_{rs}(\Theta) = F_{rs}(\theta, \phi, \psi) = \exp(-ir\theta) d^2_{rs}(\phi) \qquad (34)$$

After a consideration of the motional properties of bilayers mentioned above, the form of the total correlation function becomes:

$$G_p(\tau) = (\frac{3}{4}e^2qQ)^2 A_{2,p}^2 [\sum_{q=-2}^{2} \sum_{k\neq 0} \sum_{n\neq 0} [D_{pq}^2(\Omega)]^2$$

$$\times < F_{qk}(\delta\Omega)_{t=0} F_{qk}(\delta\Omega)^*_{t=\tau} > \exp(\frac{-t}{\tau_c})$$

$$\times < F_{kn}(\Omega')_{t=0} F_{kn}(\Omega')^*_{t=\tau} > \exp(\frac{-t}{\tau_b}) < D_{n0}^2(\Omega'')_{t=0} D_{n0}^2(\Omega'')^*_{t=\tau} >$$

$$+ \sum_{q=-2}^{2} \sum_{k\neq 0} [D_{pq}^2(\Omega)]^2 < F_{qk}(\delta\Omega)_{t=0} F_{qk}(\delta\Omega)^*_{t=\tau} > \exp(\frac{-t}{\tau_c})$$

$$\times < D_{k0}^2(\Omega')_{t=0} D_{k0}^2(\Omega')^*_{t=\tau} >< D_{00}^2(\Omega'')_{t=0} D_{00}^2(\Omega'')^*_{t=\tau} >$$

$$+ \sum_{q=-2}^{2} \sum_{n\neq 0} [D_{pq}^2(\Omega)]^2 < D_{q0}^2(\delta\Omega)_{t=0} D_{q0}^2(\delta\Omega)^*_{t=\tau} >$$

$$\times < F_{0n}(\Omega')_{t=0} F_{0n}(\Omega')^*_{t=\tau} > \exp(\frac{-t}{\tau_b}) < D_{n0}^2(\Omega'')_{t=0} D_{n0}^2(\Omega'')^*_{t=\tau} >$$

$$+ \sum_{q=-2}^{2} [D_{pq}^2(\Omega)]^2 < D_{q0}^2(\delta\Omega)_{t=0} D_{q0}^2(\delta\Omega)^*_{t=\tau} >< D_{00}^2(\Omega')_{t=0} D_{00}^2(\Omega')^*_{t=\tau} >$$

$$\times < D_{00}^2(\Omega'')_{t=0} D_{00}^2(\Omega'')^*_{t=\tau} >] \qquad (35)$$

If β' and β'' are taken to be constant on the NMR time scale, the following substitutions are possible:

$$< D_{00}^2(\Omega')_{t=0} D_{00}^2(\Omega')_{t=\tau} >= S_{\beta'}^2 \qquad (36a)$$

$$< D_{00}^2(\Omega'')_{t=0} D_{00}^2(\Omega'')_{t=\tau} >= S_{\beta''}^2 \qquad (36b)$$

The total correlation function becomes:

$$G_p(\tau) = (\frac{3}{4}e^2qQ)^2 A_{2,p}^2 [\sum_{q=-2}^{2} \sum_{k\neq 0} \sum_{n\neq 0} [D_{pq}^2(\Omega)]^2$$

$$\times < F_{qk}(\delta\Omega)_{t=0} F_{qk}(\delta\Omega)^*_{t=\tau} > \exp(\frac{-t}{\tau_c}) < F_{kn}(\Omega')_{t=0} F_{kn}(\Omega')^*_{t=\tau} > \exp(\frac{-t}{\tau_b})$$

$$\times < D^2_{n0}(\Omega'')_{t=0} D^2_{n0}(\Omega'')^*_{t=\tau} >$$

$$+ \sum_{q=-2}^{2} \sum_{k\neq 0} [D_{pq}^2(\Omega)]^2 < F_{qk}(\delta\Omega)_{t=0} F_{qk}(\delta\Omega)^*_{t=\tau} > \exp(\frac{-t}{\tau_c})$$

$$\times < D^2_{k0}(\Omega')_{t=0} D^2_{k0}(\Omega')^*_{t=\tau} > S^2_{\beta''})$$

$$+ \sum_{q=-2}^{2} \sum_{n\neq 0} [D_{pq}^2(\Omega)]^2 < D^2_{q0}(\delta\Omega)_{t=0} D^2_{q0}(\delta\Omega)^*_{t=\tau} >$$

$$\times < F_{0n}(\Omega')_{t=0} F_{0n}(\Omega')^*_{t=\tau} > \exp(\frac{-t}{\tau_b}) < D^2_{n0}(\Omega'')_{t=0} D^2_{n0}(\Omega'')^*_{t=\tau} >$$

$$+ \sum_{q=-2}^{2} [D_{pq}^2(\Omega)]^2 < D^2_{q0}(\delta\Omega)_{t=0} D^2_{q0}(\delta\Omega)^*_{t=\tau} > S^2_{CD}] \qquad (37)$$

As mentioned previously, motions of $\delta\gamma$ and γ' are much faster than any other motions in the lipid bilayer system. The exponential decays with rates τ_c^{-1} and τ_b^{-1}, therefore, will have decayed to very small values long before significant changes in other Euler angles have occurred. Consequently, in the first three terms of Eqn. (37), the time dependence of other angles may be neglected.

Furthermore, the last term in Eqn. (37) may be simplified using the approximations in Eqn. (20). Only terms that are linear in $\delta\beta$ need be retained. This leads to the restriction that $q = \pm 1$. The final form of the total correlation function becomes:

$$G_p(\tau) = (\frac{3}{4}e^2qQ)^2 A_{2,p}^2 [\sum_{q=-2}^{2} \sum_{k\neq 0} \sum_{n\neq 0} [D_{pq}^2(\Omega)]^2$$

$$\times[F_{qk}(\delta\Omega)]^2[F_{kn}(\Omega')]^2[D^2_{n0}(\Omega'')]^2\exp(\frac{-t}{\tau_c})\exp(\frac{-t}{\tau_b})$$

$$+\sum_{q=-2}^{2}\sum_{k\neq 0}[D^2_{pq}(\Omega)]^2[F_{qk}(\delta\Omega)]^2[D^2_{k0}(\Omega')]^2 S^2_{\beta''})\exp(\frac{-t}{\tau_c})$$

$$+\sum_{q=-2}^{2}\sum_{n\neq 0}[D^2_{pq}(\Omega)]^2[D^2_{q0}(\delta\Omega)]^2[F_{0n}(\Omega')]^2[D^2_{n0}(\Omega'')]^2\exp(\frac{-t}{\tau_b})$$

$$+\sum_{q=\pm 1}[D^2_{pq}(\Omega)]^2 < D^2_{q0}(\delta\Omega)_{t=0}D^2_{q0}(\delta\Omega)^*_{t=\tau} > S^2_{CD}] \qquad (38)$$

where

$$< D^2_{\pm 1}(\delta\gamma)_{t=0}D^2_{\pm 1}(\delta\gamma)^*_{t=\tau} >= \frac{2}{3} < \delta\beta(0)\delta\beta(\tau) > \qquad (39)$$

The Fourier transform of this correlation function is:

$$J_p(\omega) = (\frac{3}{4}e^2qQ)^2A^2_{2,p}[\sum_{q=-2}^{2}\sum_{k\neq 0}\sum_{n\neq 0}[D^2_{pq}(\Omega)]^2$$

$$\times[F_{qk}(\delta\Omega)]^2[F_{kn}(\Omega')]^2[D^2_{n0}(\Omega'')]^2\frac{\tau_b\tau_c}{\tau_c+\tau_b}$$

$$+\sum_{q=-2}^{2}\sum_{k\neq 0}[D^2_{pq}(\Omega)]^2[F_{qk}(\delta\Omega)]^2[D^2_{k0}(\Omega')]^2 S^2_{\beta''})\tau_c$$

$$+\sum_{q=-2}^{2}\sum_{n\neq 0}[D^2_{pq}(\Omega)]^2[D^2_{q0}(\delta\Omega)]^2[F_{0n}(\Omega')]^2[D^2_{n0}(\Omega'')]^2\tau_b$$

$$+\sum_{q=\pm 1}\frac{2}{3}[D^2_{pq}(\Omega)]^2 S^2_{CD}\int_{-\infty}^{+\infty} < \delta\beta(0)\delta\beta(\tau) > \exp(-i\omega\tau)d\tau] \qquad (40)$$

The spectral density, therefore, consists of two types of terms. The first three terms are dependent on very rapid motions of a single molecule. Because $J_1(\omega)$ and $J_2(\omega)$ are sensitive to the faster motions, these spectral densities should be dominated by the first three terms of Eqn. (40). Consequently, T_1^{-1} relaxation will be due primarily to uncorrelated lipid motions.

The last term in the spectral density expression reflects the slow, collective motions of the instantaneous directors. Since $J_0(0)$ and $J_0(2\omega')$ are most sensitive to slow motions, these spectral densities should be dominated by the last term in Eqn. (40). The expression for $J_0(\omega)$ is:

$$J_0(\omega) = (\frac{3}{4}e^2qQ)^2A^2_{2,0}[\sum_{q=-2}^{2}\sum_{k\neq 0}\sum_{n\neq 0}[D^2_{0q}(\Omega)]^2$$

$$\times[F_{qk}(\delta\Omega)]^2[F_{kn}(\Omega')]^2[D^2_{n0}(\Omega'')]^2\frac{\tau_b\tau_c}{\tau_c+\tau_b}$$

$$+\sum_{q=-2}^{2}\sum_{k\neq 0}[D^2_{0q}(\Omega)]^2[F_{qk}(\delta\Omega)]^2[D^2_{k0}(\Omega')]^2S^2_{\beta''}\tau_c$$

$$+\sum_{q=-1,1}\sum_{n\neq 0}[D^2_{0q}(\Omega)]^2[D^2_{0q}(\delta\Omega)]^2[F_{0n}(\Omega')]^2[D^2_{n0}(\Omega'')]^2\tau_b$$

$$+\sum_{q=-1,1}\frac{2}{3}[D^2_{0q}(\Omega)]^2S^2_{CD}\int_{-\infty}^{+\infty}<\delta\beta(0)\delta\beta(\tau)>\exp(i\omega\tau)d\tau] \qquad (41a)$$

where

$$[D^2_{0\pm1}(\Omega)^2] = \frac{1}{12}\sin^2(2\beta) \qquad (41b)$$

This work is concerned with a characterization of cooperative lipid motions, and the changes in these collective motions upon addition of other lipids or peptides to a lipid bilayer. Because $J_0(0)$ and $J_0(2\omega')$ are the dominant terms in the expressions for T_2^{-1} and $T_{1\rho}^{-1}$, respectively, these relaxation rates should be most sensitive to cooperative motions. For this reason, $T_{1\rho}^{-1}$ and T_2^{-1} measurements have been chosen as the method by which cooperative motions will be studied.

Eqn. (41a) predicts that a plot of $J_0(\omega)$ or, equivalently, $T_{1\rho}^{-1}$ and T_2^{-1} against S^2_{CD} should yield a straight line whose slope should be proportional to the rate of director fluctuation. The y-intercept of this line should reflect uncorrelated

motions. In chapter 3, perdeuterated DML bilayers, selectively deuterated lipid mixtures, and mixtures of GA′ with selectively deuterated DML are studied. A different S_{CD} is associated with the powder pattern of each deuteron along the hydrocarbon chain, the powder pattern of deuterons in each lipid mixture, and the powder pattern of deuterons in each GA/DML recombinant. In order to determine if the rates of chain fluctuations in these systems are identical, the T_2^{-1} of each system is plotted against S_{CD}^2. If the points fall on a straight line, one may conclude that chain motions of the lipid systems are similar.

Eqn. (40b) also predicts that T_2^{-1} will vary with the angle made by the average director to the external magnetic field. In particular, T_2^{-1} should be minimum at the 90° singularities of the powder pattern.

In conclusion, a correlation function has been derived whose time dependence is due both to uncorrelated chain motions and to fluctuations of the chains about the mean director orientation. In the following chapters, the linear dependence of T_2^{-1} on S_{CD}^2 for deuterons at different positions in a perdeuterated lipid bilayer and the angular dependence of T_2^{-1} in a selectively deuterated lipid bilayer will be used to prove the existence of cooperative director fluctuations in lipid bilayers. Subsequently, an expression for the time dependence of these fluctuations will be derived and used to describe the perturbation of a lipid system by incorporation of dissimilar lipids or proteins.

The Chemical Shift Hamiltonian

I. *The Chemical Shift Hamiltonian in High Magnetic Field*

Because electrons are charged, their motion produces a local magnetic field. In the presence of an external magnetic field, electronic motion will create a magnetic field which reinforces or opposes the external one. In an atom, the field generated by electronic motion, therefore, will either de-shield or shield the nucleus from the external magnetic field. Electronic de-shielding and shielding alter the resonant frequency of the nucleus and, thus, produce a chemical shift. If the electron cloud is asymmetric, the chemical shift will depend on the orientation of the molecule with respect to the external magnetic field. This is known as chemical shift anisotropy (CSA). An asymmetric electron cloud may result from polarization by nearby nuclei or an asymmetric distribution of electrons in orbitals such as *p* and *d*. In the absence of rapid motional averaging, CSA results in a powder type NMR spectrum.

In the presence of high power proton decoupling, the chemical shift interaction is the dominant perturbation on the Zeeman energy levels of the ^{31}P nucleus. Because of anisotropic motion in lipid bilayers, ^{31}P-NMR of a phospholipid head group yields a powder pattern. The phase of a lipid system is easily determined by the width and shape of this powder pattern.

The chemical shift Hamiltonian may be written as:

$$H^{cs} = \gamma_I \hat{\mathrm{I}} \cdot \hat{\sigma} \cdot B_0 \tag{42}$$

where γ_I is the magnetogyric ratio of the nucleus of interest, $\hat{\sigma}$ is the chemical shift tensor, and B_0 is the magnetic field vector. As with the electric field gradient, the chemical shift tensor may be expressed in a coordinate system in which it is diagonal. This system has axes represented by (1,2,3) with diagonal elements σ_{11}, σ_{22}, and σ_{33}. Writing H^{cs} as a product of space and spin spherical tensors, the

following expression is obtained:[1]

$$H^{cs} = \gamma_I B_0 \sum_{l=0}^{2} \sum_{m=-2}^{2} \sigma_{l,m} A'_{l,-m} \tag{43}$$

where the non-zero space components are:

$$\sigma_{00} = -(\frac{1}{\sqrt{3}})(\sigma_{11} + \sigma_{22} + \sigma_{33}) = -\frac{1}{\sqrt{3}} Tr(\hat{\sigma}) \tag{44a}$$

$$\sigma_{20} = \sqrt{\frac{3}{2}}(\sigma_{33} - \frac{1}{3} Tr(\hat{\sigma})) \tag{44b}$$

and the non-zero spin components are:

$$A_{0,0} = \frac{-1}{\sqrt{3}} I_z \tag{45a}$$

$$A_{2,0} = \sqrt{\frac{2}{3}} I_z \tag{45b}$$

The chemical shift tensor is not traceless. In a system undergoing isotropic motion, therefore, the average chemical shift Hamiltonian will have a non-zero value equal to the trace of the chemical shift tensor. Because anisotropic motions are of great interest in lipid bilayers, the isotropic contribution to the chemical shift interaction is eliminated by invoking a laboratory frame rotating at the isotropic shift frequency. The anisotropic component of the chemical shift Hamiltonian is:

$$H^{cs'} = \gamma_I B_0 \sigma_{zz} I_z \tag{46}$$

where:

$$\sigma_{zz} = \sum_{m=-2}^{2} \sigma_{2,m} D^2_{m,0} \tag{47}$$

II. *The CSA Hamiltonian in Bilayer Phase*

The treatment of the chemical shift Hamiltonian in bilayers is very similar to that of the quadrupolar interaction in bilayers. Although the phosphorus chemical shift tensor is not axially symmetric, rapid averaging about the instantaneous director orientation results in an axially symmetric spectrum. By making stepwise transformations from the molecular interaction frame into the laboratory frame, the following Hamiltonian results:

$$< H_0^{cs'} >_{bilayer} = \gamma_I B_0 D_{00}^2(\Omega) < D_{00}^2(\Omega') >< D_{00}^2(\Omega'') > \sigma_{33} I_z \qquad (48a)$$

or

$$< H_0^{cs'} >_{bilayer} = \gamma_I B_0 S_{\beta'} S_{\beta''} \frac{1}{2}(3cos^2\beta - 1)\sigma_{33} I_z \qquad (48b)$$

For lipid multilayers, this Hamiltonian again produces a powder pattern. Because ^{31}P is a spin I=1/2 nucleus, only the nuclear transition between I_z=-1/2 and I_z=+1/2 is possible. The ^{31}P-NMR spectrum, therefore, is similar to half of a ^{2}H-NMR spectrum. The splitting between the low and high field singularities is designated $\Delta\sigma$.

III. *The CSA Hamiltonian in Hexagonal Phase*

For lipids in hexagonal phase (H_{II}), an additional axis of averaging exists. This axis is illustrated in Figure 5. The lipids diffuse rapidly about the symmetry axis of the cylindrical structures. This may be treated simply by introducing an additional rotation from the coordinate sytem of the average director orientation into the coordinate system of the cylinder axis. Ω''' will represent the Euler angles

Figure 5: The additional axis of averaging available to lipids in H_{II} phase.[15]

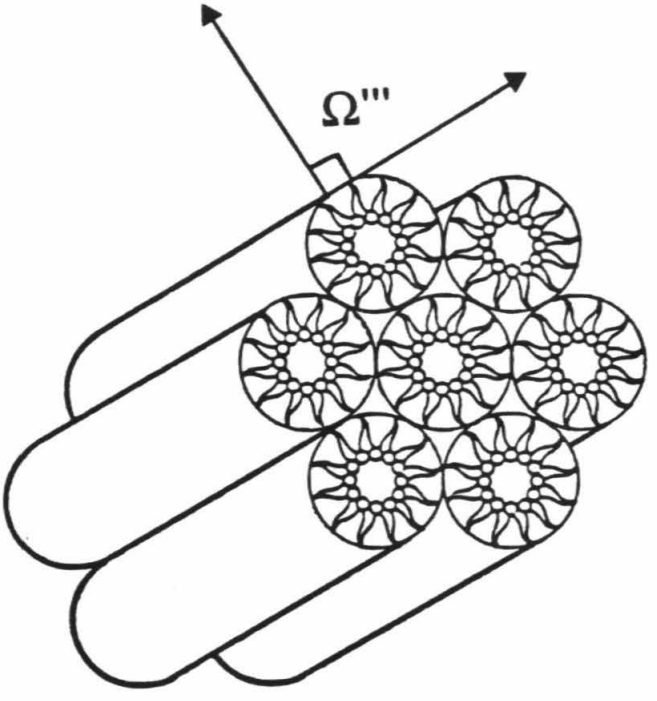
Ω'''

associated with this rotation. Since there is obviously cylindrical symmetry about this axis, only $D^2_{00}(\Omega''')$ need be considered. This leads to the following expression:

$$< H_0^{cs'} >_{HII} = \gamma_I B_0 D^2_{00}(\Omega) < D^2_{00}(\Omega') > D^2_{00}(\Omega''') < D^2_{00}(\Omega'') > \sigma_{33} I_z \qquad (49)$$

Furthermore, on the time scale of interest, the angle between the average chain orientation and the cylinder axis remains constant at 90°. As a result, $D^2_{00}(\Omega''') = -\frac{1}{2}$. This leads to:

$$< H_0^{cs'} >_{HII} = \gamma_I B_0 - \frac{1}{2} S_{\beta'} S_{\beta''} \frac{1}{2}(3cos^2\beta - 1)\sigma_{33} I_z \qquad (50)$$

and

$$< H_0^{cs'} >_{bilayer} = -\frac{1}{2} < H_0^{cs} >_{HII} \qquad (51)$$

The $\Delta\sigma$ observed for H_{II} phase is half of the bilayer $\Delta\sigma$ and of opposite sign. This characteristic makes H_{II} phase readily distinguishable from bilayer phase. The ^{31}P-NMR spectra for these two cases are compared in Figure 6.

Conclusion

In this chapter, the expressions necessary for simulating ^{2}H-NMR spectra of deuterated lipids in bilayer phase have been presented. In addition, the spectral density relationships necessary to calculate T_1^{-1}, $T_{1\rho}^{-1}$, and T_2^{-1} have been presented. The spectral density expressions are based on a motional model which includes cooperative director fluctuations in the lipid bilayer. This model predicts

Figure 6: A comparison of simulated ^{31}P-NMR spectrum for lipids in the bilayer and H_{II} phases: (a) the bilayer phase spectrum and (b) the H_{II} phase spectrum.

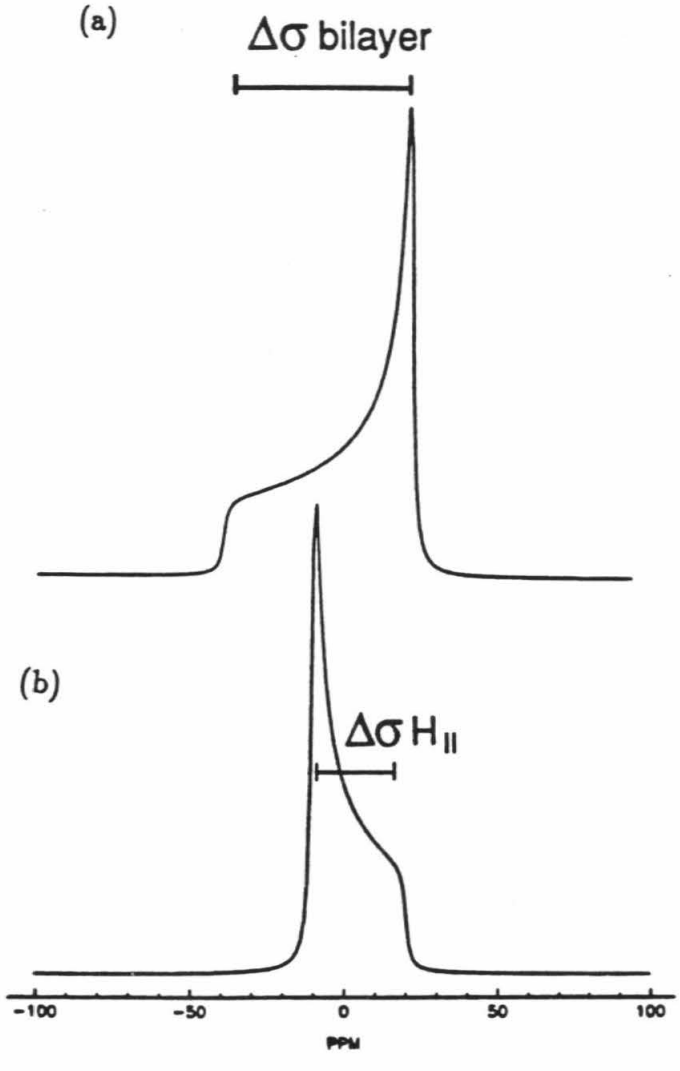
(a)
Δσ bilayer
(b)
Δσ H||
-100
-50
0
50
100
PPM

that T_2^{-1} will be proportional to S_{CD}^2 and that T_2^{-1} will show a $\sin^2(2\beta)$ dependence on molecular orientation with respect to the external magnetic field. In Chapter 3, these two predictions will be tested by experiment. In Chapters 4 and 5, the spectral density relationships will be used in conjunction with a model for cooperative director motion to obtain elastic constants and cooperative lengths for mixed lipid and protein/lipid recombinant bilayers.

Finally, the expressions necessary for calculating ^{31}P-NMR spectra of lipids in both bilayer and hexagonal phase have been derived. It has been shown that:

$$\Delta\sigma^{HII} = -\frac{1}{2}\Delta\sigma^{bilayer}$$

In chapters 5 and 6, this relationship will be used to determine the phase of phospholipids containing Gramicidin A.

References

1. M. Mehring, **High Resolution NMR in Solids**, Springer-Verlag, New York, 1983).
2. J. Seeling, *Quart. Rev. Biophys.*, **10**, 353-418 (1977).
3. M. F. Brown, *J. Mag. Res.*, **35**, 203-215 (1979).
4. R. J. Pace and S. I. Chan, *J. Chem. Phys.*, **76**, 4228-4240 (1982).
5. A. Abragam, **Principles of Nuclear Magnetism**, (Oxford University Press, New York, 1961).
6. M. E. Rose, **Elementary Theory of Angular Momentum**, (Wiley, New York, 1957).
7. S. I. Chan, D. F. Bocian, and N. O. Petersen, *Membrane Spectroscopy*, (Springer-Verlag, New York, 1981).
8. R. J. Pace and S. I. Chan, *J. Chem. Phys.*, **76**, 4217-4227 (1982).
9. J. W. Doane and D. L. Johnson, *Chem. Phys. Lett.*, **6**, 291-295 (1970).
10. L. T. Pearson, S. I. Chan, B. A. Lewis, and D. M. Engelman, *Biophys. J.*, **43**, 167-174 (1983).
11. L. T. Pearson, J. Edelman, and S. I. Chan, *Biophys. J.*, **45**, 863-871 (1984).
12. C. P. Slichter, **Principles of Magnetic Resonance**, (Springer-Verlag, New York, 1980).
13. J. B. Marion, **Classical Dynamics of Particles and Systems**, (Academic Press, New York, 1970).
14. H. Hauser, I. Pascher, R. H. Pearson, and S. Sundell, *Biochim. Biophys. Acta*, **650**, 21-51 (1981).
15. S. M. Gruner, P. R. Cullis, M. J. Hope, and C. P. S. Tilcock, *Ann. Rev. Biophys. Biophys. Chem.*, **14**, 211-238 (1985).

Chapter III

A Characterization of the Spin-Spin Relaxation Rate in Pure Lipid Bilayers, Lipid Mixtures, and Peptide/Lipid Membrane Systems

Introduction

In the preceding chapter, it was shown that low frequency motions dominate T_2^{-1} relaxation in lipid bilayers. These motions are hypothesized to arise from large scale cooperative fluctuations of the lipid bilayer directors. In biological membranes, coupling of these motions to membrane-bound transporters or enzymes may enhance or inhibit the conformational fluctuations necessary to the function of these proteins. The glucose transporter, for instance, has been shown to be sensitive to the motional state of the surrounding lipid.[1]

In this chapter, experimental measurements of T_2^{-1} in pure deuterated lipid bilayers will be shown to be consistent with cooperative director fluctuations. Subsequently, other lipids and proteins will be added to the pure lipid bilayer, and their effect on director fluctuations will be studied.

DML will be used for all studies of pure lipid bilayers. DML is a phospholipid with a choline head group and two fourteen carbon chains. In these experiments, DML will either be deuterated at the 2 position of both chains, the 9 and 10 positions of both chains, or deuterated at every position on both chains. The structure of fully protonated DML is shown in Figure 1.

In a pure DML bilayer, the S_{CD}'s of deuterons at positions 3 to 10 along the lipid hydrocarbon chain are approximately equal. Because of structural constraints, the S_{CD} of each deuteron on a two position carbon is very different. Deuterons towards the end of the hydrocarbon chain experience greater motional freedom.[2] For positions greater than 10, therefore, S_{CD} decreases. In this chapter, the relationship between T_2^{-1} and S_{CD}^2 will be studied for deuterons at several positions along the lipid hydrocarbon chain. As discussed in chapter 2, if director

Figure 1: The structure of DML.

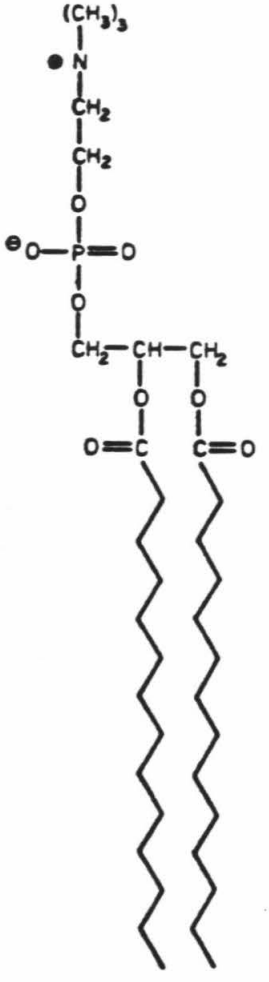

fluctuations are present in the lipid bilayer, a linear relationship is expected.

A multilamellar dispersion of a selectively deuterated lipid has been shown to produce a powder-type spectrum. This arises in randomly oriented bilayer systems because the quadrupolar interaction is dependent on the orientation of the average director with respect to the external magnetic field. The model of director fluctuations predicts a dependence of T_2^{-1} on $\sin^2(2\beta)$, where β is the angle between the average director orientation and the magnetic field. This prediction is tested by measuring T_2^{-1} at several positions in the ^2H NMR spectrum of a selectively deuterated lipid in a multilamellar dispersion.

It has been shown that the inclusion of dissimilar lipids or peptides in a pure lipid bilayer changes the motional properties of the bilayer.[3–6] In order to examine this effect systematically, several mixed lipid and protein/lipid membrane systems will be studied. These include mixtures of DML with distearoyllecithin (DSL), myristic acid (MA), cholesterol, chlorophyll *a* (chl *a*), phytol, and GA′. The structures of the lipids are shown in Figure 2.

DSL has a head group identical to that of DML. The hydrocarbon chains of DSL are four carbons longer than DML. DSC and freeze-fracture electron microscopy experiments show these two lipids to be only slightly miscible in the gel state and non-ideally miscible in the liquid crystalline state.[7–9] In a preparation with a 1:1 ratio of these two lipids maintained at a temperature between the phase transition temperatures of DSL and DML, one might expect to find liquid crystalline patches enriched in DML surrounded by gel state lipid enriched in DSL. In such a system, one might study the effect of a rigid boundary on cooperative director motions.

At pH 7.4, MA is a neutral fatty acid with a hydrocarbon chain identical to

Figure 2: The structures of (a) DSL, (b) myristic acid, (c) chlorophyll *a* , (d) phytol, and (e) cholesterol.

(a)

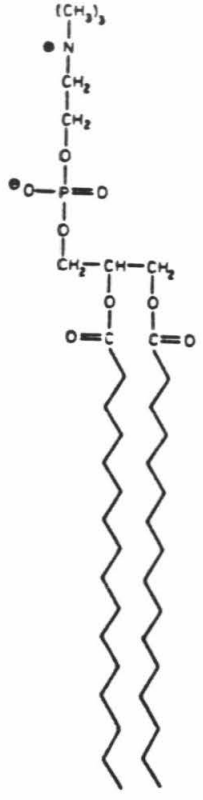

(b)

(c)

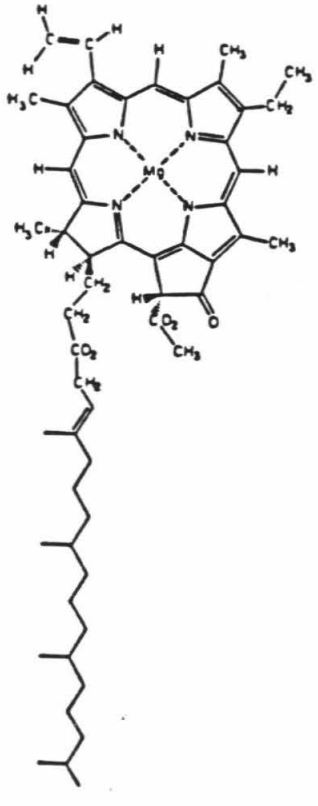

(d)

(e)

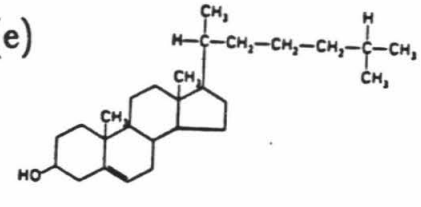

that of DML.[10,11] MA will contribute bulk to the hydrocarbon region of the DML bilayer. The T_2^{-1} of the MA/DML system should reflect the effect of close packing of lipid chains in the hydrocarbon region of the bilayer.

The hydrophobic portion of cholesterol consists of a hydrocarbon chain attached to four joined carbon rings. An -OH functionality at the end of the final carbon ring constitutes the hydrophilic portion of the molecule. The hydrophobic portion of cholesterol is very different from that of DML, and the head group of cholesterol is small.

The chl *a* head group is composed of a porphyrin ring with a central magnesium atom. The ring is attached to a 17 carbon chain with methyl groups protruding from every fourth carbon atom. The hydrocarbon chain of the phytol molecule is identical to that of chl *a* . Phytol, however, has a small alcohol -OH head group. A comparison of T_2^{-1} in chl *a* /DML and phytol/DML mixtures will reveal the effect of introducing a bulky porphyrin ring into the head group region of the DML bilayer.

Finally, the response of cooperative director motions to GA′ will be studied. GA′ is a pentadecapeptide which forms an ion channel in bilayers. The primary sequence of gramicidin A is shown below:

formyl-l-Val^{1}-Gly^{2}-l-Ala^{3}-d-Leu^{4}-l-Ala^{5}-d-Val^{6}
-l-Val^{7}- d-Val^{8}-l-Trp^{9}-d-Leu^{10}-l-Trp^{11}-d-Leu^{12}
-l-Trp^{13}-d-Leu^{14}-l-Trp^{15}-ethanolamine

GA′ is actually a mixture of gramicidins A, B, and C. The primary sequence of these three peptides differs only at position 11. In gramicidin A, this amino acid is a tryptophan. In gramicidins B and C, the eleventh amino acid is a phenylalanine

and a tyrosine, respectively. The ratio of these peptides in the GA′ mixture is 85 % gramicidin A, 10 % gramicidin B, and 5 % gramicidin C. All forms of GA′ are believed to span the DML bilayer as end to end dimers.[12,13] The dimer consists of two GA′ molecules connected at their N-termini by four hydrogen bonds. The channel has an approximate length of 30Å . The inner diameter of the channel is 4Å . Four bulky trp residues, located at the C-terminus of GA′, produce an outer diameter of 137Å at either end of the GA′ channel. The region of the channel in the center of the bilayer has an outer diameter of only 47Å .[14] The channel conformation of GA′ is shown in Figure 3. The experiments using GA′ reconstituted in DML represent a first attempt to characterize the effect of proteins on cooperative director fluctuations in the bilayer.

Experimental Section

I. *Materials and Methods*

DSL and perdeuterated DML (d_{54}-DML) were purchased from Avanti Polar Lipids. GA′ was purchased from Boehringer Mannheim Biochemicals. Cholesterol and phytol were purchased from Sigma Chemical Co. 6,6-d_2-myristic acid (6,6-MA) was synthesized by MSD Isotopes.

1,2-(2,2,2′,2′)-d_4-DML (d_4-DML) was synthesized by attaching MA deuterated at the 2 position to a glycerophosphocholine head group. The procedure of Regen et al. was used.[15] The MA used in the d_4-DML synthesis was deuterated at the 2 position by the procedure of Aasen, Lauer, and Holman.[16]

1,2-dimyristoyl-9,9′,10,10′-d_4-phosphatidylcholine (9,10-DML) was kindly

Figure 3: The channel conformation of GA′: (a) The conformation of the GA′ dimer in a lipid bilayer.[24] (b) The cone shape of a GA′ monomer in a $\beta^{6.3}$ helix.[25]

(a)

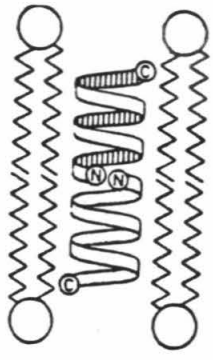

(b)

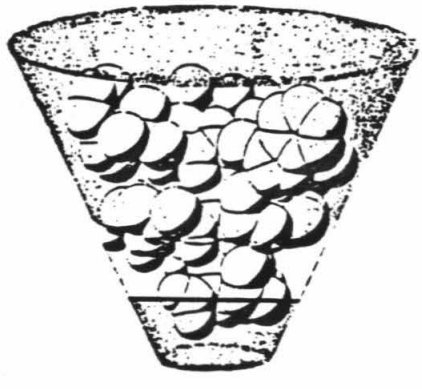

supplied Dr.Phoebe Dea. This lipid was synthesized by the following modification of the balloon technique used in the catalytic hydrogenation of unsaturated dicarboxylic acids.[17] On one side of a twin flask, deuterium is generated from sodium borodeuteride and concentrated deuterium chloride. On the other side, tris(triphenylphosphine)chlororhodium catalyzes the reduction of dimyristoleoyl lecithin. Silica gel thin-layer chromatography (TLC) was used to check the purity of the lipid. For this analysis, a mobile phase consisting of chloroform-methanol-water (65:25:4,v/v/v) was employed. Gas-liquid chromatographic analysis of the esterified fatty acid methyl ester was carried out using a diethylene glycol succinate on chromosorb W 60-80 mesh column at 160°C.[18]

Multilamellar dipersions were formed using the following protocol. The lipid or mixture of lipids was dissolved in chloroform and then transferred to a 5 mm sample tube. Most of the chloroform was then evaporated under a stream of nitrogen. The last traces of the solvent were removed by drying the sample under high vacuum for at least eight hours. The dried film was hydrated with a 25 mM Tris buffer solution (pH 7.0), and the sample tube was sealed. The lipid was then dispersed by alternately vortexing and warming to just above the gel-to-liquid crystalline phase transition temperature of the phospholipid. The vortexing was continued until a uniform suspension was formed ($\approx$ 5 minutes).

Experiments using d_4-DML were done within hours of hydration. This was necessary because deuterons at the two position are fairly acidic. Over a period of days, these deuterons exchange quite rapidly with protons in the aqueous environment.

All samples containing chl *a* were prepared and handled in the dark to avoid production of free radicals.

The procedure for the preparation of GA′ /DML samples differed slightly from that used for the mixed lipid samples. GA′ was dissolved in methanol and then added to 9,10-DML in appropriate amounts. When necessary, additional methanol was used to dissolve the lipid. The organic solution was placed under low vacuum until most of the solvent evaporated. The sample was then placed under high vacuum overnight. The GA′/DML film was hydrated in a 40 mM NaCl, 400 mM Tris buffer (pH 7.4). In order to reach an equilibrium distribution of GA′ in the bilayer, it was necessary to incubate samples above the phase transition temperature for approximately twelve hours.

All lipid mixtures and GA′/DML preparations contained less than 20 percent lipid by weight with respect to water. All experiments were performed at temperatures well above the gel-to-liquid crystalline phase transition temperature of DML.

II. *Instrumentation*

Relaxation experiments were conducted on a Bruker WM 500 spectrometer for lipid mixtures and on a Bruker AM 500 spectrometer for GA′ /DML samples. On both consoles, the transmitter pulse was attenuated to 1 volt peak/peak. On the Bruker AM 500 console, the TLO transmitter output was used. The attenuated transmitter pulse was used to drive an Amplifier Research 200L amplifier. The amplified pulse was then fed into a home built high power deuterium probe. This arrangement provided a 3.5 μs 90° pulse.

III. *Pulse Sequence*

A pulse sequence, developed by Mueller et al.[19] was used to determine the

of these lipid systems.[19] A diagram of this pulse sequence is shown below:

$$90_x - t_1/4 - 180_x - t_1/4 - 90_y - t_1/4 - 180_x - t_1/4 - \text{acquire}$$

The first central 180_x pulse is included to refocus resonant offset at the time of the 90_y solid echo pulse.[21] For longer t_1 values, even a small offset of the carrier may interfere significantly with formation of the solid echo.

T_2^{-1} experiments were carried out in two ways. In most experiments, the t_1 increment was constant throughout the series. This allowed two dimensional transformation of the data. The transformed data then yielded line widths in the ω_1 dimension and the usual one-dimensional spectrum in the ω_2 dimension.

Some experiments were designed to use larger time increments between the longer t_1 values. Although two-dimensional transformation was no longer possible in the latter design, the experiments required much less instrument time.

IV. *Data Analysis*

For T_2^{-1} experiments using a constant t_1 increment, a two dimensional transformation of the data was performed. Analysis of the transformed data was carried out by fitting cross-sections in the ω_1 dimension to a single Lorentzian line shape. Except in the study of the angular dependence of T_2^{-1}, all line widths were measured at the cross-section corresponding to a 90° singularity of the one-dimensional spectrum.

For experiments in which t_1 values were unevenly spaced, the intensity at a 90° singularity of the deuterium powder pattern was recorded for each time point. The array of intensities was then fit to a single exponential decay using an International Mathematical Statistical Library (IMSL) non-linear least squares fit

subroutine (ZXSSQ).

Results

I. *9,10-DML*

In order to characterize the T_2^{-1} of pure lipid bilayers, the DML bilayer was studied in detail. A one dimensional spectrum of 9,10-DML taken at a field strength of 11.7 Tesla is shown in Figure 4. In the absence of a strong magnetic field, bilayers in multilamellar dispersions are randomly oriented. The high intensity of the 90 degree singularities and the unusually low intensities at central and outer frequencies indicate that in an 11.7 T magnetic field, the bilayers are oriented with directors perpendicular to the magnetic field direction. This type of interaction between the magnetic field and the bilayer is commonly observed at high field strengths.[20,21] Although the degree of orientation was consistently high in these experiments, the precise extent of orientation varied from experiment to experiment.

Based on a model of cooperative order fluctuations, a dependence of T_2^{-1} on the angle β has been predicted. In order to test this prediction, the angular dependence of T_2^{-1} was measured for 9,10-DML. The results of this measurement are shown in Figure 5 both as a function of β and resonant frequency.

II. *d_{54}-DML*

Figure 6 shows a one-dimensional spectrum of d_{54}-DML. T_2^{-1} 's were measured at all resolvable singularities. The model of cooperative director fluctuations

Figure 4: The one-dimensional ^{2}H-NMR spectrum of a 9,10-DML multilayer preparation at 303K.

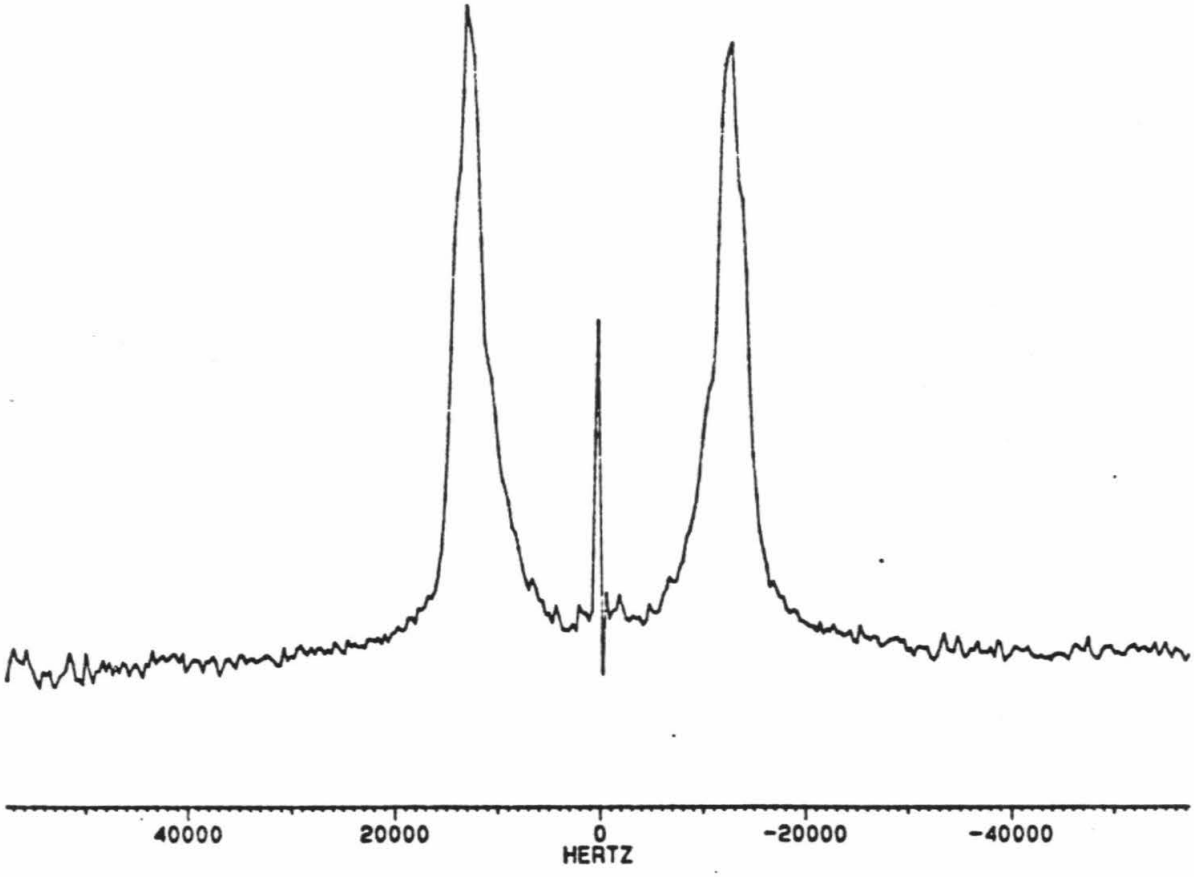
40000
20000
0
-20000
-40000
HERTZ

Figure 5: The dependence of T_2^{-1} on the orientation of the 9,10-DML bilayer director with respect to the external magnetic field. β indicates the angle between the director and the external magnetic field.

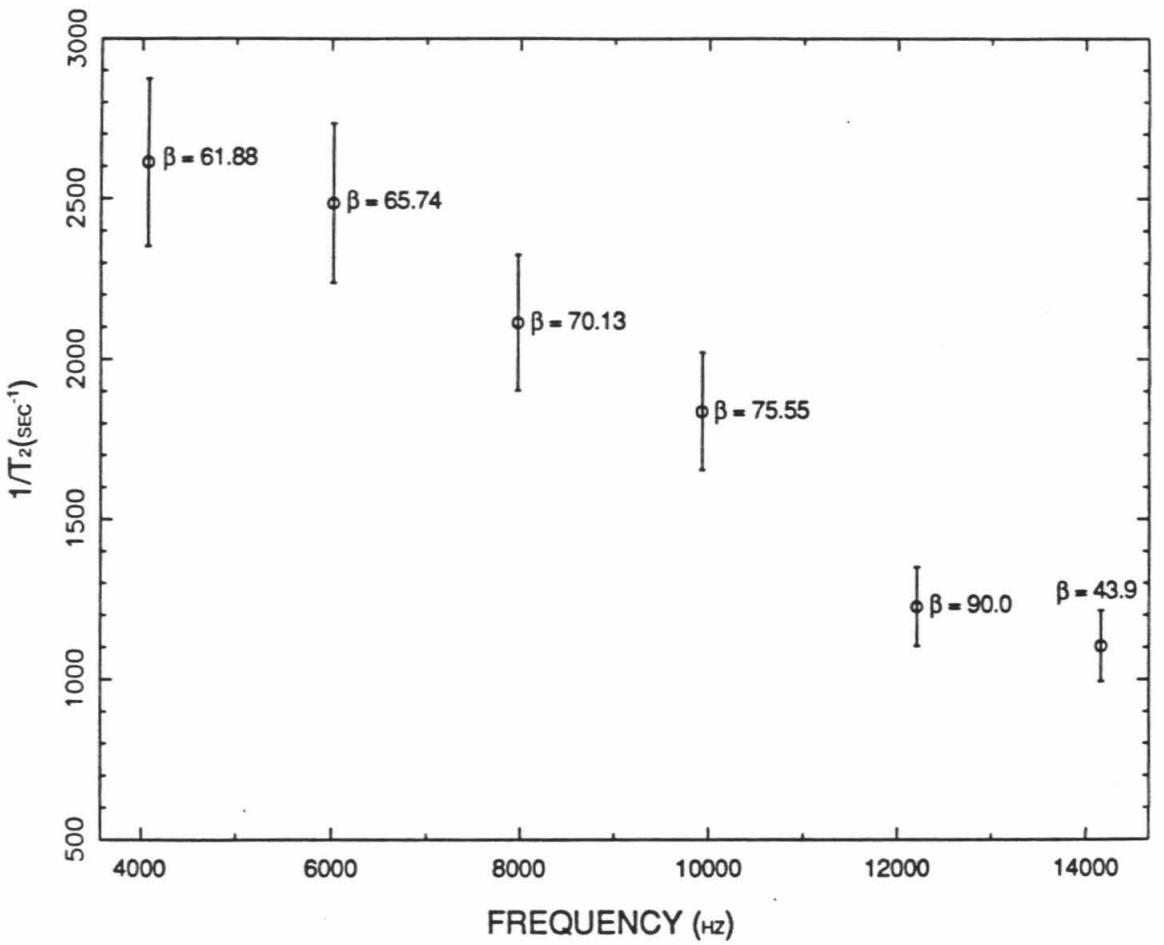
3000
2500
2000
1500
1000
500
1/T2(SEC-1)
β = 61.88
β = 65.74
β = 70.13
β = 75.55
β = 90.0
β = 43.9
4000
6000
8000
10000
12000
14000
FREQUENCY (HZ)

Figure 6: A one-dimensional ^{2}H-NMR spectrum of d_{54}-DML multilayers.

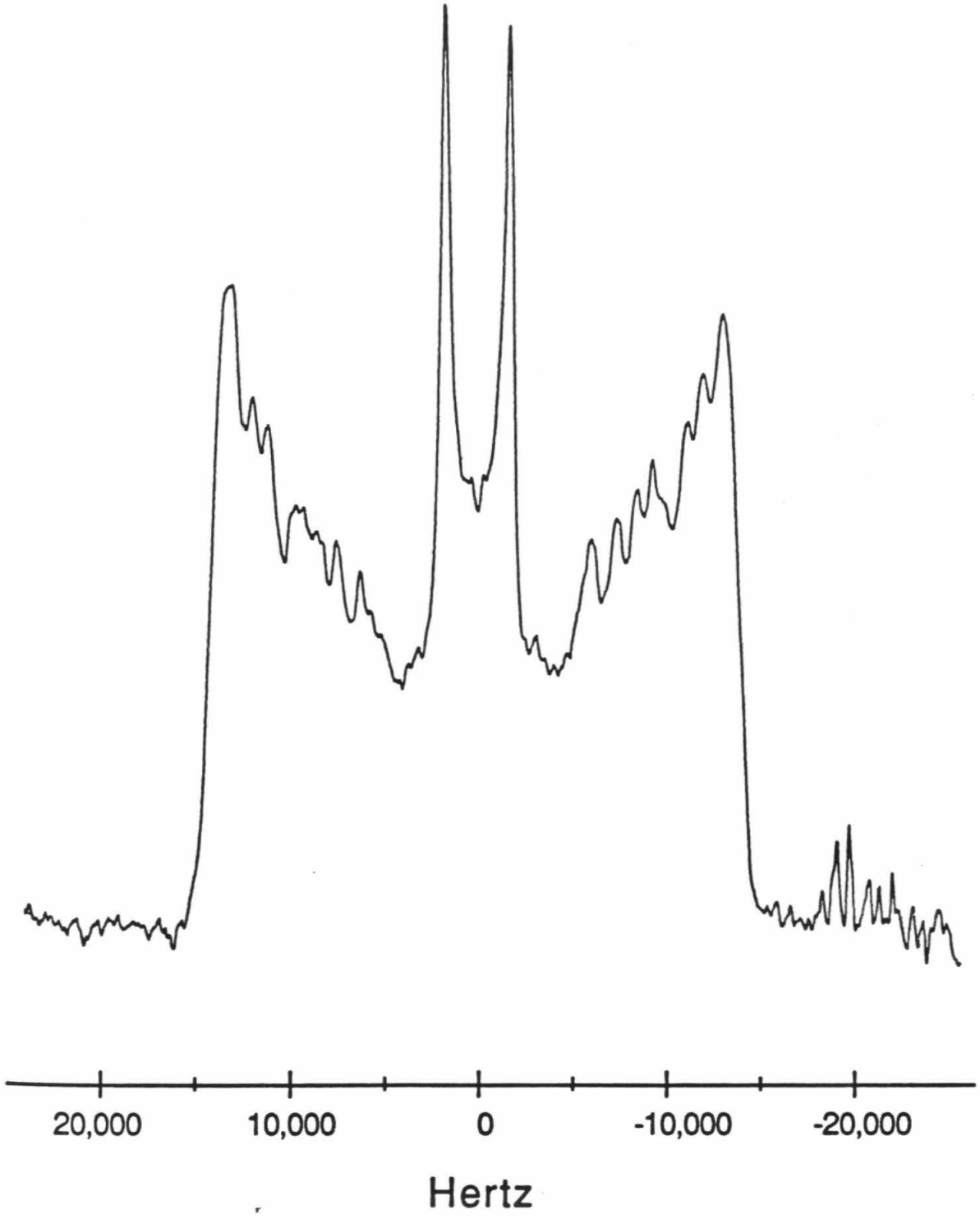
20,000
10,000
0
-10,000
-20,000
Hertz

predicts that a plot of T_2^{-1} vs. S_{CD}^2 should yield a straight line for deuterons experiencing similar cooperative fluctuations. Because deuterons at different positions on the same lipid chain are associated with the same director, it is expected that they will experience the same director fluctuations. If a plot of T_2^{-1} vs. S_{CD}^2 is made for deuterons on a perdeuterated lipid chain, therefore, a straight line should result. The experimental plot is shown in Figure 7. The line drawn through the points has been calculated using a linear least-squares fit program. The equation describing this 'best fit' line is:

$$T_2^{-1} = 11,926\text{sec}^{-1} S_{CD}^2 + 329\text{sec}^{-1} \qquad (1)$$

III. *d_4-DML*

If the lipid head group does not take part in the motions of the hydrocarbon chains, fluctuations of deuterons near the lipid head group may be curtailed. This should be reflected in the T_2^{-1} of deuterons near the lipid head group. A comparison of the relaxation rates in d_4-DML and 9,10-DML illustrate the differences in motion near the lipid head group. The one dimensional spectrum of d_4-DML is shown in Figure 8. Again, a high degree of orientation is observed. Due to orientation, all four deuterons are resolved. Each peak is labelled with its experimental relaxation value. These values are very different from those observed in 9,10-DML.

IV. *Lipid Mixtures and GA′/DML Membrane Systems*

To understand the effect of other lipids and GA′ on the T_2^{-1} of DML bilayers, the T_2^{-1} of DSL/9,10-DML, 6,6-MA/DML, cholesterol/9,10-DML, phytol/9,10-DML, chl *a* /9,10-DML, and GA′/9,10-DML bilayers were compared with the

Figure 7: A plot of T_2^{-1} vs. S_{CD}^2 for d_{54}-DML multilayers. The data are fit to a straight line whose slope is 11,926±306s^{-1} and whose y-intercept is 329±7s^{-1}.

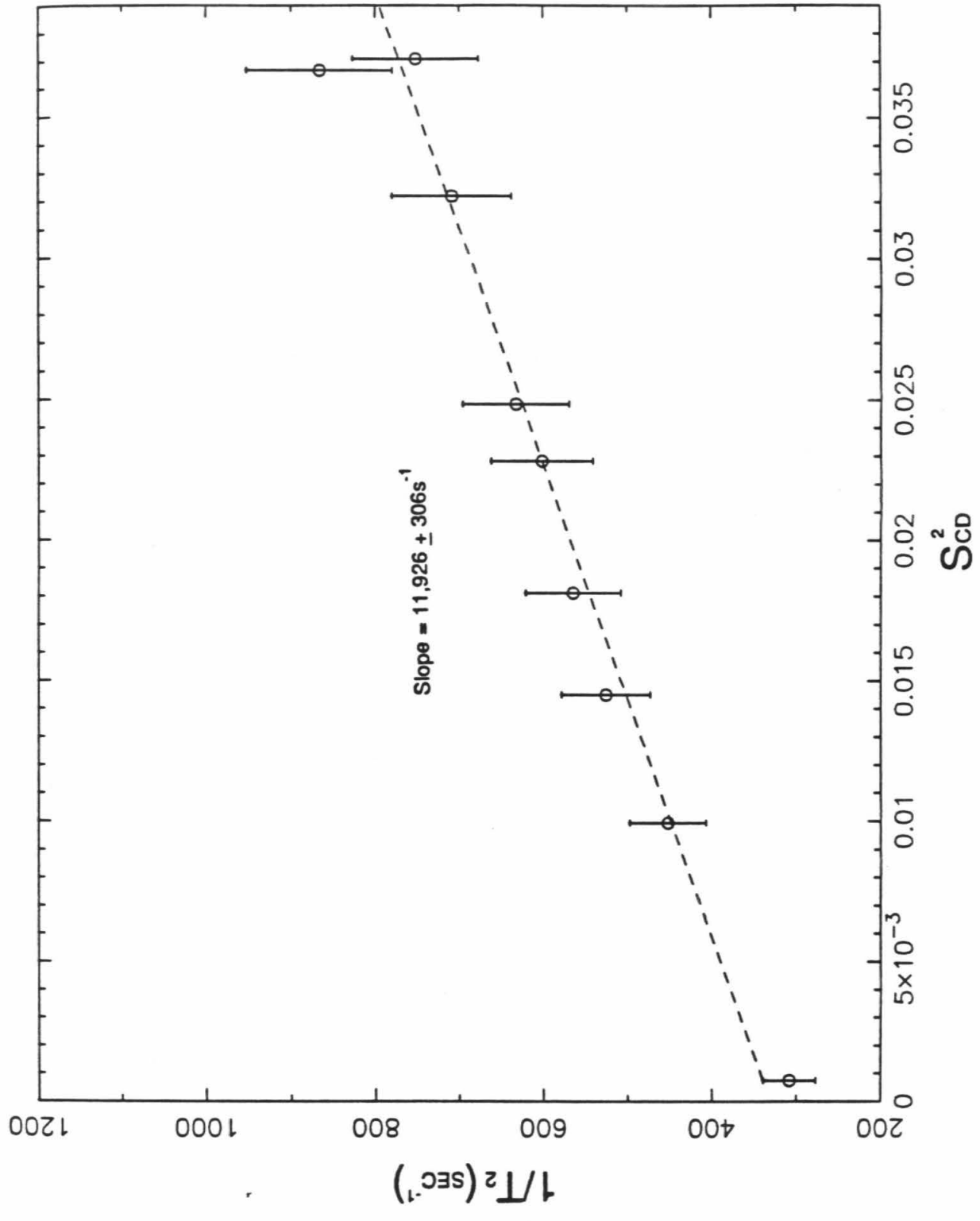
Slope = 11,926 ± 306s^{-1}
$1/T_2$ (sec^{-1})
S^2_{CD}
0
200
400
600
800
1000
1200
5×10^{-3}
0.01
0.015
0.02
0.025
0.03
0.035

Figure 8: A one-dimensional ^{2}H-NMR spectrum of d_4-DML multilayers. A powder pattern is observed for each of the four deuterons. Each powder pattern is labelled with its T_2^{-1} .

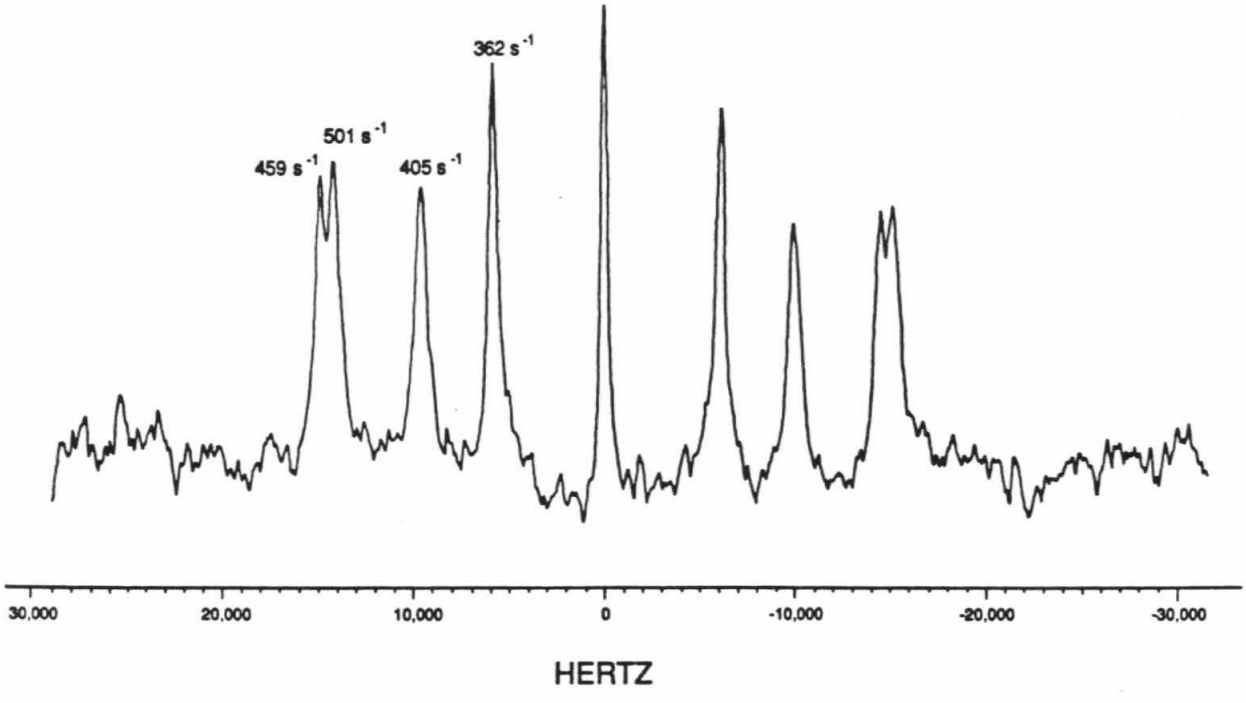
362 s-1
501 s-1
459 s-1
405 s-1
30,000
20,000
10,000
0
-10,000
-20,000
-30,000
HERTZ

relaxation rate measured for pure 9,10-DML bilayer. It was possible to divide these systems into the following two groups: (1) one in which T_2^{-1} remained similar to that of the pure lipid and (2) one in which it changed radically. Mixtures falling into the former category are 9,10-DML in DSL (1:1), 20 mol % 6,6 MA/DML, 30 mol % cholesterol/9,10-DML, and 8 and 20 mol % phytol/9,10-DML.

Mixtures of chl *a*/9,10-DML and GA′ combined with 9,10-DML exhibited a large change in T_2^{-1}. These results are plotted vs. mol % of solute in Figures 9 and 10. In both systems, T_2^{-1} increases with increasing solute concentration.

Discussion

Before examining the T_2^{-1} measurements in detail, the effects of spectral overlap on the T_2^{-1} measurement must be considered. This may interfere with the characterization of cooperative motions in the lipid bilayer.

I. *Effects of Resonance Overlap on the T_2^{-1} of 9,10-DML*

The ^2H spectrum of a selectively deuterated lipid bilayer consists of two overlapping powder patterns. These powder patterns arise from nuclear spin state transitions of opposite sign, namely $\Delta m = \pm 1$. A given resonant frequency corresponds to different orientations of the bilayer with respect to the external magnetic field for transitions of opposite sign. Different angular orientations, therefore, overlap in the NMR spectrum. The following relationship exists between the two angles which give rise to equivalent resonances in powder spectra of lipid bilayers:

Figure 9: A plot of T_2^{-1} vs. mole percent chlorophyll *a* in 9,10-DML multilayers.

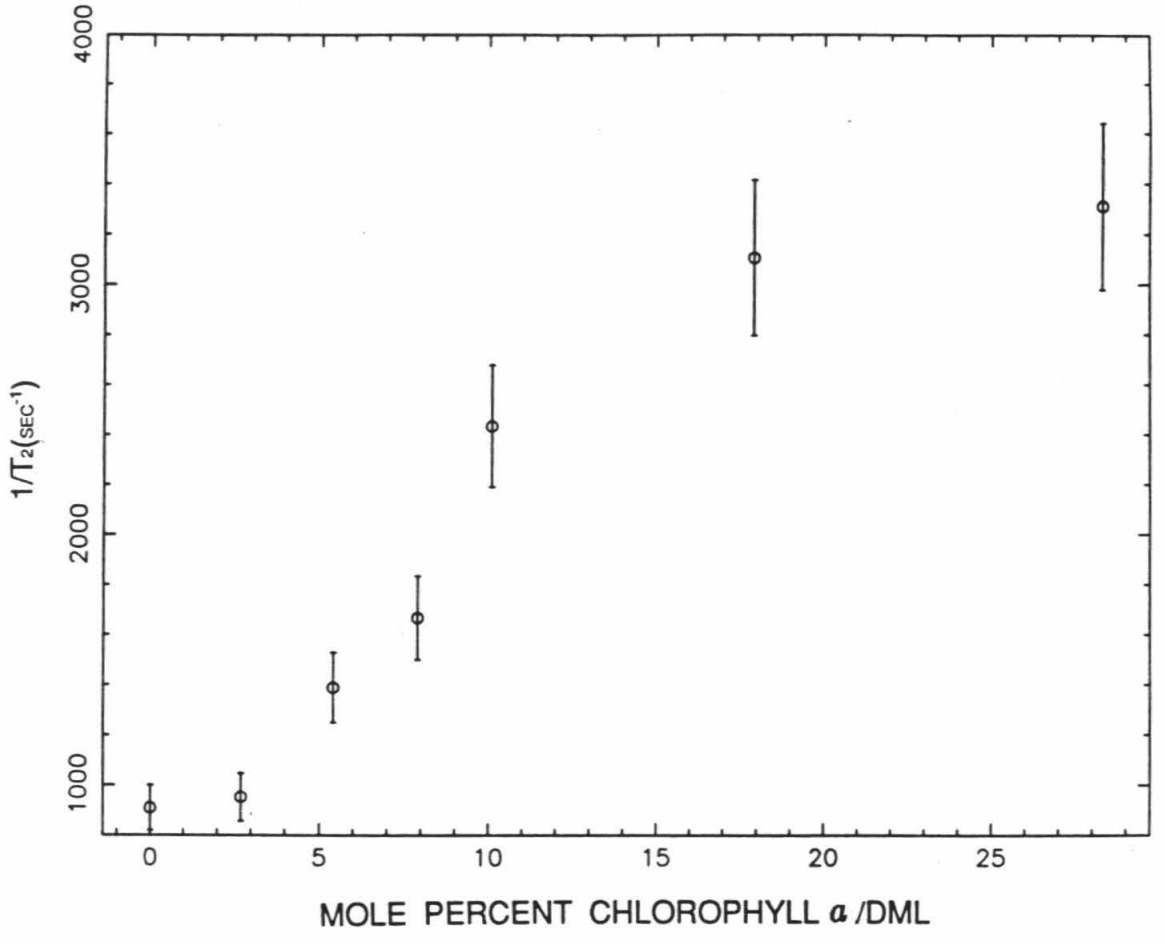
4000
3000
2000
1000
1/T2(SEC-1)
0
5
10
15
20
25
MOLE PERCENT CHLOROPHYLL a /DML

Figure 10: A plot of T_2^{-1} vs. mole percent Gramicidin A′ in 9,10-DML multilayers.

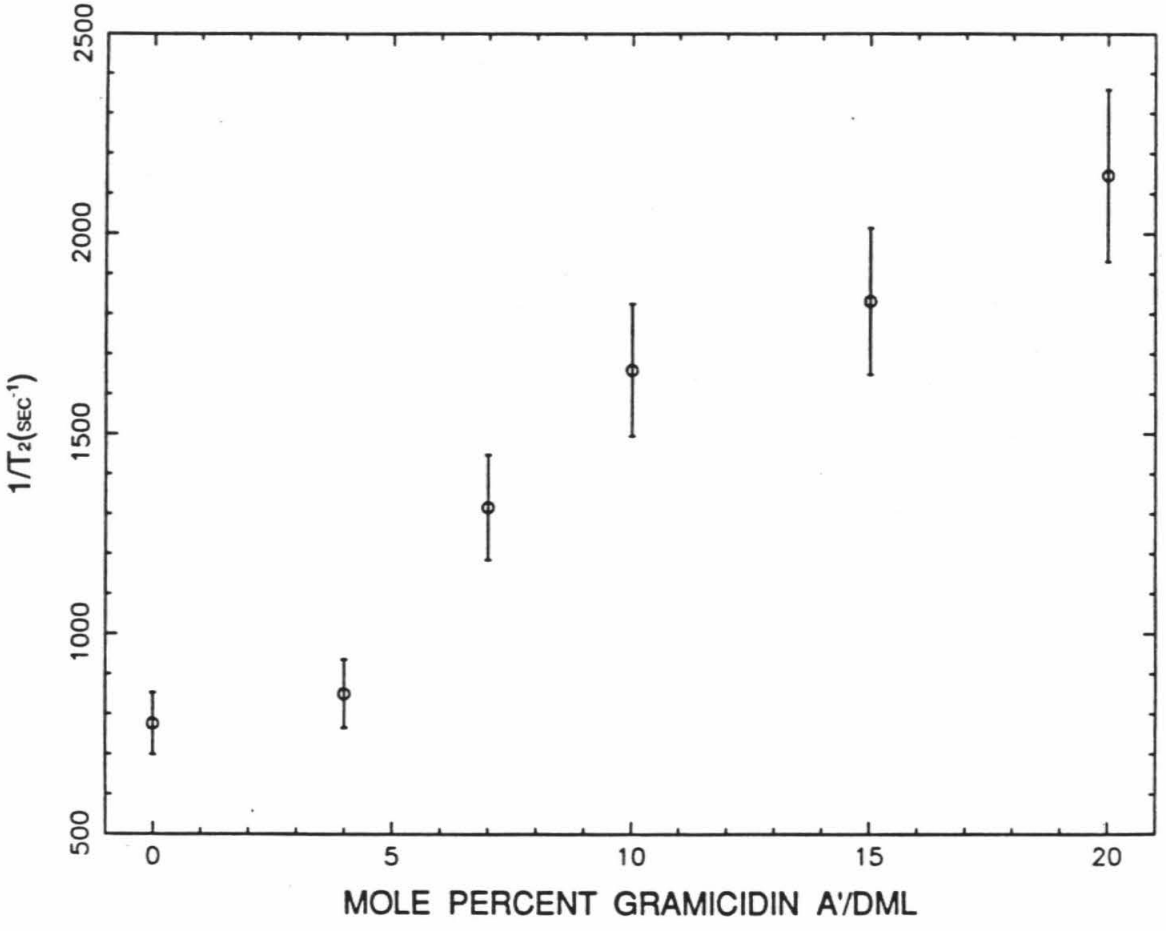
2500
2000
1500
1000
500
1/T2(sec-1)
0
5
10
15
20
MOLE PERCENT GRAMICIDIN A'/DML

$$cos(\beta_1) = \sqrt{2/3 - cos^2(\beta_2)} \qquad (2)$$

Given the marked angular dependence of T_2^{-1} in a bilayer powder pattern, overlap of different orientations may complicate the T_2^{-1} measurement. As described in chapter 2, the intensity at a given orientation β of the bilayer director with respect to the external magnetic field is given by $\sin(\beta)$. Using the above relationship, an orientation of approximately 35.26° to the magnetic field should yield a resonance overlapping with the 90° position. When the spectral intensity of bilayer directors oriented at $\beta = 90°$ is scaled to 1.00, the signal intensity of directors oriented at 35.26° should be 0.58. The total intensity measured at the spectral singularity will be 1.58. In an unoriented sample, the contribution to the 90° spectral singularity from lipids oriented at 35.26° will be approximately 1/3 of the total intensity.

Because of extreme director orientation at the magnetic field strengths used in these experiments, however, the contribution of $\beta = 35.26°$ to the spectral singularity is actually much less than this. Furthermore, because of the $\sin^2(2\beta)$ dependence of T_2^{-1}, the intensity of the $\beta = 35.26°$ resonance will decay much more rapidly than that of the $\beta = 90°$ resonance. The T_2^{-1} measurements at spectral singularities, therefore, should be dominated by resonances arising from directors oriented at $\beta = 90°$.

II. *Effect of Resonance Overlap on T_2^{-1} of d_{54}-DML*

By using perdeuterated lipids, the ^2H relaxation rates of deuterons at several positions on a lipid chain may be measured in one experiment. The spectrum of d_{54}-DML, for example, is composed of several superimposed powder patterns with varying order parameters. Each powder pattern corresponds to a different

position or group of positions on the lipid chain. With the exception of position 2, powder patterns which overlap because of identical order parameters arise from motionally similar deuterons. These deuterons are most likely located at neighboring positions on the hydrocarbon chain. These deuterons should also have similar T_2^{-1} 's. Overlap of their respective powder patterns, therefore, should not lead to a measurement of multi-exponential T_2^{-1} 's.

Resonances due to chain positions with very different order parameters, however, may interfere significantly with the measurement of T_2^{-1} at the spectral singularities. These contributions arise from orientations very different from $\beta = 90°$. In 9,10-DML, a large dependence of T_2^{-1} on β is observed. Careful consideration, therefore, must be given to resonances arising from director orientations with $\beta \neq 90°$.

Overlap due to powder patterns with differing order parameters, however, does not appear to interfere significantly with the measurement of T_2^{-1} at the singularities. The T_2^{-1} at the 90° orientation in the ^2H spectrum of 9,10-DML is 900 sec^{-1}. The T_2^{-1} at the corresponding frequency in the perdeuterated spectrum is approximately 720 sec^{-1}. Given approximately 20 % error in the measurements, these numbers are within experimental error of each other. One must conclude, therefore, that the effect of overlap is not great.

III. *Cooperative Fluctuations in the Lipid Bilayer*

The theory presented in chapter 2 predicts that the T_2^{-1} of a deuterated lipid bilayer will show a $\sin^2(2\beta)$ dependence. This dependence arises from the assumption that the director fluctuations, which are represented by $\delta\beta$, must have very small amplitude. T_2^{-1}, therefore, should be minimum at the 90° singularities

and should increase towards the center of the spectrum. The angular dependence of T_2^{-1} which is observed for 9,10-DML bilayers does, in fact, follow this trend. This is consistent with small amplitude director fluctuations.

The model of lipid bilayer motion presented in chapter 2 also predicts that positions 3 through 10 of the hydrocarbon chain will be coupled to cooperative fluctuations of the director. These deuterons, therefore, should exhibit similar rates of chain fluctuation. As discussed in chapter 2, T_2^{-1} relaxation due primarily to director fluctuations should be linearly proportional to both the rate of director fluctuation and S_{CD}^2. This proportionality results from the assumption that director fluctuations are uncoupled to motions such as bond rotation and lateral diffusion which involve individual lipid molecules. The T_2^{-1} 's of deuterons experiencing similar rates of director fluctuation, therefore, should yield a straight line when plotted against their respective S_{CD}^2's. The slope of this line is proportional to the correlation function associated with director fluctuations. A plot of T_2^{-1} vs. S_{CD}^2 for the various chain positions of the perdeuterated lipid is shown in Figure 7. The experimental points fit the straight line which is given by Eqn. (1) remarkably well. This demonstrates that cooperative director fluctuations in bilayers are not coupled to uncorrelated lipid motions in bilayers. In section V, possible origins of the y-intercept of this line will be discussed.

Both the angular dependence of T_2^{-1} and the linear relationship of T_2^{-1} with S_{CD}^2 have been predicted theoretically by a model of cooperative director fluctuations. These predictions have been borne out by T_2^{-1} measurements in DML bilayers. The experimental results suggest that, indeed, cooperative director fluctuations are the dominant cause of T_2^{-1} relaxation in lipid bilayers.

IV. *The Role of the Head Group in Cooperative Fluctuations*

There are two ways in which the lipid head group might affect cooperative fluctuations. Cooperative fluctuations may originate in the hydrophilic region of the bilayer. In this case, the motions of the hydrocarbon chains merely reflect those of the attached head group, and the rate of director fluctuation exhibited by deuterons at the two position on the hydrocarbon chain should be similar to that of deuterons at all other positions. Alternatively, the head group may act as anchor in the bilayer about which these director fluctuations occur. In this scenario, deuterons in the upper portion of the lipid chain do not experience the full effect of the director fluctuations. This restriction of cooperative motion will result in a slower rate of director fluctuation for deuterons at the 2 position of the hydrocarbon chain. As suggested above, this decrease in the rate of director fluctuation should be reflected in the slope of a plot of T_2^{-1} versus S_{CD}^2 for deuterons at the 2 position.

The extreme orientation of the multilayers in the magnetic field allows resolution of four signals corresponding to the four deuterium labels in d_4-DML. NMR studies show that the inner two powder patterns correspond to the 2 chain (closer to head group) of the lipid, while the outer two correspond to the 1 chain. X-ray crystallographic studies of crystalline lipids reveal a kink in the 2 chain. As a result, the deuterium labels at the 2 position of the 2 chain are oriented perpendicular to the head group. This kink presumably allows the ester linkage to interact with the polar head group or solvent exterior. The angle about which averaging occurs with respect to the average director is quite different for deuterium labels at the 2 position of each chain. A difference in the axis of averaging, rather than the rate, leads to dissimilar order parameters.

The d_4-DML T_2^{-1} 's are plotted against S_{CD}^2 in Figure 11. The line calculated for the perdeuterated system is shown for comparison. The plot of the d_4-DML T_2^{-1} 's versus S_{CD}^2 fits a straight line quite well. The slope of this line, however, is approximately a factor of five smaller than that of the line corresponding to experiments on the perdeuterated lipid. Because the rate of chain fluctuation is directly proportional to the slope, cooperative motions must be hindered at the two position. This suggests that, indeed, the lipid head groups anchor their chains in the bilayer.

V. *The Y-Intercept in Eqn. (1)*

In Eqn. (41a) of chapter 2, an expression for $J_0(\omega)$ is presented which includes contributions from both uncorrelated or uni-molecular lipid motions and from cooperative director motions. Only the cooperative contribution depends on S_{CD}^2. If $T_2^{-1} \approx J_0(0)$, this expression implies that the y-intercept in a plot of T_2^{-1} vs. S_{CD}^2 should be proportional to the contribution of uncorrelated motions to T_2^{-1}. Because uncorrelated motions are quite fast, however, they are not expected to contribute significantly to T_2^{-1}. One predicts, therefore, a linear dependence of T_2^{-1} on S_{CD}^2 with a zero y-intercept.

Experiment shows, however, that a large part of T_2^{-1} does not depend on S_{CD}^2. The y-intercept in Eqn. (1) is 306 sec^{-1}, while the intercept for a plot of T_2^{-1} vs. S_{CD}^2 in d_4-DML bilayers is 345 sec^{-1}. The constant contribution to T_2^{-1}, therefore, is similar at all positions on the lipid chain.

It is unlikely that uncorrelated motions are responsible for the constant contribution to T_2^{-1}. Because T_1^{-1} and $T_{1\rho}^{-1}$ are both approximately 5 % of T_2^{-1} in pure lipid bilayers (results not shown), uncorrelated motions contributing to

Figure 11: Plots of T_2^{-1} vs. S_{CD}^2 are compared for d_{54}-DML and d_4-DML multilayers. Each is fit to a straight line. Although the y-intercepts of these lines are comparable, the slope of the line corresponding to d_4-DML is 1/5 that of the slope corresponding to d_{54}-DML.

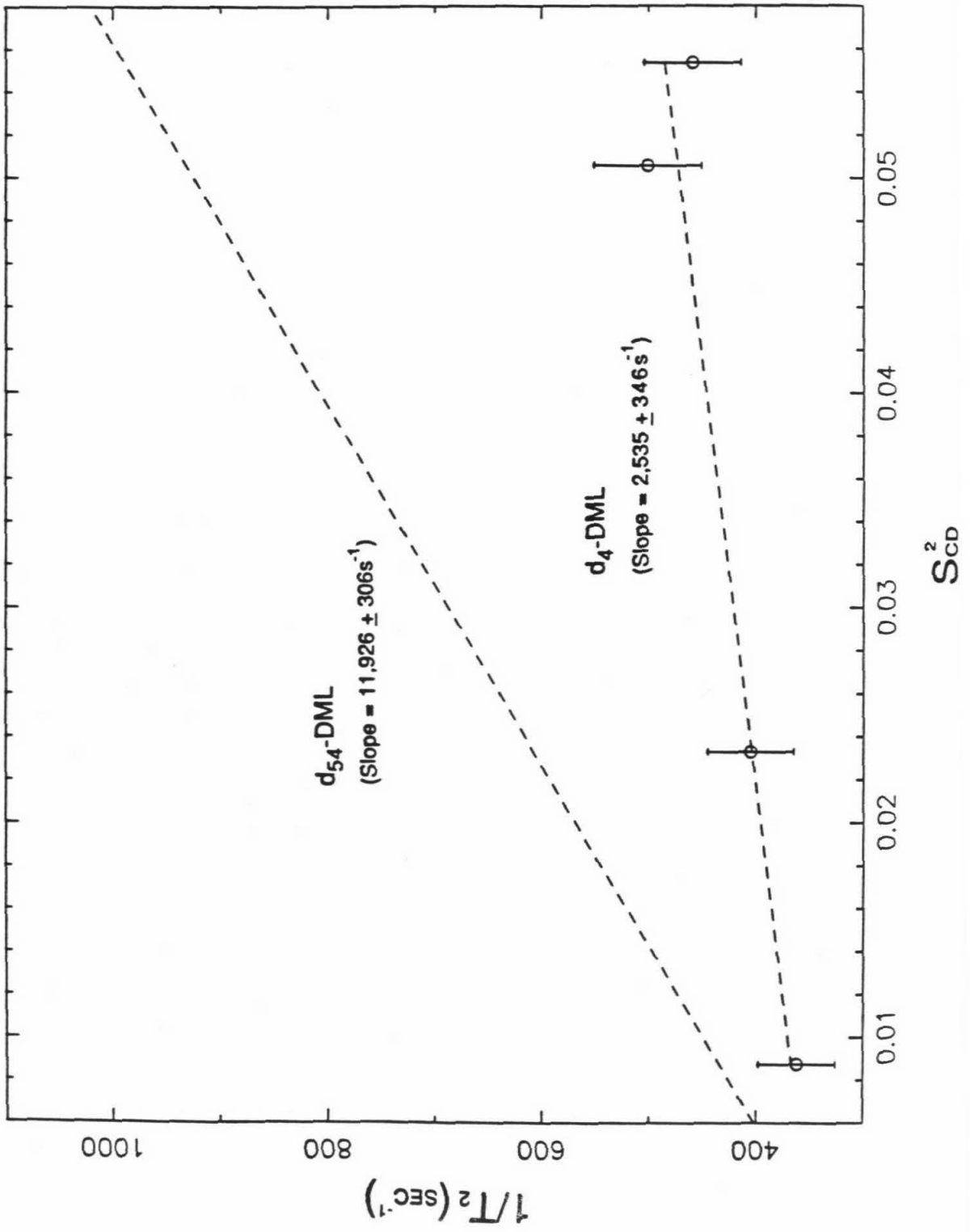
d_{54}-DML
(Slope = 11,926 ± 306s^{-1})
d_4-DML
(Slope = 2,535 ± 346s^{-1})
1/T$_2$ (sec^{-1})
400
600
800
1000
0.01
0.02
0.03
0.04
0.05
S^2_{CD}

T_2^{-1} would have to be extremely slow to account for such a large portion of T_2^{-1}. Lateral diffusion of the lipid molecule about the liposome, however, might be responsible for the y-intercept. Lateral diffusion may affect the T_2^{-1} measurement in two ways. First of all, lateral diffusion may contribute directly to the intrinsic T_2^{-1}. Secondly, it may cause motional broadening of the ^{2}H-NMR lipid bilayer spectrum. The resonant frequency of a ^{2}H label on a lipid hydrocarbon chain depends on β. Because liposomes are curved, the resonant frequency of the ^{2}H nucleus will change as the lipid diffuses about the liposome. The T_2^{-1} experiment employs a series of echo pulse sequences which rely on the nucleus retaining the same resonant frequency during the course of the experiment. If rotational diffusion about the liposome is significant on the time scale of the NMR experiment, refocussing of the NMR signal will be incomplete, and the T_2^{-1} will appear larger.

The relative importance of these two effects of lateral diffusion may be evaluated by calculating the rotational correlation time associated with lateral diffusion about the curved bilayer surface. The correlation time for diffusion of a lipid molecule about a liposome of radius r has been shown to be:[22]

$$\frac{1}{\tau_c} = \frac{6}{r^2}(D_t + D_{diff}) \tag{3}$$

where D_{diff} is the lateral diffusion coefficient of a lipid molecule in a bilayer. D_t, the diffusion coefficient for a sphere of radius r, is given by:

$$D_t = \frac{k_B T}{8\pi r \eta} \tag{4}$$

where η is the viscosity of the surrounding medium at temperature T. Thus, the correlation time for lipid diffusion depends on the radius of the liposome. ^{31}P-NMR spectra of pure DML bilayers are broad powder patterns of $\Delta\sigma \approx 40$ ppm.

In this case, the minimum liposomal radius may be taken to be 5,000Å .[22] Using Eqn. (4) at 30°,a value of 4.18 x 10^{-9} cm^2/sec is obtained for D_t. D_{diff} for DML at 30°C has been measured by Sackmann et al.[23] to be 1.28 x 10^{-7} cm^2/sec. Insertion of these diffusion coefficients in Eqn. (3) yields a value of 3.15 ms for τ_c.

τ_c is approximately three times the T_2 measured for a pure DML bilayer. It is unlikely, therefore, that lateral diffusion will contribute directly to T_2^{-1} relaxation. The lipid molecule, however, will diffuse a significant distance on the NMR time scale. This will lead to motional broadening of the NMR signal, and a larger T_2^{-1} measurement.

The non-zero y-intercept found in pure lipid bilayers, therefore, is probably due to motional broadening arising from lateral diffusion. Upon addition of GA′ or any of the lipids used in this work to the bilayer, it is unlikely that the rate of lateral diffusion or the distribution of liposomal radii changes significantly. Changes in T_2^{-1} upon addition of these lipids or proteins to the DML bilayer, therefore, are not attributed to changes in rates of rotational diffusion in the bilayer.

VI. *Lipid Mixtures and GA′ /DML Membrane Systems*

It has been determined that cooperative director fluctuations are consistent with the type of motions observed in the hydrocarbon region of the pure DML bilayer. The effect of other lipids or GA′ on these cooperative motions may be studied by measuring the T_2^{-1} of deuterated DML in mixed bilayers. A comparison of the T_2^{-1} 's and S_{CD}'s of the mixed lipid and GA′ /DML systems with Eqn. (1) leads to a subdivision of the experimental systems into two groups. Group (1) includes those systems whose relaxation rates and order parameters satisfy Eqn. (1). These are 20 mol % 6,6-MA in DML (pH 7.4), 30 % cholesterol in 9,10-DML,

8 mol % phytol in 9,10-DML, 23 mol % phytol in 9,10-DML, and 50 mol % 9,10-DML in DSL at 313 K. The T_2^{-1} values for these systems are compared with the line described by Eqn. (1) in Figure 12. Group (2) includes various concentrations of chl *a* in 9,10-DML and GA′ in 9,10-DML. The T_2^{-1}'s and S_{CD}'s of these systems are not solutions to Eqn. (1). The data for systems belonging to group (2) are shown in Figures 13 and 14.

In the plot of T_2^{-1} vs. S_{CD}^2 for systems in group (1), most T_2^{-1} values fall near the line described by Eqn. (1). This suggests that the contribution of cooperative director fluctuations to T_2^{-1} in these mixed systems is similar to the contribution in the pure DML bilayer. For systems falling into group (2), there is no correlation between the line of Eqn. (1) and the T_2^{-1} of the mixed system. The T_2^{-1}'s of these systems increase with increasing lipid or protein concentration. Addition of lipid or protein, therefore, increases the contribution of the term in the spectral density function due to correlated motions.

If the structures of the lipids which have been mixed with DML are compared, certain conclusions may be drawn concerning features which affect cooperative director motion in lipid bilayers.

DML Surrounded by DSL in the Gel State

In the DSL/DML system, lipids with similar head groups but unlike chain lengths are mixed. The (1:1) mixture of unlabelled DSL and 9,10-DML was studied at 313 K. This is below the gel-to-liquid crystalline phase transition temperature of DSL but above the phase transition temperature of DML. This system might be visualized as liquid crystalline patches enriched in DML surrounded by gel state lipid enriched in DSL. The T_2^{-1} of gel-state DML is at least one order of magnitude larger than that of DML in the liquid crystalline state. Because T_2^{-1} of DML in

Figure 12: A plot of T_2^{-1} vs. S_{CD}^2 for lipids falling into group (1). The best fit line for the d_{54}-DML data is included for comparison.

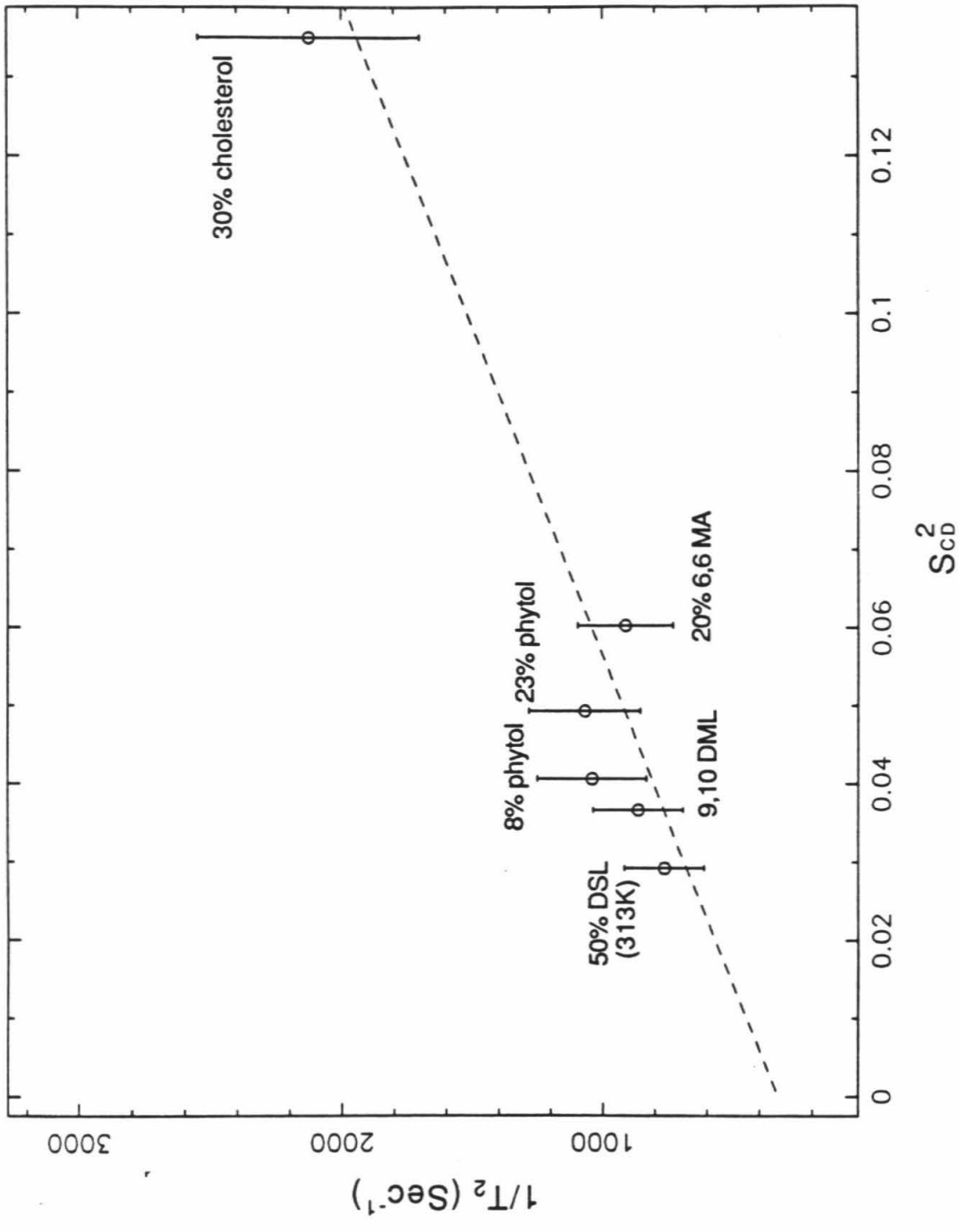
30% cholesterol
8% phytol
23% phytol
20% 6,6 MA
9,10 DML
50% DSL
(313K)
1/T2 (Sec-1)
3000
2000
1000
0
0.02
0.04
0.06
0.08
0.1
0.12
SCD2

Figure 13: A plot of T_2^{-1} vs. S_{CD}^2 for the chl *a* /9,10-DML system. Points are labelled with the experimental chl *a* concentrations. The best fit line for the d_{54}-DML data is included for comparison.

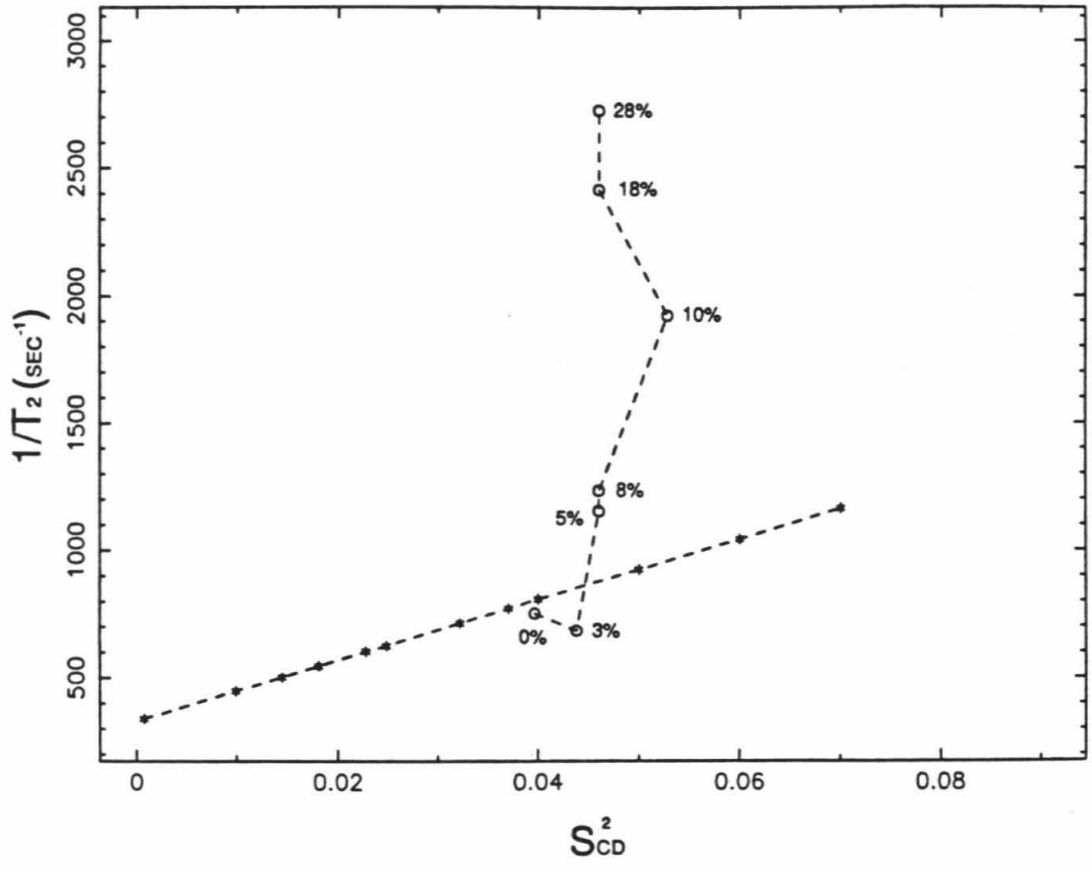
1/T2 (SEC-1)
3000
2500
2000
1500
1000
500
0
0.02
0.04
0.06
0.08
SCD2
28%
18%
10%
8%
5%
3%
0%

Figure 14: A plot of T_2^{-1} vs. S_{CD}^2 for the GA′/9,10-DML system. Points are labelled with the relevant GA′ concentrations. The best fit line for the d_{54}-DML data is included for comparison.

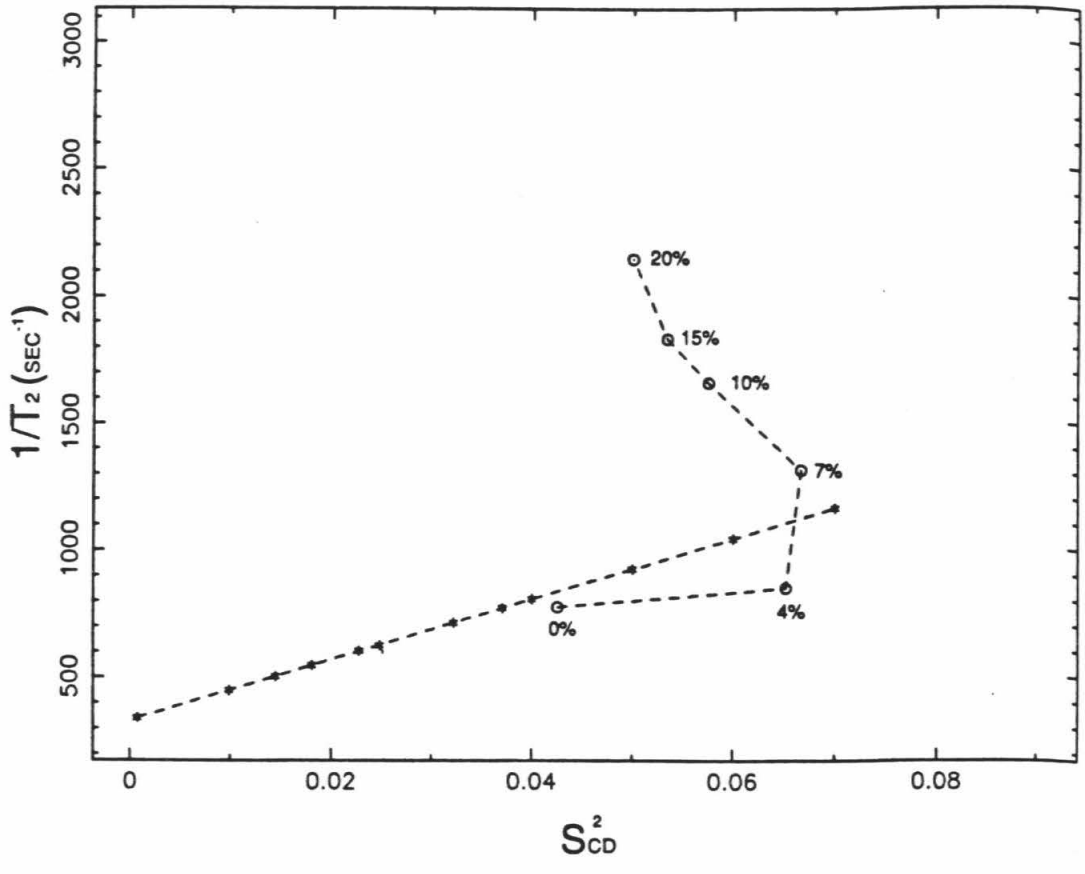
1/T2 (SEC-1)
3000
2500
2000
1500
1000
500
0
0.02
0.04
0.06
0.08
S2CD
20%
15%
10%
7%
4%
0%

the DML/DSL mixture is very similar to that of the pure liquid crystalline DML bilayer, one may conclude that the liquid crystalline domains have very little gel character. The rigid gel state boundaries, therefore, do not interfere with motions in the liquid crystalline patches of DML.

Two conclusions may be drawn from this observation. First of all, coupling between liquid crystalline and gel state phases is weak in this system. In other words, gel state motions are not transmitted far into the liquid crystalline domains. In addition, cooperative motions in the liquid crystalline domains are not curtailed by the gel state boundaries. In other words, the distances over which cooperative motions extend must be much smaller than the size of the liquid crystalline domains.

Cholesterol, Phytol and 6,6-MA in DML

Phytol, cholesterol, and 6,6-MA (pH 7.4) are all lipids with small, neutral head groups. The organic acid and alcohol head group functionalities of these three lipids differ from the phosphatidylcholine head group of DML. Although the hydrocarbon chains of 6,6-MA and phytol are similar to that of DML, the hydrocarbon portion of cholesterol is quite different from that of DML. The hydrocarbon chain of MA is identical in length and structure to that of DML. A methyl group protrudes from every fourth carbon of the phytol saturated hydrocarbon chain. In contrast, the hydrocarbon portion of cholesterol includes three six membered rings and one five membered ring. These cyclic structures differ considerably from the linear saturated chains of DML. None of these three lipids has an effect on cooperative motions in the DML bilayer. Small structural differences between the head group of DML and that of an added lipid, therefore, do not interfere with cooperative motion in the bilayer. Furthermore, significant differences between

the hydrocarbon region of DML and that of an added lipid seem to have little effect on cooperative motions in the bilayer.

Phytol and Chl a in DML

A comparison of the effects of phytol and chl *a* on T_2^{-1} underscores the importance of the head group in bilayer motions. The phytol head group is merely an -OH functionality, while the chl *a* head group is a bulky porphyrin moiety. Bilayer motions are not perturbed by addition of the phytol chain. This contrasts strongly with the change in motion upon addition of chl *a*. Because phytol and chl *a* differ only in the head group region, one must conclude that head group interactions play an important role in bilayer motion. This effect is analyzed in detail below.

GA′ in DML

GA′ is similar to chl *a* in that it perturbs motion in the DML bilayer. The origin of this perturbation is difficult to determine. GA′ is very different from a lipid. In the bilayer, it exists as a beta helical dimer. An ethanolamine moiety at the C-terminus of the peptide presumably protrudes into the head group region of the bilayer. The ethanolamine moiety is not large enough to perturb bilayer interactions in the same way that the porphyrin group of chl *a* does. The beta helix of GA′, however, is cone-shaped, while the DML molecule is approximately cylindrical. This difference in shape might alter lipid motion.

Further Discussion

Cooperative director fluctuations in bilayers may be likened to the motions of a series of coupled oscillators. Van der Waals interactions between the lipid chains may act as a restoring force in these coupled director oscillations. As the distance between neighboring chains is increased, the restoring forces decay rapidly, and

the oscillators begin to move independently.

The following structural features of chl *a* and GA′ might lead to such a change in the restoring forces between lipid chains. The bulky porphyrin head group of chl *a* is attached to a single phytol chain. Accommodation of the porphyrin ring in the head group region of the DML bilayer may introduce large distances between lipid chain. These distances will lead to weaker van der Waals interactions and, therefore, weaker coupling between bilayer directors. Because of the four bulky tryptophans near the C-terminus of GA′, the GA′ channel is approximately three times wider at the C-terminus than the N-terminus. Since the C-terminus is located near the head group region of the bilayer, and the N-terminus is located in the center of the bilayer, GA′ may also create larger spaces in the hydrophobic region of the bilayer.

In conclusion, it seems likely that the addition of both chl *a* and GA′ to the DML bilayer uncouple director fluctuations inthe lipid bilayer.

Conclusions

The measurements discussed above reveal several characteristics of the motions which effect T_2^{-1} relaxation in DML bilayers. Both cooperative fluctuations and uncorrelated motions contribute to T_2^{-1}. The lipid head group participates only in uncorrelated motions. In cooperative motions of the hydrocarbon chains, the head group serves as an anchor about which these fluctuations occur. In mixed lipid/DML systems, lipids with small head groups do not perturb the cooperativity of director fluctuations in the DML bilayer. Lipids with very different hydrophobic moieties also do not perturb cooperative fluctuations when added to the DML bilayer. GA′ and lipids with large head groups, however, interfere greatly with these cooperative motions.

References

1. A. Carruthers and D. L. Melchior, *Biochemistry*, **23**, 6901-6911 (1984).
2. J. Seelig and A. Seelig, *Quart. Rev. Biophys.*, **13**, 19-61 (1980).
3. B. A. Cornell, M. M. Sacre, W. E. Peel, and D. Chapman, *FEBS Lett.*, **90**, 29-35 (1978).
4. D. Rice and E. Oldfield, *Biochemistry*, **18**, 3272-3279 (1979).
5. B. A. Cornell, R. G. Hiller, J. Raison, F. Separovic, R. Smith, J. C. Vary, and C. Morris, *Biochim. Biophys. Acta*, **732**, 473-478 (1983).
6. P. F. Devaux, G. L. Hoatson, E. Favre, P. Fellmann, B. Farren, A. L. Mackay, and M. Bloom, *Biochemistry*, **25**, 3804-3812 (1986).
7. S. Mabrey and J. Sturtevant, *Proc. Natl. Acad. Sci. USA*, **73**, 3862-3866 (1976).
8. P. W. M. Van Dijck, A. J. Kaper, H. A. J. Oonk, and J. De Gier, *Biochim. Biophys. Acta*, **470**, 58-69 (1977).
9. E. J. Luna and H. M. McConnell, *Biochim. Biophys. Acta*, **509**, 462-473 (1978).
10. M. Ptak, M. Egret-Charlier, A. Sanson, and O. Bouloussa, *Biochim. Biophys. Acta*, **600**, 387-397 (1980).
11. S. E. Schullery, T. A. Seder, D. A. Weinstein, and D. A. Bryant, *Biochemistry*, **20**, 6818-6824 (1981).
12. S. Weinstein, B. A. Wallace, E. R. Blout, J. S. Morrow, and W. Veatch, *Proc. Natl. Acad. Sci. USA*, **76**, 4230-4234 (1979).
13. B. A. Cornell, F. Separovic, A. J. Baldassi, and R. Smith, *Biophys. J.*, **53**, 67-76 (1988).
14. J. A. Killian and B. De Kruijff, *Biophys. J.*, **53**, 111-117 (1988).
15. S. Regen, K. Yamaguchi, N. K. P. Samuel, and M. Singh, *J. Am. Chem.*, **105**, 6345-6356 (1983).
16 A. J. Aasen, W. M. Lauer, and R. T. Holman, *Lipids*, **5**, 869-877 (1970).

17. L. S. Fieser, **Organic Experiments**, (Heath, New York, 1967).

18. K. A. Devor and J. B. Mudd, *J. Lip. Res.*, **12**, 396-402 (1971).

19. L. Mueller and S. I. Chan, *J. Chem. Phys.*, **78**, 4341-4348 (1983).

20. B. J. Gaffney and H. McConnell, *Chem. Phys. Lett.*, **24**, 310-313 (1974).

21. J. Seelig, F. Borle, and T. A. Cross, *Biochim. Biophys. Acta*, **814**, 195-198 (1985).

22. E. B. Burnell, P. R. Cullis, and B. De Kruijff, *Biochim. Biophys. Acta*, **603**, 63-69 (1980).

23. H. J. Galla, W. Hartmann, U. Theilen, and E. Sackmann, *J. Membr. Biol.*, **48**, 215-236 (1979).

24. B. A. Wallace, *Biopolymers*, **22**, 397-402 (1983).

25. R. Brasseur, V. Cabiaux, J. A. Killian, B. De Kruijff, and J. M. Ruysschaert, *Biochim. Biophys. Acta*, **855**, 317-324 (1986).

Chapter IV

The Effect of Chlorophyll *a* on Director Fluctuations in the Dimyristoyllecithin Bilayer

Introduction

In a living cell, ion transport, transmembrane signalling, and enzymatic functions of membrane-bound proteins may depend on large amplitude conformational fluctuations in the protein. The probability of the occurrence of such fluctuations depends, in part, on the interaction of the protein with the surrounding cell membrane. In chapter 3, slow, cooperative director fluctuations were shown to exist in lipid bilayers. When the frequencies of conformational fluctuations in the protein are matched to those in the lipid bilayer, the lipid and protein motions may couple. Thus, the activity of the protein may be enhanced or inhibited by motions in the surrounding lipid membrane. Director fluctuations in lipid bilayers are characterized by their cooperativity. These motions, therefore, may also induce cooperative motion in nearby protein molecules. Of all the motions present in lipid bilayers, therefore, director fluctuations are the most likely to influence conformational fluctuations in proteins. In order to assess the importance of such coupling mechanisms in protein activity, the frequency profiles of both director fluctuations in the lipid bilayer and protein fluctuations must be determined. This work is concerned primarily with director fluctuations.

Preliminary studies show that the extent of slow motion in the lipid bilayer increases dramatically upon reconstitution with membrane-bound proteins.[1–3] A similar effect is observed upon addition of chl *a* to the DML bilayer. In this chapter, the effect of chl *a* on the lipid bilayer is used as a simple model for the motional changes produced in a lipid bilayer by the addition of a membrane-bound protein. An analysis of the effect of chl *a* on lipid motion is simpler than the analysis of the effect of a protein on lipid motion for the following reasons.

First of all, the structure of a protein is very different from that of a lipid.

Consequently, it is difficult to identify particular aspects of the lipid/protein interaction which alter bilayer motion in a reconstituted bilayer system. Chl *a*, however, only differs significantly from DML in its large porphyrin head group. The phytol chain of chl *a* is quite similar to DML's acyl chain. Because the inclusion of phytol in the DML bilayer has no effect on slow motion (see chapter 3), the changes in bilayer motion which are observed upon addition of chl *a* must be due to the influence of the porphyrin head group on the DML bilayer.

Furthermore, this study is concerned with changes in the bulk properties of cooperative director fluctuations in the lipid bilayer upon addition of an unlike lipid or protein. The mass of a protein may be several times that of a lipid. If a complex is formed between the lipid and the protein, the fluctuations of complexed lipids will not be correlated. The effect of complex formation may, thus, overshadow the effect of bulk changes in cooperative properties of director fluctuations. Chl *a* and DML, however, are similar in mass. Although short-lived complexes between DML and chl *a* molecules may form, it is unlikely that the brief encounter of these two lipids would drastically affect correlated motions in the DML bilayer. Changes in the slow motions of the DML bilayer upon addition of chl *a*, therefore, must arise from changes in the bulk properties of the cooperative director fluctuations.

The distances over which director fluctuations extend are much larger than the dimensions of a single lipid molecule. In this case, continuum theory, which is commonly used to describe distortions in liquid crystals, may be applied to director fluctuations in lipid bilayers.[4] This theory permits the characterization of cooperative director fluctuations in bilayers by correlation lengths and elastic constants. The correlation length corresponds to the distance over which cooperative director motions extend. The elastic constants describe the resistance of the

hydrophobic region of the bilayer to specific distortions. The correlation lengths and elastic constants associated with certain distortional modes of the director in the DML bilayer are expected to change upon addition of chl *a*. $T_{1\rho}^{-1}$ and T_2^{-1} measurements may be used to identify the changes in elastic constants and cooperative lengths induced by the addition of chl *a*. By characterizing these changes in a relatively simple mixed lipid bilayer system such as chl *a* in DML, a strong foundation is laid to support subsequent studies of more complex protein-lipid systems.

EXPERIMENTAL SECTION

I. *Materials and Methods*

Chl *a*/DML samples were prepared as described in Chapter 3. All experiments were done at 30°C. This temperature is well above the gel-to-liquid crystalline phase transition of pure DML.

II. *Instrumentation*

Relaxation experiments were conducted on a Bruker WM 500 spectrometer. For T_1 and T_2 experiments, the transmitter pulse was attenuated and used to drive an Amplifier Research 200L amplifier. The amplified pulse was then fed into a home built high power deuterium probe. This arrangement provided a 3.5 μs 90° pulse. For $T_1\rho$ experiments, the pulse was fed directly from the transmitter driver into the high power amplifier. This was necessary because the spectrometer transmitter could not sustain a pulse for the length of time required in $T_1\rho$ spin-

locking. To avoid sample heating, the amplifier was run at a maximum power of 100 Watts. This provided a 90° pulse of 8.5 μs corresponding to a spin-locking frequency of approximately 25 KHz.

III. *Pulse Sequences*

A two dimensional deuterium pulse sequence, developed by Mueller et al. was used to measure T_2.[5] A diagram of this pulse sequence is shown below:

$$90_x - t_1/4 - 180_x - t_1/4 - 90_y - t_1/4 - 180_x - t_1/4 - \text{acquire}$$

The first central 180_x pulse is included to refocus resonant offset at the time of the 90_y solid echo pulse.[21] For longer t_1 values, even a small offset of the carrier frequency from the center of the ^2H powder pattern may interfere significantly with formation of the solid echo.

Deuterium T_1's were measured by the inversion-recovery technique using a composite 180° pulse followed by a solid echo 'read' sequence. A refocussing delay of 30 μs was used to avoid receiver saturation. This sequence is shown below:

$$90_x - 90_y - 90_y - 90_x - \tau - 90_x - t_1 - 90_y - t_1 - \text{acquire}$$

To measure ^2H $T_{1\rho}$'s, the customary spin locking sequence was modified to include a final 90°_y pulse. This achieved the required terminal solid echo sequence. This pulse sequence is shown below:

$$90_x - (\theta)_y - t_1 - 90_y - t_1 - \text{acquire}$$

To avoid sample heating, the spin-locking pulse was limited to 1 percent of the total duty cycle.

IV. *Data Analysis*

Intensities at the 90° singularities of the deuterium powder pattern were recorded for T_1^{-1} and $T_{1\rho}^{-1}$ data and then fit to single exponential decays using an International Mathematical Statistical Library (IMSL) non-linear least squares fit subroutine (ZXSSQ). Analysis of T_2 data was carried out by performing a two dimensional transform, fitting cross-sections in the ω_1 dimension to a single Lorentzian lineshape, and finally measuring the line width at half-height. Excluding a study of the frequency dependence of T_2^{-1}, all cross-sections were taken at frequencies corresponding to the 90° singularities in the one-dimensional spectrum.

Theoretical Background

In chapter 2, an expression for $J_0(\omega)$ was derived which contained contributions from uncorrelated motions and cooperative director fluctuations in the lipid bilayer. Each uncorrelated motion was approximated as one-dimensional circular diffusion about the appropriate axis and described by a single correlation time. The correlation function for an uncorrelated motion, therefore, may be described by a single decaying exponential. In order to interpret $T_{1\rho}^{-1}$ and T_2^{-1} measurements quantitatively, the correlation function $< \delta\beta(0)\delta\beta(\tau) >$, which describes director fluctuations, must be expressed in terms of the correlation times for these fluctuations. $< \delta\beta(0)\delta\beta(\tau) >$ is equivalent to $< \delta\hat{n}(0)\delta\hat{n}(\tau)^* >$, where $\delta\hat{n}(t)$ represents

the displacement of the instantaneous director orientation at a time t. Continuum theory is used to describe the types of distortions undergone by fluctuating directors. This allows expression of $< \delta\hat{n}(0)\delta\hat{n}(t) >$ in terms of the cooperative and elastic properties of the hydrocarbon region of the bilayer.

I. *Continuum Theory of the Nematic State as Applied to Lipid Bilayers*

In order to apply continuum theory to director fluctuations, the hydrocarbon region of the lipid bilayer must be treated as a continuous, fluid medium. This approach is valid for a lipid bilayer if the correlation length for director fluctuations is much greater than the cross-sectional area of the hydrophobic portion of the lipid molecule.[4] The forces producing director fluctuations are much weaker than the intermolecular forces responsible for local alignment of the directors. As a result, directors fluctuate cooperatively, and the correlation lengths of these deformations are great. Thus, the continuum approach is valid.

Continuum theory has previously been applied to the study of director fluctuations in liquid crystals.[6–8] The types of liquid crystal phases are shown in Figure 1. In the nematic phase, molecules are oriented parallel to an average director, but no organization is observed in any other dimension. In neat smectic phases, the liquid crystals are arranged in contiguous layers.[9] Within these layers, the molecules are oriented parallel to the average director. The vector perpendicular to the surface defined by a smectic layer is defined as the layer normal. This is represented by $\hat{n}$ in Figure 1. In smectic A phase, the molecules are perpendicular to the layer normal, while the molecules are tilted with respect to the layer normal in smectic C phase. The lipid bilayer has a smectic A arrangement in the liquid crystalline phase and a smectic C arrangement in the gel phase. The continuum

Figure 1: A depiction of the (a) nematic, (b) smectic A, and (c) smectic C type liquid crystals.[9]

(a)

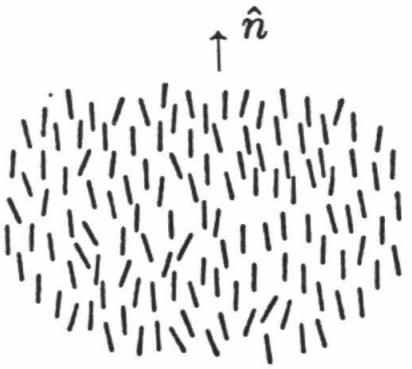

(b)

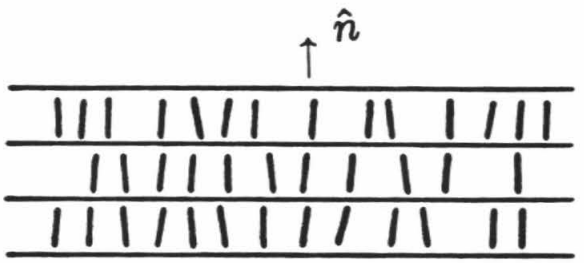

(c)

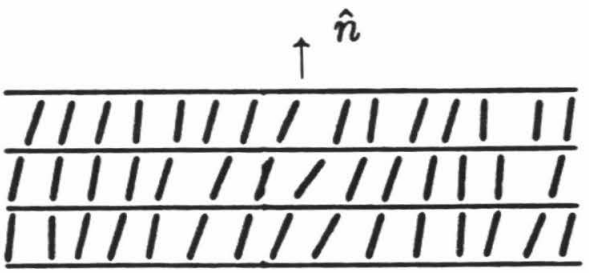

theory of the smectic phase differs from that of nematic phase in that distortions which alter the spacing of the layers are not allowed.

In excess water, lipid multilayers are separated by approximately 30 Å of water. This water may be forced out during compression of the multilayers. Hence, for lipid multilayers, distortions which alter the interlayer spacings are allowed inspite of the smectic arrangement of the bilayers.[10] For this reason, the continuum theory of the nematic state is applied to director fluctuations in lipid multilayers. The following treatment is taken from texts by de Gennes[9] and Chandrasekhar.[4]

II. *Distortions of the Lipid Bilayer*

In continuum theory, director fluctuations are treated as time-dependent, elastic deformations, which are characterized by correlation lengths and elastic constants. Splay, twist, and bend are the three deformations allowed in nematic liquid crystals and lipid bilayers. These deformations are illustrated in Figure 2 and represented mathematically below:

$$\frac{\partial n_x}{\partial x}, \frac{\partial n_y}{\partial y} \Rightarrow \text{splay} \tag{1a}$$

$$\frac{\partial n_y}{\partial x}, \frac{\partial n_x}{\partial y} \Rightarrow \text{twist} \tag{1b}$$

$$\frac{\partial n_x}{\partial z}, \frac{\partial n_y}{\partial z} \Rightarrow \text{bend} \tag{1c}$$

k_{11}, k_{22}, and k_{33} are the elastic constants associated with the splay, twist, and bend deformations, respectively. Splay and twist deformations are associated with correlated director fluctuations within a single bilayer. The correlation length for

Figure 2: Three types of deformations allowed in the bilayer according to the continuum theory of the nematic state: (a) splay, (b) twist, and (c) bend.[31]

(a)

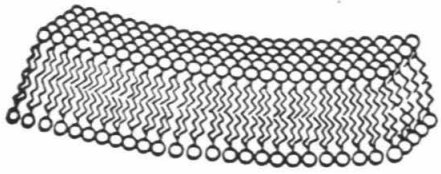

(b)

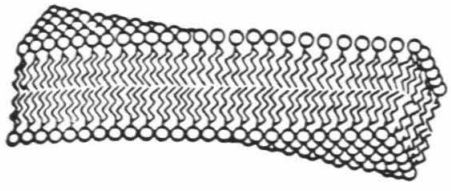

(c)

these deformations is measured in a direction perpendicular to the average director and is represented by $\lambda_\perp$. The bend deformation is associated with correlated fluctuations of directors in distinct, stacked bilayers. The correlation length associated with the bend deformation is measured in a direction parallel to the average director and is represented by $\lambda_\parallel$. Because the angular displacements of the instantaneous director were shown to be small in chapter 3, the splay, twist, and bend distortions may also be considered small. As a result, higher order derivatives of n_i may be ignored.

III. *Director Fluctuations in Wave Space*

The correlation function for director fluctuations is expressed most simply if the displacement of the director at a position $\hat{r}$ and time t is decomposed into its Fourier components in wave space. These components may be represented as follows:

$$\delta\hat{n}(\hat{q},t) = \delta\hat{n}(\hat{r},t)\exp(i\hat{q}\cdot\hat{r}) \tag{2}$$

where $\hat{q}$ is the wave vector in reciprocal space. All director fluctuations may be expressed as linear combinations of (splay + bend) and (twist + bend) terms. Each term is represented by $\delta\hat{n}_\alpha(\hat{q},t)$, where $\alpha = 1$ corresponds to a (splay + bend) deformation, and $\alpha = 2$ corresponds to a (twist + bend) deformation. The total correlation function for director fluctuations is expressed in terms of the $\delta\hat{n}_\alpha(\hat{q},t)$ as follows:

$$< \delta\hat{n}(0)\delta\hat{n}(\tau)^* >= \sum_{\alpha=1,2}\int_{\hat{q}} < \delta\hat{n}_\alpha(\hat{q},0)\delta\hat{n}_\alpha(\hat{q},\tau)^* > d\hat{q} \tag{3}$$

The elastic constant associated with each α deformation is given by:

$$k_\alpha(\hat{q}) = k_{33}q_{\|}^2 + k_{\alpha\alpha}q_{\perp}^2 \tag{4}$$

where $q_{\|} = \lambda_{\|}^{-1}$ and $q_{\perp} = \lambda_{\perp}^{-1}$.

IV. *The Time Dependence of* $\delta\hat{n}_\alpha(\hat{q},t)$

To obtain an expression for the time dependence of $\delta\hat{n}_\alpha(\hat{q},t)$, the following differential equation must be solved:

$$\frac{\partial(\delta\hat{n}_\alpha(\hat{q},t))}{\partial t} = \frac{1}{\tau_\alpha(\hat{q})}\delta\hat{n}_\alpha(\hat{q},t) \tag{5}$$

where $\tau_\alpha(\hat{q})$ is the correlation time for the particular director deformation. The solution to this standard first order differential equation is:

$$\delta\hat{n}_\alpha(\hat{q},t) = \delta\hat{n}_\alpha(\hat{q},0)\exp[-t/\tau_\alpha(\hat{q})] \tag{6}$$

For nematic liquid crystals, $\tau_\alpha(\hat{q})^{-1}$ has been characterized by light scattering techniques. Light scattered from a liquid crystalline material exhibits a Lorentzian frequency distribution. $\tau_\alpha(\hat{q})^{-1}$ may be estimated by measuring the half-height width of the frequency distribution of the scattered light. In nematic liquid crystals, $\tau_\alpha(\hat{q})^{-1}$ is found to be proportional to the elastic constant, $k_\alpha(\hat{q})$, for a given deformation and inversely proportional to the viscosity of the medium, η_α, with respect to a given deformation. This is represented as:

$$\frac{1}{\tau_\alpha(\hat{q})} = \frac{k_\alpha(\hat{q})}{\eta_\alpha} = \frac{(k_{\alpha\alpha}q_{\perp}^2 + k_{33}q_z^2)}{\eta_\alpha} \tag{7}$$

Substituting Eqns. (6) and (7) into the correlation function for a given deformation, the following expression is obtained:

$$< \delta\hat{n}_\alpha(\hat{q},0)\delta\hat{n}_\alpha(\hat{q},\tau)^* >=< \delta\hat{n}_\alpha(\hat{q},0)^2 > \exp[\frac{-\tau(k_{\alpha\alpha}q_\perp^2 + k_{33}q_z^2)}{\eta_\alpha}] \qquad (8)$$

V. *The Initial Distribution of Director Orientations*

In order to express the entire correlation function in terms of elastic constants and correlation lengths, $< \delta\hat{n}_\alpha(q,0)^2 >$ must also be expressed in terms of these variables. The average value theorem is used for this purpose, and the following expression is obtained:[11]

$$< \delta\hat{n}_\alpha(\hat{q},0)^2 >= \frac{\int_0^\infty \delta\hat{n}_\alpha(\hat{q},0)^2 \exp(-\Delta E_{\delta\hat{n}_\alpha}(\hat{q})/K_BT)d\delta\hat{n}_\alpha}{\int_0^\infty \exp(-\Delta E_{\delta\hat{n}_\alpha}(\hat{q})/K_BT)d\delta\hat{n}_\alpha} \qquad (9)$$

In the continuum theory of the nematic state, the equilibrium free energy of distortion is given by:

$$F = \frac{1}{2}k_{11}(\nabla\cdot\hat{n})^2 + \frac{1}{2}k_{22}(\hat{n}\cdot\nabla\times\hat{n})^2 + \frac{1}{2}k_{33}(\hat{n}\times\nabla\times\hat{n})^2 \qquad (10a)$$

An identical expression is used for fluctuations of directors in lipid bilayers. In wave space, the equivalent expression is:

$$\Delta E_{\delta\hat{n}_\alpha}(\hat{q}) = \frac{1}{2}\sum_\alpha k_\alpha(\hat{q})|\delta\hat{n}_\alpha(\hat{q})|^2 \qquad (10b)$$

where, in analogy to Hooke's law, $k_\alpha(\hat{q})$ is the elastic constant, and $|\delta\hat{n}_\alpha|$ is the displacement of the director from the zero position. Substituting Eqn. (10b) into Eqn. (9), the following expression is obtained:

$$< \delta\hat{n}_\alpha(\hat{q},0)^2 >= \frac{K_BT}{k_{33}q_\parallel^2 + k_{\alpha\alpha}q_\perp^2} \qquad (11)$$

VI. *Evaluation of the Total Correlation Function*

If Eqn. (11) is now substituted into Eqn. (8), the correlation function $< \delta\hat{n}_\alpha(\hat{q},0)\delta\hat{n}_\alpha(\hat{q},\tau) >$ may be expressed solely in terms of elastic constants and correlation lengths as follows:

$$< \delta\hat{n}_\alpha(\hat{q},0)\delta\hat{n}^*_\alpha(\hat{q},t) >= \frac{K_B T}{k_{33}q_{\|}^2 + k_{\alpha\alpha}q_\perp^2} \exp[\frac{-t(k_{\alpha\alpha}q_\perp^2 + k_{33}q_z^2)}{\eta_\alpha}] \qquad (12)$$

To evaluate the correlation function $< \delta\hat{n}(0)\delta\hat{n}(\tau) >$, Eqn. (12) is made use of in Eqn. (4). The following expression results:

$$< \delta\hat{n}(0)\delta\hat{n}(\tau) >= \sum_{\alpha=1,2} \int_{q_\perp^l}^{q_\perp^u} \int_{q_{\|}^l}^{q_{\|}^u} \frac{k_B T}{k_{33}q_{\|}^2 + k_{\alpha\alpha}q_\perp^2}$$

$$\times \exp[\frac{-\tau(k_{\alpha\alpha}q_\perp^2 + k_{33}q_z^2)}{\eta_\alpha}] 2\pi dq_{\|} dq_\perp \qquad (13)$$

where $q_{\|}^u = (\lambda_{//}^u)^{-1}$, $q_{\|}^l = (\lambda_{//}^l)^{-1}$, $q_\perp^u = (\lambda_\perp^u)^{-1}$, and $q_\perp^l = (\lambda_\perp^l)^{-1}$. The superscripts u and l refer to the minimum and maximum possible wave numbers, respectively for director fluctuations in a lipid bilayer.

k_{33}, $\lambda_{//}^l$, and $\lambda_{//}^u$ may be estimated from x-ray diffraction and freeze fracture electron microscopy data. Freeze fracture data show that curved, layered stacks of bilayers are present in lipid suspensions.[12] The stacks consist of six to ten lipid bilayers separated by approximately 30 Å of water. Correlations of director fluctuations in the direction parallel to the director involve the interactions of directors in neighboring bilayers of a given stack. First of all, because the stacked bilayers are separated by water, one may infer that k_{33}, the elastic constant for cooperative deformations parallel to the director, must be quite small. Secondly, $\lambda_{//}^l$, the minimum correlation length possible for cooperative deformations parallel

to the director, is the length of one bilayer. X-ray diffraction experiments show this length to be approximately 34Å for the DML bilayer in the liquid crystalline phase.[13] Finally, $\lambda^u_{//}$ may be approximated. If multilamellar structures consist of approximately six lipid bilayers, $\lambda^l_{//}$ is approximately 204Å for the DML bilayer. k_{33}, $\lambda^l_{||}$, and $\lambda^u_{||}$ are not expected to change upon addition of chl *a* to the DML bilayer.

Certain approximations may also be made concerning $k_{\alpha\alpha}$ and $\lambda^l_\perp$.[10] First of all, splay and twist deformations are both associated with correlated director fluctuations within a single bilayer. Thus, the elastic constants for the splay and twist distortions must be very similar. For simplicity, the approximation that $(k_{11} = k_{22})$=(k_{11}, k_{22}) is made. Secondly, $\lambda^l_\perp$, the minimum possible correlation length for fluctuations perpendicular to the director, must be the diameter of one lipid molecule. X-ray diffraction shows this to be approximately 4.6Å. $\lambda^l_\perp$ is also unlikely to change upon addition of chl *a* to the DML bilayer.

Two parameters remain to be determined. These are $(k_{11} = k_{22})$ and $\lambda^u_\perp$. In this work, $T^{-1}_{1\rho}$ and T^{-1}_2 are measured experimentally. Because $T^{-1}_{1\rho} \approx J_0(2\omega'_D)$ and $T^{-1}_2 \approx J_0(0)$, $T^{-1}_{1\rho}$ and T^{-1}_2 measurements yield approximate values for $J_0(0)$ and $J_0(2\omega'_D)$. Substituting Eqn. (13) into the expression for $J_0(\omega)$ which is given in Eqn. (40) of chapter 2, independent equations for $J_0(0)$ and $J_0(\omega)$ may be constructed which contain (k_{11}, k_{22}) and $\lambda^u_\perp$. By the simultaneous solution of these two equations, values for (k_{11}, k_{22}) and $\lambda^u_\perp$ may be obtained.

Many assumptions are made in these calculations. The resulting values of (k_{11}, k_{22}) and $\lambda^u_\perp$, therefore, should not be treated as absolute values. Instead, the calculated values for a mixed lipid system must be compared to calculated values for the pure lipid system. The changes in (k_{11}, k_{22}) and $\lambda^u_\perp$ which are

observed as chl *a* is added to the DML bilayer are indicative of changes in the absolute cooperative lengths and elastic constants of the DML bilayer.

In this section, an expression for $< \delta\hat{n}(0)\delta\hat{n}(\tau) >$ has been obtained. This expression depends solely on elastic and cooperative parameters describing the lipid bilayer. This correlation function may be used to evaluate the relaxation rate expressions presented in chapter 2.

Chl *a* is positioned in a DML bilayer with its porphyrin head group in the polar region of the bilayer and its phytol chain in the hydrophobic region. The director fluctuations which show correlation within the bilayer, therefore, should be most sensitive to the addition of chl *a*. Because $\lambda_{\perp}^{u}$ and (k_{11}, k_{22}) involve correlated director fluctuations within a single bilayer, these parameters are of interest in the chl *a* /DML system.

The changes in $\lambda_{\perp}^{u}$ and (k_{11}, k_{22}) as chl *a* is added to the DML bilayer will be traced using $T_{1\rho}^{-1}$ and T_2^{-1} measurements. Certain correlation lengths and elastic constants for pure DML and chl *a* /DML bilayers have been approximated using freeze fracture and x-ray diffraction data. Using $T_{1\rho}^{-1}$ and T_2^{-1} measurements in addition to these approximations, an evaluation of the relaxation rate equations for $T_{1\rho}^{-1}$ and T_2^{-1} yields estimates of $\lambda_{\perp}^{u}$ and (k_{11}, k_{22}) .

Results

Figure 3 shows representative one dimensional traces at several delays in the T_1^{-1} , $T_{1\rho}^{-1}$, and T_2^{-1} experiments, respectively. At all chl *a* concentrations, only one spectral component was observed. This is in agreement with most NMR

Figure 3: Spectral traces of the 10.1 mol % chl *a* samples at various delay times for each ofthe relaxation experiments. The pulse sequences are as described in the text. For all experiments, the ^{2}H frequency is 76 MHz, the dwell time is 3μs, and the repetition rate is at least 0.5 s. The temperature is 30° for each experiment. (a) A series of T_1 traces. The number of scans taken is 4096. The delay time for each trace is shown at the right. (b) A series of $T_{1\rho}$ traces. The number of scans taken is 2184. Each trace is labelled at the right by the delay time. (c) A series of T_2 traces. The number of scans taken is 2016. These traces correspond to cross-sections in the ω_2 dimension of a doubly transformed experiment. Delay times are given at the right.

(a)

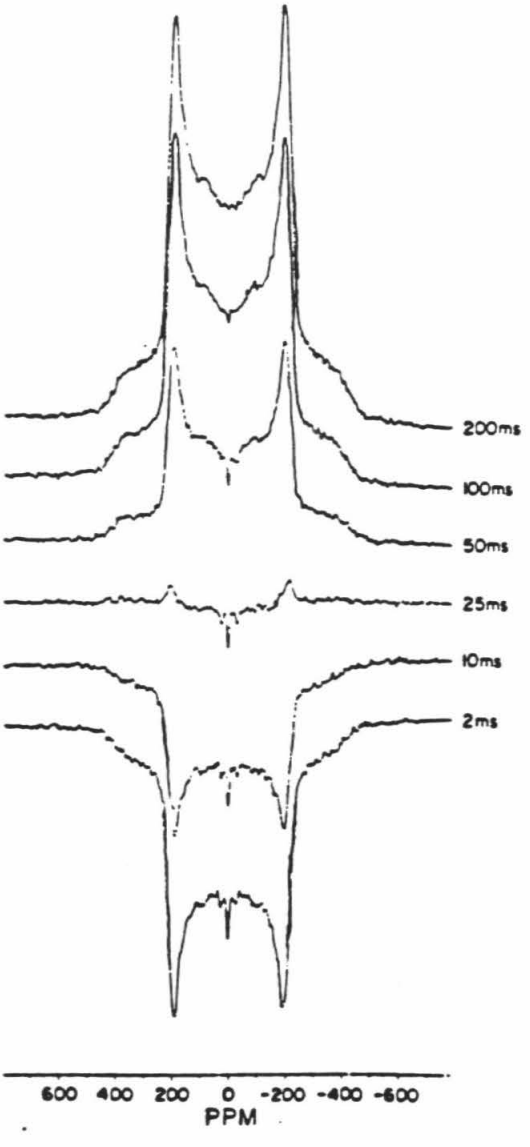

(b)

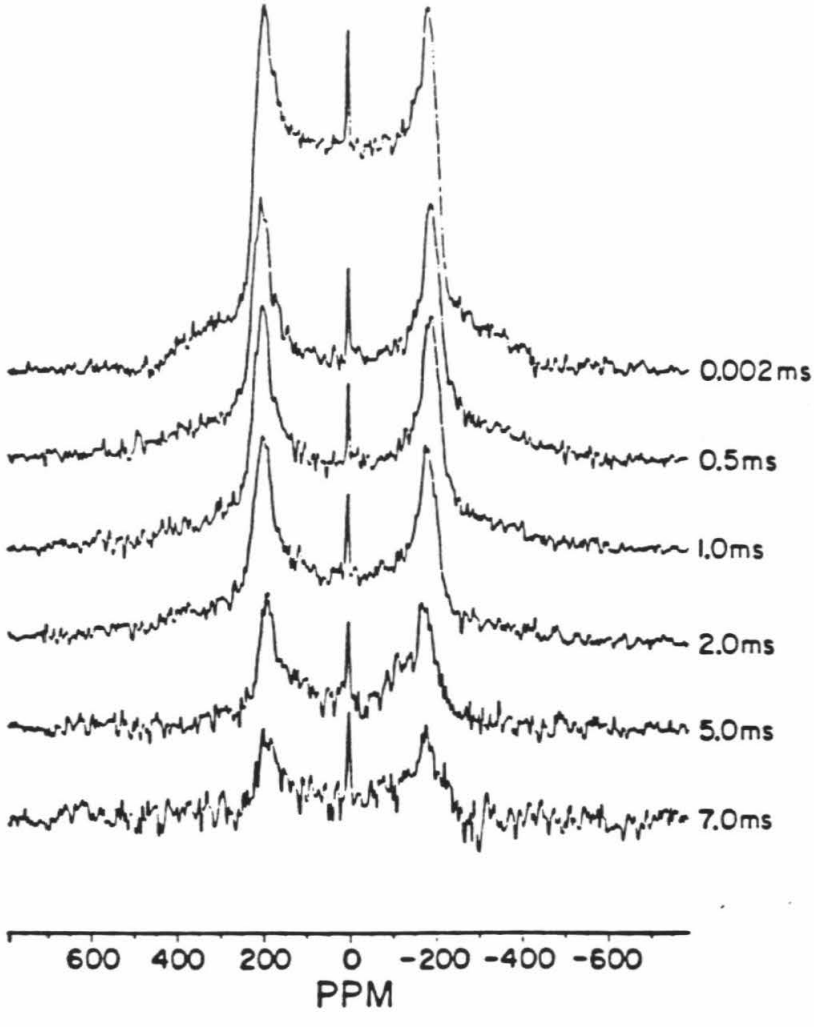

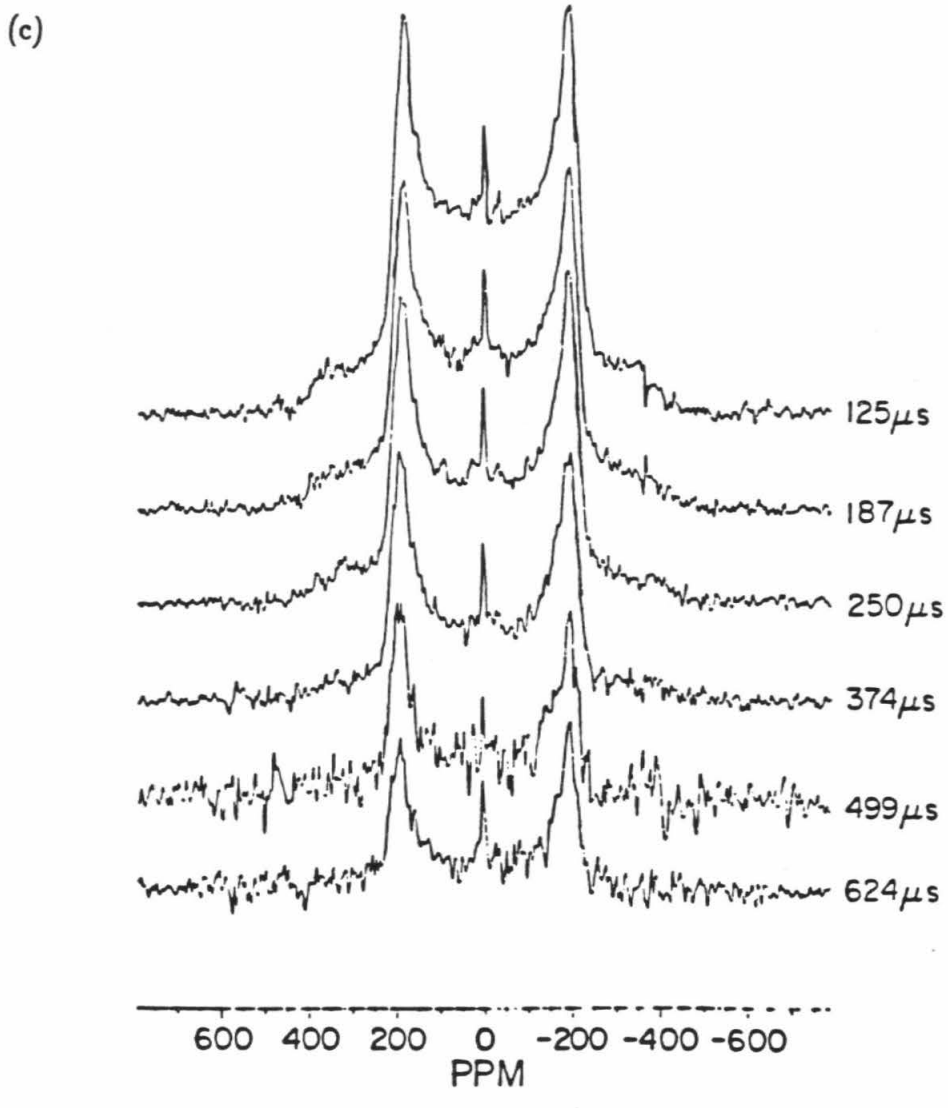
(c)
125μs
187μs
250μs
374μs
499μs
624μs
600 400 200 0 -200 -400 -600
PPM

experiments of protein/lecithin and chl *a* /lecithin bilayer systems above the gel-to-liquid crystalline phase transition temperature.[14–17] In contrast, several researchers have presented ESR results as evidence for the existence of more than one lecithin environment in protein-lecithin systems.[18–20] Because the NMR timescale is approximately three orders of magnitude slower than that of ESR, results from these two techniques may be reconciled by invoking an exchange rate between sites which is slow on the ESR timescale, and yet fast on the NMR timescale. Alternatively, by performing detailed spectral simulations of both lipid dispersions and aligned lipids, Freed et al. have shown that ESR spectra of protein-lipid systems may be quite accurately reproduced using a single site model involving microscopic order and macroscopic disorder (MOMD). According to their model, the lipid molecules are treated as undergoing anisotropic motion of a single mean rotational correlation time in well-aligned domains.[21] Either rationalization of the discrepancy between the ESR and NMR results, however, indicates that the relaxation rates obtained from the NMR experiments are best approximated by single exponentials. Representative fits of the data to single exponentials are shown in Figure 4. Although multiple measurements show the uncertainties in T_1 measurements to be on the order of 1 % and the uncertainties in the $T_{1\rho}$ and T_2 values to be on the order of 10%, the uncertainties calculated by the fitting routine were much smaller.

Figure 5 shows the dependence of T_1^{-1} , $T_{1\rho}^{-1}$, and T_2^{-1} of 9,10-DML on chl *a* concentration. As the concentration of chl *a* is increased, T_1^{-1} remains virtually unaffected. This is true even at 28 mole percent chl *a*, where there is approximately one chl *a* molecule to every three lipid molecules. The behaviors of $T_{1\rho}^{-1}$ and T_2^{-1}, however, are significantly affected by the addition of chl *a*.

Figure 4: Representative fits for the various experimental relaxation measurements. (a) A T_1 fit of the 4.7 mol % chl *a* sample. The calculated T_1 relaxation time is 42.6±0.3 ms. (b) A fit of the $T_{1\rho}$ decay for the 17.9 mol % chl *a* sample. The calculated relaxation time is 3.3±0.2ms. (c) A fit of a cross-sectional line width obtained from the two-dimensional T_2 experiment for the 28 mol % chl *a* sample. The $\frac{1}{\pi T_2}$ value obtained is 5.45±0.06 ppm.

(a)

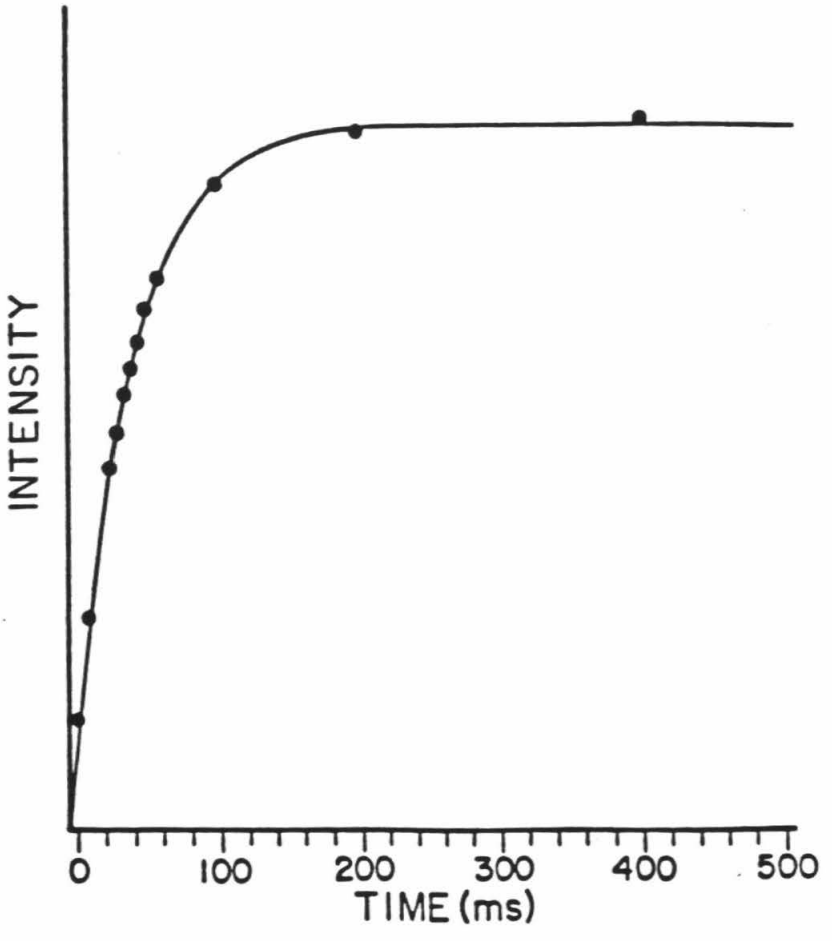

(b)

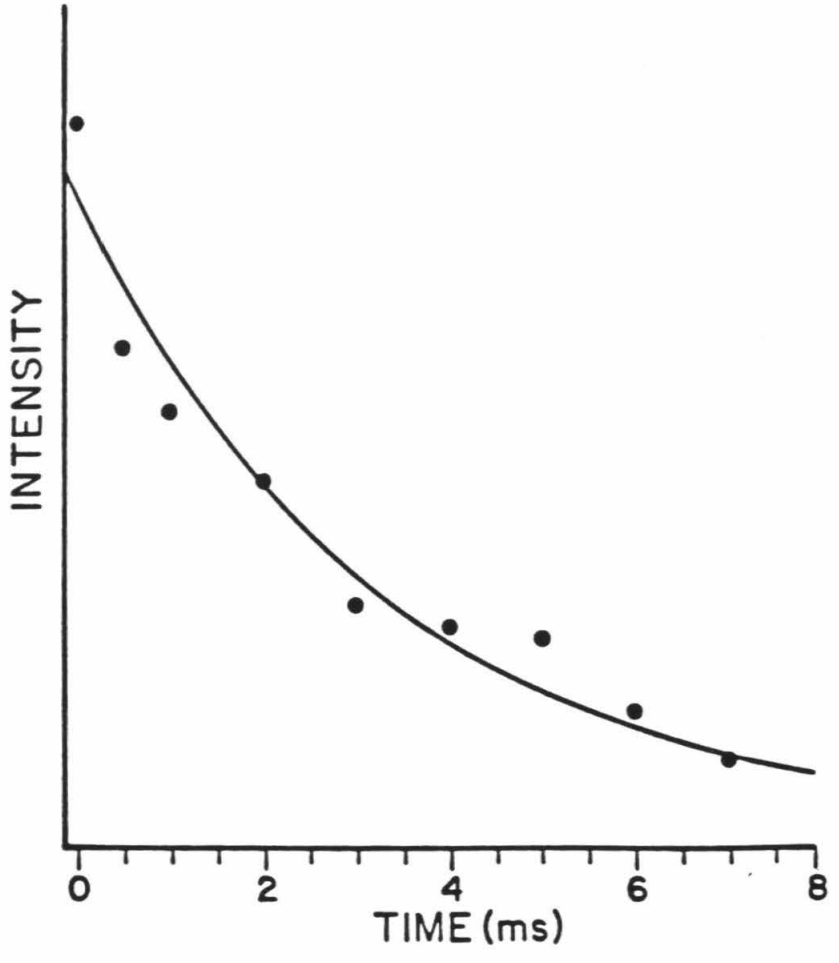

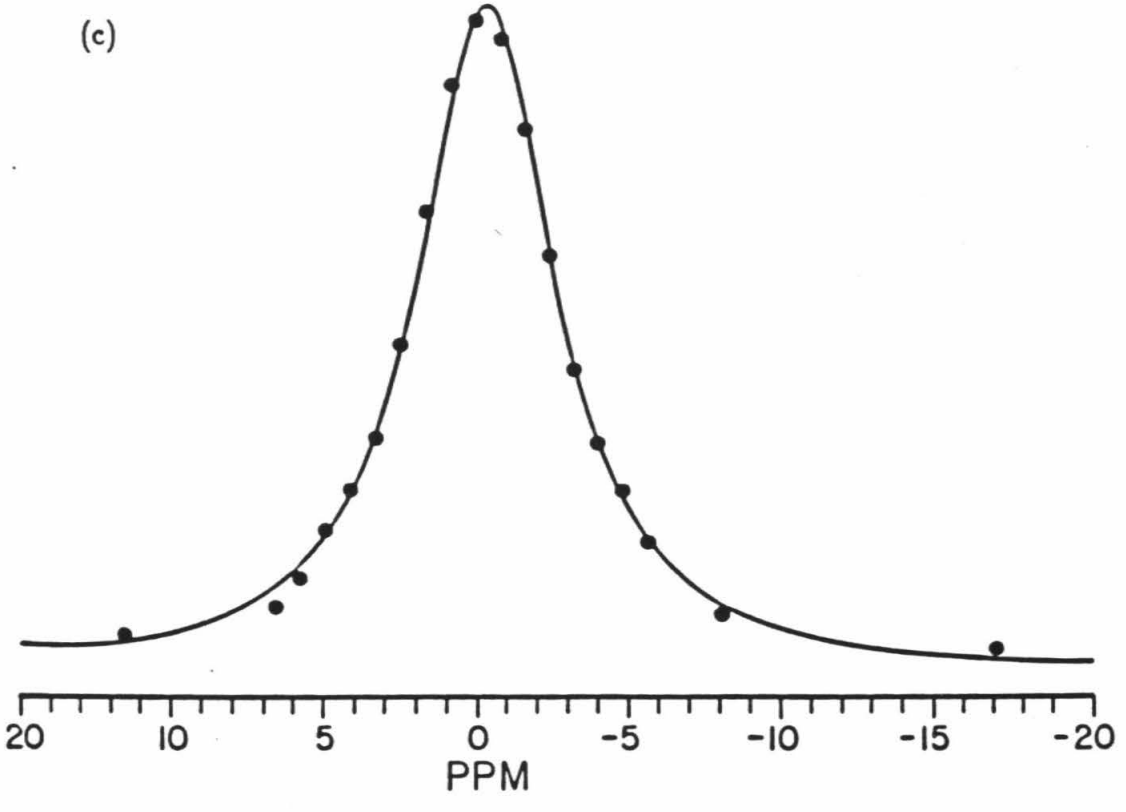
(c)
20
10
5
0
-5
-10
-15
-20
PPM

Figure 5: The relaxation rates measured for various chl *a* concentrations. The relaxation rates are represented by the following symbols, respectively: ■ : $1/T_1$, ▲: $1/T_{1\rho}$, and ● :$1/T_2$. All rates were measured at the 90° singularities of the ^{2}H-NMR spectra.

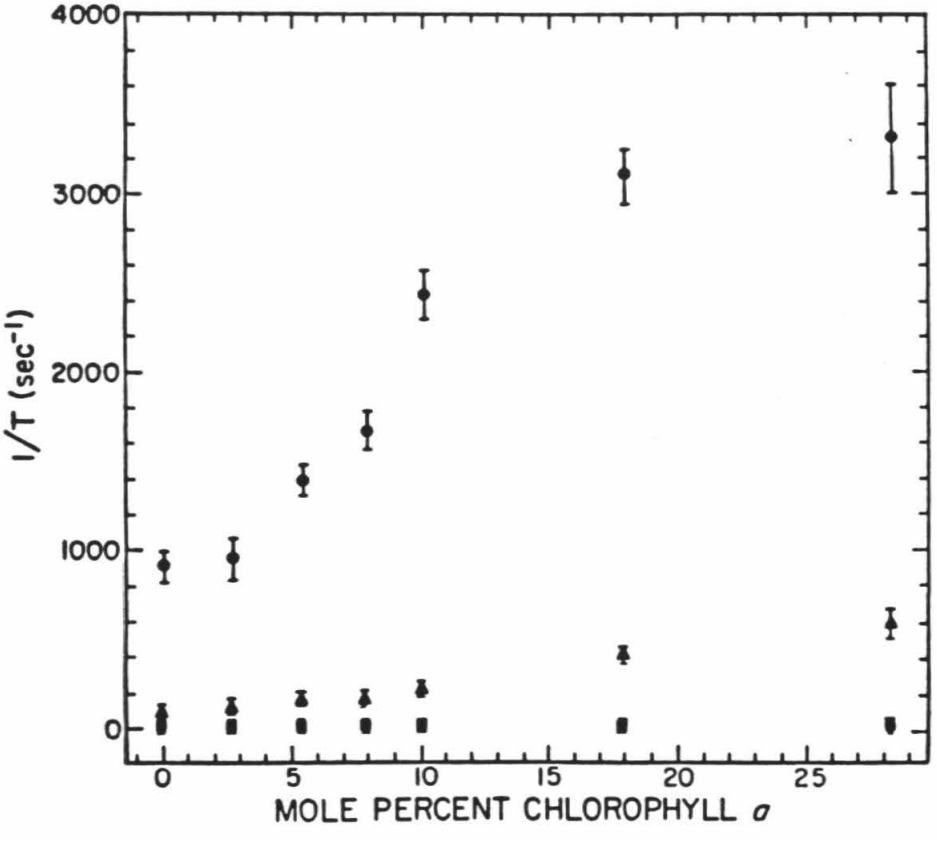
4000
3000
2000
1000
0
1/T (sec⁻¹)
0
5
10
15
20
25
MOLE PERCENT CHLOROPHYLL a

In these calculations, it is assumed that both lateral diffusion coefficients and the distribution of liposome sizes in multilamellar DML suspensions do not vary with chl *a* content. To demonstrate the validity of this assumption, T_2^{-1} 's at several positions in the deuterium powder pattern have been measured for all concentrations of chl *a*. The dependence of T_2^{-1} on resonant frequency or, equivalently, on β, the angle the average director makes with respect to the magnetic field, is a direct indication of the amount of averaging taking place as a result of diffusion of the lipid molecule. In Figure 6, the dependence of T_2^{-1} on resonant frequency is shown for several concentrations of chl *a*. For 0.0 and 2.5 mol % chl *a*, there is a slight increase in frequency dependence which subsequently remains constant. It is clear that the rate of angular lipid diffusion does not increase upon addition of chl *a*. Furthermore, the change in the rate of angular displacement of the DML moleules as chl *a* is added to the lipid bilayer is small.

DISCUSSION

In order to quantitate the apparent differences in behavior between T_1^{-1}, $T_{1\rho}^{-1}$, and T_2^{-1}, the explicit relaxation rate equations for the deuterium nucleus must be examined. As mentioned previously, spectral densities at several frequencies contribute to T_1^{-1}, $T_{1\rho}^{-1}$, and T_2^{-1}. $T_{1\rho}^{-1}$ and T_2^{-1} are expected to be most sensitive to slow motions since they include $J_0(2\omega_D')$ and $J_0(0)$, respectively. The relaxation rate measurements shown in Figure 5, then, demonstrate unequivocally that very slow motional modes are either newly excited or enhanced by the addition of chl *a*. $T_{1\rho}^{-1}$ is sensitive to motional frequencies around 50 KHz, while T_2^{-1} is sensitive

Figure 6: The dependence of line width on spectral frequency. The following mole percents of chl *a* correspond to the illustrated symbols:□:0.0, ✱:2.7, ✕:4.7, ○:10.1, and +:28.0.

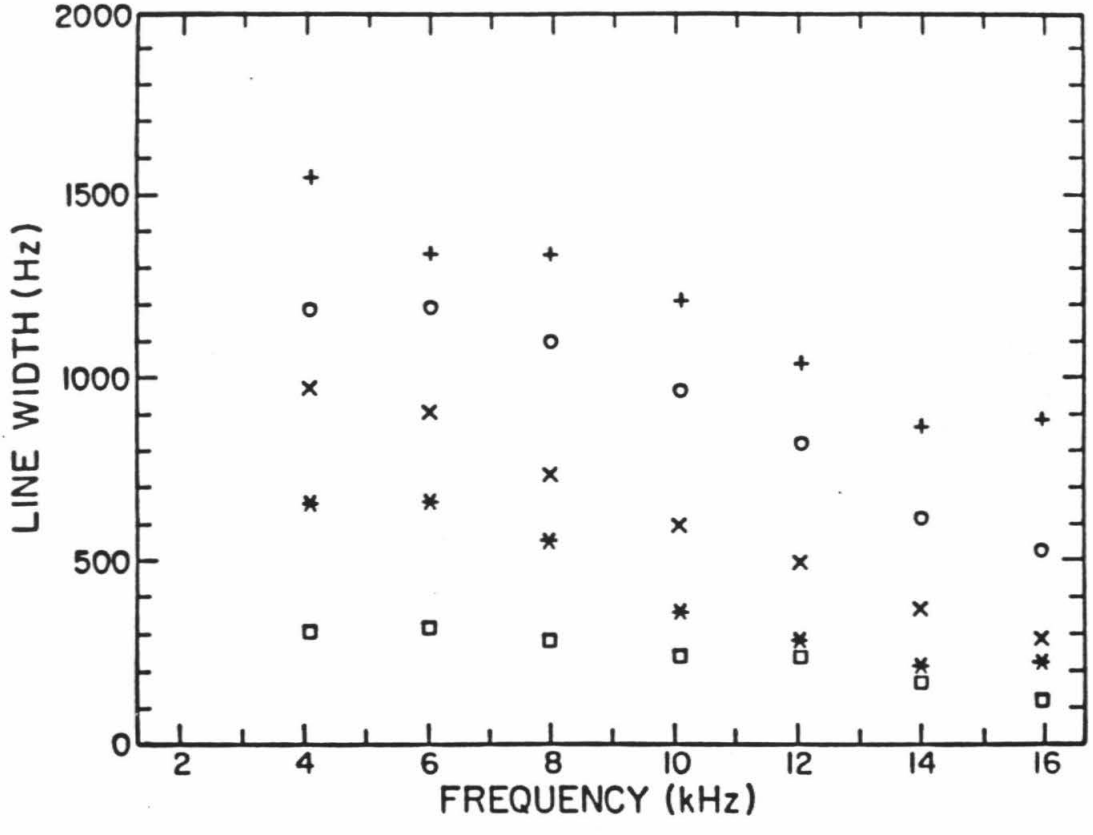
2000
1500
1000
500
0
LINE WIDTH (Hz)
2
4
6
8
10
12
14
16
FREQUENCY (kHz)

to motional frequencies around zero KHz. Since the addition of chl *a* to the DML bilayer produces a much greater increase in T_1^{-1} than in $T_{1\rho}^{-1}$, chl *a* must preferentially enhance motional frequencies in the DML bilayer which are much less than 50 KHz.

I. $J_1(\omega_D)$,$J_2(2\omega_D)$

It is possible to estimate the contribution of $J_1(\omega_D)$ and $J_2(2\omega_D)$ to $T_{1\rho}^{-1}$ and T_2^{-1}. Temperature dependence studies show that motions contributing to T_1^{-1} at higher frequencies are in the extreme narrowing regime.[22] In this case, $J_1(\omega_D) \approx J_2(2\omega_D)$. The collective contribution of $J_1(\omega_D)$ and $J_2(2\omega_D)$ to each of the relaxation rates $T_{1\rho}^{-1}$ and T_2^{-1} is 16.8 sec^{-1}. A comparison of this value with $T_{1\rho}^{-1}$ and T_2^{-1} measurements show the contributions of $J_1(\omega_D)$ and $J_2(2\omega_D)$ to be negligible in comparison with $J_0(2\omega'_D)$ and $J_0(0)$.

II. $J_0(2\omega'_D)$,$J_0(0)$

Several types of fluctuations experienced by a C-D bond vector in the hydrocarbon region of a lipid bilayer may contribute to $J_0(0)$ and $J_0(2\omega'_D)$. To determine which of these contributions is significant, the frequency of each type of motion must be calculated. The motions to be considered are rotations of the C-D bond about the long axis of the lipid molecule, diffusion of lipid molecules through lateral movement within the bilayer as well as rotation of the entire liposome, and cooperative director fluctuations.

C-D Bond Rotation

Motions on the timescale of 10^{-10} to $10^{-11}sec^{-1}$, recorded by several re-

searchers, have been attributed to C-D bond rotations.[23–25] Because this motion is in the extreme narrowing regime, its contribution to $J_0(0)$ and $J_0(2\omega'_D)$ must be comparable to its contribution to $J_1(\omega_D)$ and $J_2(2\omega_D)$. Since it has been shown that $J_1(\omega_D)$ and $J_2(2\omega_D)$ are themselves very small in comparison with $J_0(0)$ and $J_0(2\omega'_D)$, the contribution of bond rotation to $J_0(0)$ and $J_0(2\omega'_D)$ must also be negligible.

Diffusion

In chapter 3, a correlation time of approximately 3.15 msec was calculated for the angular diffusion of lipid molecules in a liposome. Although the rate of lateral diffusion is too slow to contribute to $J_0(0)$ and $J_0(2\omega'_D)$, it does alter the T_2^{-1} measurement through motional broadening. Lateral diffusion has been identified as the origin of approximately 1/3 of the T_2^{-1} measured for the pure 9,10-DML bilayer.

Because the rate of lateral diffusion is not altered by addition of chl *a* to the DML bilayer, the contribution of lateral diffusion to $J_0(0)$ is also expected to remain constant as chl *a* is added to the bilayer. Lateral diffusion, therefore, simply results in a constant offset in T_2^{-1} and does not cause the increase in T_2^{-1} which is observed as chl *a* is added to the 9,10-DML bilayer.

Director Fluctuations

The contribution of director fluctuations to $J_0(2\omega'_D)$ and $J_0(0)$ may be estimated using Eqn. (13). By approximating η_α, (k_{11}, k_{22}) and $\lambda_\perp^u$, it is possible to calculate the range of correlation times for director fluctuations and the total contribution to $J_0(2\omega'_D)$ and $J_0(0)$. η_1 and η_2, the microviscosities of the splay and

twist modes of a lipid bilayer, have each previously been estimated by Pace and Chan to be 1 Poise in the liquid crystalline phase.[26] In nematic liquid crystals, k_{11} and k_{22} are on the order of 10^{-6} dynes.[9] In lipid bilayers, these elastic constants are assumed to be similar to those in nematic liquid crystals, or $4.3\text{x}10^{-6}$ dynes.

If $\lambda_{\perp}^{u}$ is taken to be 9,000 Å, the calculated contributions of director fluctuations to $T_{1\rho}^{-1}$ and T_2^{-1} are 91 sec^{-1} and 903 sec^{-1}, respectively. These values match the experimental values of 90 sec^{-1} and 909 sec^{-1} quite well. Using these estimated parameters in Eqn. (7), inverse correlation times ranging from $1.7\text{x}10^{-11}$ sec^{-1} to $1.9\text{x}10^{-3}$ sec^{-1} are obtained.

Director fluctuations exhibit a range of correlation times and correlation lengths. Some director fluctuations have very long correlation lengths and correlation times. The correlation function for director fluctuations expressed in Eqn. (13) includes an integration over $\lambda_{\perp}$. As the variable of integration, $\lambda_{\perp}$ may take on a wide range of values. Thus, the value of this integral is quite large, and director fluctuations swamp contributions to $J_0(0)$ and $J_0(2\omega_D')$ from any type of diffusive or rotational motion. Thus, order director fluctuations are the primary contributors to $T_{1\rho}^{-1}$ and T_2^{-1} .

III. *The Calculation of* (k_{11}, k_{22}) *and* $\lambda_{\perp}^{u}$ *for Chl a /DML Bilayers*

In the following calculations, experimental $T_{1\rho}^{-1}$ and T_2^{-1} rates have been reproduced by varying $\lambda_{\perp}^{u}$ as well as (k_{11}, k_{22}). To illustrate the variation of relaxation rates with (k_{11}, k_{22}) and $\lambda_{\perp}^{u}$, calculated relaxation rates have been plotted against each of these parameters in Figure 7. Figures 7a and 7b show the calculated change in $T_{1\rho}^{-1}$ and T_2^{-1} , respectively, as (k_{11}, k_{22}) are varied. $\lambda_{\perp}^{u}$ is held constant at 9,000 Angstroms, and all other parameters are as stated above.

Figure 7: Plots of $1/T_{1\rho}$ and $1/T_2$ vs. (k_{11}, k_{22}) and $\lambda_{\perp}^{u}$. Values have been calculated using a model of fluctuating directors. In all calculations, the following values have been used:η=1 P, T=30°K, $k_{33} \approx 0$, $\lambda_{//}^{u}$ =60Å, $\lambda_{//}^{l}$ =360Å, and $\lambda_{\perp}^{l}$ =5.3Å. (a) The dependence of $1/T_{1\rho}$ on (k_{11}, k_{22}). In this calculation, $\lambda_{\perp}^{u}$ is held constant at 9000Å. (b) The dependence of $1/T_2$ on (k_{11}, k_{22}). (k_{11}, k_{22}) and $\lambda_{\perp}^{u}$ are treated as in (a). (c) The dependence of $1/T_{1\rho}$ on $\lambda_{\perp}^{u}$. In this calculation, (k_{11}, k_{22}) is held constant at 1×10^{-6} dyn. (d) The dependence of $1/T_2$ on $\lambda_{\perp}^{u}$. (k_{11}, k_{22}) are treated as in (c).

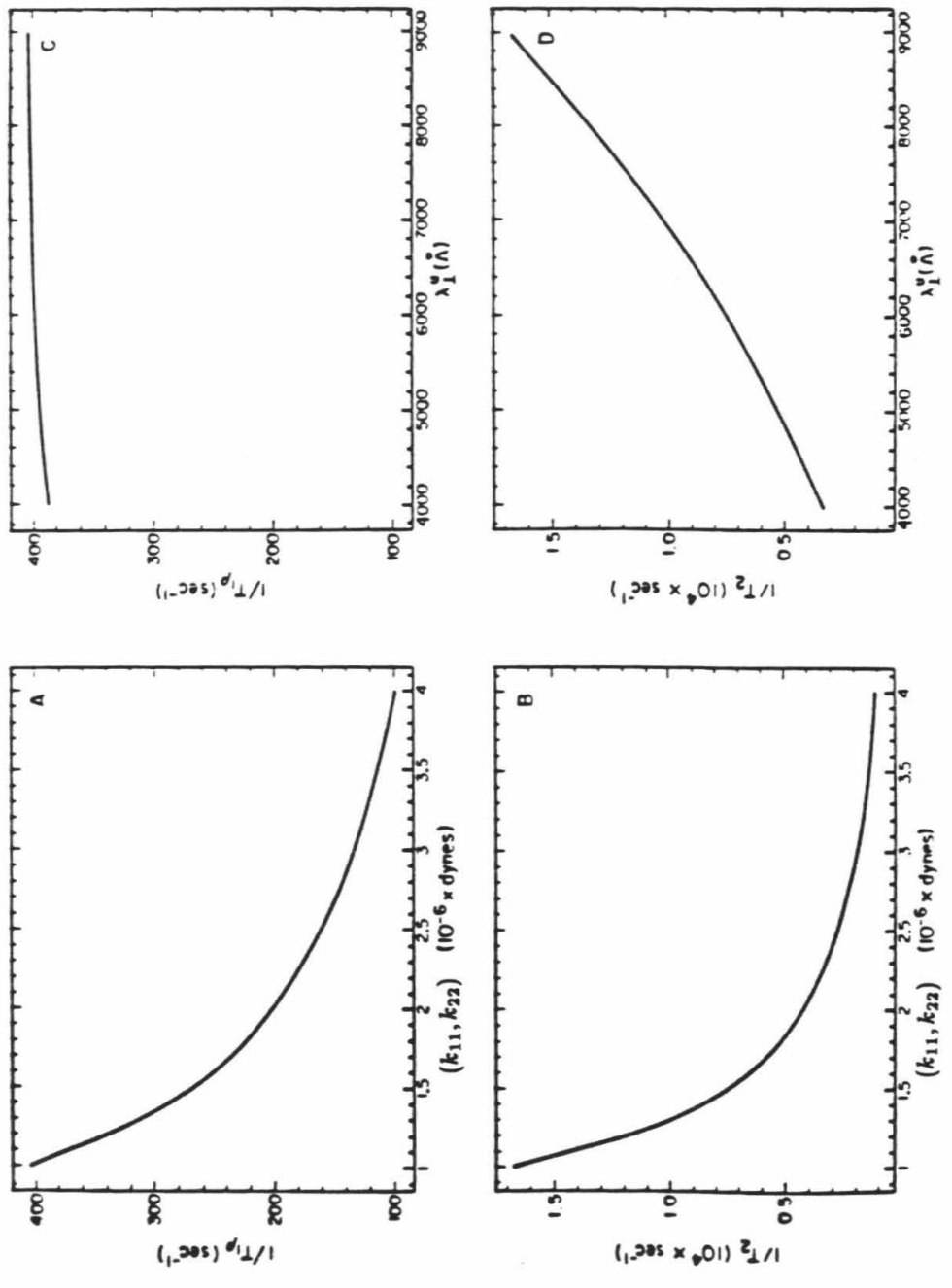
A
B
C
D
$1/T_{1\rho}$ (sec^{-1})
$1/T_2$ (10^4 × sec^{-1})
(k_{11}, k_{22}) (10^{-6} × dynes)
λ^{-1} (Å^{-1})

Figures 7c and 7d show calculated $T_{1\rho}^{-1}$ and T_2^{-1} values, respectively, plotted against $\lambda_\perp^u$. (k_{11}, k_{22}) is fixed at $1x10^{-6}$ dynes.

A decrease in (k_{11}, k_{22}) increases the calculated $T_{1\rho}^{-1}$ and T_2^{-1} substantially. An increase or decrease in upper cutoff , however, affects T_2^{-1} much more drastically than $T_{1\rho}^{-1}$. In these calculations, $T_{1\rho}^{-1}$ has been matched by varying (k_{11}, k_{22}). Subsequently, T_2^{-1} has been brought into the appropriate range by adjusting $\lambda_\perp^u$. In all cases, experimental and calculated rates have been brought to within a few inverse seconds of each other. Figures 8 and 9 show the calculated $\lambda_\perp^u$ and (k_{11}, k_{22}), respectively, for each concentration of chl *a*. There is a decrease in both $\lambda_\perp^u$ and (k_{11}, k_{22}) with increasing chl *a* content. This trend, however, is reversed for very high chl *a* content. In addition, for each concentration of chl *a*, the τ_α^{-1} associated with $\lambda_\perp^u$ is shown in Figure 10.

Further Discussion

In the chl *a* /lecithin bilayer, the phytol chain of chl *a* is embedded in the hydrophobic portion of the bilayer, while the prophyrin ring protrudes into the hydrophilic region. DSC experiments indicate that chl *a* is homogeneously distributed in the DML bilayer.[27] Circular dichroism measurements of chl *a* in lecithin bilayers have shown that the porphyrin ring is inclined at an angle of 45°-55° with respect to the bilayer normal.[28] The Mg^{+2} atom in the porphyrin ring of chl *a* has been shown to coordinate a fifth and possibly a sixth ligand.[29] In chl *a* /lecithin bilayer, ^{31}P-NMR experiments indicate that the two coordination positions of chl *a* are filled by the phosphate moiety of the lecithin head group.[30]

Figure 8: The variation of $\lambda_{\perp}^{u}$ in DML systems of several chl *a* contents.

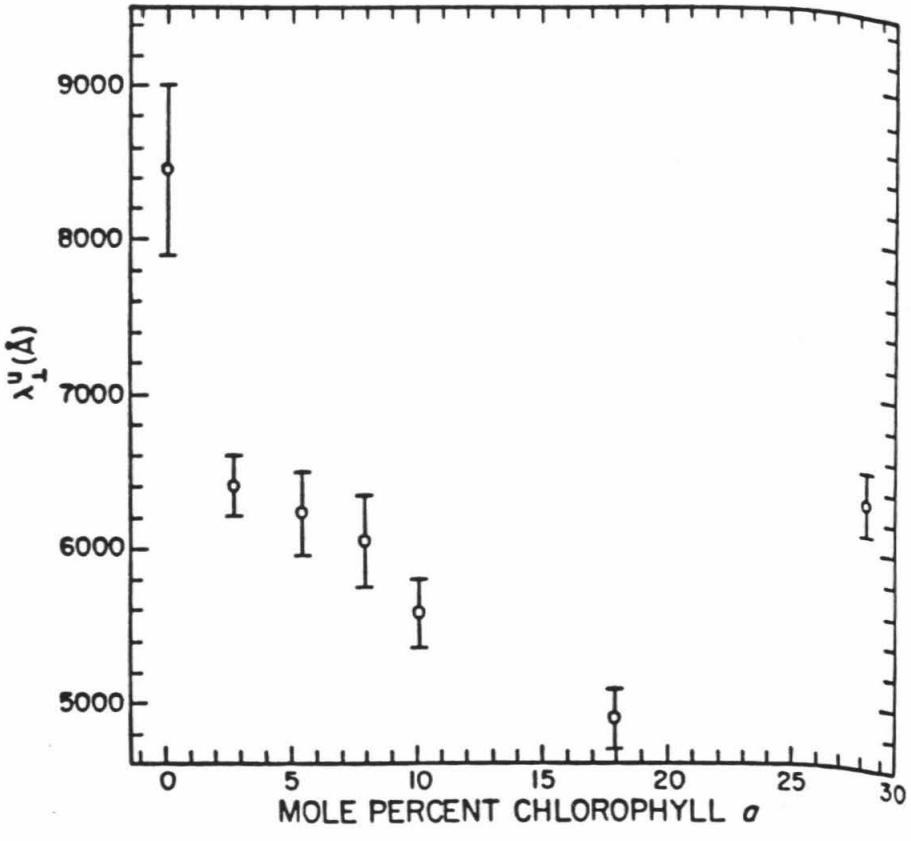
9000
8000
7000
6000
5000
$\lambda_{\perp}^{u}$(Å)
0
5
10
15
20
25
30
MOLE PERCENT CHLOROPHYLL *a*

Figure 9: The dependence of (k_{11}, k_{22}) on chl *a* concentration.

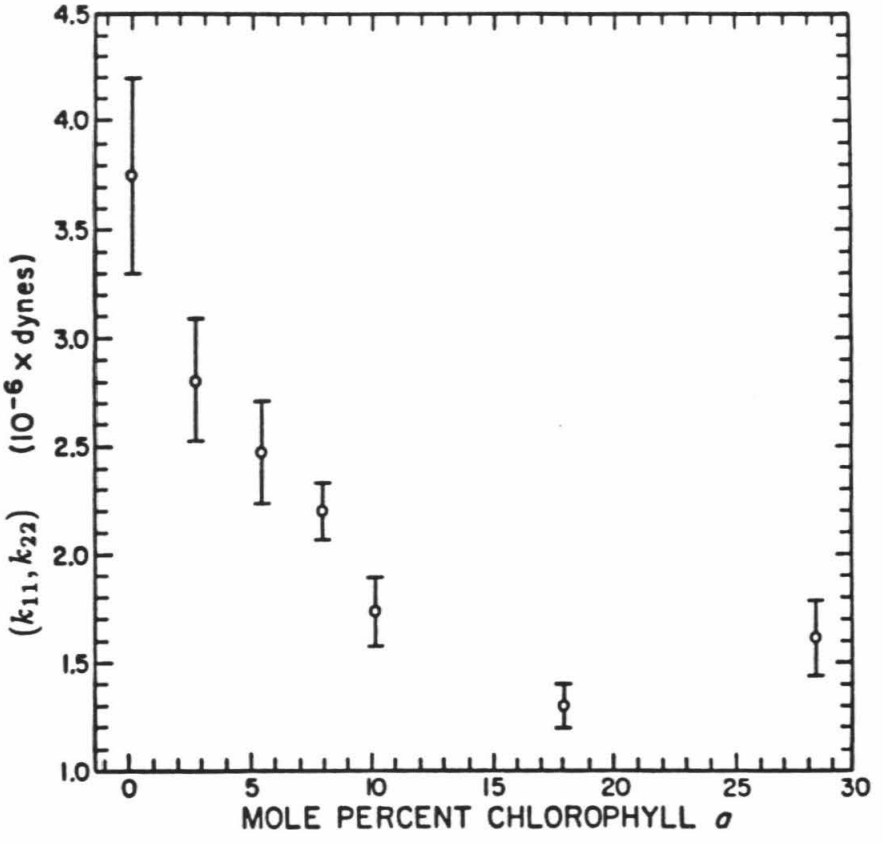
4.5
4.0
3.5
3.0
2.5
2.0
1.5
1.0
(k_{11}, k_{22}) $(10^{-6} \times \text{dynes})$
0
5
10
15
20
25
30
MOLE PERCENT CHLOROPHYLL *a*

Figure 10: The variation of τ_α^{-1} with chl *a* concentration. The calculated correlation times are associated with motions having $\lambda_\perp^u$ and (k_{11}, k_{22}) as graphed in Figures 8 and 9.

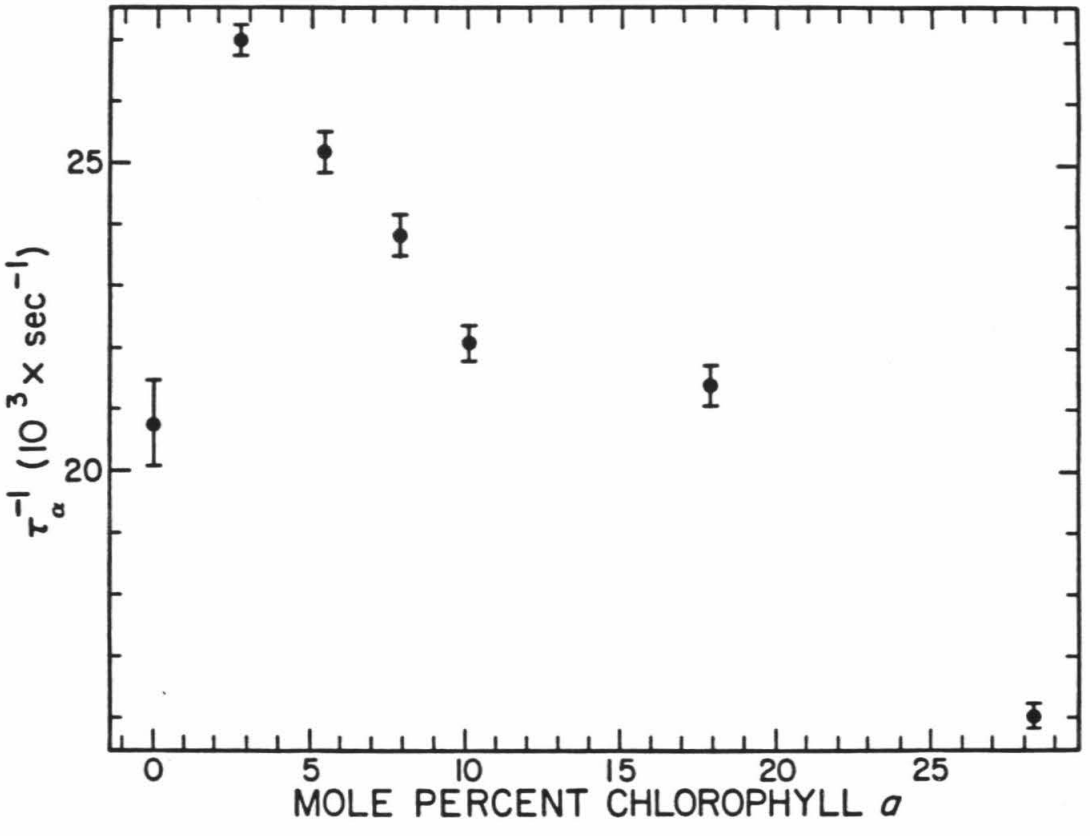
25
20
τ_α^{-1} ($10^3 \times sec^{-1}$)
0
5
10
15
20
25
MOLE PERCENT CHLOROPHYLL *a*

The geometry of the chl *a* molecule may explain the effect of chl *a* on the cooperative and elastic properties of the DML bilayer. The chl *a* molecule is composed of a bulky porphyrin group attached to a single phytol chain. The diameter of the porphyrin group is slightly larger than that of a DML molecule in a bilayer. The diameter of the phytol chain, however, is approximately half that of a DML molecule. When the porphyrin ring inserts into the hydrophilic region of the DML bilayer, it creates a space in the hydrophobic region of the bilayer which the phytol chain is unable to fill completely. The acyl chains of DML, therefore, must expand to fill these voids. As a result, the steric and van der Waals interactions between chains, which lead to cooperative director motion, are weakened. Thus, the elastic constants associated with correlated director fluctuations become smaller, and the distance over which these correlated motions extend is also decreased.

As the concentration of chl *a* is increased, interactions between chl *a* molecules become significant. The tilted porphyrin rings approach each other and may stack in order to minimize the exposure of the underlying hydrocarbon chains to the aqueous environment. As a result, lipid acyl chains again approach each other closely, and the cooperativity of phytol and acyl chain motion increases. Thus, a rise in the correlation lengths and elastic constants for director fluctuations is observed at high concentrations of chl *a* in the DML bilayer.

CONCLUSIONS

Director fluctuations in the pure DML bilayer are highly cooperative. If

liposomes in a multilamellar suspension are on the order of 10,000 Angstroms in diameter, then these fluctuations encompass approximately one third of the liposome. As small amounts of chl *a* are added to the bilayer, the correlation length for director fluctuations decreases rapidly. Chl *a*, therefore, impedes the propagation of director fluctuations in the lipid bilayer. As more chl *a* is added to the bilayer, however, the cooperative distance levels off and eventually begins to increase again.

(k_{11}, k_{22}) has been measured for chl *a* /DML bilayers. The value obtained is in agreement with the (k_{11}, k_{22}) value measured for nematic liquid crystals. The changes seen in (k_{11}, k_{22}) upon addition of chl *a* to the DML bilayer parallel those observed for the cooperative length of director fluctuations. At low chl *a* concentrations, a sharp decrease in (k_{11}, k_{22}) is seen, indicating that the chl *a* is disrupting interactions between the hydrocarbon chains. At the highest concentration of chl *a*, however, only a slight increase (k_{11}, k_{22}) is observed.

It is suggested that at low concentrations of chl *a* in the DML bilayer, chl *a* increases the spacing of the DML acyl chains. As a result, the forces leading to cooperative motion are weakened, and the elastic constants and the correlation lengths for director fluctuations decrease. At high concentrations of chl *a*, the porphyrin rings of the chl *a* molecules may stack. This results in more efficient packing of the hydrocarbon chains in the bilayer. At high chl *a* concentrations, therefore, the correlation lengths and elastic constants describing director fluctuations increase.

In conclusion, $T_{1\rho}^{-1}$ and T_2^{-1} measurements may be used in conjunction with the continuum theory of nematic liquid crystals to determine the changes in the elastic properties of a lipid bilayer upon addition of another lipid or protein.

References

1. D. Rice and E. Oldfield, *Biochemistry*, **18**, 3272-3279 (1979).
2. B. A. Cornell, R. G. Hiller, J. Raison, F. Separovic, R. Smith, J. C. Vary, and C. Morris, *Biochim. Biophys. Acta*, **732**, 473-478 (1983).
3. P. F. Devaux, G. L. Hoatson, E. Favre, P. Fellmann, B. Farren, A. L. Mackay, and M. Bloom, *Biochemistry*, **25**, 3804-3812 (1986).
4. S. Chandrasekhar, **Liquid Crystals**, (Cambridge University Press, New York, 1977).
5. L. Mueller and S. I. Chan, *J. Chem. Phys.*, **78**, 4341-4348 (1983).
6. J. W. Doane and D. L. Johnson, *Chem. Phys. Lett.*, **6**, 291-295 (1970).
7. J. W. Doane, C. E. Tarr, and M. A. Nickerson, *Phys. Rev. Lett.*, **33**, 620-624 (1974).
8. R. Blinc, M. Luzar, M. Vilfan, and M. Burgar, *J. Chem. Phys.*, **63**, 3445-3451 (1975).
9. P. G. de Gennes, **The Physics of Liquid Crystals**, (Oxford University Press, New York, 1974).
10. R. J. Pace and S. I. Chan, *J. Chem. Phys.*, **76**, 4228-4240 (1982).
11. P. W. Atkins, **Physical Chemistry**, (W. H. Freeman and Company, San Francisco, 1978).
12. A. D. Bangham and R. W. Home, *J. Mol. Biol.*, **8**, 660-668 (1964).
13. B. A. Lewis and D. M. Engelman, *J. Mol. Biol.*, **166**, 211-217 (1983).
14. S. Y. Kang, H. S. Gutowsky, and E. Oldfield, *Biochemistry*, **18**, 3268-3272 (1979).
15. L. K. Tamm and J. Seelig, *Biochemistry*, **22**, 1474-1483 (1983).
16 J. Seelig, L. Tamm, L. Humel, and S. Fleischer, *Biochemistry*, **20**, 3922-3932 (1981).
17. M. R. Paddy, F. W. Dahlquist, J. H. Davis, and M. Bloom, *Biochemistry*, **20**, 3152-3162 (1981). 1967).

18. P. C. Jost, O. H. Griffith, R. A. Capaldi, and G. Vanderkooi, *Proc. Natl. Acad. Sci. USA*, **70**, 480-484 (1973).

19. P. F. Knowles, A. Watts, and D. Marsh, *Biochemistry*, **18**, 4480-4487 (1979).

20. J. Davoust and P. F. Devaux, *J. Magn. Reson.*, **48**, 475-494 (1982).

21. (a) E. Meirovitch, A. Nayeem, and J. H. Freed, *J. Phys. Chem.*, **88**, 3454-3465 (1984);(b) H. Tanaka and J. H. Freed,*J. Phys. Chem.*, **88**, 6633-6644 (1984); (c) **89**, 350-360 (1985).

22. M. F. Brown, J. Seelig, and U. Haeberlein, *J. Chem. Phys.*, **70**, 5045-5053 (1979).

23. C. H. A. Seiter and S. I. Chan, *J. Am. Chem. Soc.*, **95**, 7541-7553 (1973).

24. G. W. Feigenson and S. I. Chan, *J. Am. Chem. Soc.*, **96**, 1312-1319 (1973).

25. N. O. Petersen and S. I. Chan, *Biochemistry*, **16**, 2657-2667 (1977).

26. R. J. Pace and S. I. Chan, *J. Chem. Phys.*, **76**, 4241-4246 (1982).

27. P. Dea and S. I. Chan, *Biochim. Biophys. Acta*, **854**, 1-8 (1986).

28. (a) R. J. Cherry, K. Hsu, and D. Chapman, *Biochim. Biophys. Acta*, **267**, 512-522 (1972); (b) A. Steinemann, G. Stark, and P. Laeuger, *J. Membr. Biol.*, **9**, 177-194 (1972).

29. J. J. Katz, W. Oettmeier, and J. R. Norris, *Philos. Trans. R. Soc. London Ser. B*, **273**, 227-253 (1976).

30. K. E. Eigenberg, W. R. Croasmun, and S. I. Chan, *Biochim. Biophys. Acta*, **679**, 361-368 (1982).

31. M. Brown, *J. Biochem. Biophys. Meth.*, **11**, 71-81 (1985).

Chapter V

Hydrophobic Mismatch in Gramicidin A/Lecithin Systems

Introduction

Gramicidin A′ (GA′) is a mixture of three related linear pentadecapeptides produced by the *Bacillus brevis* bacterium. By binding to RNA polymerase, GA′ is believed to inhibit the transcription of genes involved in vegetative growth.[1] In lipid bilayers, GA′ forms a trans-membrane channel which allows the passage of monovalent anions. Although this function does not appear to be important *in vivo*, the possibility of using of GA′ as a simple model for membrane channels, membrane/protein interactions, and trans-membrane alpha helices has spurred much interest in its membrane-bound conformation.

The three peptides found in GA′ are gramicidin A (GA), gramicidin B (GB), and gramicidin C (GC). Their primary sequences are shown in Figure 1. They are present in an 85:10:5 ratio (GA:GB:GC) in GA′. Because these peptides behave similarly under most conditions, they are generally studied as the native mixture, GA′.

Evidence indicates that in many amphipathic systems, GA′ exists as a single helical dimer. NMR studies of isotopically labelled GA′ in DML have shown that most of the C terminal ends of the peptide are exposed to the hydrophilic region of the bilayer, while the N-terminal ends are buried in the hydrocarbon region.[2] This indicates that N-terminus of the GA′ monomer resides in the hydrophobic region of the bilayer and is probably the point of attachment in dimer formation.

More recent solid state NMR studies of GA′ /DML bilayers show that the magnitude of ^{13}C-^{13}C dipolar couplings in multiply labelled GA′ are consistent with a single stranded helix of pitch 6.3.[3] Infrared and Raman spectroscopic investigations of the secondary structure of GA′ indicate a β-sheet hydrogen bonding

Figure 1: The primary sequences of (a) gramicidin A, (b) gramicidin B, and (c) gramicidin C. The amino acids which differ in the three gramicidins are printed in bold face.

(a)

formyl-l-val-gly-l-ala-d-leu-l-ala

-d-val-l-val-d-val-l-trp-d-leu-**l-trp**

-d-leu-l-trp-d-leu-l-trp-ethanolamine

(b)

formyl-l-val-gly-l-ala-d-leu-l-ala

-d-val-l-val-d-val-l-phe-d-leu-**l-phe**

-d-leu-l-trp-d-leu-l-trp-ethanolamine

(c)

formyl-l-val-gly-l-ala-d-leu-l-ala

-d-val-l-val-d-val-l-trp-d-leu-**l-tyr**

-d-leu-l-trp-d-leu-l-trp-ethanolamine

pattern.[4–6]

Modelling studies show the single stranded β helix of pitch 6.3 to be 26-30Å long with an inner diameter of 4Å.[7] Because of several trp groups located near the head group region of the bilayer, the outer diameter is approximately 137Å at the ends of the GA′ dimer and approximately 47Å at the N-N junction.[8] Only four hydrogen bonds unite the two GA′ molecules. In addition, 26 intramolecular hydrogen bonds maintain the β helix structure.[7] Alternating D and L amino acids allow all side chains to face the helix exterior, while the more polar carbonyl and amino groups line the interior of the helix. This conformation of GA′, abbreviated as $\beta^{6.3}$, is illustrated in Figure 3 of chapter 3.

In DML bilayers, GA′ exhibits a circular dichroism (CD) spectrum characteristic of the $\beta^{6.3}$ conformation.[9,10] This spectrum, shown in Figure 2, consists of positive ellipticities at 217 and 237 nm. CD is a simple and direct method of determining the conformation of GA′ in an amphipathic or organic solvent system.[7]

A trans-membrane helix such as GA′ has hydrophobic and hydrophilic regions which match those of the surrounding lipid bilayer. The characteristic length of the hydrophobic region in a lipid or membrane-bound protein is known as the hydrophobic length of the molecule. When the hydrophobic lengths of the protein and the lipid into which it is reconstituted are not equal, a situation known as hydrophobic mismatch exists. In such a case, the hydrophobic length of either the lipid or the protein must adjust to compensate for this mismatch.

The hydrophobic length of a lipid bilayer varies both with the number of carbons on the acyl chain and the degree of extension of the hydrocarbon chain.[11] The bilayer thicknesses of dimyristoyllecithin (DML), dipalmitoyllecithin (DPL), and distearoyllecithin (DSL) above their respective gel-to-liquid crystalline phase

Figure 2: The CD spectrum of GA′ in DML vesicles. This spectrum is characteristic of the channel conformation of GA′ .[30]

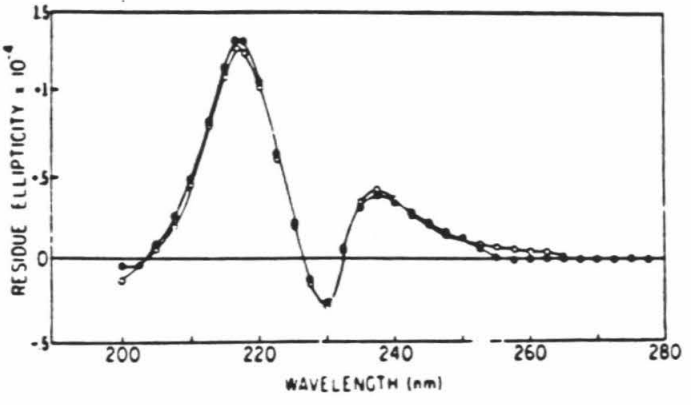
RESIDUE ELLIPTICITY x 10⁻⁴
1.5
1.0
0.5
0
-0.5
200
220
240
260
280
WAVELENGTH (nm)

transition temperatures are shown in Table I. These lipids have 14, 16, and 18 carbon chains, respectively.

Below the gel-to-liquid crystalline phase transition temperature of a lipid, the hydrocarbon chains are in an all-trans or maximally extended configuration. Above the phase transition temperature, the degree of extension of the hydrocarbon chains decreases. This corresponds to an increase in gauche conformations of the C-C chain segments. A study of ^{2}H S_{CD} values for deuterons along the hydrocarbon chain indicate that trans conformations are most heavily weighted in the first 10 carbons of the lipid chain. Gauche conformations become increasingly populated as carbon chain segments are added beyond the 10 position. Thus, long hydrocarbon chains are relatively less extended than short hydrocarbon chains, and their tails are more splayed. As the hydrocarbon tail splays, the cross-sectional area of the tail also increases. The area of the head group, however, does not vary with chain length. As a result, the ratio of the hydrocarbon area (A_C) to the head group area (A_H) increases for lipids of longer chain length.[12]

Hydrophobic mismatch has been shown to affect the interaction of many proteins with lipid bilayers.[13–15] Pearson and co-workers have suggested two ways in which the hydrocarbon region of a bilayer may deform to compensate for hydrophobic mismatch.[16,17] A lipid chain may expand by increasing the ratio of trans to gauche bonds. It may shrink either by decreasing this ratio or by tilting in the bilayer. Because the equilibrium extensions of lipid bilayers decrease with increasing chain length, short chain lipids will be better able to accommodate a compression, while long chain lipids will be better able to accommodate expansion. Furthermore, an expansion or compression of the hydrophobic region of the bilayer will lead to an increase or decrease in A_C/A_H, respectively. When the

Table I: The hydrophobic lengths of pure DML, DPL, and DSL bilayers in the liquid crystalline state.

Table I

Lipid	Liquid Crystalline Hydrophobic Length (A)
DML	27.9
DPL	29.3
DSL	30.6

energetic cost of deforming the lipid bilayer becomes greater than that of the loss in entropy due to protein aggregation, protein aggregation will occur in a lipid bilayer.

Lewis and co-workers have studied the effects of hydrophobic mismatch on the aggregation properties of bacteriorhodopsin reconstituted with diacylphosphatidylcholines of varying saturated hydrocarbon chain lengths.[14] The ideal hydrophobic match for bacteriorhodopsin was determined from a crystal structure refined to 7Å resolution. It was found that bacteriorhodopsin will aggregate when reconstituted in phosphatidylcholine bilayers whose hydrophobic length is 10Å less than the perfect match for bacteriorhodopsin, or 4Å more than the perfect match. Thus, the hydrocarbon region expands more easily than it contracts.

Hydrophobicity plots indicate seven possible trans-membrane segments for bacteriorhodopsin. The lengths of these segments vary. It is difficult, therefore, to estimate the ideal hydrophobic length of the protein. In addition, it is difficult to isolate aggregation due to hydrophobic mismatch from other causes of aggregation. Because GA′ is a single helix whose dimensions are well known, it is particularly well suited to a study of the effect of membrane thickness on lipid/protein interactions.

At low GA′ /lipid ratios and in cases of extreme hydrophobic mismatch between GA′ and a lipid, it has been shown that GA′, rather than the lipid compensates for the mismatch. At low GA′ concentrations, GA′ mediated conductance of ions through a lipid bilayer has been shown to be dependent on bilayer thickness.[18–20] Single channel recordings have been used to study the lifetime of the GA′ pore in monoacylglycerol-squalene bilayers of varying thickness. Bilayer thickness was altered by varying the number of carbons on the acyl chain of the

monoacylglycerol molecule. The channel lifetime was found to decrease for bilayers thicker than 22Å. The decrease in channel lifetime was attributed to increased GA′ dimer dissociation events. Channel lifetimes did not change for bilayers thinner than 22Å.

CD studies by Wallace of GA′ in various lipid systems confirm the sensitivity of GA′ to bilayer thickness.[9] Both above and below the phase transition, 3 mol % GA′ in DML is observed to be in the $\beta^{6.3}$ conformation. For GA′/DPL and GA′/DSL bilayers below their gel-to-liquid crystalline phase transition temperatures, the CD spectrum of GA′ appears to be a superposition of the channel spectrum and the spectrum of another GA′ conformation. It seems likely that the altered CD spectrum of GA′ is associated with the non-conducting monomeric state of the peptide observed in the single channel recording experiments. The thickness of the DML bilayer in the gel state is 38Å, while the thicknesses of DPL and DSL in the liquid crystalline state are 26Å and 30Å, respectively. Because GA′ maintains its channel conformation in the gel state DML bilayer, it is likely that the channel conformation of GA′ predominates in DPL and DSL liquid crystalline bilayers.

At higher ratios of GA′ to lipid and in cases of intermediate hydrophobic mismatch between GA′ and the lipid, the lipid adjusts to the presence of GA′. Such adjustments have been observed by Raman and infra-red (IR) spectroscopies.[21–23] The number of trans conformers in both the DML and DPL hydrocarbon region is found to increase upon addition of GA′. In addition, x-ray diffraction results show that the dioleoylphosphatidylcholine (DOPC) bilayer becomes thicker upon addition of GA′. DOPC has a head group identical to those of DML, DPL, and DSL and a 18 carbon chain with 1 trans double bond at the 9 position.[24]

In phosphatidylcholines with acyl chain lengths greater than sixteen carbons, workers in Holland have discovered the induction of hexagonal phase (H_{II}) by concentrations of GA′ above 10 mol %.[25] An elaborate mechanism has been proposed for this transition in which the GA′ monomers break apart and then reverse their orientation in the bilayer. The cone shape of the GA′ monomer leads to H_{II} formation.[8] In addition, the temperature dependence of the bilayer→H_{II} phase transition has been studied.[26] This work shows a direct transition from the gel state bilayer phase to H_{II} phase at temperatures approximately 20°C below the gel-to-liquid crystalline phase transition temperature of the pure lipid bilayer.

In this chapter, the effects of hydrophobic mismatch on the physical properties of the lipid bilayer and the factors leading to H_{II} phase formation in GA′ /lecithin systems are studied. The lipids used are DML, DPL, and DSL. ^{31}P NMR spectra of these lipids will be studied as a function of GA′ concentration. The $\Delta\sigma$ of the lecithin phosphate group ^{31}P powder pattern is indicative of the motions and orientation of the lipid head group (see chapter 2). Furthermore, since the $\Delta\sigma$ of H_{II} phase is half that of the bilayer phase and of opposite sign, these two phases are easily distinguished by ^{31}P-NMR. Mixtures of GA′ with selectively deuterated lipids will be studied by ^{2}H-NMR. $\Delta\nu_Q$ should reflect the adjustment of the lipid chains in response to the mismatch between the hydrophobic length of GA′ and the lipid hydrocarbon chains. The model of cooperative director fluctuations presented in chapters 2 and 4 will be used to extract elastic constants and cooperative lengths from $T_{1\rho}^{-1}$ and T_2^{-1} measurements on the GA′ /lipid samples. Based on the NMR measurements, the effects of hydrophobic mismatch on the properties of the bilayer will be elaborated and a possible mechanism for the bilayer to H_{II} transition in GA′ /lecithin systems will be discussed. In chapters 6 and 7,

supporting studies using Raman spectroscopy and differential scanning calorimetry (DSC), respectively, will be presented.

Experimental Section

I. *Materials and Methods*

DML, DPL, and DSL were purchased from Avanti Polar Lipids. GA′, was purchased from Boehringer Mannheim Biochemicals. DML (9,10-DML), DPL (9,10-DPL), and DSL (9,10-DSL) were deuterated at the 9 and 10 positions on both acyl chains as described in chapter 3.

GA′ was dissolved in methanol and then added to either DML, DPL, or DSL in appropriate amounts. DPL and DSL are not sufficiently soluble in methanol. In order to dissolve these lipids, chloroform was added to the GA′ /methanol solution. The organic solvent was evaporated from the GA′ /lipid samples under low vacuum until most of the solvent was removed. The sample was then placed under high vacuum overnight. Samples were hydrated in 400mM Tris, 40mM NaCl buffer (pH 7.4). All preparations contained less than 20 percent (w/w) lipid to water. In order to reach an equilibrium distribution of GA′ in the bilayer, it was necessary to incubate samples above the phase transition temperature of the mixture for approximately twelve hours. All experiments were performed well above the gel-to-liquid crystalline phase transition temperature.

Instrumentation

^{2}H-NMR experiments were conducted on a Bruker AM 500 console. The

TLO transmitter pulse was attenuated to 1 volt peak/peak and used to drive an Amplifier Research 200L amplifier. The amplified pulse was then fed into a home built high power deuterium probe. This arrangement provided a 3.5 μsec 90° pulse. The pulse sequence and methods of data analysis for the T_2^{-1} experiment have been described in chapter 3. Only variable t_1 increments were used in the T_2^{-1} experiments. T_1^{-1} and $T_{1\rho}^{-1}$ experiments have been described in chapter 4.

^{31}P-NMR spectra were obtained on a Bruker AM 400 spectrometer. A broad-band probe yielding a 10 μ sec 75° pulse was used for acquisition of spectra. ^{31}P-^{1}H dipolar couplings were eliminated using gated broad-band proton decoupling at a power of 20 Watts.

Results

The ^{31}P-NMR studies of DML, DPL, and DSL bilayers containing GA′ are summarized in Figure 3. $\Delta\sigma$ is plotted against mol %GA′ for all three lipid systems. $\Delta\sigma$ decreases identically upon addition of GA′ to all three lipid bilayers. The discontinuity observed in the $\Delta\sigma$ of DPL and DSL as GA′ is added reflects a transition from bilayer to H_{II} phase. DML remains in the bilayer phase to high concentrations, while DPL and DSL exhibit H_{II} components above 10 mol % and 4 mol % GA′, respectively.

Figure 4 shows the dependence of $\Delta\nu_Q$ on GA′ concentration for 9,10-DML, 9,10-DPL, and 9,10-DSL. For GA′ /DML, $\Delta\nu_Q$ increases by approximately 6KHz as the concentration of GA′ in the bilayer is increased from 0 mol % to 6 mol %. An increase of 3KHz occurs over a 0 mol % to 5 mol % concentration range for

Figure 3: The dependence of $\Delta\sigma$ on GA′ concentration for the three lipid systems studied. Only the $\Delta\sigma$ of the bilayer phase is shown. The following symbols are used: ⋆ :DML, ● :DPL, and ▲ :DSL.

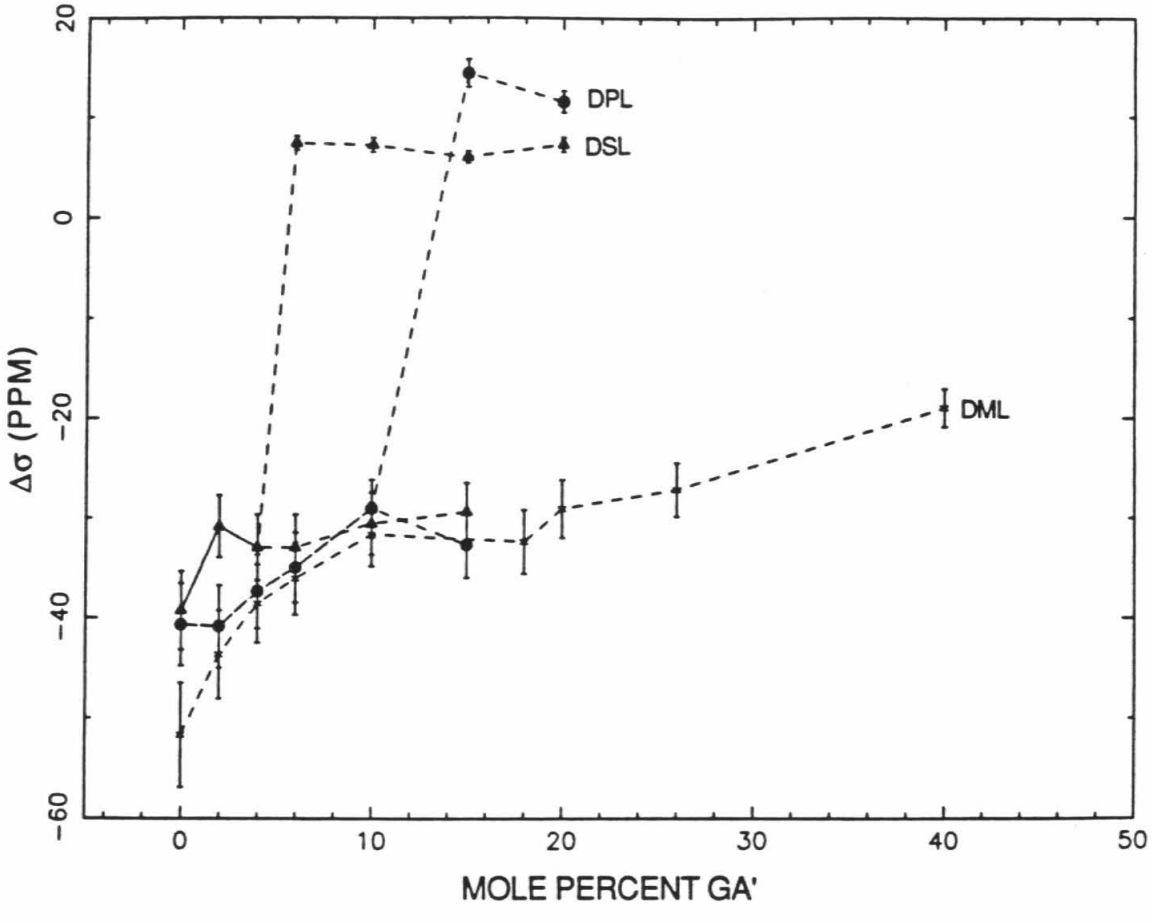
20
0
−20
−40
−60
Δσ (PPM)
DPL
DSL
DML
0
10
20
30
40
50
MOLE PERCENT GA'

Figure 4: The dependence of $\Delta\nu_Q$ on GA′ concentration. The three lipid systems are represented as follows: * :DML, ● :DPL, and ▼ :DSL. Values are only shown for the bilayer phase.

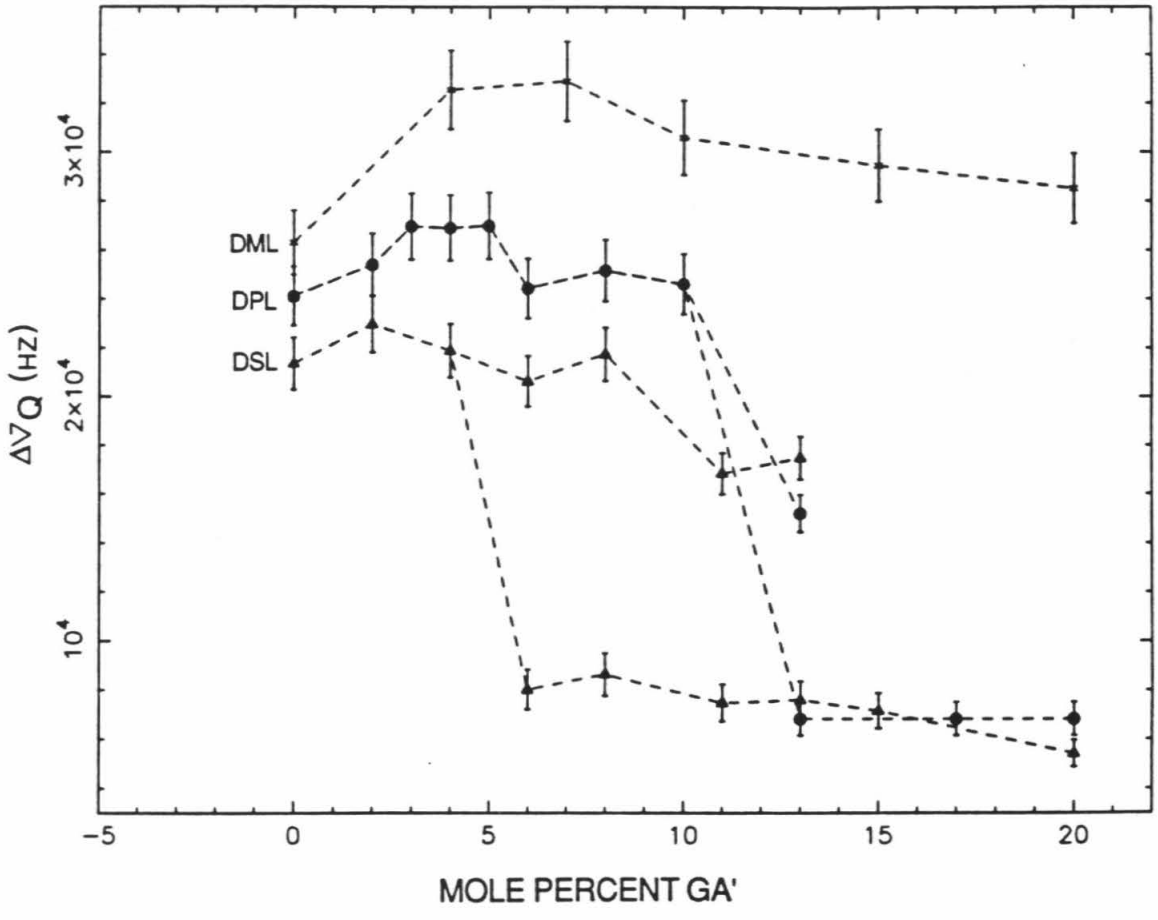
DML
DPL
DSL
$\Delta\nu_Q$ (HZ)
3×10^4
2×10^4
10^4
−5
0
5
10
15
20
MOLE PERCENT GA'

DPL. In DSL, $\Delta\nu_Q$ remains constant for GA′ concentrations of 0 mol % through 8 mol %. In DPL and DSL, the discontinuities in $\Delta\nu_Q$ at 13 mol % and 6 mol % GA′, respectively, again reflect transitions to H_{II} phase.

In ^2H spectra which exhibit both bilayer and H_{II} phase lipids, the components of each phase are observed. The ratio of lipid in H_{II} phase to total lipid has been obtained by spectral simulation. In Figure 5, these results are plotted against mol % GA′ for DML, DPL and DSL. Only the bilayer phase is observed in DML. In both DPL and DSL, co-existence of bilayer and H_{II} phases implies a higher solubility of GA′ in the H_{II} phase than in the bilayer phase. In DPL, co-existence is only observed at a concentration of 13 mol % GA′. In DSL, co-existence is observed from 6 mol % through 20 mol % GA′. Both the onset of phase co-existence at lower concentrations of GA′ and the observation of coexistence over a wider GA′ concentration range in DSL indicate that the difference between the solubilities of GA′ in the bilayer and H_{II} phases is greatest for DSL.

T_1^{-1}, $T_{1\rho}^{-1}$, and T_2^{-1} for the 9 and 10 deuterons on the hydrocarbon chains of DML, DPL, and DSL have been measured as a function of GA′ concentration. In Figure 6, the dependence of these relaxation rates on GA′ concentration is compared for each of the three lipid systems. In all lipid systems, T_1^{-1} is significantly less than $T_{1\rho}^{-1}$ and T_2^{-1}. In the H_{II} phase of GA′/DPL and GA′/DSL systems, $T_{1\rho}^{-1}$ and T_2^{-1} increase rapidly with increasing GA′ concentration. Furthermore, the gap between $T_{1\rho}^{-1}$ and T_2^{-1} widens as GA′ is added to the H_{II} phase.

As GA′ is added to the bilayer phase of each GA′/lipid mixture, the S_{CD} as well as the T_2^{-1} of the deuterated lipid changes. As discussed in chapter 2, if a plot of T_2^{-1} versus S_{CD}^2 does not yield a straight line, then the change in T_2^{-1} must be due to a change in motions undergone by lipid molecules in the bilayer.

Figure 5: The ratio of the moles of lipid in H_{II} phase to the total moles of lipid as a function of GA′ concentration. The ratio was obtained by simulating ^{2}H-NMR spectra as a superposition of H_{II} and bilayer powder patterns. The following symbols are used: ✱:DML, ●:DPL, and ▲:DSL.

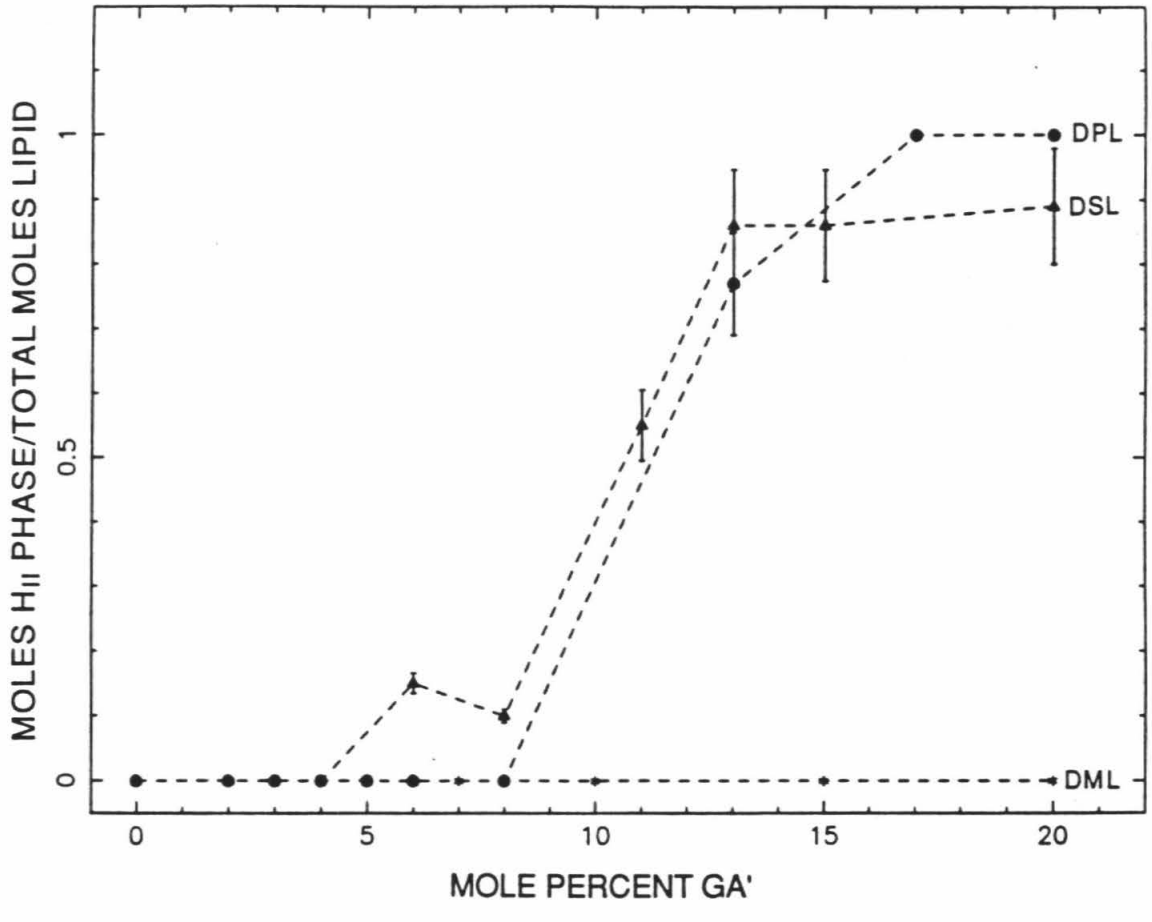
MOLES H_{II} PHASE/TOTAL MOLES LIPID
0
0.5
1
0
5
10
15
20
MOLE PERCENT GA'
DPL
DSL
DML

Figure 6: T_1^{-1} , $T_{1\rho}^{-1}$, and T_2^{-1} for various concentrations of GA′ in (a) DML, (b) DPL, and (c) DSL systems. ● represents T_1^{-1} , ⁎ represents $T_{1\rho}^{-1}$, and ▲represents T_2^{-1} .

(a)

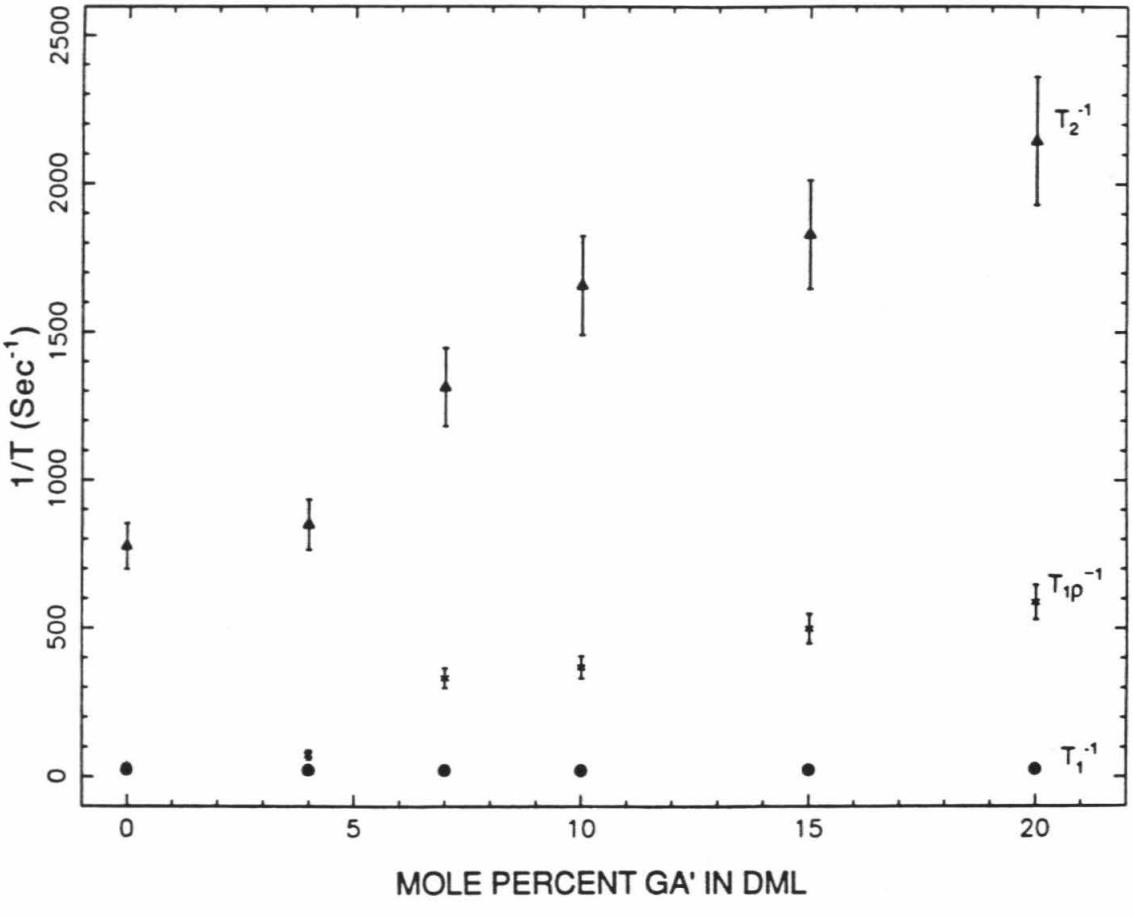
1/T (Sec^{-1})
0
500
1000
1500
2000
2500
0
5
10
15
20
MOLE PERCENT GA' IN DML
T_2^{-1}
$T_{1\rho}^{-1}$
T_1^{-1}

(b)

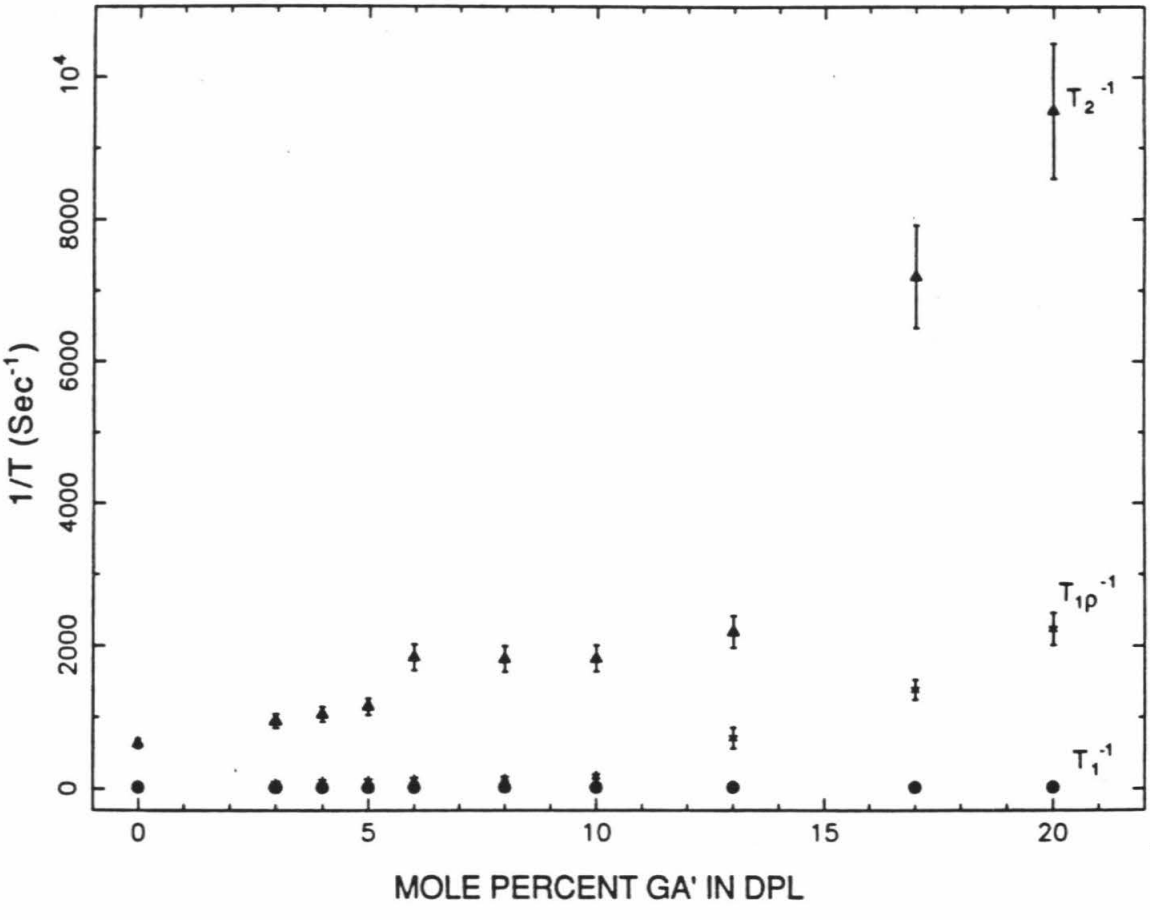
1/T (Sec^{-1})
0
2000
4000
6000
8000
10^4
0
5
10
15
20
MOLE PERCENT GA' IN DPL
T_2^{-1}
$T_{1\rho}^{-1}$
T_1^{-1}

(c)

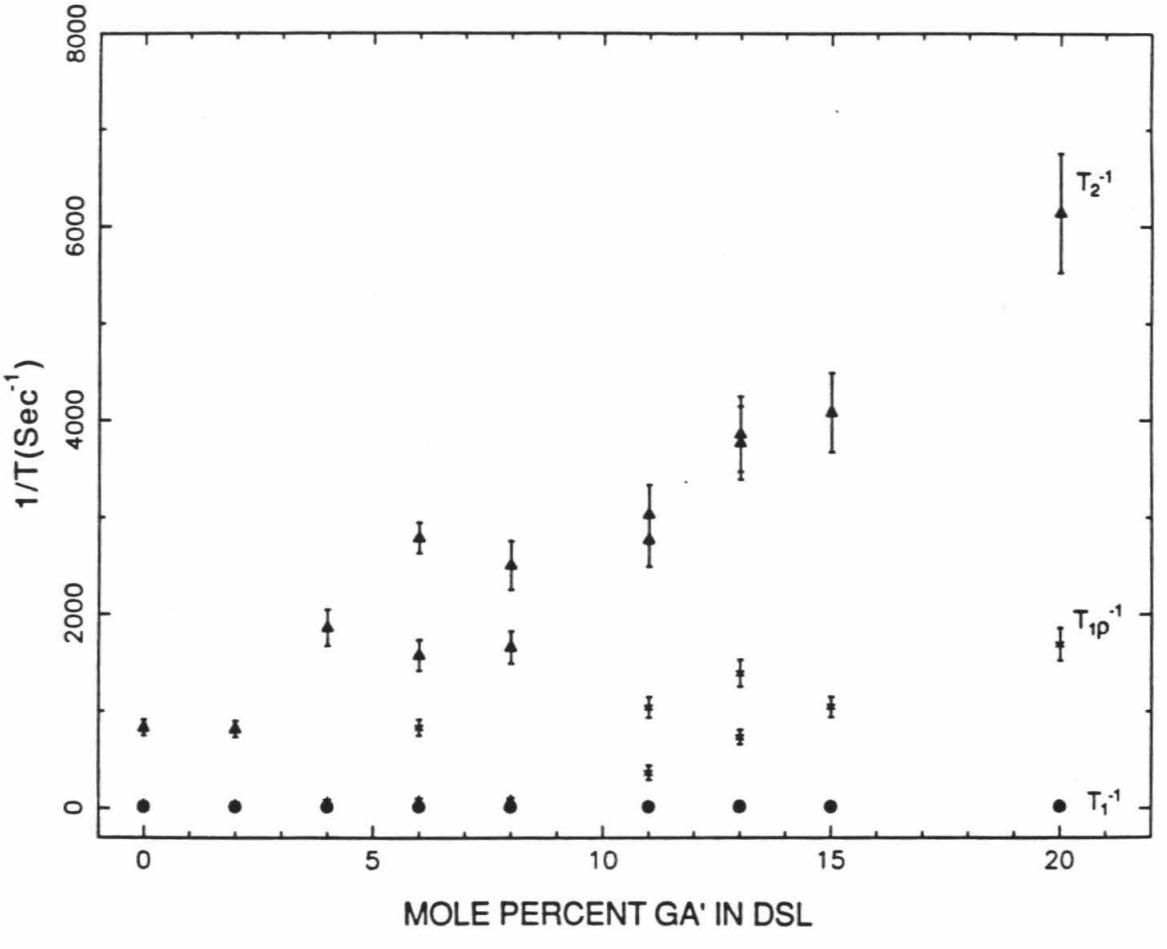
8000
6000
4000
2000
0
1/T(Sec^{-1})
T_2^{-1}
$T_{1\rho}^{-1}$
T_1^{-1}
0
5
10
15
20
MOLE PERCENT GA' IN DSL

In Figure 7, the ^{2}H-NMR T_2^{-1} 's of 9,10-DML, 9,10-DPL, and 9,10-DSL bilayers containing varying concentrations of GA′ are plotted against S_{CD}^2. A plot of T_2^{-1} versus S_{CD}^2 for deuterons along the hydrocarbon chain of the DML lipid bilayer yield a straight line. This line is included in Figure 7 for comparison. A linear dependence of T_2^{-1} on S_{CD}^2 is not observed for any of the GA′/lipid bilayer systems studied. Furthermore, upon addition of GA′, therefore, motions of the bilayer become very different from those of the pure lipid bilayer.

In Figure 8, the dependence of each relaxation rate on GA′ concentration is compared for all three lipid systems. Only values for the bilayer phase are included. At higher concentrations of GA′ in DPL and DSL, bilayer and H_{II} type spectra are superimposed, and it is especially difficult to extract relaxation rates for the bilayer components. At high mol % of GA′ in DPL and DSL, therefore, relaxation rates reported for the bilayer component may be artificially high. T_1^{-1} is very similar for all three lipid systems. In addition, the T_1^{-1} 's for the bilayer phases of the three lipid systems are not sensitive to the incorporation of GA′. The $T_{1\rho}^{-1}$'s and T_2^{-1} 's of all bilayer systems increase noticeably upon addition of GA′. The magnitude of increase, however, is different in each of the lipid systems. $T_{1\rho}^{-1}$ increases dramatically for DML but only shows a small increase in DPL and DSL. In contrast, T_2^{-1} increases more rapidly in DPL and DSL. These differences indicate that addition of GA′ to DML increases relaxation arising from motion in the MHz regime, while addition of GA′ to DPL and DSL increases relaxation arising from motion at much lower frequencies.

In chapters 2 and 4, a model for cooperative director fluctuations in bilayers was proposed. The amplitude and frequency of these fluctuations are determined by (k_1, k_2) , the elastic constants, and $\lambda_\perp^u$, the maximum cooperative length of

Figure 7: The relationship between T_2^{-1} and S_{CD}^2 for several concentrations of GA′ . Each point is labelled with the appropriate GA′ concentration. (a) GA′ in DML. (b) GA′ in DPL. (c) GA′ in DSL.

(a)

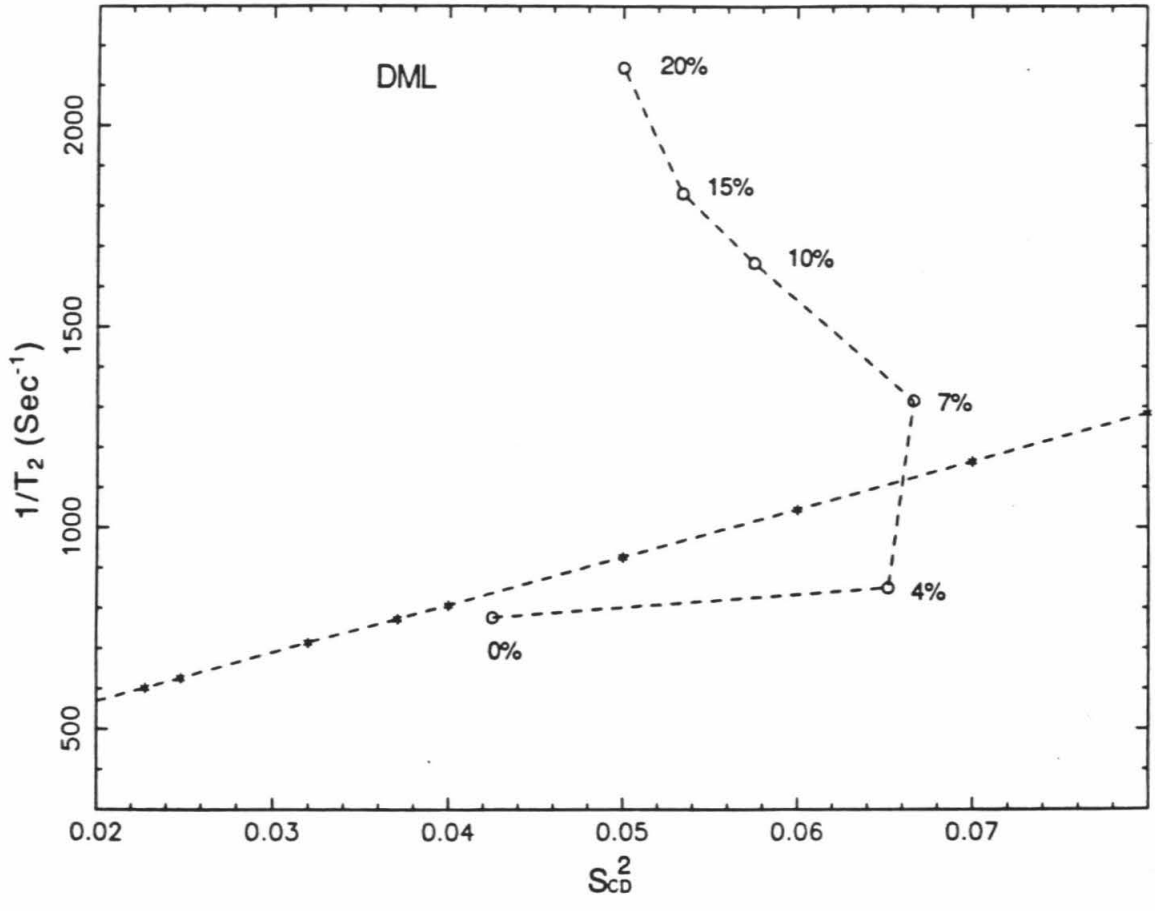
DML
20%
15%
10%
7%
4%
0%
1/T2 (Sec-1)
500
1000
1500
2000
0.02
0.03
0.04
0.05
0.06
0.07
SCD2

(b)

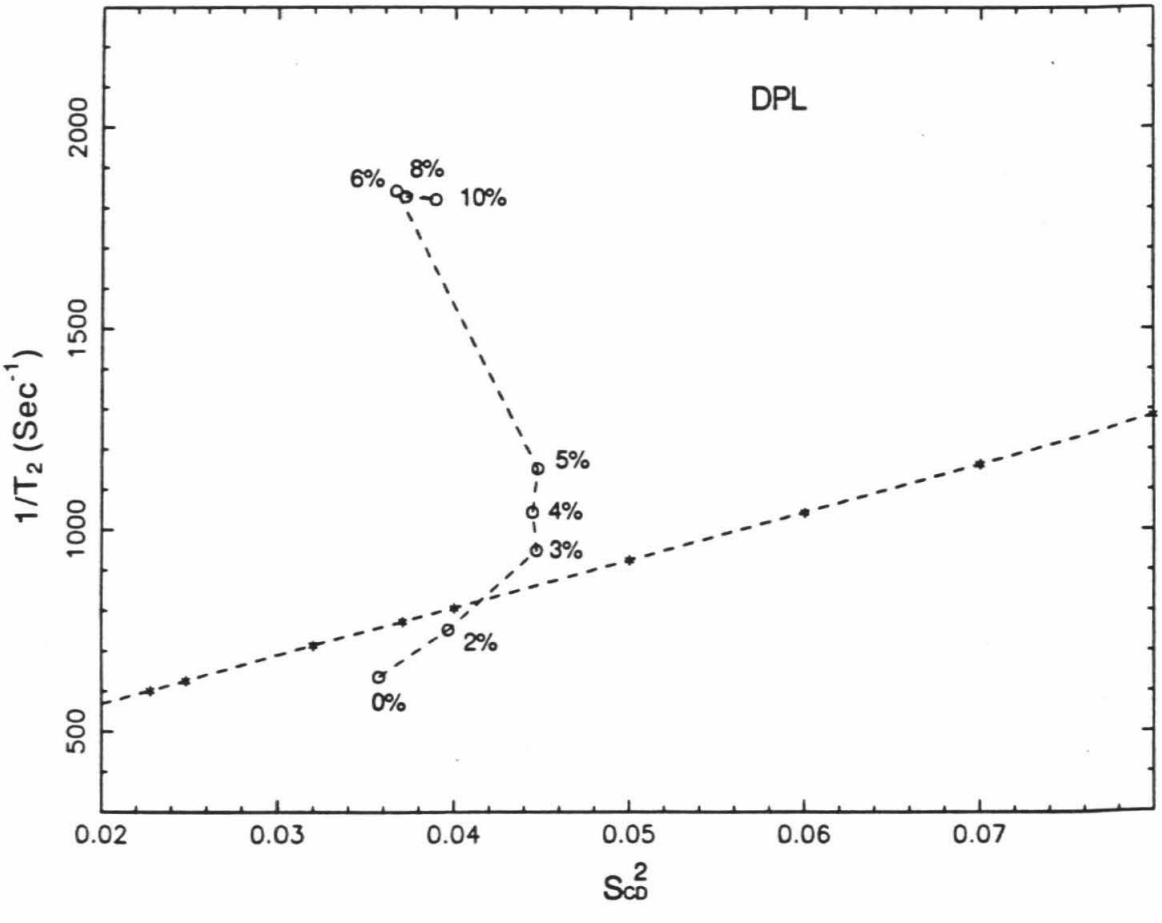
DPL
6%
8%
10%
5%
4%
3%
2%
0%
2000
1500
1000
500
1/T2 (Sec-1)
0.02
0.03
0.04
0.05
0.06
0.07
SCD2

(c)

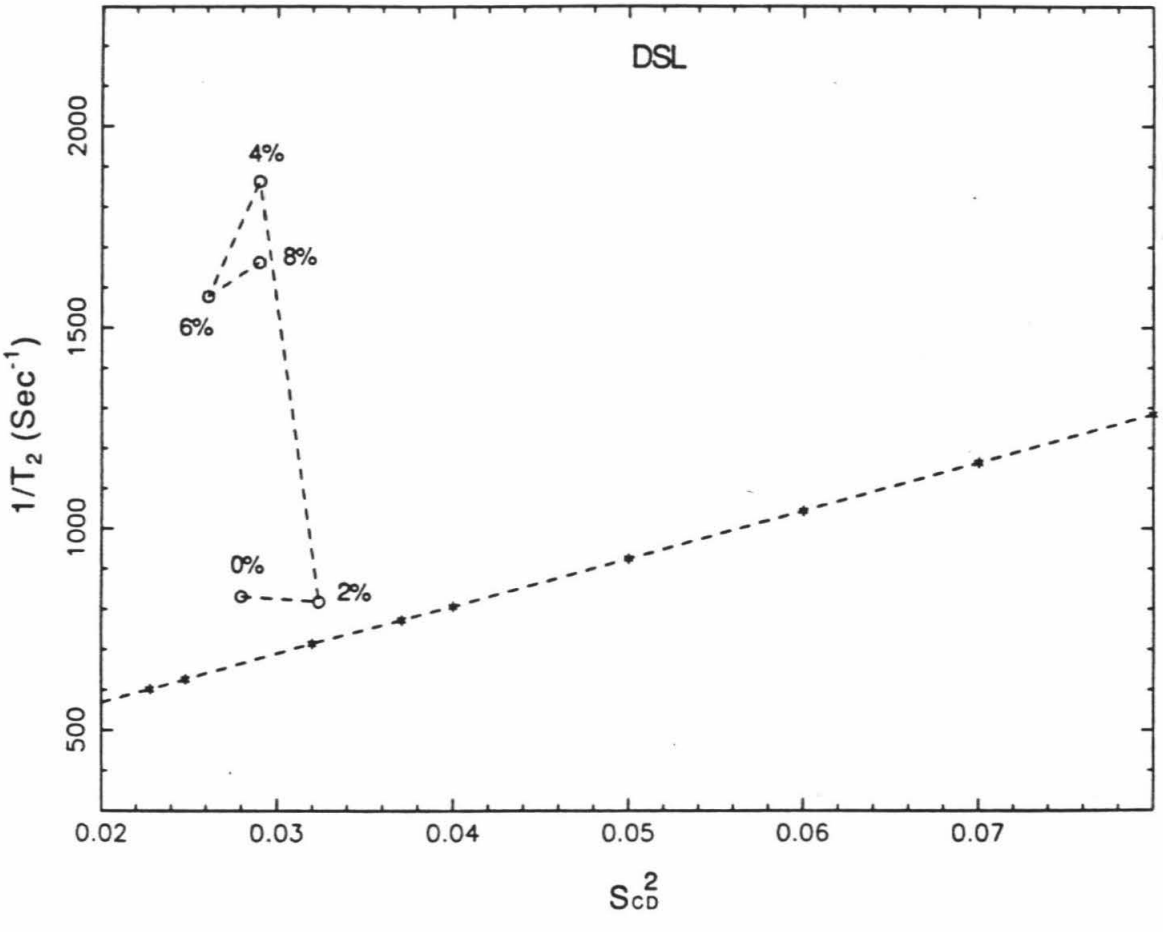
DSL
4%
8%
6%
0%
2%
2000
1500
1000
500
1/T2 (Sec-1)
0.02
0.03
0.04
0.05
0.06
0.07
SCD2

Figure 8: A comparison of the dependence of the relaxation rate on GA′ concentration for the three lipid systems studied. Only values for the the bilayer phase are shown. The lipid systems are represented by the following symbols: * :DML, ● :DPL, and ▲ :DSL. The relaxation rates measured are: (a) T_1^{-1} , (b) $T_{1\rho}^{-1}$, and (c) T_2^{-1} .

(a)

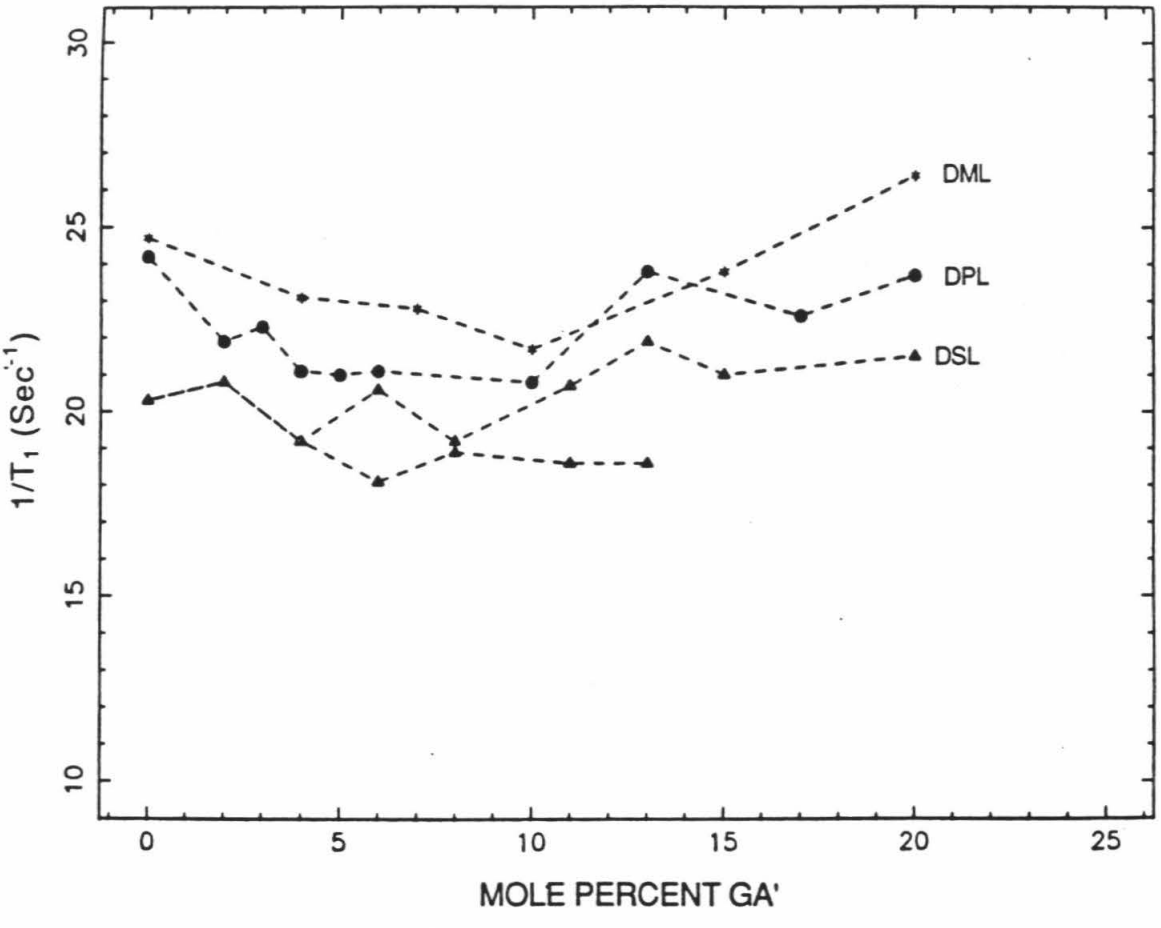

(b)

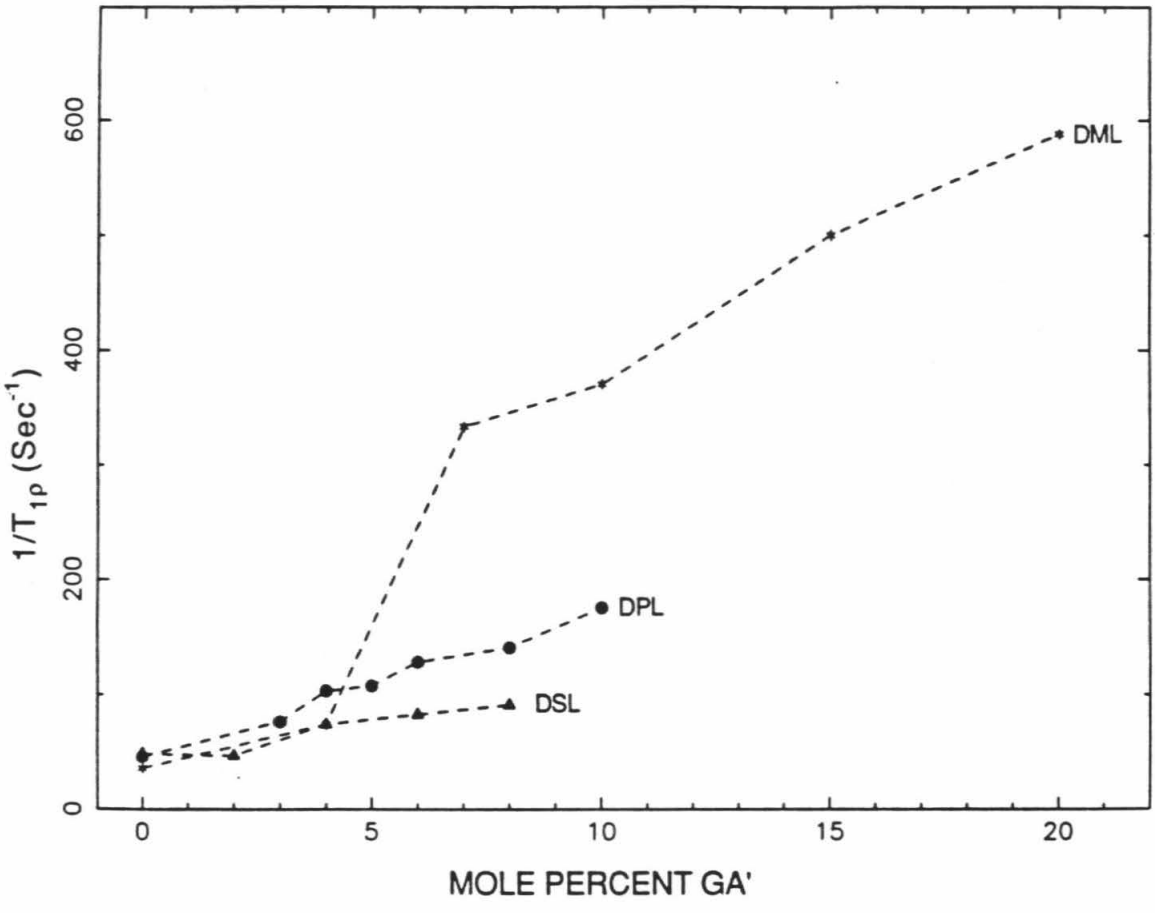
600
400
200
0
$1/T_{1\rho}$ (Sec^{-1})
DML
DPL
DSL
0
5
10
15
20
MOLE PERCENT GA'

(c)

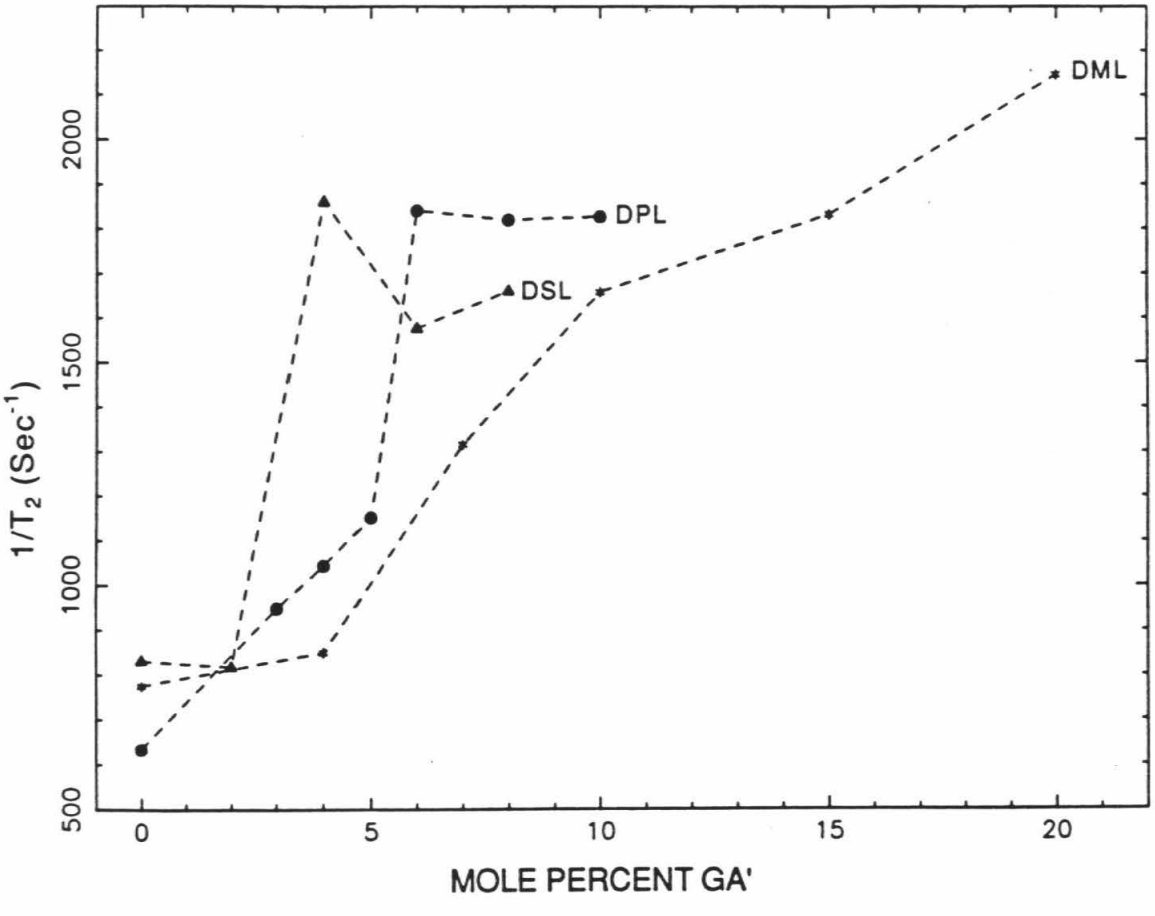
DML
DPL
DSL
2000
1500
1000
500
$1/T_2$ (Sec^{-1})
0
5
10
15
20
MOLE PERCENT GA'

director fluctuation in the bilayer. $T_{1\rho}^{-1}$ and T_2^{-1} measurements may be used to extract $\lambda_\perp^u$ and (k_1, k_2) of a particular lipid system. Such calculations have been carried out for DML, DPL, and DSL bilayers containing varying concentrations of GA′. In Figure 9a, the resulting elastic constants for these three bilayer systems have been plotted against mol % GA′. In pure lipid bilayers, the (k_1, k_2) of DML is much higher than that of DPL and DSL. As GA′ is added to each of the bilayers, however, their elastic constants converge.

In Figure 9b, the $\lambda_\perp^u$ of the three lipid systems are plotted as a function of GA′ concentration. In the pure bilayers, the $\lambda_\perp^u$ of DML is greater than that of DPL and DSL. As GA′ is added to the bilayers, however, the $\lambda_\perp^u$ of DML decreases much more rapidly than that of DPL or DSL. Consequently, at high concentrations of GA′, the $\lambda_\perp^u$ length of the DML bilayer is shorter than that of the other two lipids, the $\lambda_\perp^u$ of DPL is intermediate, and the DSL bilayer has the longest $\lambda_\perp^u$.

In the H_{II} phases of both GA′/DPL and GA′/DSL, further addition of GA′ causes a sharp rise in the T_2^{-1} of deuterons at the 9 and 10 positions on the lipid hydrocarbon chain. This increase in T_2^{-1} should be apparent in the line widths of the corresponding one-dimensional ^2H spectrum. If the lipid head groups are affected in a similar manner, the line width of the H_{II} ^{31}P-NMR spectrum should also increase upon addition of GA′. In Figure 10, ^2H spectra of 9,10-DPL containing 13 and 20 mol % GA′ are compared. The 13 mol % spectrum is a superposition of bilayer and H_{II} phase spectra. The powder pattern with the smaller $\Delta\nu_Q$ corresponds to H_{II} phase lipids. Simulations show that the $\Delta\nu_Q$ of the H_{II} phase spectra are equivalent at 13 mol % and 20 mol % GA′ in DPL. The line width of the 20 mol % spectrum is so great, however, that $\Delta\nu_Q$ is obscured. In the H_{II} phase of DPL, therefore, slow motions in the hydrocarbon chains increase

Figure 9: The model which was presented in chapter 4 is used to extract both the elastic constant and the cooperative length of director fluctuations from $T_{1\rho}^{-1}$ and T_2^{-1} measurements. (a) The elastic constant (k_{11}, k_{22}) is plotted vs. GA′ concentration for GA′ in DML($*$), DPL ($\bullet$), and DSL ($\blacktriangle$) bilayers. (b) The cooperative length, $\lambda_{\perp}^{u}$, is plotted as a function of GA′ concentration in DML, DPL, and DSL bilayers. Symbols representing each of the lipid systems are the same as in (a).

(a)

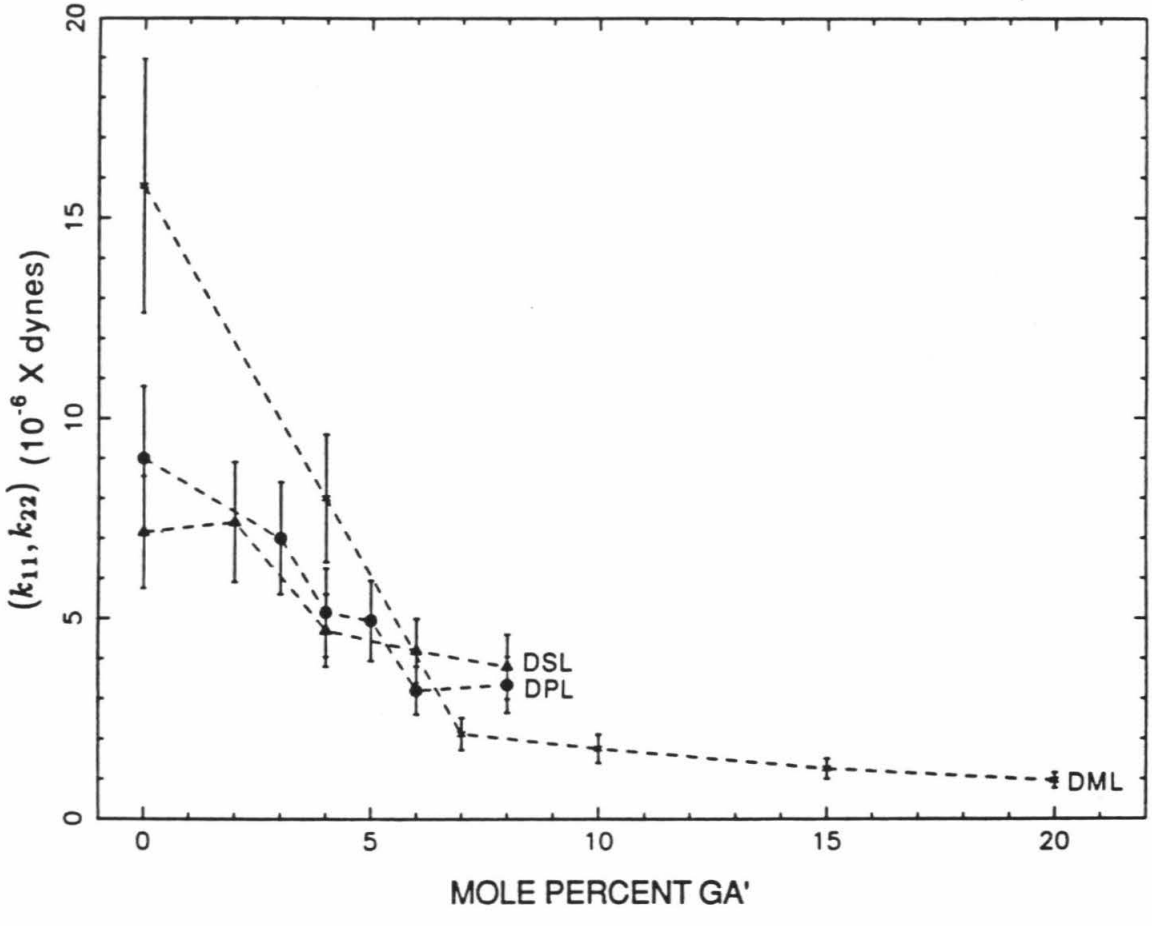

(b)

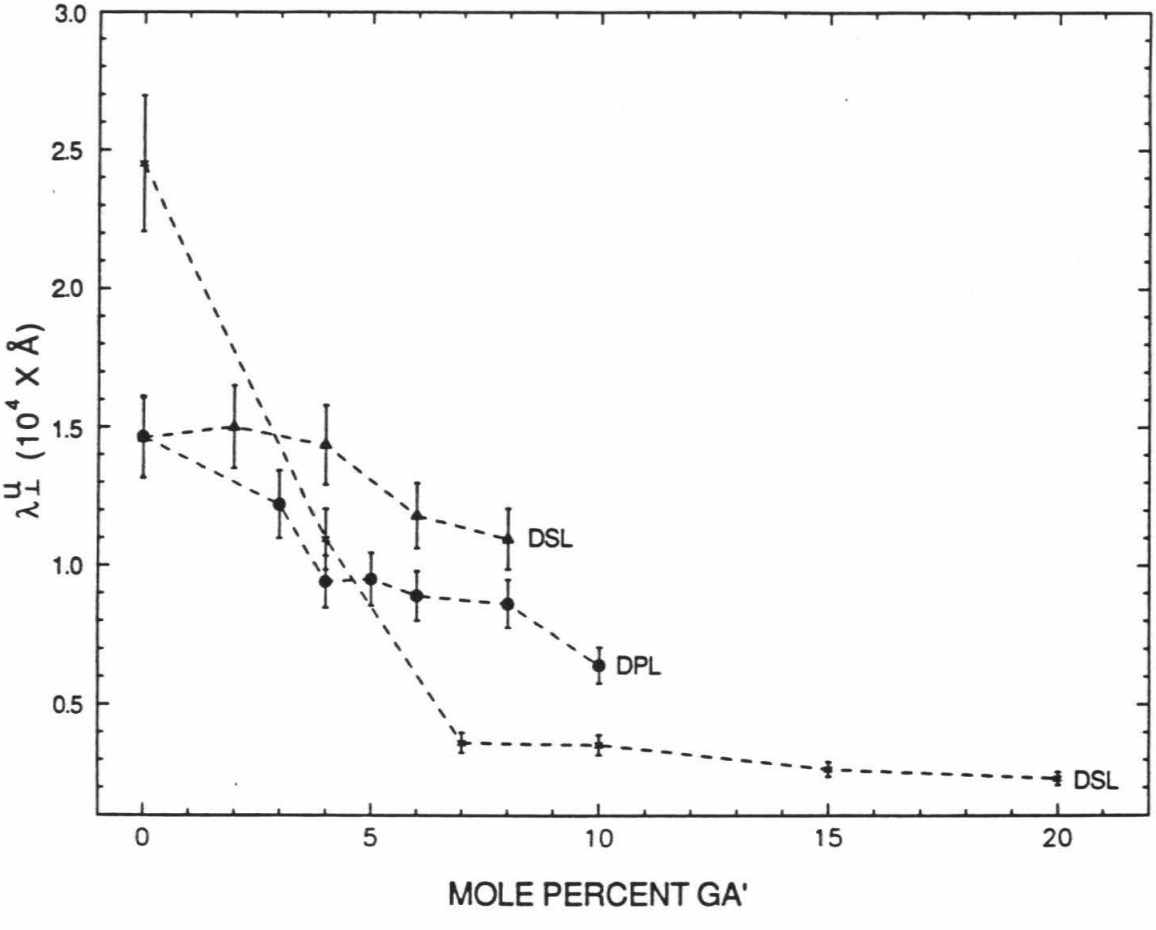
3.0
2.5
2.0
1.5
1.0
0.5
$\lambda_{\perp}^{u}$ (10^4 X Å)
DSL
DPL
DSL
0
5
10
15
20
MOLE PERCENT GA'

Figure 10: The ^{2}H-NMR spectra of (a) 20 mol % GA′ in DPL and (b) 13 mol % GA′ in DPL.

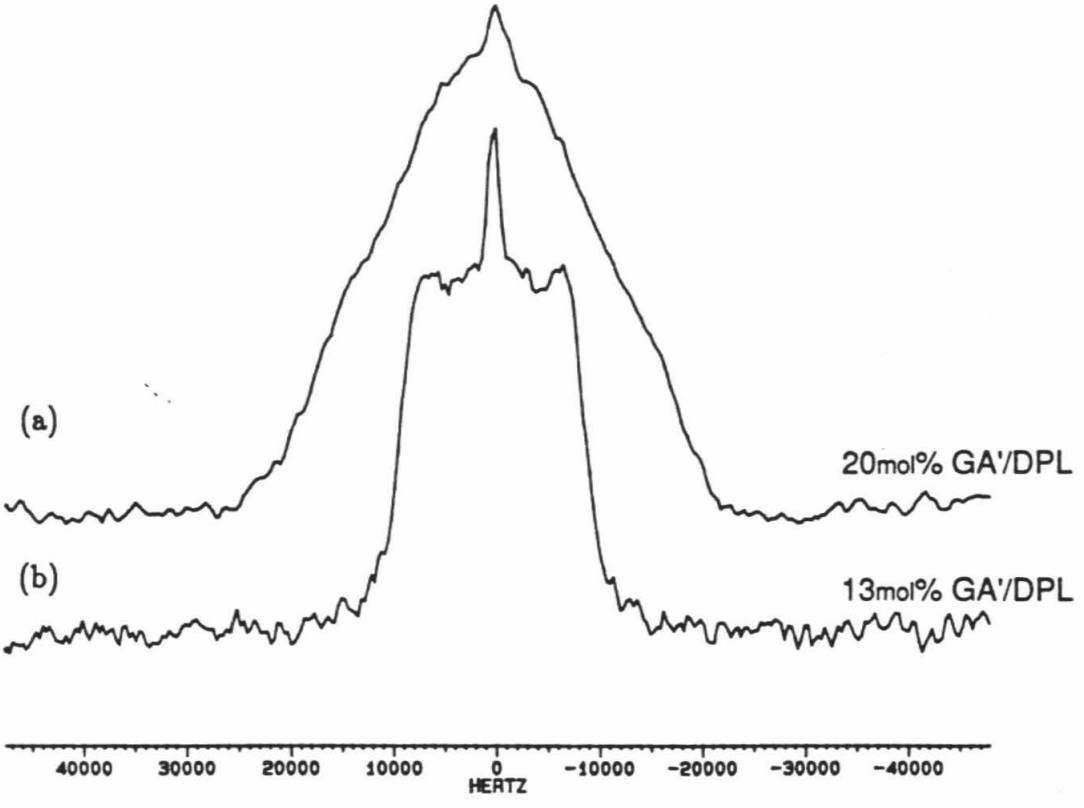
(a)
20mol% GA'/DPL
(b)
13mol% GA'/DPL
40000
30000
20000
10000
0
-10000
-20000
-30000
-40000
HERTZ

as GA′ is added.

In Figure 11, the ^{31}P-NMR spectra of DPL combined with 15 mol % and 20 mol % GA′ are presented. Both the bilayer and H_{II} phases of DPL are present at 15 mol % GA′. The singularity at 7.8 ppm corresponds to the spectrum of the H_{II} phase. Neither the $\Delta\sigma$'s nor the line widths of the 15 mol % and 20 mol % GA′ spectra are drastically different. In H_{II} phase, therefore, motions in the lipid head group do not change as GA′ is added. Furthermore, the similarity of $\Delta\sigma$ and $\Delta\nu_Q$ for DPL H_{II} systems containing varying amounts of GA′ suggest that further addition of GA′ does not affect the orientations of the lipid head groups and chains with respect to the director.

Discussion

I. *Hydrophobic Mismatch in GA′/Lecithin Bilayer Systems*

Hydrophobic mismatch in GA′/lecithin bilayers has been studied by ^{31}P and ^{2}H-NMR. GA′ has been incorporated into DML, DPL, and DSL bilayers. These lipids have similar head groups and hydrocarbon chains of 14, 16, and 18 carbons, respectively. ^{31}P NMR shows that $\Delta\sigma$ decreases uniformly as GA′ is added to each of these three bilayers. $\Delta\nu_Q$, however, increases most for DML, increases less for DPL, and remains essentially constant for DSL as GA′ is added. These trends suggest that GA′ interacts equivalently with the head groups of all the bilayers but perturbs the hydrocarbon chains of each bilayer differently.

$\Delta\nu_Q$ depends on both β'', the angle between the C-D bond vector and the chain segment orientation, and β', the angle between the chain segment and the

Figure 11: The ^{31}P-NMR spectra of (a) 20 mol % GA′ in DPL and (b) 15 mol % in DPL.

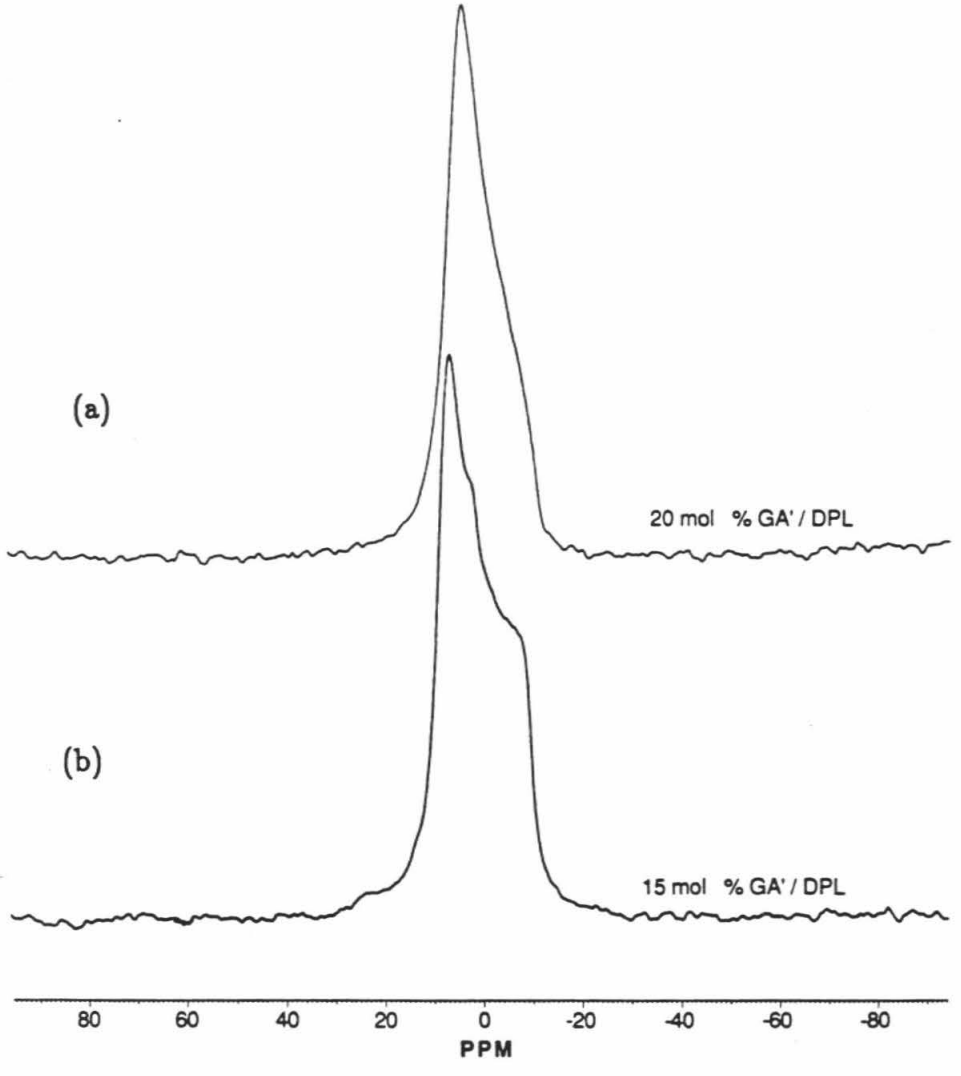
(a)
20 mol % GA' / DPL
(b)
15 mol % GA' / DPL
80
60
40
20
0
-20
-40
-60
-80
PPM

director. $\Delta\nu_Q$ is related to β'' and β' by the following equation:

$$\Delta\nu_Q = \frac{3}{4}\frac{e^2qQ}{\hbar}| < \frac{1}{2}(3\cos^2\beta' - 1) >< \frac{1}{2}(3\cos^2\beta'' - 1) > |$$

It is unlikely that the bond angle β'' will change with the addition of any perturbing substance to a lipid bilayer. It will be assumed, therefore, that only the orientation of the chain segment with respect to the director changes upon addition of GA′. In particular, this change is attributed to adjustment of the lipid chains to hydrophobic mismatch. Note that the sign of $\Delta\nu_Q$ cannot be determined because of the axial symmetry of the ^{2}H spectrum. As a result, there is some ambiguity in the value of the angle β'. In pure lipid bilayers, the average β' value for a methylene carbon in a lipid chain has been shown to be approximately 70°. If this angle increases slightly, $\Delta\nu_Q$ will increase. Likewise, if this angle decreases, $\Delta\nu_Q$ will decrease. The addition of GA′, therefore, increases β' of the 9-10 position hydrocarbon chain segment to varying amounts in the three lipid systems. Because the value of β' is smaller for a gauche conformer than for a trans conformer, an increase in β' corresponds to an increase in the population of trans conformers at the 9-10 position chain segment in the bilayer. One may conclude, therefore, that the population of trans conformers in this region of the bilayer increases as GA′ is added to DML and DPL. This is consistent with Raman and IR spectroscopic findings.[21–23] The ratio of trans to gauche conformers remains constant as GA′ is added to DSL.

If the hydrophobic length of the lipid bilayer is less than that of the added protein, an increase in trans conformers of the lipid hydrocarbon region will compensate for hydrophobic mismatch between a protein and a lipid bilayer. The results of $\Delta\nu_Q$ measurements, therefore, indicate that the hydrophobic length of

GA′ is longer than that of DML and DPL and nearly equal to that of DSL. Table 1 shows the hydrophobic lengths of pure DML, DPL and DSL bilayers in the liquid crystalline phase to be 27.9Å, 29.3Å, and 30.6Å, respectively. The length of the $\beta^{6.3}$ GA′ dimer is 30Å. A comparison of the hydrophobic lengths of the three lipid bilayers with the entire length of GA′ suggests that most or all of the GA′ molecule prefers a hydrophobic environment.

Upon addition of GA′ to the three bilayer systems studied, $\lambda_{\perp}^{u}$ decreases. The difference in this decrease for the three lipid systems parallels the chain length dependence observed for $\Delta\nu_Q$. The cooperative length of the DML bilayer decreases most in response to GA′, the cooperative length of the DPL bilayer decreases less, and the cooperative length of DSL decreases only slightly. The largest change in cooperative length is observed for the system in which hydrophobic mismatch is most severe. Thus, hydrophobic mismatch, which results in extension of the lipid hydrocarbon chains, also decreases the cooperative length of director fluctuation. The ratio of A_C to A_H may be used to understand this effect. As the lipid hydrocarbon chains extend, A_C decreases relative to A_H. As a result, hydrophobic contacts between the chains become weaker, and cooperative motions of the bilayer decay more quickly.

II. *The Bilayer to Hexagonal Transition in GA′/Lecithin Systems*

In order to understand the transition from bilayer to H_{II} phase in GA′/lecithin systems, an analogy is drawn to two geometrically similar transitions. One is a transition from the micellar phase to the bilayer phase observed in GA′/lysopalmitoyllecithin (LPL),[27] and the other is a transition from the bilayer phase to H_{II} phase observed in palmitic acid (PA)/DPL at pH 4.0.[28]

Because the head group area of pure LPL is much greater than the hydrocarbon area, LPL forms micelles. When a sufficient amount of GA′ is added, however, a bilayer phase is formed.

An analogy may also be drawn to the bilayer→H_{II} transitions in a mixture of 66 mol % palmitic acid (PA) in DPL (pH 4.0). PA acts as an additional lipid chain. At high mol % of PA to DPL, H_{II} phase is induced. A study of the temperature dependence of the bilayer→H_{II} phase transition shows a direct transformation from the bilayer gel state into H_{II} phase. In other words, the liquid crystalline state is bypassed completely. This is also observed for GA′/DPL mixtures.

In the GA′/LPL and PA/DPL systems, the GA′ or PA molecules add to the hydrophobic region of the existing lipid structure. As A_C/A_H increases, a phase change is induced. In both cases, the new phase is better able to accommodate the larger value of A_C/A_H. By analogy to the transitions described above, it is deduced that GA′ also increases A_C/A_H. When this ratio is sufficiently large, a transition from bilayer to H_{II} phase occurs. Several characteristics of this transition, however, remain to be explained.

First of all, the transition is chain length dependent. The transition occurs most readily in lipid bilayers whose hydrophobic lengths nearly match or exceed that of GA′. The transition does not occur at all in DML whose hydrophobic length is much less than that of GA′.

Secondly, both the $T_{1\rho}^{-1}$ and T_2^{-1} of deuterons at the 9,10 positions of DPL and DSL increase drastically and abruptly upon addition of GA′ to the H_{II} phase. Although precise relaxation experiments have not been performed, ^{31}P-NMR spectra of the phospholipid head groups in H_{II} phase indicate little change in T_2^{-1} upon addition of GA′. In H_{II} phase, therefore, GA′ interferes significantly with chain

motion, but appears to have no effect on the motion of the lipid head groups.

Lastly, in GA′/dioleoyllecithin bilayers, De Kruijff and co-workers have observed a reversion to bilayer phase at low water contents.[29] Although this phenomenon has been observed in other systems, it is opposite to lipid systems such as phophatidylethanolamine (PE) which favor H_{II} at low water contents.

A simple geometric model presented by Kirk et al. may be used to understand the characteristics of the bilayer to H_{II} transition in GA′/lecithin systems.[30–32] In this model, a lipid system has an intrinsic radius of curvature (R_0). This is the radius of curvature of the surface created by the lipid head groups in the minimum energy conformation. For micelles, R_0 is negative. In a bilayer, R_0 is infinite. If R_0 is small, H_{II} phase forms. R_0 decreases when A_C/A_H increases. According to this model, the R_0 of the DPL bilayer decreases as GA′ is added to the bilayer. At 10 mol % GA′, R_0 has decreased sufficiently to allow the lipid system to assume H_{II} phase. For DSL, R_0 also decreases upon addition of GA′. H_{II} phase, however, appears at 6 mol % GA′. In the DML bilayer, addition of GA′ does not decreases R_0 enough to stabilize H_{II} phase.

Several factors may contribute to the chain length dependence of H_{II} phase formation in GA′/lecithin bilayers. First of all, because of the splay of the hydrocarbon chain tails in longer chain lipids, these lipids simply have larger hydrophobic areas. Thus, A_C/A_H is larger, and R_0 is smaller. This effect, however, does not induce H_{II} formation in pure DML, DPL, or DSL bilayers. The decrease in R_0 due to chain length, therefore, is not sufficient to cause of H_{II} formation.

It has been suggested that the shorter lipid hydrocarbon chains extend to match the hydrophobic length of GA′. This extension is accomplished at the expense of the gauche conformers in the tail of the lipid hydrocarbon chain. A_C,

therefore, decreases with no corresponding decrease in A_H. Thus, A_C/A_H decreases, and R_0 increases. The magnitude of this effect varies with the extent of hydrophobic mismatch. The hydrocarbon chains of DML must extend the most. The hydrocarbon chains of DPL also extend somewhat. Consequently, H_{II} phase becomes less favorable for DML and DPL. In contrast, the hydrocarbon chains of DSL need not extend at all. With regard to this effect, H_{II} phase remains equally favorable in the presence of GA′. The extension effect, therefore magnifies the propensity of short chain lipids to remain in the bilayer phase.

Lastly, GA′ has been shown to insert completely into the lipid hydrocarbon region if permitted by the hydrocarbon chain length. Analogies to phase transitions in the GA′/LPL and PA/DPL systems indicate that GA′ may reduce R_0 by adding its own area to the area of the lipid hydrophobic region. This is equivalent to adding several additional hydrocarbon chains to the hydrophobic region of the bilayer with no corresponding addition to the head group region. Thus, A_C/A_H increases, and R_0 becomes very small. By greatly reducing the R_0 of lecithin bilayers, therefore, GA′ induces H_{II} phase. The addition of GA′ increases A_C/A_H much more than a simple extension or compression of the lipid hydrocarbon chains. As a result, these effects may be neglected.

DML does not undergo the transition to H_{II} phase upon addition of GA′. A_C/A_H, therefore, must not increase sufficiently to induce H_{II} phase in this system. If the DML hydrocarbon chain is not able to stretch sufficiently to contain the GA′ molecule in the hydrophobic region of the bilayer, the GA′ molecule may protrude into the head group region of the bilayer. In this case, increases in the hydrophobic area of the bilayer, will be counteracted to some extent by a similar increase in the head group area. Thus, both A_C/A_H and R_0 change less in DML

than in DPL and DSL, and H_{II} phase will never be stabilized.

Finally the inhibition of H_{II} phase by low water contents must be addressed. This effect has been observed in dioleoyllecithin/dodecane systems.[33] At all water contents, the aqueous inner tube of the H_{II} cylinder must be completely filled with water. As the water content is decreased, therefore, the radius of this inner tube must shrink. High concentrations of GA′ alter the R_0 of DPL and DSL bilayers sufficiently to induce H_{II} phase in excess water. At very low water contents, however, the water present may only be sufficient to fill a narrow H_{II} cylinder. If the radius of this cylinder is much smaller than R_0, only the bilayer phase will be energetically accessible to the GA′/lipid system at low water contents.

Conclusion

NMR studies have shown that the hydrophobic length of the DSL bilayer best matches GA′. Hydrophobic mismatch is encountered when GA is added to DML and DPL bilayers. The lipid hydrocarbon chains, rather than the head groups, accommodate this mismatch. In particular, they extend by increasing trans conformers in the chain. This extension leads to a decrease in the cooperative length of the bilayer.

Intermediate concentrations of GA′ induce H_{II} phase in DPL and DSL bilayers. DML, however, does not undergo a bilayer to H_{II} phase transition at any concentration of GA′. It is proposed that GA′ prefers to be contained in the hydrocarbon region of the bilayer. Addition of GA′ to the bilayer, therefore, increases the ratio of the hydrocarbon chain area to the head group area. This leads to a

decrease in R_0. When R_0 is sufficiently small, H_{II} phase is formed. The DML hydrocarbon region, however, is too short to contain GA′ completely. Thus, GA′ protrudes into the hydrophilic region. The ratio of the hydrocarbon area to the head group area increases much more slowly. As a consequence, R_0 never becomes small enough to stabilize H_{II} phase.

References

1. R. Fisher and T. Blumenthal, *Proc. Natl. Acad. Sci. USA*, **79**, 1045-1048 (1982).
2. S. Weinstein, B. A. Wallace, E. R. Morrow, and W. Veatch, *Proc. Natl. Acad. Sci. USA*, **76**, 4230-4234 (1979).
3. B. A. Cornell, F. Separovic, A. J. Baldassi, and R. Smith, *Biophys. J.*, **53**, 67-76 (1988).
4. Z. Iqbal and Weidekamm, *Arch. Biochem. Biophys.*, **202**, 639-649 (1980).
5. V. M. Naik and S. Krimm, *Biophys. J.*, **45**, 109-112 (1984).
6. V. M. Naik and S. Krimm, *Biophys. J.*, **49**, 1147-1154 (1986).
7. W. R. Veatch, E. T. Fossel, and E. R. Blout, *Biochemistry*, **13**, 5249-5256 (1974).
8. J. A. Killian and B. De Kruijff, *Biophys. J.*, **53**, 111-117 (1988).
9. B. A. Wallace, W. R. Veatch, and E. R. Blout, *Biochemistry*, **20**, 5754-5760 (1981).
10. A. Spisni, I. Pasquali-Ronchetti, E. Casali, L. Lindner, P. Cavatorta, L. Masotti, and D. W. Urry, *Biochim. Biophys. Acta*, **732**, 58-68 (1983).
11. B. F. Cornell and F. Separovic, *Biochim. Biophys. Acta*, **733**, 189-198 (1983).
12. J. N. Israelachvili, D. J. Mitchell, and B. W. Ninham, *Biochim. Biophys. Acta*, **470**, 185-201 (1977).
13. A. Kusumi and J. S. Hyde, *Biochemistry*, **21**, 5978-5983(1982).
14. B. A. Lewis and D. M. Engelman, *J. Mol. Biol.*, **166**, 203-210 (1983).
15. J. Riegler and H. Moehwald, *Biophys. J.*, **49**, 1111-1118 (1986).
16. L. T. Pearson, S. I. Chan, B. A. Lewis, and D. M. Engelman, *Biophys. J.*, **43**, 167-174 (1983).
17. L. T. Pearson, J. Edelman, and S. I. Chan, *Biophys. J.*, **45**, 863-871 (1984).
18. S. B. Hladky and D. A. Haydon, *Biochim. Biophys. Acta*, **274**, 294-312 (1972).

19. H. A. Kolb and E. Bamberg, *Biochim. Biophys. Acta*, **464**, 127-141 (1977).

20. J. R. Elliot, D. Needham, J. P. Dilger, and D. A. Haydon, *Biochim. Biophys. Acta*, **735**, 95-103 (1983).

21. D. Chapman, B. A. Cornell, A. W. Eliasz, and A. Perry, *J. Mol. Biol.*, **113**, 517-538 (1977).

22. D. C. Lee, A. A. Durrani, and D. Chapman, *Biochim. Biophys. Acta*, **769**, 49-56 (1984).

23. D. Aslanian, M. Negrerie, and R. Chambert, *Eur. J. Biochem.*, **160**, 395-400 (1986).

24. J. A. Killian, C. W. van den Berg, H. Tournois, S. Keur, A. J. Slotboom, G. J. M. van Scharrenburg, and B. De Kruijff, *Biochim. Biophys. Acta*, **857**, 13-27 (1986).

25. C. J. A. Van Echteld, B. De Kruijff, A. J. Verkleij, J. Leunissen-Bijvett, and J. De Gier, *Biochim. Biophys. Acta*, **692**, 126-138 (1982).

26. V. Chupin, J. A. Killian, and B. De Kruijff, *Biophys. J.*, **51**, 395-405 (1987). (1980).

27. D. W. Urry, T. L. Trapane, K. U. Prasad, *Science*, **221**, 1064-1067 (1983).

28. D. Marsh and J. M. Seddon, *Biochim. Biophys. Acta*, **690**, 117-123 (1982).

29. J. A. Killian and B. De Kruijff, *Biochemistry*, **24**, 7890-7898 (1985).

30. G. L. Kirk, S. M. Gruner, and D. L. Stein, *Biochemistry*, **23**, 1093-1102 (1984).

31. G. L. Kirk and S. M. Gruner, *J. Physique*, **46**, 761-769 (1985).

32. S. M. Gruner, *Proc. Natl. Acad. Sci. USA*, **82**, 3665-3669 (1985).

33. M. Sjolund, G. Lindblom, L. Rilfors, and G. Arvidson, *Biophys. J.*, **52**, 145-153 (1987).

Chapter VI

Raman Spectroscopic Studies of Gramicidin A′ Conformations in Crystalline Form and in Lecithin Environments

Introduction

In chapter 5, the effect of hydrophobic mismatch on three GA′/lecithin systems was examined. It was proposed that the equilibrium length of the acyl region of DSL most closely matches the hydrophobic length of GA′. The acyl chains of DML and DPL must extend to varying amounts to accommodate the hydrophobic length of GA′.

GA′ is a mixture of three pentadecapeptides (Gramicidin A, Gramicidin B, and Gramicidin C) with sequences which differ only at position 11. In all the peptides, trptophan residues are located at positions 9, 13, and 15. The predominant form, Gramicidin A, also has a tryptophan group at position 11. In Gramicidins B and C, this tryptophan is replaced by phenylalanine or tyrosine, respectively. In all the peptides, the group nearest the C-terminus is a tryptophan. Because GA forms an N-N dimer in lipid bilayers, one might expect at least one tryptophan to be situated near the aqueous exterior in this conformation.

Hydrophobic mismatch between GA′ and the surrounding lipid may affect the tryptophan environment in the following way. If the acyl chains of the lipids cannot extend sufficiently to shield the uppermost tryptophans, they may be exposed to the more hydrophilic environment of the lipid head groups. The more severe the hydrophobic mismatch is, the more polar an environment the tryptophans of GA′ will experience. Thus, the environment of GA′ should be most hydrophilic in the DML bilayer.

Raman spectroscopy has proven useful in monitoring the hydrophobicity of the tryptophan environment. Recently, Miura et al. have suggested that the fre-

quency of the 880 cm^{-1} tryptophan vibrational mode is indicative of the extent of hydrogen bonding of the indole NH.[1,2] In non-hydrogen bonding environments, this band appears at 882-883 cm^{-1}. In more strongly hydrogen bonding environments, this band shifts to lower frequencies.Another significant feature of the trptophan spectrum is a Fermi resonance doublet which arises from a fundamental skeletal stretching vibration and a combination band arising from indole ring vibrational modes. The components of the doublets appear at approximately 1360 cm^{-1} and 1342 cm^{-1}. The ratio of their intensities is indicative of the polarity of the indole ring environment. This ratio is defined as:

$$R = \frac{I_{1360}}{I_{1342}}$$

For hydrophilic environments, this ratio is in the range of 0.65 to 0.92. In the presence of aromatic groups, the ratio increases to 1.23-1.32. For saturated carbon environments such as lipid environments, the range is 1.0-1.2. Raman spectroscopy, therefore, will be used to test the hypothesis that the overall tryptophan environment is more polar for shorter chain length lipids.

Normal mode calculations have predicted measurable differences in Raman backbone amide vibrations of double and single GA′ helices of varying pitch.[3] Some Raman studies have supported these calculations,[4] and some have not.[5] In this work, Raman spectroscopy will be used to establish the similarity of GA′ conformations in the DML, DPL, and DSL environments.

In lipid systems, GA′ is assumed to be in a single $\beta^{6.3}$ helix. By x-ray crystallography, crystalline GA′ has been shown to be in an anti-parallel, double helical conformation.[6] By comparing the Raman spectra of GA′/lecithin systems with that of crystalline GA′, the possibility of distinguishing the $\beta^{6.3}$ helical and the

anti-parallel double helical conformations of GA′ using Raman spectroscopy will be assessed.

In summary, Raman spectroscopy will be used to determine the effect of hydrophobic mismatch on the polarity of the tryptophan environment in GA′/lecithin systems. In addition, the conformation of the amide backbone of GA′ in the various lecithin systems will be monitored by Raman spectroscopy.

Experimental Section

I. *Materials and Methods*

DML, DPL, and DSL were purchased from Avanti Polar Lipids. GA′, a mixture of 85 % gramicidin A and 15 % gramicidins B and C, was purchased from Boehringer Mannheim Biochemicals.

GA′ was dissolved in methanol and then added to DML, DPL, or DSL in the appropriate amounts to obtain a 20 mol % concentration of GA′ in lipid. Addition of chloroform was necessary to dissolve the longer chain lipids mixed with GA′. The organic solvent was evaporated from the GA′/lecithin sample under low vacuum until most of the solvent was removed. The sample was then placed under high vacuum overnight. Samples were then hydrated in excess 400mM Tris, 40mM NaCl buffer (pH 7.4). In order to reach an equilibrium distribution of GA in the lipid, it was necessary to incubate samples above the phase transition temperature of the respective GA′/lecithin mixtures for approximately twelve hours. The suspensions were then transferred to quartz capillaries and stored at room temperature until Raman spectra were acquired. All experiments were performed

at room temperature.

II. *Raman Instrumentation*

In these experiments, the sample was held in a liquid capillary backscattering mount. A Spex 1mm double monochromator was used with an increment of 1 pt/cm^{-1}. The 488 nm band of an Ar^+ laser, operated at a power level of 500 mWatts, served as the excitation source. The emitted intensities were amplified using a photomultiplier tube in photon counting mode. A SCAMP computer from Spex, Inc. controlled both the monochromator increment and data aquisition. For all samples, four scans were averaged in order to obtain adequate signal-to-noise.

Results and Discussion

Figure 1 shows the region from 600 cm^{-1} to 1700 cm^{-1} in the Raman spectra of crystalline GA′ and 20 mol % GA′ in the DML, DPL, and DSL systems. There are no detectable differences in the frequencies of any of the peptide bands for the three lipid systems studied. Thus, one may conclude that the conformation of GA′ does not vary drastically with the acyl chain length of the surrounding lipid environment.

Of special interest is the amide I band of GA′. Table I shows the frequencies predicted by Naik and Krimm for possible GA conformations. X-ray diffraction has demonstrated that crystalline GA′ is in an anti-parallel $\beta^{5.6}$ double helical conformation. In a lipid environment, however, GA′ is believed to assume a $\beta^{6.3}$ helical conformation.[7] In Figure 2, an expanded view of the amide I region is presented for the four GA′ samples studied. The amide I band appears at 1668 cm^{-1} in all systems. The shape and frequency of this band shows little dependence on the conformation of GA′. Contrary to the calculations of Naik and Krimm,

Figure 1: The region from 600 cm^{-1} to 1700 cm^{-1} in the Raman spectra of (a) pure crystalline GA′, (b) 20 mol % GA′ in DML, (c) 20 mol % GA′ in DPL, and (d) 20 mol % GA′ in DSL. All spectra were taken at room temperature.

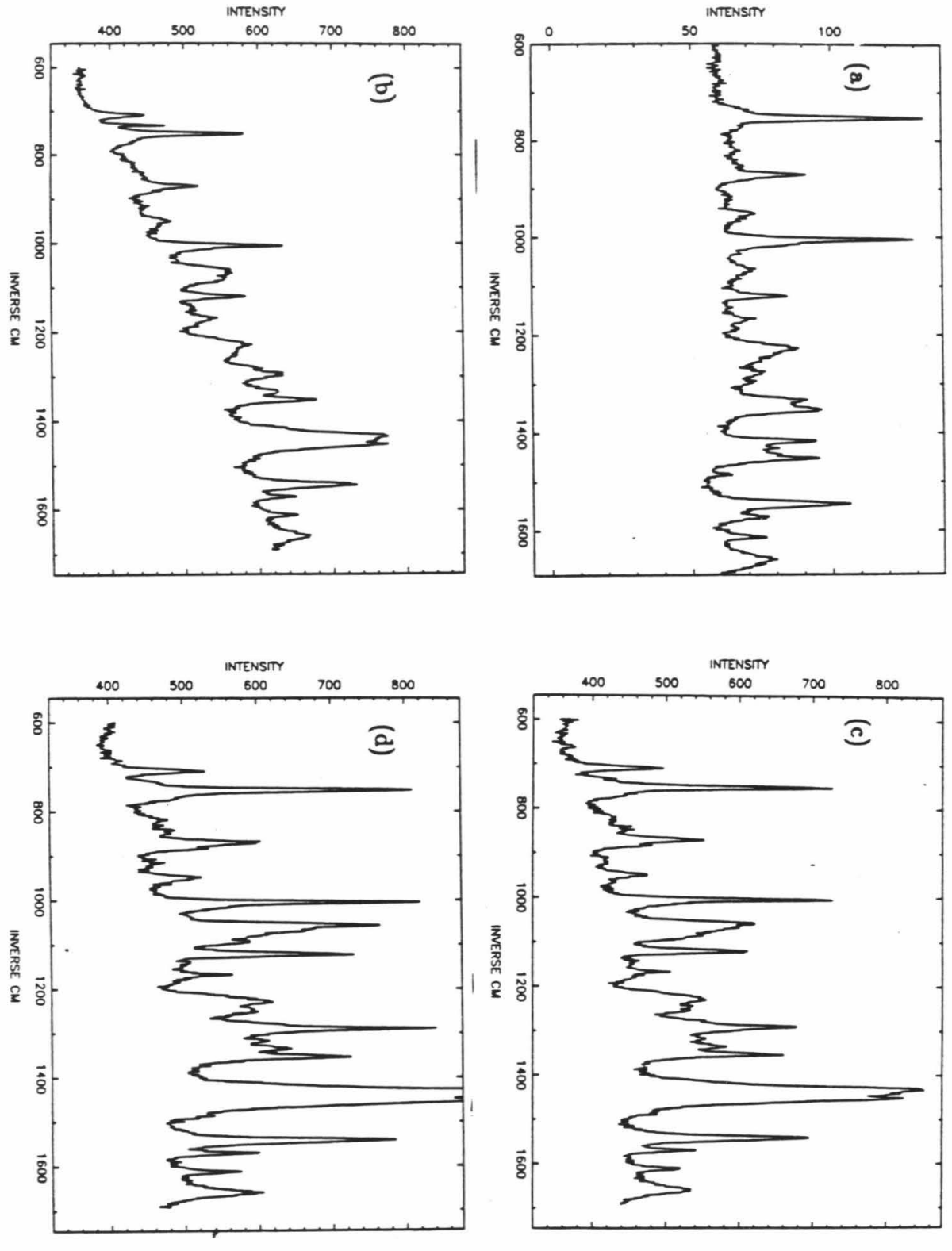
(a)
INTENSITY
0
50
100
600
800
1000
1200
1400
1600
INVERSE CM
(b)
INTENSITY
400
500
600
700
800
600
800
1000
1200
1400
1600
INVERSE CM
(c)
INTENSITY
400
500
600
700
800
600
800
1000
1200
1400
1600
INVERSE CM
(d)
INTENSITY
400
500
600
700
800
600
800
1000
1200
1400
1600
INVERSE CM

Table I: The amide I frequencies predicted by Naik and Krimm[3] for the Raman spectrum of various GA′ structures. The single helices represent possible conformations of GA′ in the lipid bilayer, while the double helices represent possible conformations of GA′ in pure crystalline form and in organic solvents.

Table I

Structure	Predicted Amide I Frequency (cm^{-1})
Single Helices:	
$Beta^{4.4}$	1648-53
$Beta^{6.3}$	1652-54
Double Helices:	
$Beta^{5.6}$	1656-75
$Beta^{7.2}$	1651-86

Figure 2: An expanded view of the Amide I region of the GA′ Raman spectrum. GA′ in the following environments is shown: (a) pure crystalline GA′, (b) GA′ in DML, (c) GA′ in DPL, and (d) GA′ in DSL. All spectra were taken at room temperature.

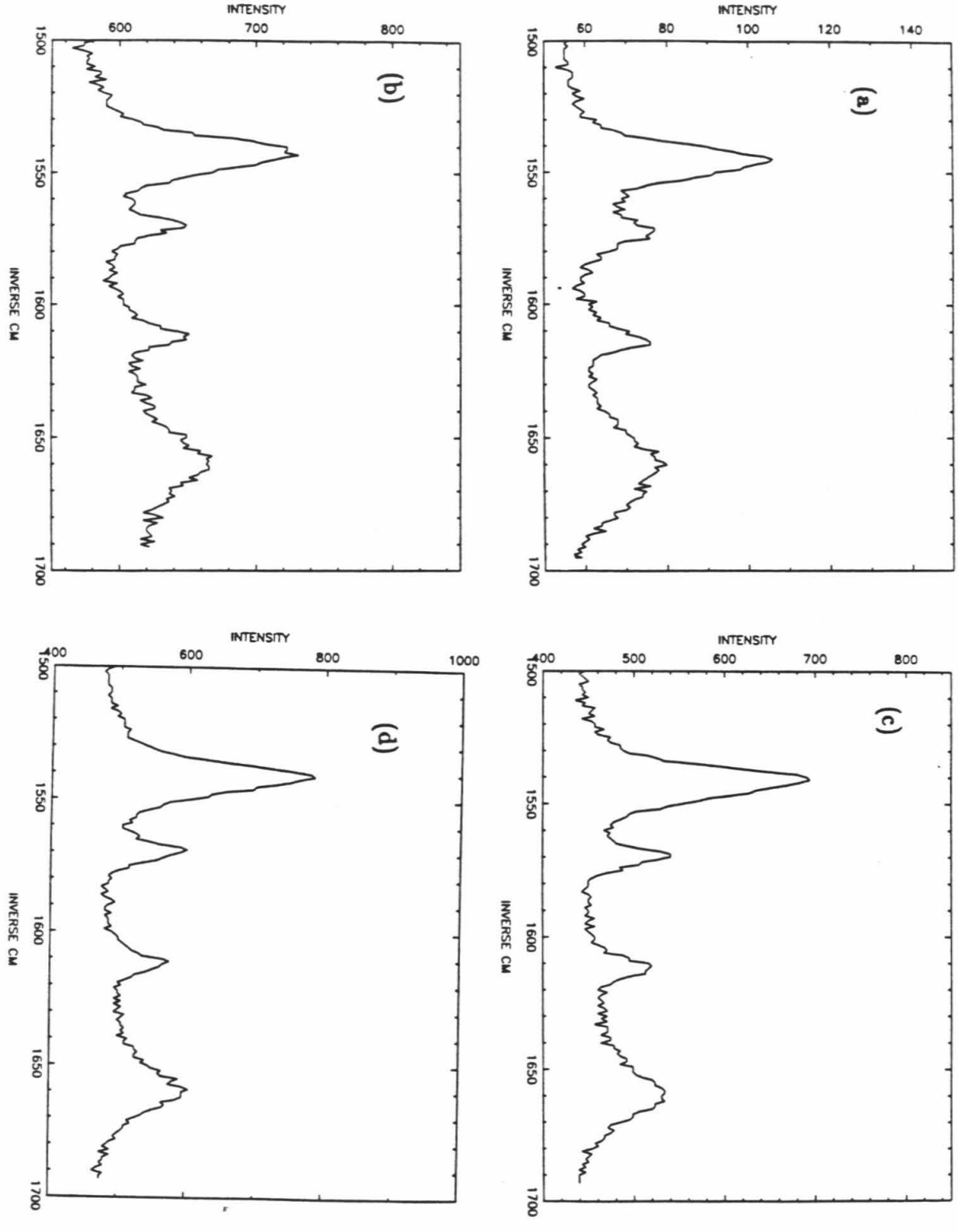
(a)
INTENSITY
60
80
100
120
140
1500
1550
1600
1650
1700
INVERSE CM
(b)
INTENSITY
600
700
800
1500
1550
1600
1650
1700
INVERSE CM
(c)
INTENSITY
400
500
600
700
800
1500
1550
1600
1650
1700
INVERSE CM
(d)
INTENSITY
400
600
800
1000
1500
1550
1600
1650
1700
INVERSE CM

therefore, these studies show that Raman spectroscopy cannot distinguish between the various conformations of GA′.

In Figure 3, expanded plots of the 880 cm^{-1} tryptophan band are shown for crystalline GA′ and GA′ in all lecithin systems. The frequency and intensity of the bands are listed in Table II. This band appears at 870 cm^{-1} in the spectrum of crystalline GA′. This suggests an tryptophan indole -NH environment which is highly hydrogen bonding. The hydrogen bonding environment is probably provided by neighboring GA′ molecules. The 870 cm^{-1} band, therefore, is indicative of intermolecular GA′ interactions.

In all the DML, DPL, and DSL systems, an additional GA′ tryptophan band appears at 882 cm^{-1}. This band corresponds to a tryptophan indole -NH in a very non-hydrogen bonding environment. The GA′ molecules in this environment are probably surrounded by lipid molecules. By analogy to the Raman spectrum of crystalline GA′, the 870 cm^{-1} band of GA′ in the lecithin systems probably arises from GA′ molecules in direct contact with other GA′ molecules. In all GA′/lecithin systems, the ratio of the 870 cm^{-1} band to the 882 cm^{-1} band is approximately two. At 20 mol % GA′, therefore, peptide-peptide contacts are extensive in all the lipid systems studied.

In Table II, the intensity ratio (R) of the Fermi doublet is listed for crystalline GA′ and GA′ in each lipid system. In Figure 4, the region of the Raman spectrum containing this doublet is shown for each system. The band frequencies are similar in all spectra. The R's, however, differ. The R of crystalline GA′ falls in the range predicted for an aromatic environment. This probably corresponds to tryptophan-tryptophan stacking interactions. X-ray crystallographic studies of the anti-parallel double helical conformation of GA′ show that

Figure 3: An expanded view of the 880 cm^{-1} band of th tryptophans of GA′ is shown. (a) pure crystalline GA′ . (b) GA′ in DML. (c) GA′ in DPL. (d) GA′ in DSL.

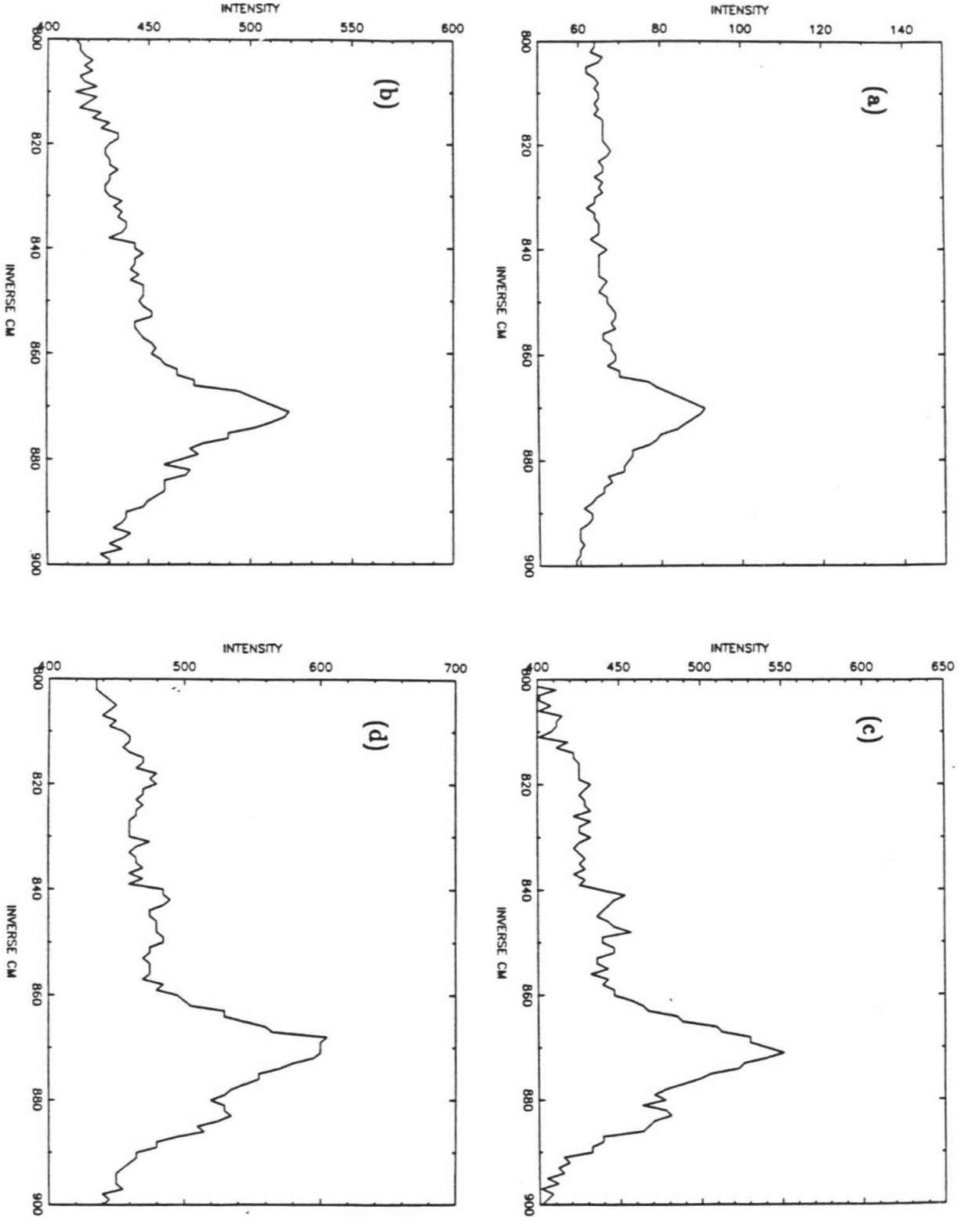
(a)
INTENSITY
60
80
100
120
140
INVERSE CM
800
820
840
860
880
900
(b)
INTENSITY
400
450
500
550
600
INVERSE CM
800
820
840
860
880
900
(c)
INTENSITY
400
450
500
550
600
650
INVERSE CM
800
820
840
860
880
900
(d)
INTENSITY
400
500
600
700
INVERSE CM
800
820
840
860
880
900

Table II: The frequencies and intensities for the 880 cm^{-1}, 1340 cm^{-1}, and 1360 cm^{-1} bands for the Raman spectra of the tryptophans in GA′. R, the ratio of the 1360 cm^{-1} band intensity to the band intensity of the 1340 cm^{-1} band, is also calculated. Data are tabulated for GA′ in pure crystalline form and in DML, DPL, and DSL environments. All data are reported for room temperature spectra.

Table II

Sample	880 cm^{-1} Band	Intensity	1340 cm^{-1} Band	Intensity	1360 cm^{-1} Band	Intensity	R
GA'	870	25	1332	45.7	1354	50.0	1.09
GA'/DML	871 882	88 40	1333	41.8	1352	63.6	1.52
GA'/DPL	871 883	126 57	1334	130.0	1353	202.5	1.56
GA'/DSL	870 883	145 84	1334	147.2	1343	226.4	1.54

Figure 4: An expanded view of the 1360 cm^{-1}/1340 cm^{-1} Fermi doublet of the tryptophans in GA′. (a) pure crystalline GA′. (b) GA′ in DML. (c) GA′ in DPL. (d) GA′ in DSL.

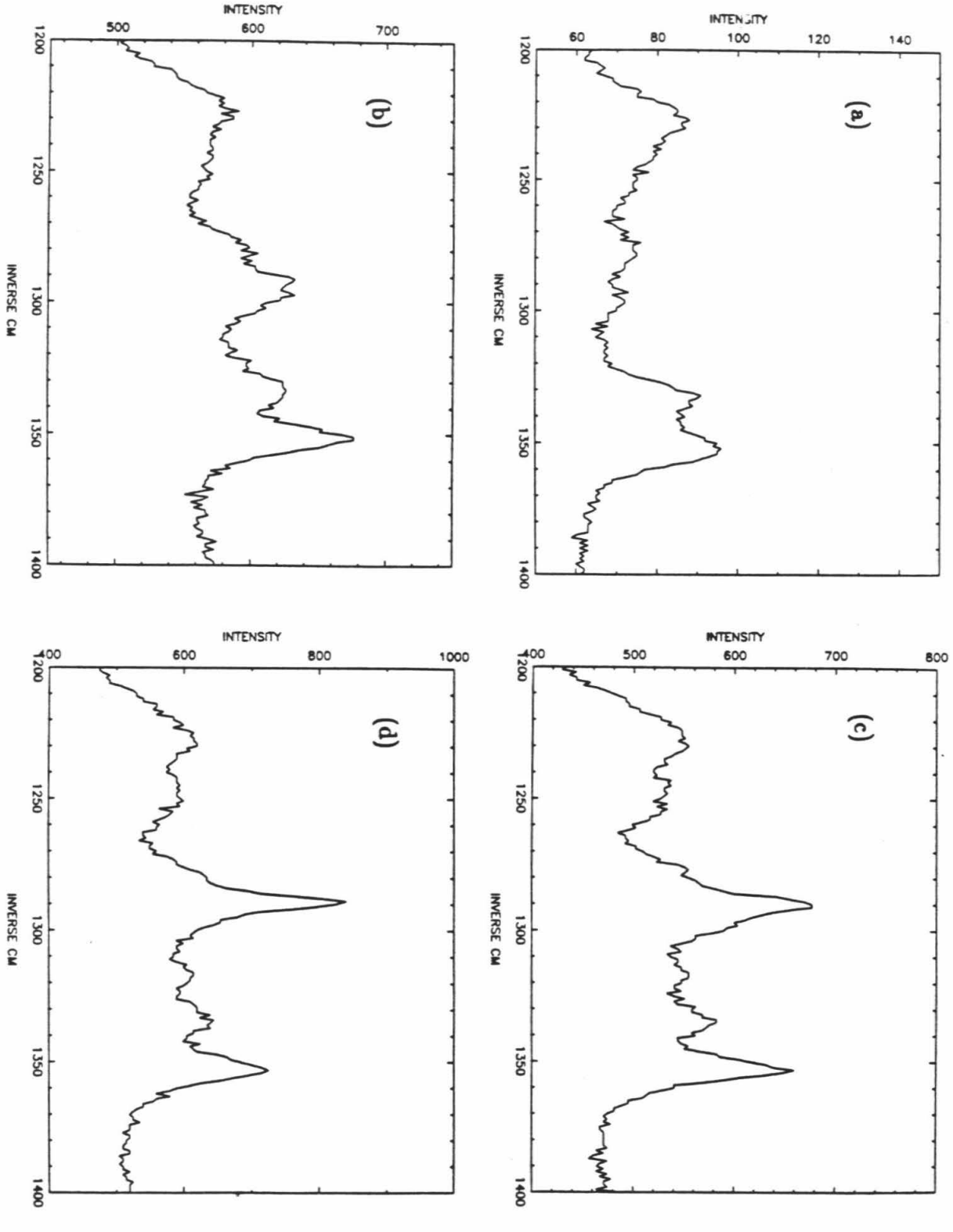
(a)
INTENSITY
60
80
100
120
140
1200
1250
1300
1350
1400
INVERSE CM
(b)
INTENSITY
500
600
700
1200
1250
1300
1350
1400
INVERSE CM
(c)
INTENSITY
400
500
600
700
800
1200
1250
1300
1350
1400
INVERSE CM
(d)
INTENSITY
400
600
800
1000
1200
1250
1300
1350
1400
INVERSE CM

intramolecular tryptophan-tryptophan interactions are unlikely. Thus, intermolecular tryptophan-tryptophan interactions must be present in crystalline GA′.

The R value for the tryptophans of GA′ in lecithin systems clearly indicates a very hydrophobic environment. Furthermore, the R of GA′ in DPL and DSL is slightly larger than that of GA′ in DML. A comparison of the spectra in Figure 4 shows that the difference in R between the three GA′ /lecithin systems studied is probably not an artifact of the peak height measurement. The environment of tryptophan in DML, therefore, may be slightly more hydrophilic than its environment in DPL or DSL. This supports the conclusions of chapter 5 suggesting that GA′ may protrude from the acyl chain region in the DML bilayer. This exposes the tryptophans nearest the C-terminus of GA′ to the hydrophilic environment of the polar lipid head groups.

Conclusions

Although Raman spectroscopy cannot distinguish between the different types of β-helical structures assumed by GA′, the Raman spectra of the various GA′/lecithin systems studied indicate that no major changes in the conformation of GA′ occur as the thickness of the lipid environment is altered.

Raman spectroscopy has also been used to determine the hydrophobicity of the tryptophan environment for GA′ in crystalline form and in DML, DPL, and DSL environments. The 870 cm^{-1} band of crystalline GA′ indicates the presence of GA′-GA′ interactions. In all lecithin systems, an additional band is observed at 882 cm^{-1}. This band probably arises from GA′ surrounded by lipid molecules.

A comparison of R for GA′ in the three lipid systems shows the tryptophans

of GA′ to be in a slightly more polar environment in DML than they are in either DPL or DML. As was proposed in chapter 5, the acyl chain of DML may be unable to extend sufficiently to match the hydrophobic length of GA′. As a result, the tryptophans of GA′ have more contact with the head group region of the DML bilayer. Raman spectroscopy of the GA′/lecithin systems, therefore, supports the conclusion that the hydrophobic thickness of GA′ is most poorly matched to that of DML and better matched to longer chain lecithins such as DPL and DSL.

References

1. I. Harada, T. Miura, and H. Takeuchi, *Spectrochim. Acta*, **42A**, 307-312 (1986).
2. T. Miura, H. Takeuchi, and I. Harada, *Biochemistry*, **27**, 88-94 (1988).
3. V. M. Naik and S. Krimm, *Biophys. J.*, **49**, 1131-1145 (1986).
4. V. M. Naik and S. Krimm, *Biophys. J.*, **49**, 1147-1154 (1986).
5. K. W. Short, B. A. Wallace, R. A. Myers, S. P. A. Fodor, and A. K. Dunker, *Biochemistry*, **26**, 557-562 (1987).
6. B. A. Wallace, *Biophys. J.*, **49**, 295-306 (1986).
7. S. Weinstein, B. A. Wallace, E. R. Morrow, and W. Veatch, *Proc. Natl. Acad. Sci. USA*, **76**, 4230-4234 (1979).

Chapter VII

Differential Scanning Calorimetric Studies of Gramicidin A in DML, DPL, and DSL Systems

Introduction

Mismatch between the hydrophobic length of a membrane-bound protein and that of the surrounding lipid may alter many properties of the lipid system. The effect of hydrophobic mismatch on cooperative director fluctuations in lipid bilayers was presented in chapter 5. In addition, hydrophobic mismatch may alter the gel-to liquid crystalline phase transition temperature of the lipid bilayer (T_c).[1,2] In this chapter, the effect of GA′ on the T_c of the DML, DPL, and DSL systems will be examined by DSC. Less detailed studies of GA′ in DML and DPL have been presented by Chapman et al. and Macdonald et al.[3,4]

Mouritsen and Bloom have recently presented a thermodynamic 'mattress' model of the gel-to liquid crystalline phase transition.[5] This model predicts the shift in the T_c of a lipid bilayer upon addition of a membrane-bound protein of whose hydrophobic thickness differs from that of the lipid. In this model, the lipid and protein are described as one dimensional springs with associated equilibrium lengths and elastic constants. Three effects of hydrophobic mismatch are considered in this model. These are (1) extension of the lipid or protein 'spring' to compensate for the mismatch in hydrophobic lengths, (2) the energetically favorable interaction of the hydrophobic regions of the lipid and protein, and (3) the energetically unfavorable interaction between hydrophobic regions of the lipid with hydrophilic regions of the protein or vice-versa. The latter interaction is results from insufficient extension of the lipid or protein to accommodate the mismatch in hydrophobic length. The mattress model does not consider protein-protein interactions. It is only valid, therefore, at low protein/lipid ratios and

under non-aggregated protein conditions.

The GA′/lecithin system provides an ideal test of the mattress model. The hydrophobic length of GA′ in the lipid bilayer is fairly well characterized. In its $\beta^{6.3}$ helical conformation, the GA′ dimer is approximately 30Ålong. In chapter 5, it was shown that the hydrophobic length of GA′ is best matched to the DSL bilayer. Because the hydrophobic length of DSL is 30.6Å, it is apparent that the entire length of GA′ must prefer a hydrophobic environment. The hydrophobic lengths of lecithin bilayers both above and below T_c are also well known.[6,7] The model, therefore, may be tested on a well-defined system. In this chapter, the phase diagram for DML, DPL, and DSL mixed with up to 20 mol % GA′ is presented. At low GA′ concentrations, the phase diagrams of the GA′/lecithin systems have been used to test the mattress model of the membrane. At high GA′ concentrations, ^{31}P-NMR has been used to label the phase boundaries observed in the DSC traces.

Experimental Section

I. *Materials and Methods*

DML, DPL, and DSL were purchased from Avanti Polar Lipids. GA′, a mixture of 85 % gramicidin A and 15 % gramicidins B and C, was purchased from Boehringer Mannheim Biochemicals.

GA′ was dissolved in methanol. Appropriate amounts of GA′ were then added test tubes containing DML, DPL, or DSL. 5mgs of lipid were used to obtain DSC traces of pure lipid samples. Because the width of the phase transition increased

with GA′ concentration, 10 mgs of lipid were used to obtain good signal to noise at intermediate GA′ concentrations. At the highest GA′ concentrations, 15 mgs of lipid were used. Most of the organic solvent was allowed to evaporate under low vacuum. The GA′/lecithin mixture was then transferred quantitatively to 8 × 15 mm thin-walled glass sample container. The remaining organic solvent was then evaporated under low vacuum. The sample was placed under high vacuum overnight to remove any trace amounts of solvent. Samples were then hydrated in 20λ-40λ of 400mM Tris, 40mM NaCl buffer (pH 7.4). In order to reach an equilibrium distribution of GA in the lipid suspension, samples were incubated above the phase transition for approximately twelve hours. The sample containers were then placed directly in the stainless-steel ampoules of the DSC.

II. *DSC Instrumentation*

The calorimetric studies were carried out on a Hart Scientific Model S7708 high-sensitivity differential scanning calorimeter (Hart Scientific, Provo, Utah) which was interfaced to an IBM PC/XT microcomputer. The DSC was equipped with four ampoules, three of which were used for experimental samples and one of which was used as a reference. The reference ampoule contained a glass container similar to that of the GA′/lecithin samples with an equivalent volume of buffer solution. Both samples and reference were heated at a uniform rate of 10°C/Hr. The digitized data were collected every ten seconds and stored in the computer. The measured voltage signals were converted to microWatt units using electrical calibrations.

III. *Data Analysis*

The DSC data were transferred from the IBM XT to a VAX computer. Phase

transition temperatures were measured from the top of each peak in the DSC spectra. At lower concentrations of GA′, it was possible to deconvolute peaks and, thus, measure transition temperatures and enthalpies more accurately. The data were processed in six steps. The names of the programs used to process the data are:

(1) DSCRED

(2) BASELINE

(3) POLYFIT

(4) MIDDLEFIT4

(5) INTEGRATE2

(6) CONVERTDSC

This approach assumes that the phase transitions are first order and that the two peaks in the DSC trace represent parallel rather than sequential phase transitions. DSCRED rewrites the data in a standard two column format. BASELINE fits the baseline of a DSC curve to a polynomial of maximum order 15. The order of the polynomial to be used in the fit is left as an input parameter. A polynomial of order 2 yielded an excellent fit of baselines for all DSC traces. In addition, up to two regions of the trace may be excluded from the fit. These regions were generally reserved for the pretransition signal and the signal due to multiple overlapping main transitions.

Two strongly overlapping signals corresponding to main transitions were observed in the DSC traces of bilayers with low mol % GA′. For clarity, the T_c of the transition occurring at lower temperature will be referred to T_c^1, and that occurring at higher temperature will be referred to as T_c^2. In order to determine the T_c's and enthalpies of these peaks, they were deconvoluted using an iterative

procedure.

First, T_c^1 and T_c^2 were estimated. The part of the DSC trace containing the two peaks were divided into the following three regions: (1) $T<T_c^1$, (2) $T_c^1 <T<T_c^2$, and (3) $T>T_c^2$. Overlap was greatest in region 2. The overlap in regions (1) and (3) was not significant. For this reason, regions (1) and (3) were first fit to polynomials of order 15 or less, respectively, using the POLYFIT program. At lower GA′ concentrations, DSC peaks were quite sharp, and higher order polynomials were necessary to obtain good fits. In a first approximation, the two peaks were assumed to be symmetric about their respective phase transitions. Intensities in region 2 were generated by reflecting the polynomials generated to fit regions (1) and (3) about T_c^1 and T_c^2, respectively. The intensities in region (2)produced by this method were too high.

The MIDDLEFIT4 program was used to refine the results of POLYFIT by fixing the polynomial describing one of the peaks while varying the other. Input parameters include which of the polynomials will be varied and which of the three regions of the DSC trace will be fitted.

The approximate phase transition temperatures were refined in the following way. Most DSC traces contained a dominant peak whose T_c could be accurately determined. Thus, by fixing the polynomial fit of the dominant peak and varying that of the smaller peak, a more accurate estimate of the smaller peak's T_c could be obtained. A typical result of the T_c refinement is shown in Figure 1.

Using the new, more exact T_c's, the limits of regions (1), (2), and (3) were redefined, and POLYFIT program was used to fit regions (1) and (3). The MIDDLEFIT4 program was then used iteratively in each of the three regions in order to obtain a best fit to the experimental data. The result of such a fit is shown in

Figure 1: The result of using the computer programs described in the text to locate the T_c of the minor peak in a DSC endotherm. The DSC trace of 4 mol % GA′ in DPL is simulated. The solid line is the experimental trace. The dotted lines represent simulations of the low and high temperature endotherms. The stars represent the sum of the low and high temperature endotherm simulations. There is a very good match between the experimental data and the sum of the low and high temperature endotherm simulations.

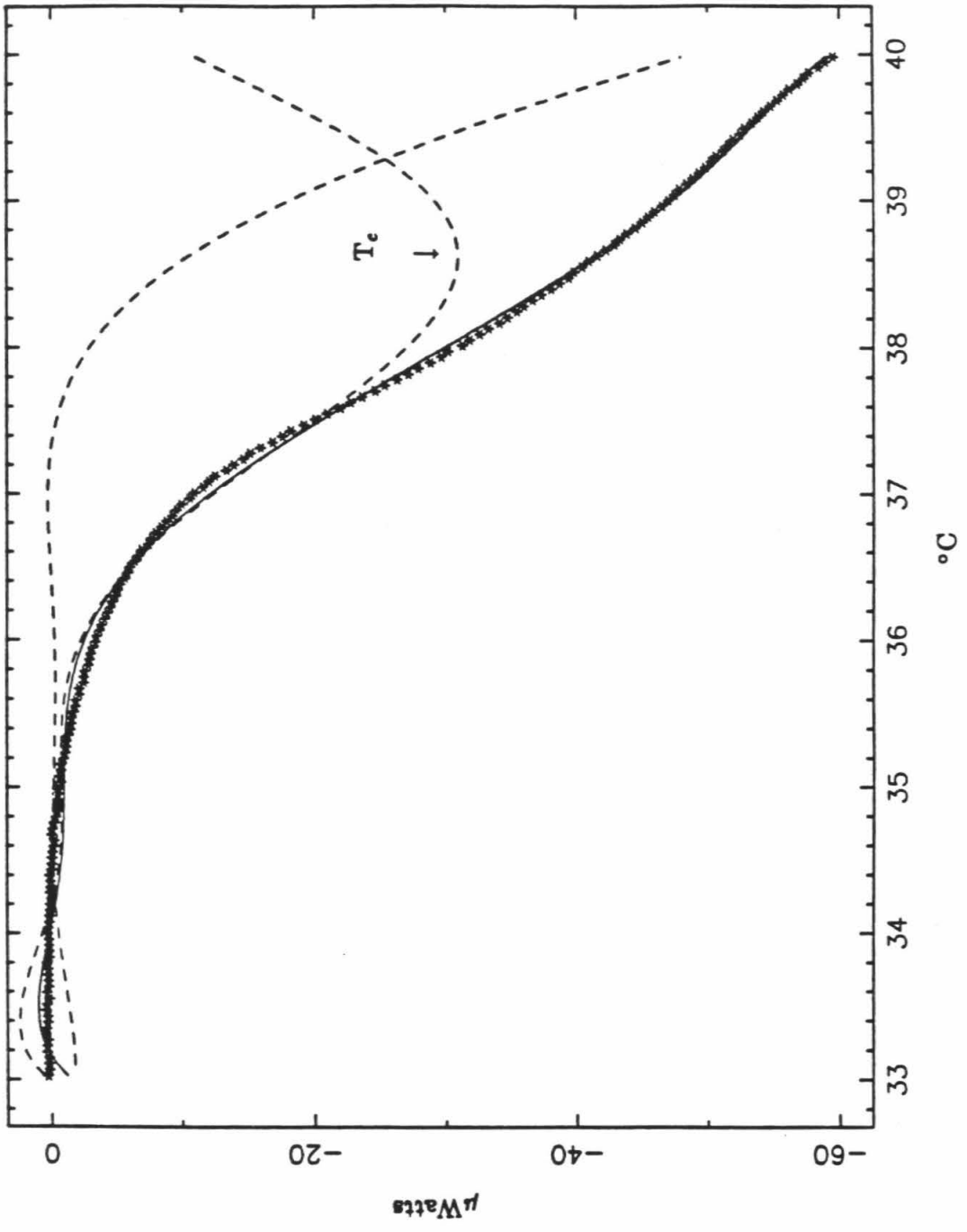
Tc
0
−20
−40
−60
μWatts
33
34
35
36
37
38
39
40
°C

Figure 2. The result depended heavily on which polynomial was chosen to remain constant in the first iteration. In general, the dominant peak in each region was varied. For example, in region (1), the polynomial corresponding to the lower temperature peak was varied first. Thus, a single peak was described by a different polynomial in each region of the DSC trace, and peak symmetry was not assumed in these calculations. Best fits were obtained when the two peaks were of comparable intensity or separated by 1°C or more.

Subsequently, the coefficients of the two polynomials were fed into the INTEGRATE2 program. This program calculated the areas under the two polynomials in each of the three regions of the DSC trace. The areas, therefore, were calculated from the polynomial fits rather than from the experimental data. The areas of each peak in the three regions were summed. The final error in area varied with the intensities and temperature separations of the two peaks. In general, it was probably in the range of 20 %. Finally, CONVERTDSC was used to convert the areas from μWatt to millicalories.

In summary, a series of programs were written which allowed the calculation of T_c's and enthalpies for two strongly overlapping DSC endotherms.

Results

In Figure 3, typical traces are shown for low and high concentrations of GA′ in each of the lipid bilayers. In Figure 4, the complete phase diagrams for up to 20 mol % GA′ in DML, DPL, and DSL are shown. All GA′/lipid systems

Figure 2: A full simulation of the main endotherms in the DSC trace of 4 mol % GA′ in DPL. The dotted lines represent the respective simulations of the low and high temperature endotherms as described in the text. The * represent the sum of these endotherms. The solid line which represents the experimental data is barely visible under the simulated trace.

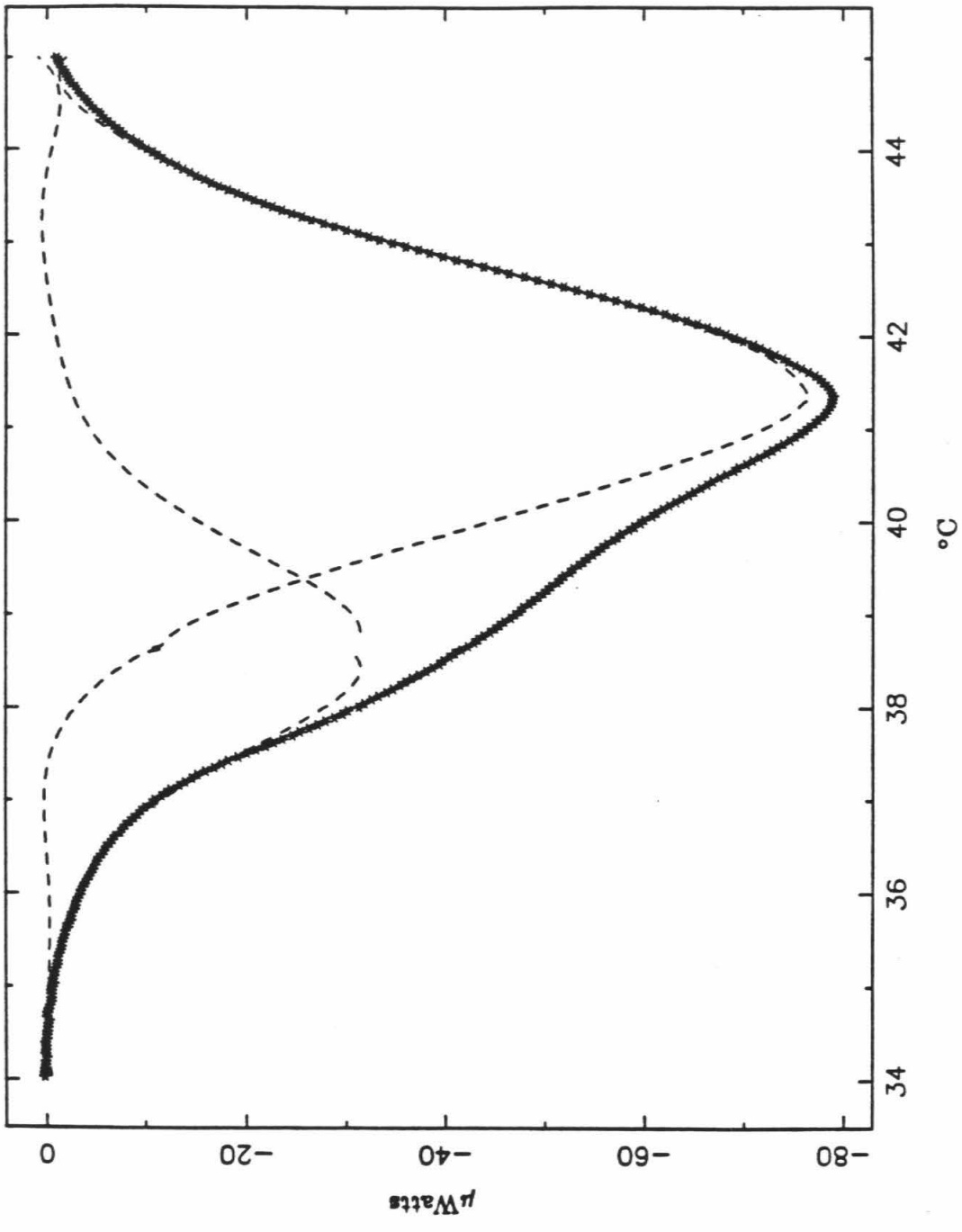
0
−20
−40
−60
−80
μWatts
34
36
38
40
42
44
°C

Figure 3: DSC traces of low and high concentrations of GA′ in the DML, DPL, and DSL systems. Before each DSC experiment, samples were incubated above their respective gel-to-liquid crystalline phase transition temperatures for 12 hours.(a) 2 mol % GA′/DML. (b) 8 mol % GA′/DML. (c) 2 mol % GA′/DPL. (d) 10 mol % GA′/DPL. (e) 2 mol % GA′/DSL. (f) 5 mol % GA′/DSL. (g) 10 mol % GAP/DSL.

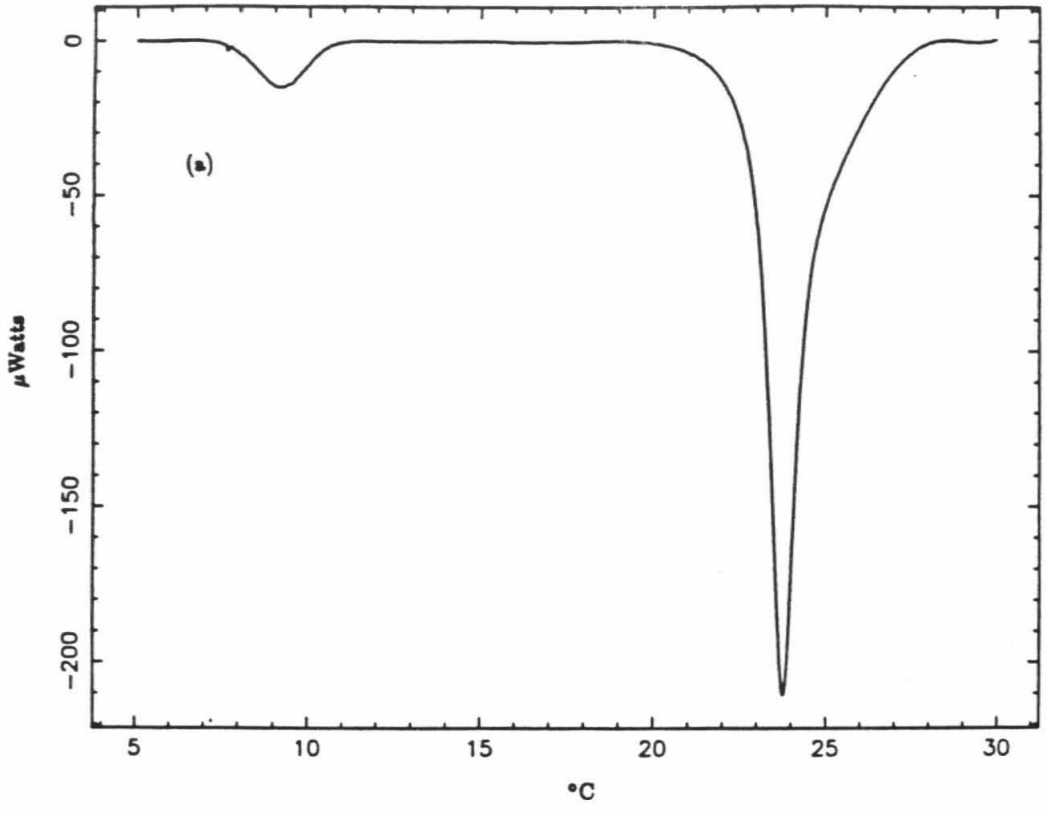
(a)
0
−50
−100
−150
−200
μWatts
5
10
15
20
25
30
°C

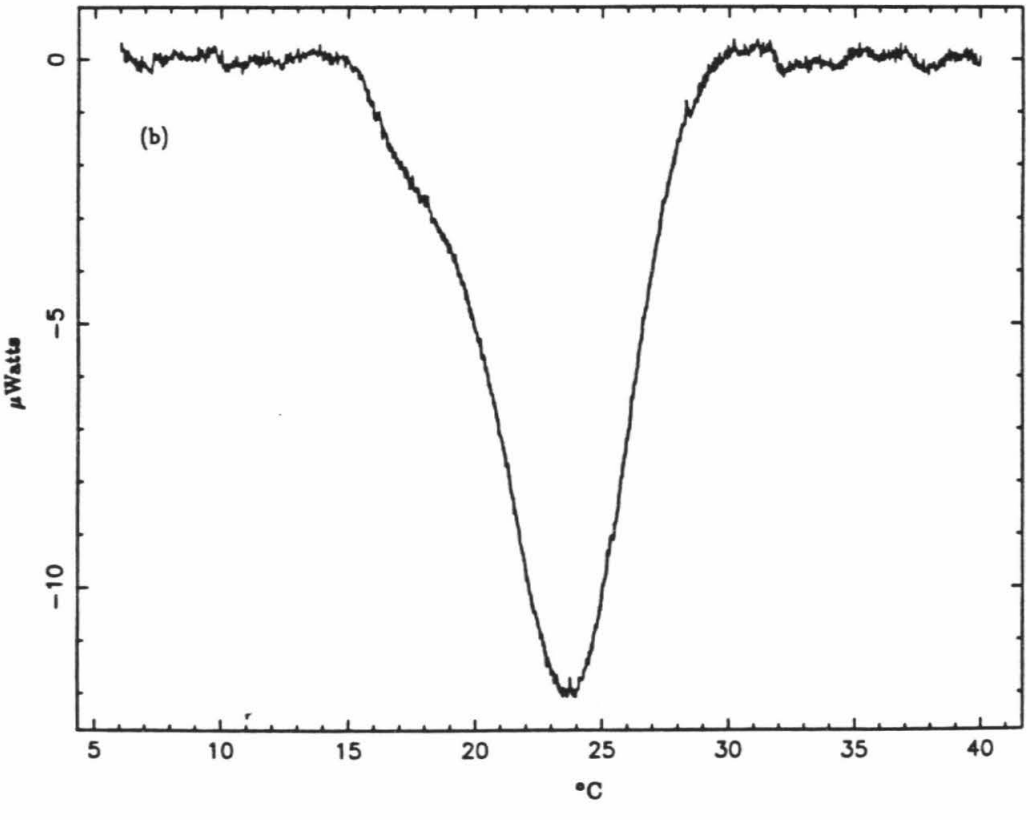
(b)
0
−5
−10
μWatts
5
10
15
20
25
30
35
40
°C

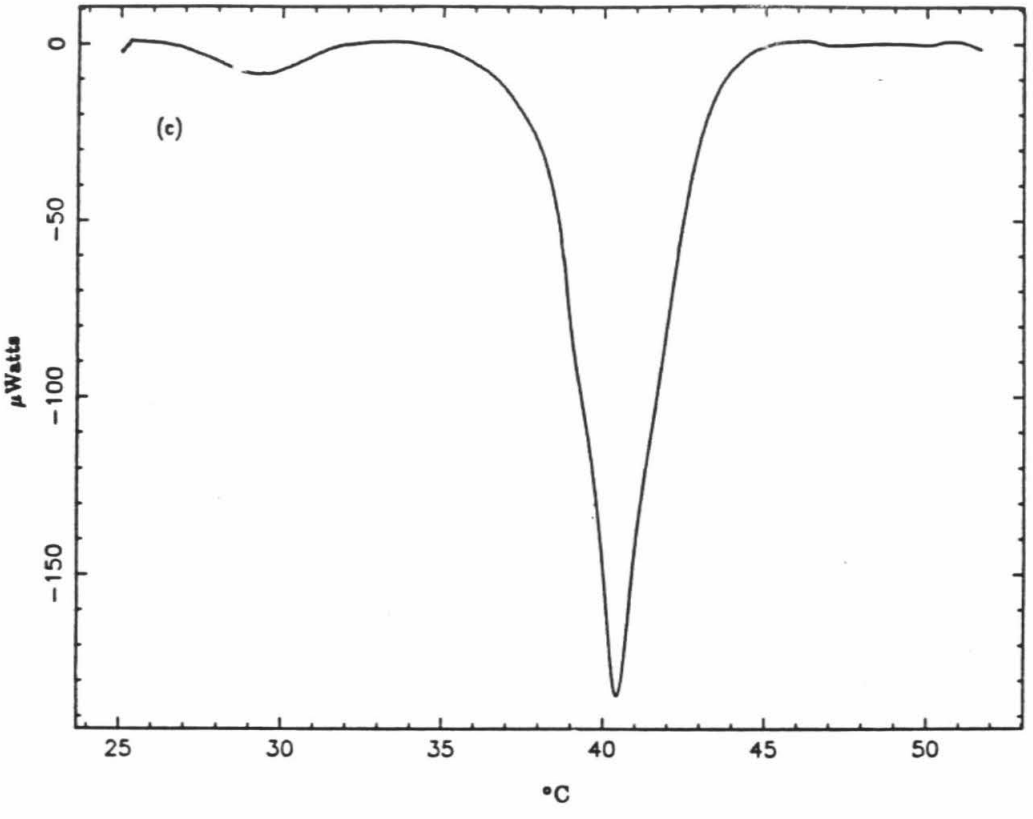
(c)
0
−50
−100
−150
µWatts
25
30
35
40
45
50
°C

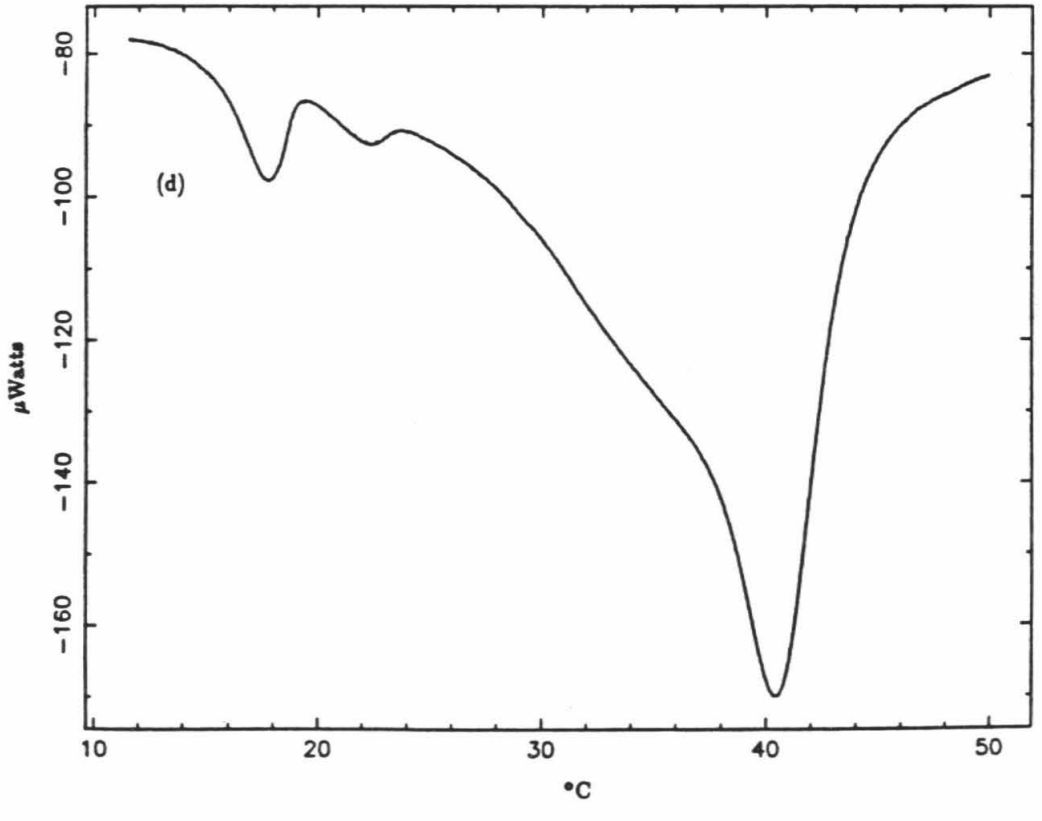
(d)
−80
−100
−120
−140
−160
µWatts
10
20
30
40
50
°C

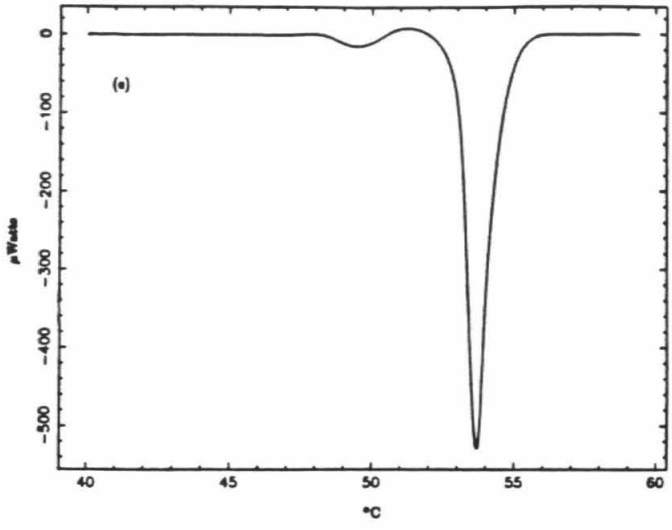
(e)
0
-100
-200
-300
-400
-500
μWatts
40
45
50
55
60
°C

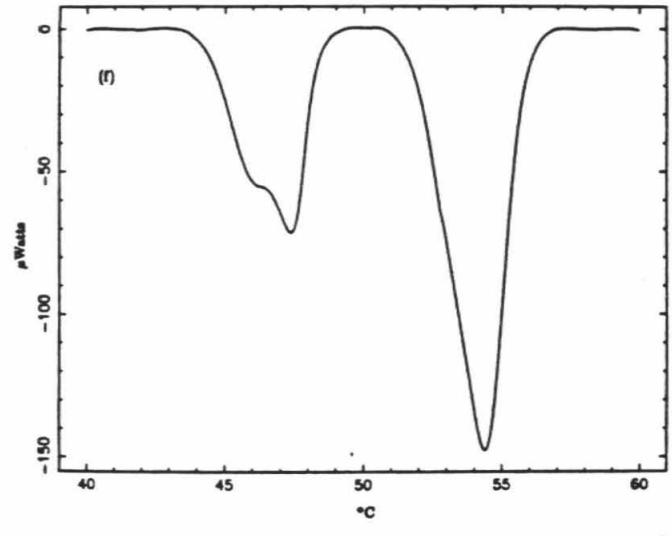
(f)
0
-50
-100
-150
μWatts
40
45
50
55
60
°C

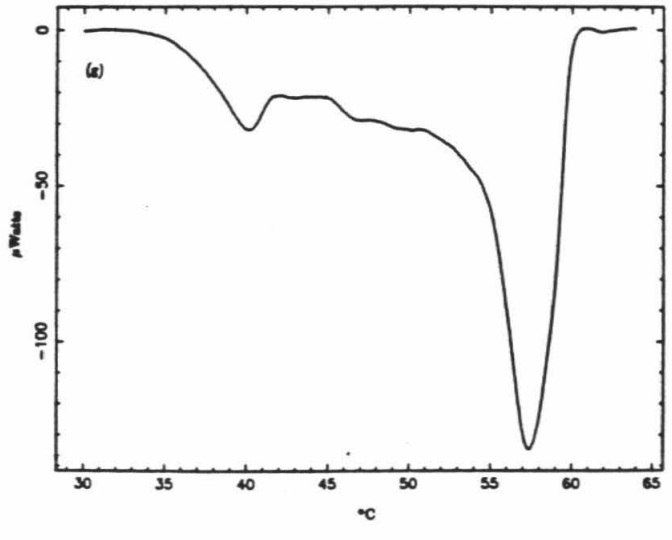
(g)
0
-50
-100
μWatts
30
35
40
45
50
55
60
65
°C

Figure 4: The phase diagrams for up to 20 mol % GA′ in the (a) DML, (b) DPL, and (c) DSL lipid systems. Phase transition temperatures were measured from the bottom of each endotherm. The labels L_α, $P_{\beta'}$, and $L_{\beta'}$ indicate the liquid crystalline state, the gel state with hydrocarbon chains parallel to the bilayer normal, and gel state with chains tilted with respect to the bilayer normal, respectively. H_{II} represents the hexagonal phase. The type of interaction between the GA′ and lipid molecules are described by the labels in parentheses. S_L and S_S represent solutions of GA′ and lipid in the liquid crystalline and gel states, repsectively. C represents a compound phase of GA′ and lipid whose composition is not known.

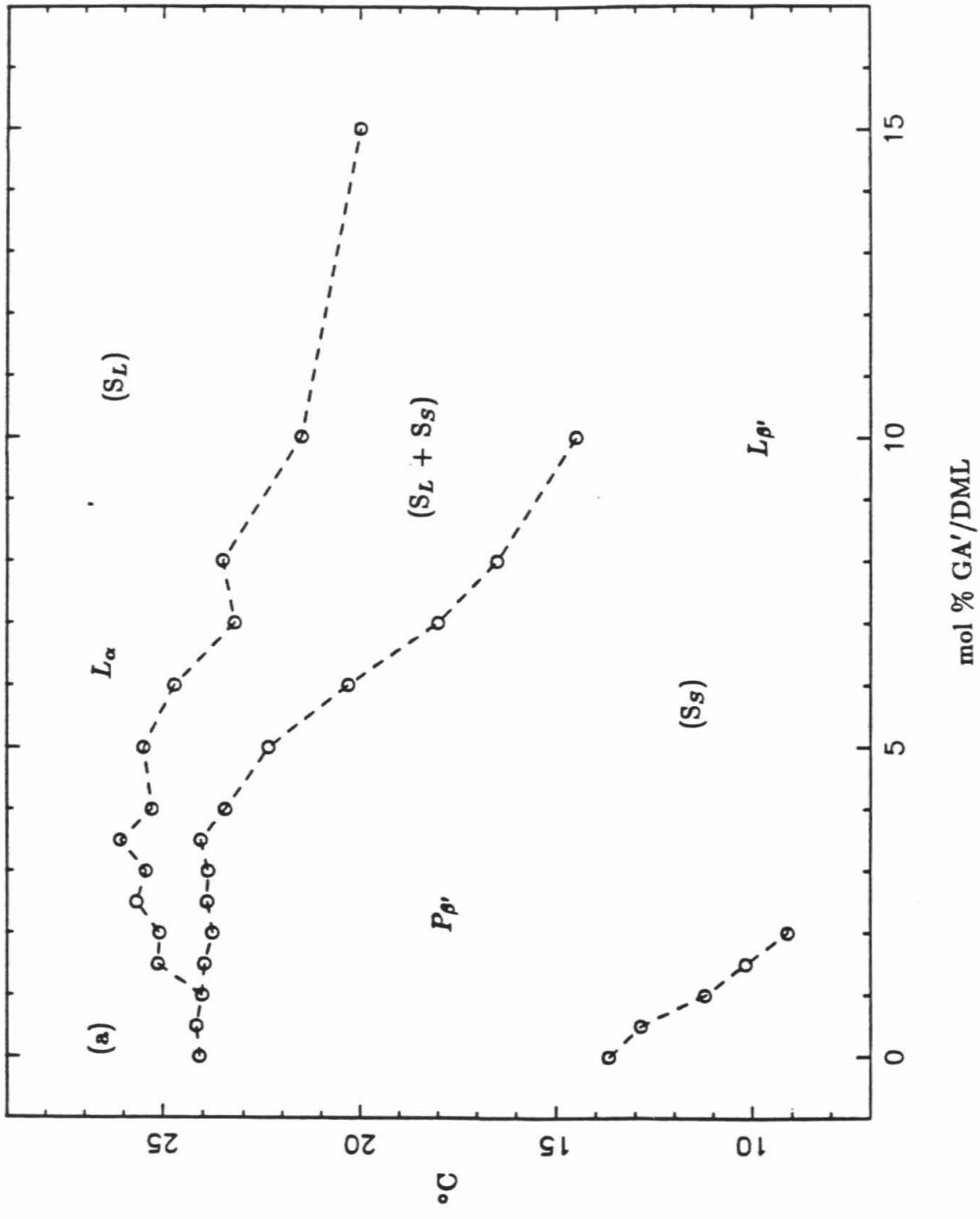
(a)
L_α
(S_L)
(S_L + S_S)
$P_{\beta'}$
(S_S)
$L_{\beta'}$
°C
25
20
15
10
0
5
10
15
mol % GA'/DML

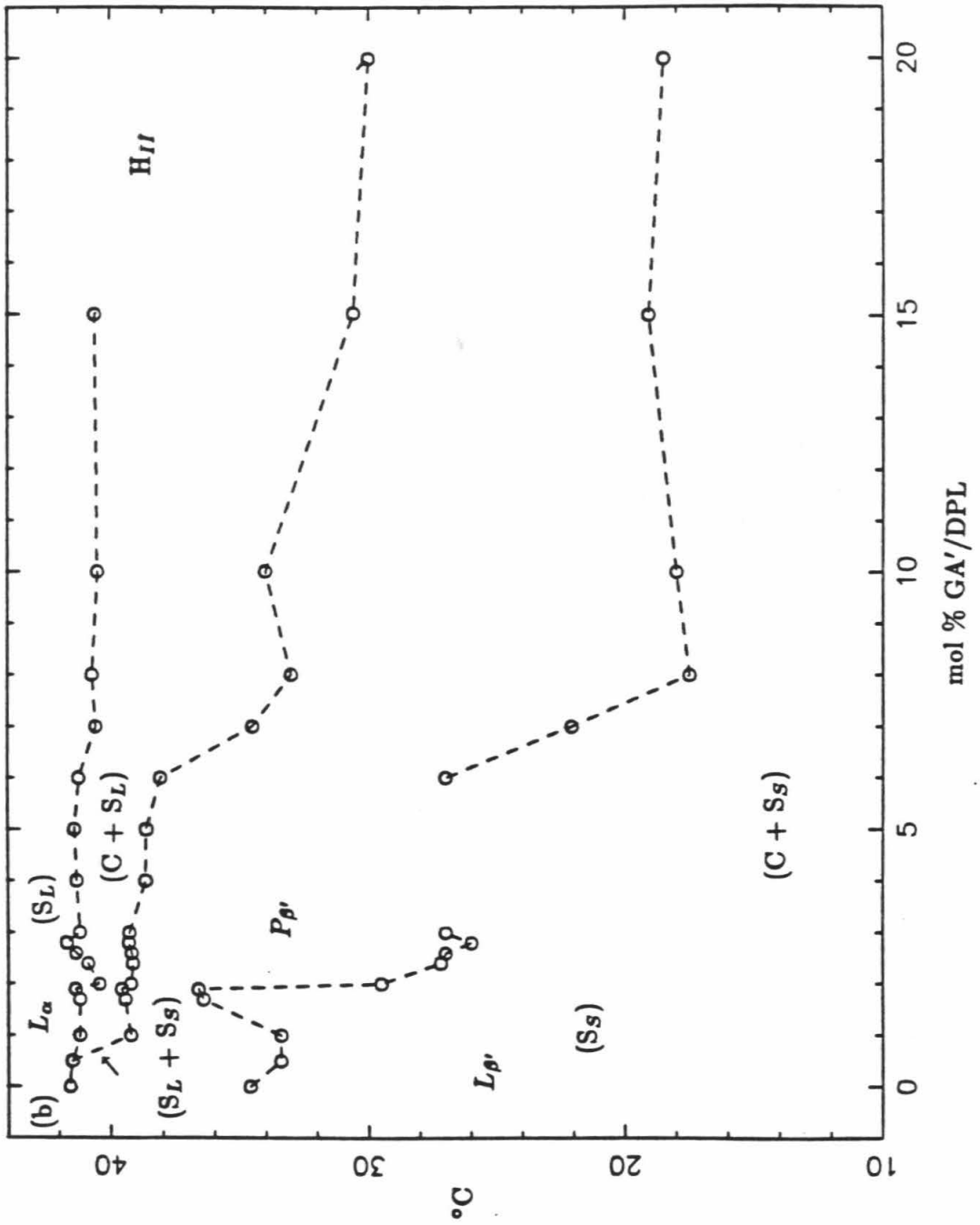
(b)
L_α
(S_L)
H_{II}
$(C + S_L)$
$(S_L + S_s)$
$P_{\beta'}$
$L_{\beta'}$
(S_s)
$(C + S_s)$
°C
10
20
30
40
0
5
10
15
20
mol % GA'/DPL

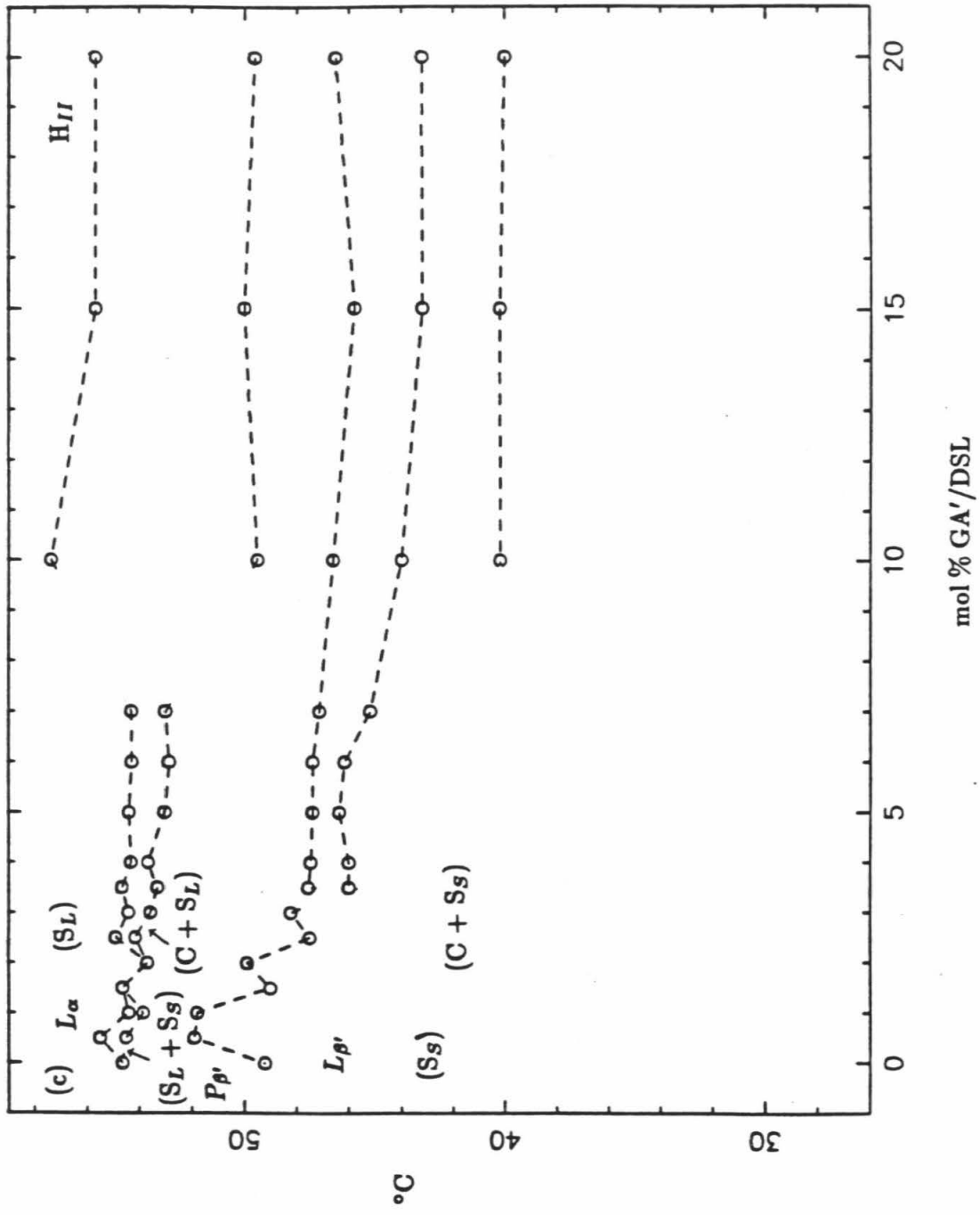
(c)
L_α
(S_L)
H_{II}
(S_L + S_s)
(C + S_L)
$P_{\beta'}$
$L_{\beta'}$
(S_s)
(C + S_s)
°C
50
40
30
0
5
10
15
20
mol % GA'/DSL

exhibit protein rich and protein poor phases at low mol % of peptide. The high temperature phase boundary represents the transition of the peptide poor phase from the L_α or liquid crystalline bilayer state into the $P_{\beta'}$ gel state.In DML, simple two phase behaviour extends to high mol % of GA′. In DPL and DSL, a eutectic point is reached at approximately 2 mol % GA′. Beyond this point a GA′/lecithin compound phase, labelled C, is formed. The actual composition of the compound phase is not known. An endotherm corresponding to the pre-transition from the $L_{\beta'}$ gel phase with tilted hydrocarbon chains to the $P_{\beta'}$ gel phase with straight hydrocarbon chains is observed in all lipid systems at low mol % of peptide. In DML, the pre-transition disappears at 2 mol % GA′, while in DPL and DSL, the pre-transitions is not observed above 3 mol % peptide.

At high mol % GA′ in DPL and DSL, a complicated DSC trace is observed. ^{31}P-NMR temperature dependence experiments show that these complicated endotherms reflect a transition from H_{II} phase into bilayer gel phase. This transition occurs at temperatures well below the gel-to-liquid crystalline phase transition temperatures of the pure lipid bilayer. A ^{31}P-NMR temperature dependence study of 20 mol % GA′ in DSL is shown in Figure 5. These spectra indicate that an isotropic phase may be an intermediate step in the transition from H_{II} phase to bilayer gel phase. Because of the large line width of ^{31}P spectra of lipid bilayers in the gel state, however, an isotropic phase is difficult to identify with certainty.

As the mattress model is particularly relevant to low protein concentrations, this part of the phase diagram has been studied in detail for all GA′/lecithin systems. In Figure 6, region of low GA′ concentration in the phase diagram of each lipid system has been expanded. The shape of the phase diagram in this region varies with the hydrocarbon chain length of the lecithin used to make the

Figure 5: The ^{31}P-NMR spectrum of a 20 mol % GA′in DSL at several temperatures. The transition from H_{II} phase to bilayer phase with decreasing temperature is illustrated (a) T=60°C. (b) T=44°. (c) T=40°. (d) T=27°.

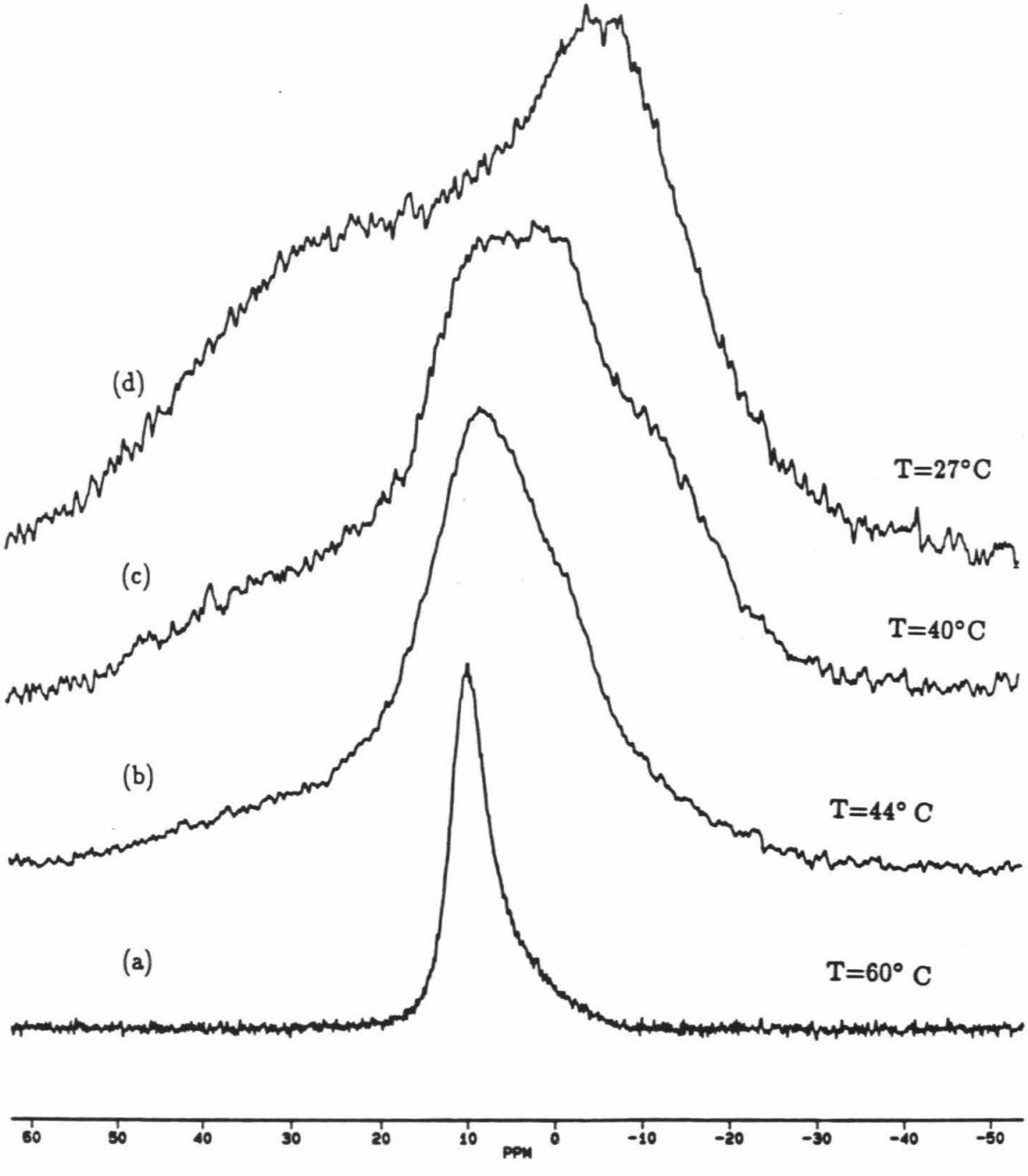
(d)
T=27°C
(c)
T=40°C
(b)
T=44° C
(a)
T=60° C
60
50
40
30
20
10
PPM
0
-10
-20
-30
-40
-50

Figure 6: An expanded view of the low mol % region of the phase diagrams for (a) GA′ in DML, (b) GA′ in DPL, and (c) GA′ in DSL. Labels are the same as in Figure 4.

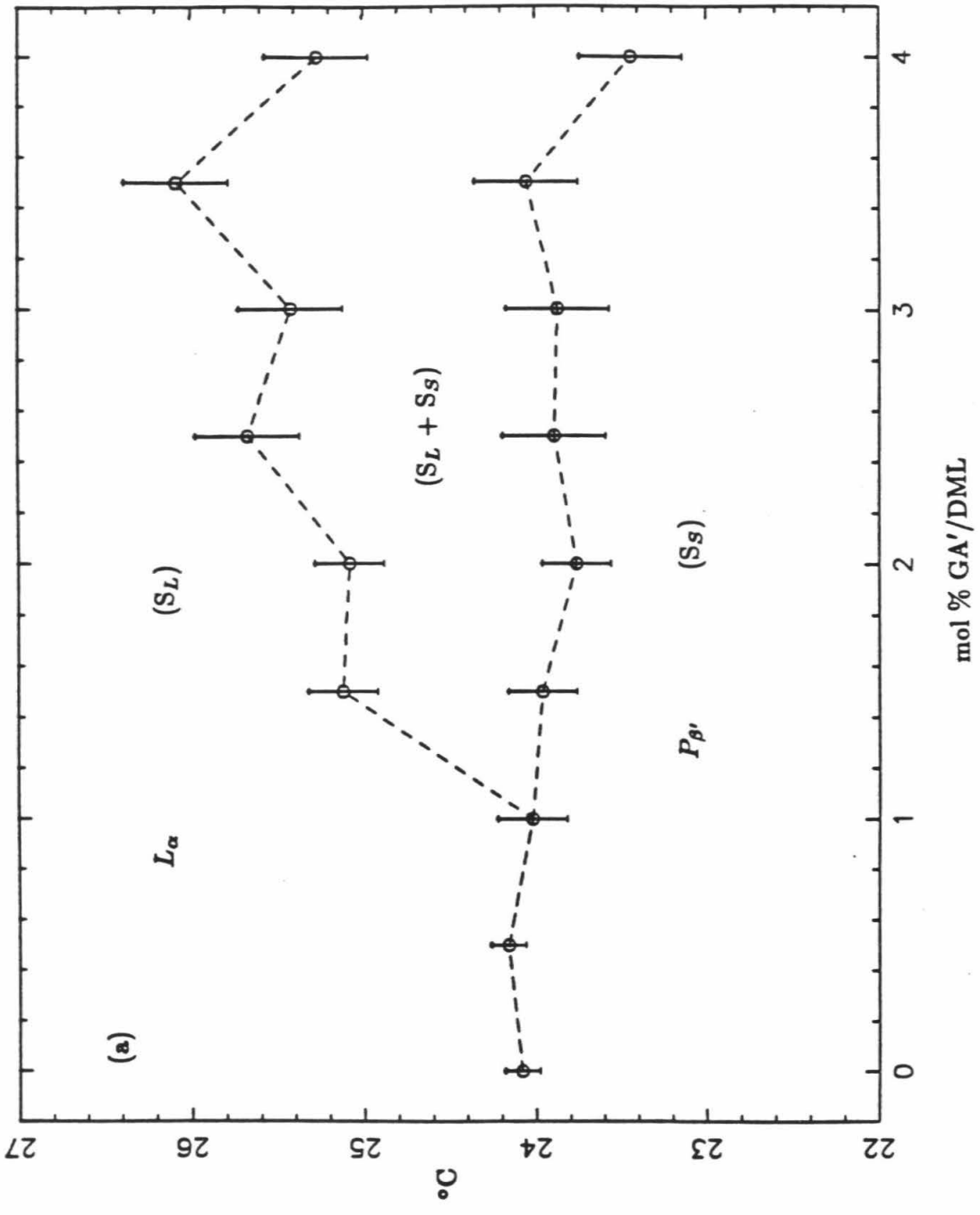
(a)
L_α
(S_L)
(S_L + S_S)
(S_S)
$P_{\beta'}$
°C
mol % GA'/DML
22
23
24
25
26
27
0
1
2
3
4

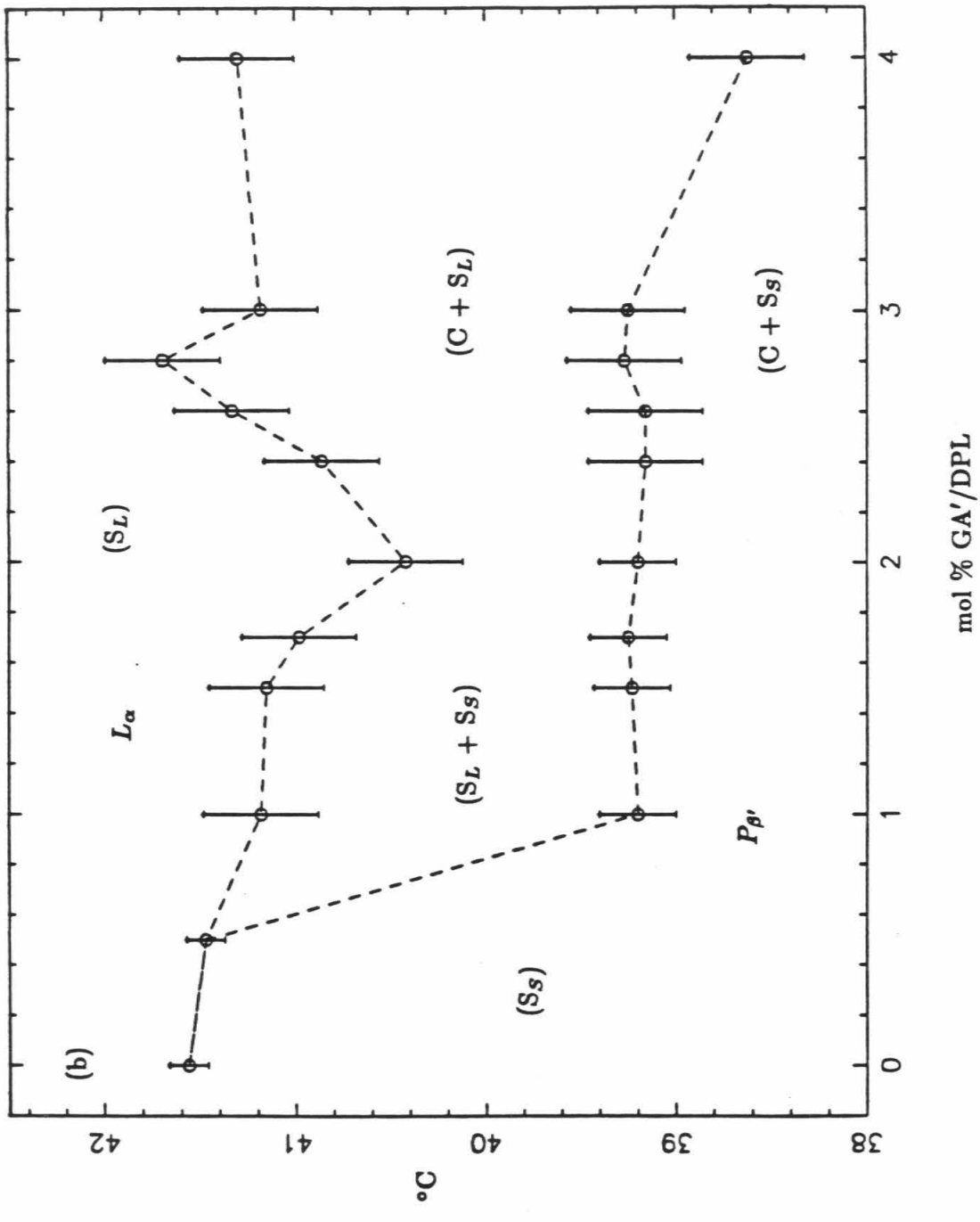
(b)
L_α
(S_L)
(S_L + S_S)
(S_S)
(C + S_L)
$P_{\beta'}$
(C + S_S)
°C
38
39
40
41
42
0
1
2
3
4
mol % GA'/DPL

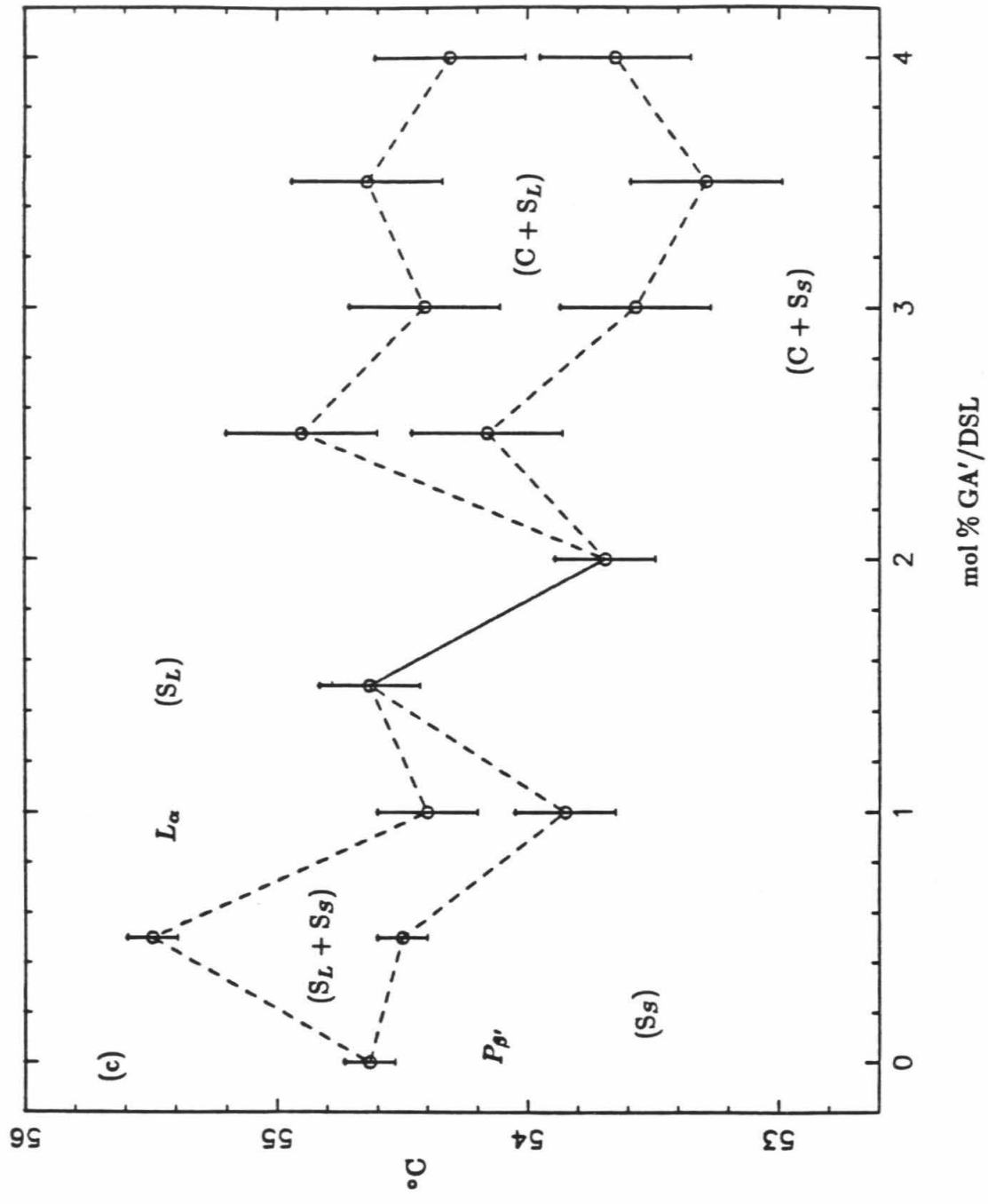
(c)
L_α
(S_L)
($S_L + S_S$)
$P_{\beta'}$
(S_S)
($C + S_L$)
($C + S_S$)
°C
56
55
54
53
0
1
2
3
4
mol % GA'/DSL

bilayer. At a GA′ concentration of 2 mol %, two main transitions are observed in the DSC traces of all lipid systems. This indicates phase segregation into protein rich and protein poor regions. The enthalpies of these peaks are shown in Figure 7. Note that the T_c of DML initially increases with GA′, while the T_c's of DPL and DSL decrease with GA′ concentration. Thus, it appears that the mattress model of the membrane may be particularly relevant to these three systems.

Theoretical Background

In this section, the mattress model of the membrane devised by Mouritsen and Bloom will be discussed briefly, and its relevance to the results of these DSC studies of GA′/lecithin systems will be considered.

First, the standard chemical potentials for the relevant lipid and protein are defined. Subsequently, the difference between the liquid crystalline and gel state chemical potentials for both the protein and the lipid will be calculated. For the lipid, the standard state is chosen to be the pure lipid bilayer. For the protein, the standard state is that of the protein at infinite dilution in the lipid bilayer. The standard chemical potential of the lipid in a state α is represented by $\mu_L^{0,\alpha}(T)$. For the liquid crystalline state of the lipid bilayer, $\alpha = f$, and $\alpha = g$ for the gel state of the lipid bilayer. If $\mu_L^{0,\alpha}(T)$ is expanded about T_c, the following expression is derived:

$$\mu_L^{0,\alpha}(T) = \mu_L^0(T_c) + \frac{h_L^\alpha}{T_c}(T - T_c) + \ldots \qquad (1)$$

If the displacement from T_c is small, the series may be truncated after the second term. As a result, the difference between the gel and liquid crystalline state

Figure 7: The enthalpies for the two main endotherms in (a) GA′/DML, (b) GA′/DPL, and (c) GA′/DSL bilayers at low GA′ concentrations are plotted as a function of GA′ concentration. Open circles represent the enthalpy of the endotherm corresponding to the GA′ poor bilayer phase. The full circles represent the enthalpy of the endotherm corresponding to the GA′ rich bilayer phase. The enthalpies are measured by fitting each endotherm to a polynomial and then integrating the polynomial over the appropriate temperature range. Because the amount of lipid contributing to each endotherm is not known, the molar enthalpies may not be determined.

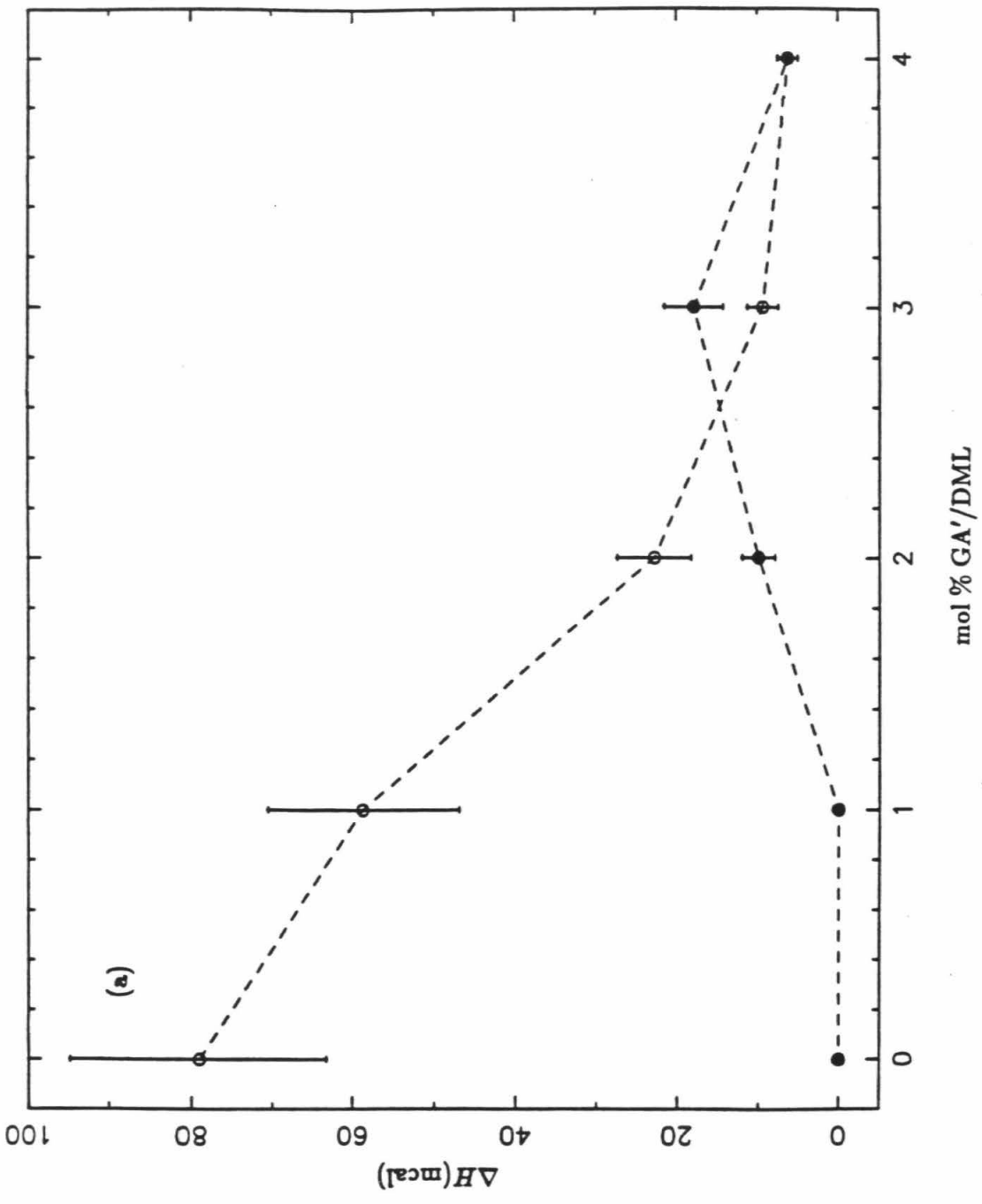
(a)
ΔH(mcal)
100
80
60
40
20
0
0
1
2
3
4
mol % GA'/DML

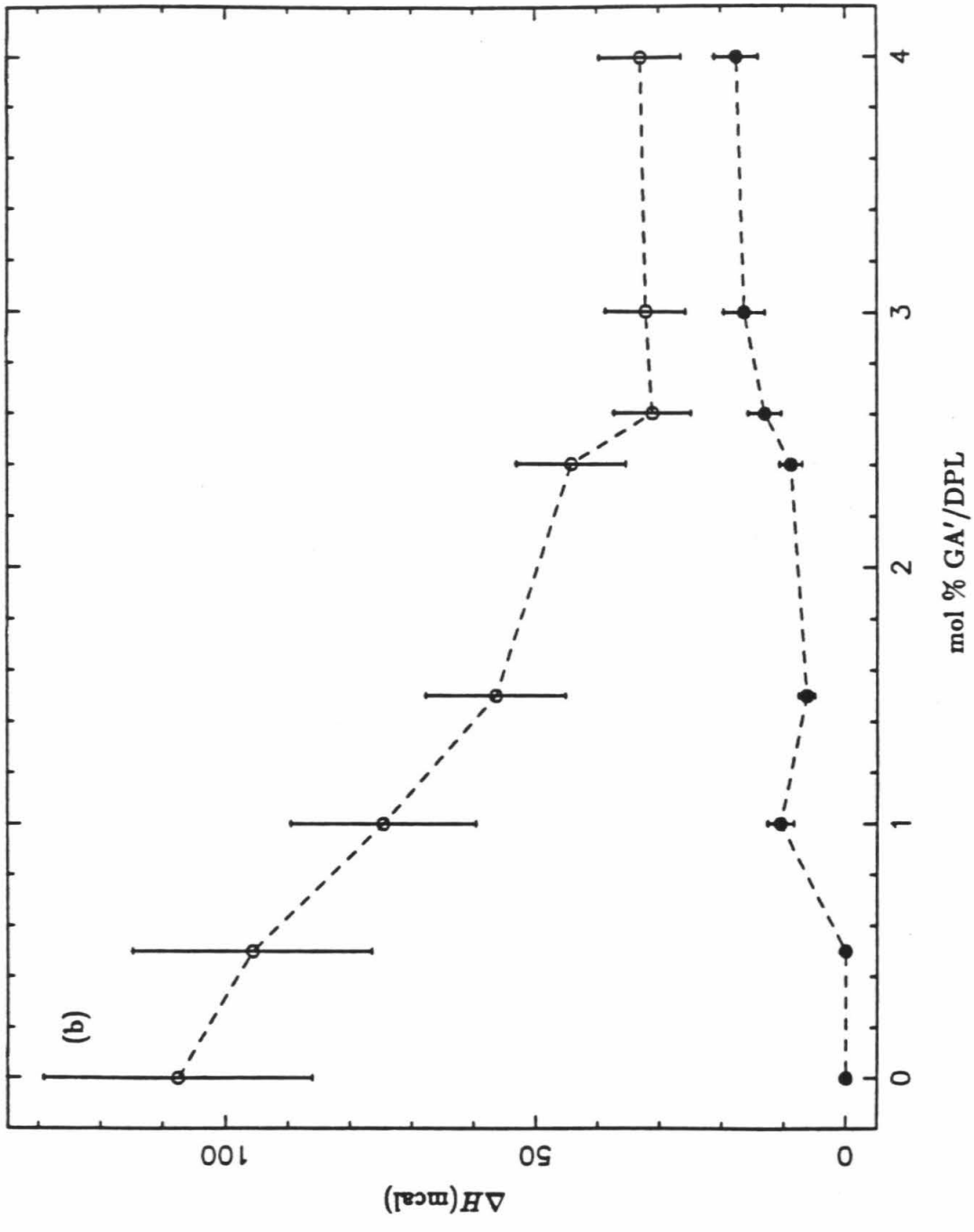
(b)
ΔH(mcal)
100
50
0
0
1
2
3
4
mol % GA'/DPL

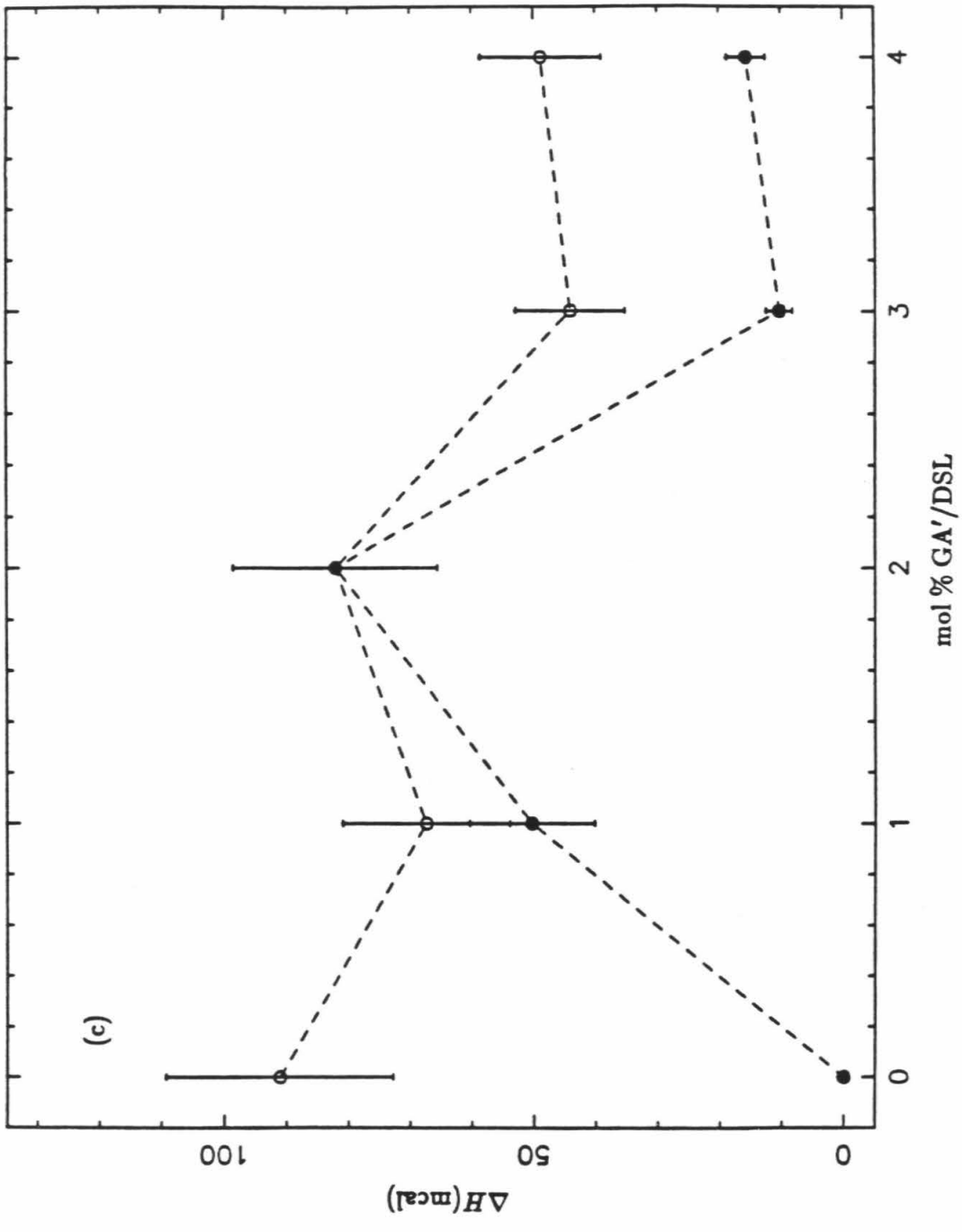
(c)
ΔH(mcal)
0
50
100
0
1
2
3
4
mol % GA'/DSL

chemical potentials of the lipid becomes:

$$\Delta\mu_L^0 = \mu_L^{0,g} - \mu_L^{0,f} = \frac{\Delta H_L}{T_c}(T - T_c) \tag{2}$$

where ΔH_L is the molar enthalpy of the transition.

The standard chemical potential for the protein includes three types of interactions. These interactions are illustrated in Figure 8. The first is an elastic term which involves the deformation of the protein 'spring' to match the hydrophobic length of the lipid bilayer. This term takes the form:

$$\mu_{P,E}^{0,\alpha} = A_P^\alpha (d_P^{s,\alpha} - d_P^0)^2 \tag{4}$$

where A_P^α is the spring constant for protein deformation, d_P^0 is the equilibrium length of the protein, and $d_P^{s,\alpha}$ is the equilibrium length of the protein at infinite dilution in the lipid. As energy is required to deform the spring, $\mu_{P,E}^{0,\alpha}$ must be positive.

Another consideration is the repulsion between adjacent hydrophobic regions of the protein and hydrophilic regions of the lipid or vice-versa. This repulsion results from insufficient expansion or contraction of the protein in response to the lipid environment. Consequently, the hydrophobic region of the protein may be exposed to hydrophilic parts of the lipid membrane, or hydrophobic regions of the bilayer may be exposed to hydrophilic parts of the protein. This interaction has the following form:

$$\mu_{P,R}^{0,\alpha} = B_{L,P}^\alpha |d_P^{s,\alpha} - d_L^{0,\alpha}| \tag{4}$$

where $d_L^{0,\alpha}$ is the hydrophobic length of the lipid, and $B_{L,P}^\alpha$ is a positive constant describing the energy of repulsion per unit length mismatch between the protein

Figure 8: Mouritsen and Bloom's mattress model of protein-lipid hydrophobic mismatch.[5] L represents the lipid bilayer, while P represents the protein. (a) The case in which the hydrophobic length of the protein is much greater than that of the lipid. (b) The case in which the hydrophobic length of the lipid is greater than that of the protein. (c) The parameters used in the mattress model. A_L^α and A_P^α are the elastic constants for deformation of the lipid or protein, respectively, in the α state. α may be the liquid crystalline or gel state. d_L^α and d_P^α are the hydrophobic lengths of the lipid and protein, respectively, in the α state and at a given lipid to protein ratio. C_{LP}^α is the interaction constant for attraction between the hydrophobic regions of the lipid and protein in the α state. B_{LP}^α is the interaction constant describing repulsion between the hydrophobic portion of the protein or lipid and the polar environment to which it may be exposed. The cross-hatched area represents a polar region.

(a)

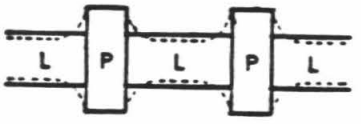

(b)

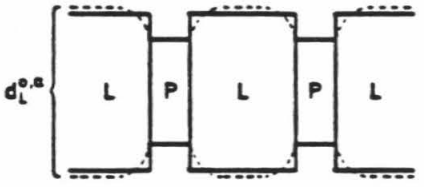

(c)

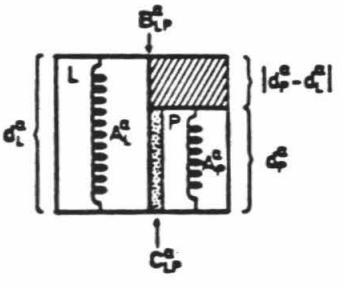

and the lipid. This term also contributes positively to $\Delta\mu_P$.

The third interaction is due to attraction between the hydrophobic region of the lipid and that of the protein. This is the only negative contribution to the chemical potential of the protein. The form of this interaction is as follows:

$$\mu_{P,A}^{0,\alpha} = C_{L,P}^{\alpha} \min(d_P^{s,\alpha}, d_L^{0,\alpha}) \tag{5}$$

where $C_{L,P}^{\alpha}$ is the attractive energy per unit length of hydrophobic contact between the protein and the lipid.

The full expression for $\mu_P^{0,\alpha}$ is obtained by summing Eqns. (3), (4), and (5). This results in the following expression:

$$\mu_P^{0,\alpha} = A_P^{\alpha}(d_P^{s,\alpha} - d_P^0)^2 + B_{L,P}^{\alpha}|d_P^{s,\alpha} - d_L^{0,\alpha}| + C_{L,P}^{\alpha} \min(d_P^{s,\alpha}, d_L^{0,\alpha}) \tag{6}$$

The mol fractions of the lipid and protein in a phase α are defined as:

$$\chi_i^{\alpha} = \frac{n_i^{\alpha}}{n_L^g + n_P^g + n_L^f + n_P^f} \tag{7}$$

and the following relationships hold:

$$\chi_L = \chi_L^g + \chi_L^f = 1 - \chi_P \tag{8}$$

χ_P^{α} must be expressed in terms of $\Delta\mu_P$ and $\Delta\mu_P$. When a protein is miscible in both the liquid crystalline and gel states of the lipid bilayer the chemical potentials of the lipid in the gel and liquid crystalline states are given by:

$$\mu_L^g = \mu_L^{0,g} + RT \ln \chi_L^g \tag{9}$$

and

$$\mu_L^f = \mu_L^{0,f} + RT \ln \chi_L^f \tag{10}$$

At equilibrium, $\mu_L^g = \mu_l^f$. Using this equality, the following expression for $\Delta\mu_L^0$ results:

$$\Delta\mu_L^0 = RT \ln(\frac{\chi_L^g}{\chi_L^f}) \tag{11}$$

If the total mol ratio of protein is much less than one, the following relationships may be derived using the relationship between χ_P and χ_L:

$$\chi_P^g \approx \frac{\Delta\mu_L^0}{RT_c(1-K_d)} \tag{12a}$$

$$\chi_P^f \approx \frac{\Delta\mu_L^0}{RT_c(K_d^{-1}-1)} \tag{12b}$$

where:

$$K_d = \frac{\chi_P^f}{\chi_P^g} = \exp(\frac{\mu_P^{0,g} - \mu_P^{0,f}}{RT_c}) \tag{13}$$

Using the relationship $\chi_P = \chi_P^g + \chi_P^f$, the displacement of the transition temperature from T_c may be expressed in terms of $\Delta\mu_P^0$ as follows:

$$T = \frac{\chi_P RT_c^2}{\Delta H_L}(\frac{1}{1-K_d} + \frac{1}{K_d^{-1}-1})^{-1} + T_c \tag{14}$$

By examining $\Delta\mu_P^0$, the value of K_d may be determined, and, thus, the relationship between T and T_c may be predicted. Namely, if $\Delta\mu_P^0 > 0$, then $K_d < 1$ and $T < T_c$. Conversely, if $\Delta\mu_P^0 < 0$, $T > T_c$. The magnitude of $\Delta\mu_0^P$ depends on the difference in interaction constants and lipid and protein hydrophobic lengths between the gel and liquid crystalline states.

The following approximations should be relevant to the GA′ /lecithin system. First of all, $B^g_{LP} = B^f_{LP} = B_{LP}$. B_{LP} is probably similar for all lipid systems studied. Furthermore, it has been shown that the length of GA′ does not vary greatly between DML, DPL, and DSL bilayers. A^{α}_{P}, therefore, is taken to be infinite, and $d^{s,f}_P = d^{s,g}_P = d^s_P$. The hydrophobic attraction between the lipid and protein molecules should also be approximately equivalent among all lipid systems studied and in all states of the bilayer.

Using these approximations, three expressions for $\Delta\mu^0_P$ may be derived subject to the following three conditions: (1) $d^0_P > d^{0,g}_L$, (2) $d^{0,g}_L > d^0_P > d^{0,f}_L$, and (3) $d^0_P \leq d^{0,f}_L$. These expressions are:

Condition 1

$$\Delta\mu_P = B_{LP}(d^{0,f}_L - d^{0,g}_L) + C_{LP}(d^{0,g}_L - d^{0,f}_L) \tag{15a}$$

Condition 2

$$\Delta\mu_P = B_{LP}(d^{0,g}_L + d^{0,f}_L - 2d^s_P) + C_{LP}(d^s_P - d^{0,f}_L) \tag{15b}$$

Condition 3

$$\Delta\mu_P = B_{LP}(d^{0,g}_L - d^{0,f}_L) \tag{15c}$$

The term including B_{LP} increases $\Delta\mu_P$, while the term including C_{LP} decreases $\Delta\mu_P$. As the length of the lipid increases with respect to the protein, the contribution of the B_{LP} term increases. As a result, $\Delta\mu_P$ also increases for longer chain lipids, and the phase transition temperature, T, shifts to lower temperatures.

Discussion

The equilibrium thicknesses of three states of pure DML, DPL, and DSL bilayers are given in Table I. The thickness in the liquid crystalline state is given in

Table I: The hydrophobic lengths of the DML, DPL, and DSL bilayers in both the L_α,[7] $L_{\beta'}$ (tilted gel), and $P_{\beta'}$ (fully extended gel)[6] states.

Table I

Hydrophobic Lengths (Å)

Lipid	Liquid Crystalline	Fully Extended Gel	Tilted Gel
DML	27.9	38.4	33.3
DPL	29.3	43.5	37.7
DSL	30.6	48.5	42.00

the first column. In the second column, the fully extended length of the hydrocarbon region is reported. At temperatures well below T_c, pure lipid bilayers are in a smectic C phase, labelled $L_{\beta'}$, with hydrocarbon chains tilted at 30° with respect to the bilayer normal. The pretransition endotherm observed in the DSC traces of pure lipid bilayers is associated with the induction of tilt in the hydrocarbon region. In column 3, the fully extended length of the hydrocarbon region has been multiplied by a factor of cos(30°). This yields the hydrophobic length of the $L_{\beta'}$ phase.

In order to evaluate the mattress model, the length of the hydrocarbon region of the bilayer below the phase transition must be known. Although the addition of high concentrations of GA′ abolishes the pretransition endotherm, at lower concentrations of GA′, the pretransition is still observed. For this reason, it will be assumed that the fully extended hydrocarbon length of the lipid bilayer must be scaled by cos(30°) to accurately describe the hydrophobic length of the GA′/lecithin bilayer in the gel state. In the theoretical section, three possible relationships between the hydrophobic length of the protein and that of the lipid bilayer in its liquid crystalline and gel state were considered. According to the known dimensions of GA′, GA′/DML and GA′/DPL mixtures satisfy condition (2), while GA′/DSL mixtures satisfy condition (3). As discussed before, terms in Eqn. (15) which include B_{LP} are positive, while terms including C_{LP} are negative. Thus, for systems satisfying condition (2), the sign of $\Delta\mu_P$ will depend on the relative contributions of terms containing B_{LP} and C_{LP}. For all systems satisfying condition (3), $\Delta\mu_P$ must be positive, and $T < T_c$. If the values from columns (1) and (3) of Table I are substituted in Eqn. (15), the following expressions result:

$$\Delta\mu_P^{DML} = 1.2B_{LP} + 2.1C_{LP} \tag{16a}$$

$$\Delta\mu_P^{DPL} = 7.0B_{LP} + 0.6C_{LP} \tag{16b}$$

$$\Delta\mu_P^{DSL} = 11.4B_{LP} \tag{16c}$$

These relationships predict that $\Delta\mu_P$ will increase with increasing chain length. This result is supported by the experimental observation that the quantity (T-T_c) decreases with increasing chain length. Simultaneous solution of the expressions in Eqn. (16) should yield approximate values of B_{LP} and C_{LP}. $\Delta\mu_P$ may be calculated using Eqns. (13) and (14). First of all, Eqn. (13) is solved for $\Delta\mu^P$ as follows:

$$\Delta\mu_P = \ln K_d \times R \times T_c \tag{17}$$

Then Eqn. (14) must be solved for K_d. This is much easier if two approximations are made. For the DML system, it is clear that $K_d \ll 0$. Thus, Eqn. (14) may be solved for K_d as follows:

$$K_d = \left[\frac{\Delta H_L}{\chi_P R T_c^2}(T - T_c) + 1\right]^{-1} \tag{18a}$$

When the appropriate physical parameters for 2 % GA′ in DML are used in Eqns. (18a) and (17), $\Delta\mu_P^{DML} = -262.1$ cals/molÅ is obtained.

For DPL and DSL, $K_d \gg 0$. In this case, the expression for K_d becomes:

$$K_d = \left(1 - (T - T_c)\frac{\Delta H_L}{\chi_P R T_c^2}\right) \tag{18b}$$

The appropriate physical parameters for 2 mol % GA′ in DPL and DSL yield $\Delta\mu_P^{DPL} = 463.1$cals/molÅ, and $\Delta\mu_P^{DSL} = 439.1$ cals/molÅ, respectively. Eqns. (16a, b, and c) may now be solved simultaneously to yield values for B_{LP} and C_{LP}.

Only two of the three expressions in Eqn. (16) are necessary to solve for B_{LP} and C_{LP}. Quite low concentrations of GA′ induce H_{II} phase in the DSL system. Because the mattress model does not treat such phase changes, Eqn. (12c), which describes GA′ in DSL, will be eliminated. Only the equations describing the DML and DPL systems will be used to calculate B_{LP} and C_{LP}. Simultaneous solution of these two equations yields $B_{LP} = 78.2$cal/molÅ and $C_{LP} = -135.7$cal/molÅ. If these values are used in Eqn. (16c), $\Delta\mu_P^{DSL}$ +891.1 cal/molÅ is obtained. This is about twice the measured value of 439.1 cal/molÅ. An attractive interaction, between GA′ molecules in the DSL bilayer, for instance, would decrease the value of $\Delta\mu_P^{DSL}$.

Conclusions

In this chapter, the phase diagrams for GA′ in DML, DPL, and DSL systems has been studied up to a concentration of 20 mol % peptide in each lipid. The mattress model of the gel-to-liquid crystalline phase transition in lipid bilayers proposed by Mouritsen and Bloom has been used in conjunction with DSC experimentation to approximate two parameters describing GA′/lecithin interactions in the lipid bilayer. B_{LP}, the constant describing the hydrophobic-hydrophilic repulsion between lipid and protein molecules, is approximately 78.17 cal/molÅ. C_{LP}, the constant describing the hydrophobic attraction between the lipid and protein, is approximately −135.7 cal/mol Å. This calculation assumes that both these constants are equal for all lecithin bilayers, and also that protein-protein

interactions are non-existent. Although the mattress model probably oversimplifies the interactions between lipids and proteins, it does predict the correct trends in phase transition temperatures as GA′ is added to lecithin bilayers of varying lengths.

References

1. M. R. Morrow, J. C. Huschilt, and J. H. Davis, *Biochemistry*, **24**, 5396-5406 (1986).
2. J. Riegler and H. Moewald, *Biophys. J.*, **49**, 1111-1118 (1986).
3. D. Chapman, B. A. Cornell, A. W. Eliasz, and A. Perry, *J. Mol. Biol.*, **113**, 517-538 (1977).
4. P. M. Macdonald and J. Seelig, *Biochemistry*, **27**, 2357-2364 (1988).
5. O. G. Mouritsen and M. Bloom, *Biophys. J.*, **46**, 141-153 (1984).
6. B. A. Cornell and F. Separovic, *Biochim. Biophys. Acta*, **733**, 189-193 (1983).
7. B. A. Lewis and D. M. Engelman, *J. Mol. Biol.*, **166**, 211-217 (1983).